LOCKHEED MARTIN ENERGY RESEARCH LIBRARIES
3 4456 0515332 0

ORNL-5266
Cy. 1

GAS-COOLED REACTOR PROGRAMS

THORIUM UTILIZATION PROGRAM PROGRESS REPORT

July 1, 1975 - September 30, 1976

A. L. Lotts
P. R. Kasten

OAK RIDGE NATIONAL LABORATORY
CENTRAL RESEARCH LIBRARY
DOCUMENT COLLECTION
LIBRARY LOAN COPY
DO NOT TRANSFER TO ANOTHER PERSON
If you wish someone else to see this
document, send in name with document
and the library will arrange a loan.
UCN-7969
(3 3-67)

OAK RIDGE NATIONAL LABORATORY
OPERATED BY UNION CARBIDE CORPORATION FOR THE ENERGY RESEARCH AND DEVELOPMENT ADMINISTRATION

Printed in the United States of America. Available from
National Technical Information Service
U.S. Department of Commerce
5285 Port Royal Road, Springfield, Virginia 22161
Price: Printed Copy $10.00; Microfiche $2.25

This report was prepared as an account of work sponsored by the United States Government. Neither the United States nor the Energy Research and Development Administration/United States Nuclear Regulatory Commission, nor any of their employees, nor any of their contractors, subcontractors, or their employees, makes any warranty, express or implied, or assumes any legal liability or responsibility for the accuracy, completeness or usefulness of any information, apparatus, product or process disclosed, or represents that its use would not infringe privately owned rights.

ORNL-5266
UC-77 — Gas-Cooled
Reactor Technology

Contract No. W-7405-eng-26

GAS-COOLED REACTOR PROGRAMS

THORIUM UTILIZATION PROGRAM PROGRESS REPORT FOR JULY 1, 1975, THROUGH SEPTEMBER 30, 1976

A. L. Lotts, Program Manager

P. R. Kasten, Program Director

Date Published: July 1977

OAK RIDGE NATIONAL LABORATORY
Oak Ridge, Tennessee 37830
operated by
UNION CARBIDE CORPORATION
for the
ENERGY RESEARCH AND DEVELOPMENT ADMINISTRATION

LOCKHEED MARTIN ENERGY RESEARCH LIBRARIES
3 4456 0515332 0

ACKNOWLEDGMENT

This report was edited by Sigfred Peterson of the Metals and Ceramics Division. Typing and composition were by the Metals and Ceramics Reports Office under the supervision of Meredith R. Hill.

CONTENTS

SUMMARY xi

1. PROGRAM MANAGEMENT AND ANALYSIS (TASK 100) 1

1.1 INTRODUCTION 1

1.2 PROGRAM MANAGEMENT 3

1.2.1 National Program Plan 3

1.2.2 Principal Contractor Program Management Plan 4

1.2.3 Requirements Documents 5

1.3 PROGRAM ANALYSIS 6

1.3.1 ^{14}C Studies 7

1.3.2 HETF Environmental Requirements 8

1.3.3 BPNL Criticality Studies 8

1.3.4 Economic Studies 9

1.3.5 Thorium Assessment 10

1.3.5.1 Conclusions 11

1.3.5.2 Recommendations 13

1.4 REFERENCES 14

2. REPROCESSING DEVELOPMENT (TASK 200) 17

2.1 INTRODUCTION 17

2.2 TASK MANAGEMENT AND COORDINATION (SUBTASK 201) 19

2.3 COLD LABORATORY DEVELOPMENT 21

2.3.1 Crushed Fuel Element Burning (Subtask 210) 21

2.3.1.1 Small Burner Design Study 21

2.3.2 Particle Classification, Crushing, and Crushed Particle Burning (Subtask 215) 21

2.3.2.1 Particle Classification 21

2.3.3 Solvent Extraction Including Feed Adjustment (Task 225) 23

2.3.3.1 Computer Code for Simulating the Acid Thorex Solvent Extraction System 23

2.3.3.2 Effect of Temperature on the Extraction of Thorium 25

2.3.3.3 Effect of Fluoride on the Extraction of Thorium 25

2.3.4 Krypton Separation (Subtask 235) 30

2.3.4.1 Sorption of Tritiated Water from Flowing Liquid CO_2 30

2.3.4.2 The Systems Kr-CO_2 and Xe-CO_2 31

2.3.4.3 The CO_2-I_2-CH_3I-H_2O System 32

2.3.4.4 Radon-220 Control in Off-Gas Streams 32

2.3.4.5 Final Krypton Concentration 37

2.3.5 Semivolatile Fission Product Collection (Subtask 240) 39

2.3.5.1 Vapor Transport of Fission Products 39

2.4 HOT LABORATORY DEVELOPMENT 43

2.4.1 Fuel Element Size Reduction (Subtask 205) 43

2.4.1.1 Properties of Irradiated Graphite 43

2.4.2 Crushed Fuel Element Burning (Subtask 210) 48

2.4.2.1 Component Tests 48

2.4.3 Particle Classification, Crushing, and Burning (Subtask 215) 52

2.4.3.1 Studies With FTE-4 Irradiated Fuel 52

2.4.3.2 Material Balances 58

2.4.3.3 Head-End Studies 58

2.4.4 Solvent Extraction, Including Feed Adjustment (Subtask 225) 59

2.4.4.1 Feed Adjustment and Solvent Extraction of Irradiated Thoria 59

2.4.5 Gaseous Effluent (Subtask 245) 60

2.4.5.1 Fuel Storage Test 60

2.4.5.2 Data on ^{85}Kr and ^{14}C Releases 62

2.4.6 Waste Processing and Scrap Recovery (Subtask 250) . . 64

2.4.6.1 Processing of Waste SiC Hulls and Semivolatile Nuclides 64

2.4.6.2 SiC Hulls and Insoluble Residues 65

2.4.6.3 Semivolatile Radionuclides 65

2.5 COLD ENGINEERING DEVELOPMENT 66

2.5.1 Krypton Separation (Subtask 235) 66

2.5.1.1 Experiments in the ORGDP Pilot Plant 67

2.5.1.2 Data From Experimental Engineering Facility at ORNL 70

2.5.1.3 Computer Modeling Studies of KALC 76

2.6 REFERENCES 77

3. REFABRICATION DEVELOPMENT (TASK 300) 83

3.1 INTRODUCTION 83

3.2 GENERAL DEVELOPMENT (SUBTASK 301) 84

3.2.1 General Coordination 84

3.2.1.1 Reference Recycle Resin Loading Flowsheet Determination 85

3.2.2 Specification and Quality Control Development 86

3.2.2.1 Specification Development 87

3.2.2.2 Quality Control Development 87

3.2.3 Safety and Safeguards Evaluation 88

3.2.3.1 Environmental, Safety, and Safeguards Evaluation — Refabrication Effluents 88

3.2.3.2 Polynuclear Aromatic Hydrocarbon Emissions from HTGR Fuel Production 89

3.2.3.3 Criticality Analysis 89

3.2.3.4 Material Flow Modeling 91

3.2.3.5 Radiation Level Analysis 92

3.3 COLD LABORATORY DEVELOPMENT 94

3.3.1 Resin Loading 94

3.3.1.1 Resin-Uranyl Nitrate Reaction Equilibria . . 94

3.3.1.2 Thorium Distribution 96

3.3.1.3 Resin Loading Rates 97

3.3.1.4 Slurry Loading of Weak-Acid Resin with Uranium in a Continuous Column 100

3.3.1.5 Density, Acidity, and Conductivity Measurements of Uranyl Nitrate-Nitric Acid Solutions 104

3.3.1.6 Resin Loading With ^{235}U 106

3.3.2 Sample Inspection (Subtask 370) 106

3.3.2.1 Determination of Defective Particle Fraction 106

3.3.2.2 Heavy Metal Assay 108

3.3.2.3 Determination of Thorium Carbide in Partially Converted Biso-Coated Thorium Oxide Fuel Particles 108

3.3.2.4 Determination of Sulfur in Fired Fuel Rods . 108

3.3.3 Waste and Scrap (Subtask 390) 108

3.4 HOT LABORATORY DEVELOPMENT 110

3.4.1 Resin Loading (Subtask 320) 110

3.4.1.1 Radiolysis Effects in Loaded Resin 110

3.4.1.2 Laboratory-Scale Test of Reference Process with ^{233}U 111

3.5 COLD ENGINEERING DEVELOPMENT 112

3.5.1 Resin Loading (Subtask 320) 112

3.5.1.1 Preparation of Feed Resin 113

3.5.1.2 Engineering-Scale Resin Loading System . . . 122

3.5.1.3 Drying of Uranium-Loaded Resin with Microwave Heating 136

3.5.1.4 Material Preparation 140

3.5.2 Resin Carbonization (Subtask 330) 144

3.5.2.1 Equipment Development 144

3.5.2.2 Process Development 147

3.5.3 Microsphere Coating (Subtask 340) 152

3.5.3.1 Equipment Development 153

3.5.3.2 Process Development: 0.13-m Coater 156

3.5.3.3 Process Development: Laboratory-Scale SiC Coating 172

3.5.3.4 Permeability of Pyrocarbon Coatings 173

3.5.3.5 X-Ray Diffraction Determination of BAF . . . 176

3.5.4 Fuel Rod Fabrication (Subtask 350) 176

3.5.4.1 Equipment Development: Fuel Rod Molding . . 177

3.5.4.2 Equipment Development: Fuel Rod Inspection 181

3.5.4.3 Nondestructive Fissile Assay 186

3.5.4.4 Process Development 193

3.5.4.5 Fabrication of Irradiation Test Sepcimens. . 206

3.5.5 Fuel Element Assembly (Subtask 360) 207

3.5.5.1 Equipment Development 207

3.5.5.2 Process Development (Cure-in-Place) 208
3.5.6 Sample Inspection (Subtask 370): Equipment Development 224
3.5.6.1 Particle Size Analysis 224
3.5.6.2 Particle Sample Transfer 225
3.5.6.3 Fuel Rod Sample Transfer 226
3.5.6.4 Sampling 226
3.5.7 Plant Management (Subtask 380) 227
3.5.7.1 Equipment Development 228
3.5.8 Waste and Scrap (Subtask 390) 231
3.5.9 Material Handling (Subtask 395) 232
3.5.9.1 Equipment Development 233
3.6 REFERENCES 234
4. WASTE TREATMENT DEVELOPMENT (TASK 400) 241
4.1 INTRODUCTION 241
4.2 REPROCESSING WASTES (Formerly Subtask 410) 242
4.2.1 Characterization Study of Reprocessing Wastes 242
4.2.2 Evaluation of Waste Processing Alternatives 244
4.2.2.1 Factors Affecting Selection of Processing Alternatives 244
4.2.2.2 General Criteria for Evaluation of Processing Alternatives 246
4.2.3 Evaluation of Options for the Disposal of ^{14}C-Contaminated CO_2 as $CaCO_3$ 246
4.2.4 Fixation of $^{14}CO_2$ as $CaCO_3$ 247
4.3 REFABRICATION WASTES (Formerly Subtask 420) 248
4.3.1 Characterization Study of Refabrication Wastes . . . 248
4.4 REFERENCES 249
5. FUELS IRRADIATION AND EXAMINATION 251
5.1 INTRODUCTION 251
5.2 PEACH BOTTOM IRRADIATIONS 252
5.2.1 Postirradiation Examination of RTE-6 252
5.2.2 Postirradiation Examination of RTE-5 256
5.2.3 Postirradiation Examination of FTE-11 262
5.3 ORR IRRADIATIONS 265

5.4 FSVR EARLY VALIDATION TESTS 265
5.5 REFERENCES 267
6. HTGR FUEL RECYCLE DEMONSTRATION FACILITY (TASK 600) 269
6.1 INTRODUCTION 269
6.2 HRDF PRECONCEPTUAL LAYOUT STUDIES 270
6.3 HRDF REQUIREMENTS DOCUMENTS 270
6.4 REFERENCES 270
7. HOT ENGINEERING TEST PROJECT 273
7.1 INTRODUCTION 273
7.1.1 Purpose 273
7.1.2 Project Objectives 273
7.1.3 Specific Technical Issues 274
7.1.4 Project Schedule 276
7.1.5 Project Status 279
7.2 DESCRIPTION OF HET PROJECT 279
7.2.1 HET-Facilities 282
7.2.2 HET Reprocessing 285
7.2.2.1 System 1100 — Fuel Size Reduction 285
7.2.2.2 System 1200 — Primary Burning 286
7.2.2.3 System 1300 — Particle Classification and Material Handling System 287
7.2.2.4 System 1400 — Particle Crushing and Secondary Burning System 289
7.2.2.5 System 1500 — Dissolution and Feed Adjustment System 291
7.2.2.6 System 1600 — Solvent Extraction System . . 292
7.2.2.7 System 1800 — Product Handling System . . . 294
7.2.3 HET Refabrication 297
7.2.3.1 System 2100 — Uranium Feed Preparation . . . 298
7.2.3.2 System 2200 — Resin Fuel Kernel Preparation 300
7.2.3.3 System 2300 — Resin Carbonization System . . 301
7.2.3.4 System 2400 — Microsphere Coating System . . 302
7.2.3.5 System 2500 — Fuel Rod Fabrication 304
7.2.3.6 System 2700 — Sample Inspection System . . . 305

7.2.3.7 System 2800 — Process Support 306
7.3 REFERENCES 307
8. COLD PROTOTYPE REFABRICATION DEVELOPMENT 309
8.1 INTRODUCTION 309
8.2 MICROSPHERE COATING 309
8.3 FUEL ROD FABRICATION 310
8.4 FUEL ELEMENT ASSEMBLY — CURE-IN-PLACE FURNACE 310
8.4.1 General Layout 310
8.4.2 Processing Chamber 311
8.4.3 Discharge Chamber 312
8.4.4 Fuel Element Unloading Equipment 313
8.4.5 Charging Chamber 313
8.4.6 Charging Chamber Loading Stand 314
8.4.7 Spacer Pallet 314
8.4.8 Thermal Gradient 314
8.4.9 Heat Removal System 314
8.4.10 Fire Protection 315
8.4.11 Furnace Purge Gas 315
8.4.12 Compressed Air 315
8.4.13 Off-Gas 315
8.4.14 Environmental Control 315
8.4.15 Instrumentation and Control Systems 316
8.4.16 Electrical 316
8.5 REFERENCES 317

SUMMARY

1. PROGRAM MANAGEMENT AND ANALYSIS

The program objective is to develop and demonstrate the technology needed to recover and recycle ^{233}U from spent HTGR fuel and to provide interim recycle services for HTGR spent fuel in support of private commitments to HTGR and HTGR fuel recycle. This will require hot and cold laboratory and hot and cold engineering development stages followed by construction of cold prototype equipment for selected items and development of procedures. The interim recycle capability will be provided by the design and construction of an HTGR Fuel Recycle Demonstration Facility (HRDF) based on the information from the development program.

A National Program Plan for HTGR Fuel Recycle was prepared to present the program objectives, define the responsibility for various tasks and subtasks of the technical work, and schedule the work so as to provide the interim recycle capability by the mid 1990s. As Principal Contractor, ORNL prepared a Program Management Plan to establish uniform engineering and management practices among the participating contractors. A requirements document concept was initiated to identify design requirements through functional analysis of HRDF and to allocate responsibility for design solutions and design verification of the solutions to the tasks and subtasks of the program.

A model for global transport of ^{14}C was assembled. This model is appropriate for the estimation of population doses corresponding to various scenarios of population growth, production of CO_2 from fossil-fuel combustion, and release of ^{14}C from HTGR fuel reprocessing. A plan was prepared for the preparation of the environmental documentation required for the construction and operation of the Hot Engineering Test Facility. An experimental plan was prepared by Battelle Pacific Northwest Laboratories under an ORNL subcontract for experimental work to fill gaps in the available data required to validate criticality calculational techniques. Computer codes were prepared to investigate the economic effects on the HTGR fuel cycle of various reactor build schedules and fuel specifications and to determine the effects on cost of enriched uranium feed to the HTGR due to various components.

The thorium fuel cycle in power reactors was assessed. The results of this study indicate that on economic and technical bases the HTGR provides the best contingency reactor in case the introduction of LMFBRs is delayed significantly. Primary emphasis should be placed on commercializing the HTGR on a time schedule such that it can capture a large share of the nuclear power market by 1995—2000.

2. REPROCESSING DEVELOPMENT (TASK 200)

Task Management and Coordination

Two review reports on reprocessing were issued, and a comparative evaluation of reprocessing costs for various thorium-based fuel cycles was prepared.

Cold Laboratory Development

An engineering design study of non-fluidized-bed burning of graphite fuel (i.e., the "whole-block burner" concept) was completed. This approach depends on recycle of burner off-gas for control.

An evaluation of fissile-fertile particle separation by gas elutriation was published.

The SEPHIS (solvent extraction in the presence of highly interacting solutes) computer code, originally written for the Purex process, has been adapted to the Thorex process. Additional data have been obtained on the effects of temperature and the presence of fluoride.

A scoping study on the viability of various solvents for the removal of tritiated water from flowing liquid CO_2 was completed. Final reports on the systems CO_2-Kr and CO_2-Xe were issued. A study of the chemistry of interactions in the systems CO_2-I_2-H_2O and CO_2-CH_3I-H_2O was completed.

The effects of ^{220}Rn on recycle operations and, in particular, the possible benefits of activity reduction via spraying and solvent extraction or ion exchange were evaluated.

The final concentration of ^{85}Kr, after preliminary concentration by the KALC process (krypton absorption in liquid carbon dioxide), was shown to be practicable by use of molecular sieves, even in the presence of xenon and some oxygen.

A transpiration apparatus was designed and built to measure the vapor pressure under controlled atmospheres of various semi-volatile species expected in the reprocessing of HTGR fuels; the system was calibrated with silver, one of the species of concern.

Hot Laboratory Development

The materials handling properties of crushed irradiated graphite are to be determined by in-cell measurements (so-called Jenike tests).

The crusher has been obtained, modified, and tested; components for the Jenike measurements are being modified for in-cell use.

A larger burner system for in-cell use was designed and is being fabricated. This system will burn up to 25 fuel rods at one time, and supply larger amounts of ash, SiC hulls, off-gas, and semivolatiles for data analysis and characterization studies. The system will include a 76-mm-diam (3-in.) burner, cyclone, condenser, and various filters. A special rod crusher was also designed.

Two representative HTGR fuels from the FTE-4 irradiations were processed in-cell to obtain data pertinent to improving material balance. Three analytical methods were used: calculation via ORIGEN code, nondestructive analysis by gamma scanning, and chemical analysis of the various process streams. The ORIGEN values were significantly improved by inputting real-time exposure histories, rather than merely the total irradiation exposure.

The final report on reprocessing experiments with RTE-7 irradiated samples of the Triso UC_2 and Triso ThC_2 type was issued.

Scouting studies on feed adjustment and batch extractions were made with irradiated thoria. Data were obtained on fission product and plutonium behavior.

In storage tests with irradiated fuel rods, about 10% of the calculated ^{85}Kr and 1% of the $^{3}H_2O$ contents were released during 300 days. Data on ^{14}C collected from the burning of two irradiated fuels indicate initial nitrogen contents of 450 and 1600 ppm, on a heavy metal basis. Initial characterization tests were completed on two classes of wastes unique to HTGR fuels: the SiC hulls and the condensed semivolatiles.

Cold Engineering Development

A second KALC (krypton absorption in liquid carbon dioxide) compaign was completed in the ORGDP pilot plant. The target objectives of ^{85}Kr decontamination by a factor of at least 100 and concentration by at least 1000 were achieved. The experimental engineering facility was used to obtain KALC data on column flooding, HTUs, and decontamination factors. An improved computer model of KALC system behavior was completed for the components CO_2-O_2-N_2-CO-Kr-Xe. The model allows modeling by specific columns.

3. REFABRICATION DEVELOPMENT (TASK 300)

Refabrication is the step in the HTGR fuel cycle that begins with the receipt of nitrate solution containing reprocessed ^{233}U and ends

with it refabricated into fuel elements for use in an HTGR. The basic steps in refabrication are very similar to fresh fuel manufacture except that the recycle fuel must be fabricated remotely in hot cell facilities; therefore, the refabrication development program is directed toward the development of processes and equipment for remote application. Its ultimate goal is to develop technology needed to design and operate the refabrication protion of an ERDA-supported HTGR Recycle Demonstration Facility (HRDF). The development program will be accomplished in five phases: (1) cold laboratory development, (2) hot laboratory development, (3) cold engineering development, (4) hot engineering development, and (5) cold prototype development. Work during this report period has primarily been in cold engineering development. Expanded work in waste and scrap handling was initiated during this report period. The work is summarized in sections parallel to the major system of the refabrication portion of the HRDF.

General Development (Subtask 301)

This subtask is responsible for the coordination and review of all functions of the refabrication development task and technical interfacing with other tasks of the Thorium Utilization Program.

A major effort during this reporting period was the development of plans for the redirection of the Program. It was decided not to construct the HTGR Fuel Refabrication Pilot Plant described in the previous report but to develop the technology required for the HTGR Recycle Demonstration Facility (HRDF) through Hot Engineering Tests of certain process steps and Cold Prototype Tests on full-scale equipment designed for remote operation and maintenance.

Other activities of this subtask included issuance of specifications for feed material, coordination of flowsheet selection for the resin-loading process, identification of chemical and radioactive effluents from HTGR fuel refabrication and analyses of the hazards of these emissions, development of a model to calculate material flow through a refabrication plant, and calculation of radiation levels to be expected in the hot cells during HTGR fuel refabrication.

Uranium Feed Preparation (Subtask 310)

No activity was scheduled.

Resin Loading (Subtask 320)

The reference fuel kernel for recycle of ^{233}U to high-temperature gas-cooled reactors (HTGRs) is prepared by loading carboxylic acid cation exhcange resins with uranium and carbonizing at controlled conditions.

Chemical development of the resin loading process has been directed primarily toward the evaluation of those chemical properties of the uranyl nitrate weak-acid resin reaction system that may affect quality control and operating procedures of the engineering process.

A systematic study of the reaction of two commercially available weak-acid resins with uranyl nitrate solutions under equilibrium conditions was conducted as a basic evaluation of the resin loading reaction. Values for the equilibrium quotients obtained from this study illustrate that the quality of the uranyl nitrate feed solution will affect both the capacity of the resin for uranium loading and the relative efficiency at which loading can be achieved. A similar study was begun to evaluate the behavior of impurity ions in the uranyl nitrate feed solution during resin loading. Experimental results obtained thus far illustrate that thorium will be strongly absorbed by the resin during its loading with uranium.

A kinetic investigation of the resin loading process has shown that the relative loading rate can be adequately described as an instantaneous equilibrium process under flow conditions proposed for the Hot Engineering Test Project. Although description of the resin loading reaction as a diffusional process may be more technically accurate, the simplified first-order reaction model developed by this program is sufficient for describing the effects of process parameters on the rate of resin loading.

A demonstration study was conducted to evaluate the application of continuous column techniques for the resin loading process. This study illustrated that feed slurries of solid UO_3 suspended in uranyl nitrate solution could be charged to a column of resin without plugging. With pulsed resin flow countercurrent to slurry feed flow, continuous operation was achieved. The concentration profile of uranium absorbed on the resin over the column length assured full uniform loading of the resin product with uranium.

A literature survey revealed that radiation-induced degradation of ion exchange resins could be appreciable during loading with ^{233}U if the resin salt is held for several days in the water swollen condition. Consequently, an experimental program was initiated to examine the effects of this contingency on the resin carbonization phase of the HTGR fuel refabrication process. To avoid chemical assessment of complex reactions associated with resin degradation, primary evaluation will be based on the results of resin carbonization and the variation in product quality as a function of sample age and moisture content.

A resin feed preparation facility was installed to process commercial resin to meet the specifications for fuel kernel size, shape, and purity. Size classification of the reference resin (Amberlite IRC-72) is by wet screening with a recycle water/resin volume ratio of 40 to give 730 ± 50 μm resin in the sodium form. The sized resin is dried

in a commercial fluidized-bed dryer. Spherical and nonspherical resin is separated on vibratory feeders specially modified to give five separators per plate. The resin is converted to the hydrogen form in either batch or continuous (Higgins-type) contactors.

A complete, integrated engineering-scale resin loading system was installed and operated with natural and depleted uranium. This system is full-scale (4 kg U/batch) for a fuel recycle pilot plant. The ^{233}U from a reprocessing plant would be uranyl nitrate solution containing excess HNO_3. The reference process for resin loading includes an amine extraction of nitric acid to maintain the acid-deficient uranyl nitrate solution required for resin loading. For a NO_3^-/U ratio of 1.6 or an average composition of $UO_2(OH)_{0.4}(NO_3)_{1.6}$, Amberlite IRC-72 can be loaded to 47.5 wt % U (dry basis) and Duolite C-464 can be loaded to 44 wt % U (dry basis). The reliability of in-line pH instrumentation for process control was demonstrated. The amine regeneration system with two water scrubs for uranium recovery results in less than 0.05% U loss (based on the uranium loaded on the resin) to the $NaNO_3$ waste solution. The solvent extraction flowsheets were improved by changing to a partial regeneration of amine and by improvements to the phase separation and interface control equipment. The integrated resin loading system was completed by demonstration of a thermosiphon evaporator to give uranium decontamination factors greater than 5×10^5. A microwave-heated dryer was demonstrated for controlled and rapid drying of the uranium-loaded resin. Over 50 loading runs were made to prepare over 400 kg of dried resin. The procedures for typical loading conditions and for special requirements were demonstrated.

Resin Carbonization (Subtask 330)

The objective of this subtask is to develop equipment and processes for carbonizing weak-acid resin microspheres. Carbonization consists of controlled heating of uranium-loaded resin in the absence of oxygen, causing evolution of volatile constituents. After being heated to about 600°C, the carbonized microspheres consist of UO_2 finely dispersed in a carbon matrix. This material can then be heated to 1600 to 1800°C to convert the desired fraction of UO_2 to UC_2. This later operation is referred to as conversion. Both operations are conducted in fluidized beds using argon as the levitating gas.

Major accomplishments during this reporting period include construction and installation of a 0.23-m-diam furnace system capable of carbonizing batches of up to 4 kg U. This furnace system includes a pneumatic transfer system for loading and unloading the furnace and transfer of the particles to an inert-atmosphere glove box. Studies of the resin carbonization process using TGA, DTA, and quadrupole mass spectrometry provided a better understanding of the resin decomposition process and permitted optimization of the carbonization cycle.

Microsphere Coating (Subtask 340)

The microsphere coating subtask has as its objective the development of equipment and processes necessary for the remote coating of HTGR fuel particles. We will obtain the data necessary to design and operate a commercial-scale remote coating system.

The equipment being developed to remotely coat recycled HTGR fuel includes a fluidized bed to deposit the carbon and silicon carbide coatings. The reference fissile particle coatings consist of low-density buffer and dense (LTI) carbon layers, a layer of silicon carbide, and an outer LTI coating. Major efforts during the year included modifying several components of the coating equipment, procuring and testing new equipment for remotely loading and unloading the furnace, and developing a better understanding of the deposition of the carbon and silicon carbide layers.

Fuel Rod Fabrication (Subtask 350)

The purpose of this work is to develop processes and equipment suitable for the remote fabrication of HTGR fuel rods. The fuel rods are 13 or 16 mm (1/2 or 5/8 in.) in diameter and 50 to 65 mm (2–2.5 in.) long and contain mixtures of fissile and fertile coated particles and graphite shim particles bonded by a matrix of pitch binder and graphite filler. The principal activities in fuel rod fabrication are dispensing particles, blending them, and loading them into molds, injecting the matrix into the beds of particles to form fuel rods, and inspecting and assaying the rods.

During this reporting period, we evaluated an experimental blender, which mixes fuel particles by fluidization with air before the fuel rod mold is loaded. The tentative conclusion is that fuel rods can be blended to meet the axial large HTGR fuel specification, but there is virtually no margin for error in some cases. To provide more conservatism in the design of the blender, a 20-way-splitter incremental blender has been designed and will be evaluated in the near future. To determine the degree of blending achieved, a nondestructive fuel rod homogeneity inspection device using multienergy gamma-ray attenuation has been designed and constructed. Other devices for rapid on-line inspection of fuel rods for mechanical defects and nondestructive fissile assay were developed.

Fuel Element Assembly (Subtask 360)

The fuel element fabrication development is divided into four areas: (1) fuel element loading, in which green (unfired) fuel rods are loaded into the fuel element block; (2) carbonization and annealing, in which the loaded fuel element block is heated to about 1000°C to

carbonize the pitch binder of the fuel rods and then annealed at 1800°C to remove residual volatiles and stabilize fuel rod dimensions; (3) end plug, dowel, and poison rod loading, in which poison rods are loaded into the element and graphite plugs and dowels are placed in the fuel holes and dowel holes and cemented into place; and (4) fuel element inspection, in which the assembled element is inspected and prepared for shipping to the reactor (or stored).

During the report period a fuel rod storage system was installed, automated, and partially evaluated. The design of a full-scale vertical cure-in-place furnace suitable for carbonizing and annealing 16 full-size HTGR fuel elements per day was nearly complete. In the area of process development, factors affecting the failure of fuel particle coatings during the cure-in-place operation were investigated. The particle crushing strength and the matrix pitch coke yield, which is highly dependent on heating rate in the range from 300 to 600°C, significantly affected particle failure. The gas permeability of the graphite fuel elements varied widely from one fuel hole to another and from one fuel element to another; however, this variation did not affect pitch coke yield or particle failure fraction significantly. Other work involved the characterization of the effluents from fuel rod carbonization, the determination of the axial swelling of the fuel column during carbonization and annealing, and the strength of the end plug-fuel element bond after this operation.

Sample Inspection (Subtask 370)

The Sample Inspection System will function as a support system for the refabrication effort. It must provide the means for obtaining representative material samples inside the hot cell at various points in the refabrication process and transferring these samples to shielded glove boxes for analysis.

During this period, efforts were directed toward the development of remotely operable sample transfer systems and a particle sampling device. The feasibility of pneumatic transfer of loose particle samples and encapsulated fuel rod samples was demonstrated.

An automatic particle size analyzer was modified for operation inside an inert-atmosphere glove box to permit analysis of pyrophoric material.

Plant Management (Subtask 380)

The objective of Subtask 380 is to develop and evaluate the instrumentation, control, and data handling technology required to support the demonstration of the remote refabrication of HTGR fuels.

The current and subsequent generations of instrumentation and control hardware appropriate for application to HTGR fuel refabrication processes involve the use of highly complex general-purpose devices such as minicomputer-based packages, microcomputers, and programmable logic controllers. These general-purpose devices will be the basic building blocks used in the design and construction of fuel recycle process control systems. Generally, recycle process control systems will comprise a network of these general-purpose devices and other types of hardware. The impact of factors such as synchronization and interfacing are obvious, creating a real-time environment, with the operation of various engineering-scale process developmental equipment that is analogous to that expected in an actual recycle facility.

A development programmable logic controller and minicomputer are being used in the control and operation of four pieces of engineering-scale mockup equipment. Three additional programmable logic controller systems were procured for the dedicated support of other engineering-scale process developmental equipment.

Waste and Scrap (Subtask 390)

Our goal is to develop waste and scrap handling technology for HTGR refabrication. During the past year, work has focused on the perchloroethylene reclamation system, with additional effort on uranium recovery from the perchloroethylene distillation bottoms and from uncarbonized fuel sticks.

Perchloroethylene is the solvent used in the off-gas scrubber systems attached to the particle carbonization and coating furnaces as well as the cure-in-place furnace. During scrubber operation, the perchloroethylene traps soots, tars, and various hydrocarbon compounds from the furnace off-gases. To maintain scrubber efficiency, the dirty perchloroethylene must be replaced by fresh solvent. This dirty perchloroethylene can be reclaimed by distillation, and thereby the volume of waste from the scrubbing operation can be reduced.

Material Handling (Subtask 395)

The objective of Subtask 395 is to verify existing and to develop new remote material handling technologies necessary to support the remote fabrication of HTGR recycle fuels. Toward this goal, work activities were planned in electromechanical manipulator position control development and advanced remote TV viewing evaluation.

4. WASTE TREATMENT DEVELOPMENT (TASK 400)

Reprocessing Wastes

A detailed analysis to identify and characterize the various reprocessing wastes was completed and published. An engineering analysis of alternative methods for treating reprocessing wastes is being carried out.

Analysis of methods to convert $^{14}CO_2$ to $CaCO_3$ (for final storage) show the direct reaction of CO_2 with slaked lime is preferred. Bench-scale experiments show that the reaction between CO_2 and $Ca(OH)_2$ in aqueous slurry has very favorable kinetics.

Refabrication Wastes

A detailed analysis to identify and characterize the various refabrication wastes was completed and published.

5. FUELS IRRADIATION AND EXAMINATION (TASK 500)

Three series of irradiation tests were funded under the ThU Program: Peach Bottom Irradiations, ORR Irradiations, and FSVR Early Validation Tests. During this reporting period, the postirradiation examination of the Peach Bottom elements was completed. Results show an equivalent performance between accelerated and real-time testing for oxides, carbides, and mixed thorium-uranium oxides. The first of the two ORR irradiation tests was reported. Irradiation of the second ORR test was completed and postirradiation examination was started. No definite results have been obtained. Fuel for the FSVR Early Validation Tests has been fabricated and partially shipped to GA.

6. HTGR FUEL RECYCLE DEMONSTRATION FACILITY (TASK 600)

Because of the program redirection during the report period, efforts on Task 600 and the HRDF have been scaled back. The low level of effort being maintained is intended to help guide program planning and development activities. The most significant of these items has been initiating a family of Requirements Documents for the HRDF, which, when completed, will become the basis upon which development activities will be selected and measured.

7. HOT ENGINEERING TEST PROJECT

Design, construction, and operation of hot engineering tests for the recycle of HTGR fuels is a supporting objective of the National Program Plan for HTGR Fuel Recycle Development. A project called the Hot Engineering Test Project has been organized to achieve this objective and is administered by the National Thorium Utilization Program.

The Hot Engineering Test Project (HETP) will use as its principal facility the Thorium Uranium Recycle Facility (TURF) located at ORNL in Oak Ridge and will provide for two major areas of HTGR nuclear fuel recycle — reprocessing and refabrication.

HET reprocessing includes systems and equipment necessary to demonstrate HTGR fuel reprocessing in the presence of high-level radioactivity from irradiated Fort St. Vrain reactor fuel elements. The important process steps to be demonstrated include primary burning, particle classification and material transport, particle crushing, secondary burning, dissolution and feed adjustment, solvent extraction, uranium-thorium product handling, and off-gas treatment.

HET refabrication includes the systems and equipment necessary to demonstrate portions of the HTGR fuel refabrication processes that may be affected by the radiation associated with ^{233}U containing significant quantities of ^{232}U. Process steps to be demonstrated include resin loading, carbonization, conversion, coating, limited rod fabrication, and inspection to produce representative "green" uncarbonized fuel rods containing ^{233}U fissile particles.

8. COLD PROTOTYPE REFABRICATION DEVELOPMENT

The objective of the cold prototype development stage is to establish the configuration and operating characteristics of equipment designed for use in HRDF. Although this development stage is cold in the sense that highly radioactive material will not be used, the cold prototype equipment will: (1) be full scale, (2) incorporate remote features that may affect the performance of equipment or the quality of the product, and (3) incorporate essential features that are required to demonstrate that equipment can be disassembled, reassembled, or otherwise maintained remotely.

During this report period, effort was concentrated on the design of a microsphere coating furnace, a fuel rod fabrication machine, and a cure-in-place furnace.

1. PROGRAM MANAGEMENT AND ANALYSIS (TASK 100)

W. H. Pechin*

1.1 INTRODUCTION

The Thorium Utilization Program is intended to extend nuclear fuel resources through the application of fuel cycles that utilize the conversion of ^{232}Th to fissile ^{233}U. Analysis of this fuel cycle (see Sect. 1.3.5) continues to indicate that its most promising application is in the High-Temperature Gas-Cooled Reactor (HTGR). Changes in the commercial status of the HTGR before the start of the current report period have altered the plan of action for commercialization of the fuel cycle.

The previous program plan was to prove the commercial feasibility of recycling ^{233}U in HTGRs by constructing two hot pilot plants — one for reprocessing to be built at Idaho National Engineering Laboratory (INEL), and one for refabrication to be built at ORNL. The current program objectives are given below.

Specific Objective. The objective of this program is to provide a demonstration plant for the recycle of HTGR fuels. The HTGR Fuel Recycle Demonstration Facility (HRDF) will demonstrate facility and equipment design and operating procedures that are licensable and commercially feasible for the reprocessing and refabrication of spent fuel from HTGRs. In addition, the HRDF will provide significant production capacity in support of early HTGRs and will include provision for the expansion of production capacity pending the construction of a full-scale commercial plant.

Supporting Objectives. The supporting objectives for the specific objective given above are as follows:

1. To design and construct a Hot Engineering Test Facility (HETF), which will be suitable for engineering-scale processing tests on irradiated HTGR fuels and ^{233}U that contains significant amounts of ^{232}U and fission products.

---

*Present address, Office of Waste Isolution, Union Carbide Nuclear Co., Oak Ridge. Responsibility for this area now assigned to M. M. Martin.

2. To conduct hot engineering tests (HET) in the HETF to determine the effects of significant levels of radiation on specific operations in the reprocessing and refabrication processes, including scrap recovery and primary waste treatment.

3. To design, construct, and test selected cold prototype equipment, which will anticipate as nearly as practicable the processing equipment to be used in the HRDF. The cold prototype equipment will include key features required for the demonstration of remote operation and maintenance.

4. To operate the cold prototype equipment for a length of time sufficient to determine that the proposed processes and equipment are commercially feasible, can be safely operated and maintained remotely, and will produce fuel with commercially acceptable performance. The cold prototype equipment will also be used to develop the operating procedures for the HRDF.

5. To conduct a program of research and development to provide the necessary basic data, information, and technology to allow the design, construction, and operation of HETF, HET, the cold prototype equipment, and HRDF.

6. To conduct a program of irradiation testing to validate the performance of the product produced by the foregoing technology and to supply material for reprocessing research and development in the hot laboratory stage.

7. To guide the above objectives by preconceptual and early conceptual design studies and to implement the results of the above objectives by the detailed design and the construction, testing, and operation of the HRDF.

8. To conduct a continuous course of studies to detect the impact on this program caused by changes in the economic, technological, regulatory, or environmental status of the nuclear industry.

9. To design, institute, and operate a management system that will ensure the orderly and efficient leadership, organization, planning, and control of all the other supporting objectives.

10. To provide for joint industry-government cooperation to include sale or lease of the HRDF to industry following the demonstration, and making program technical data available to industry.

11. To utilize the program, particluarly the HRDF, as a basis for economic evaluation of fuel recycle and as a basis for licensing actions including safeguards definition, recycle standards, and recyle safety.

12. To provide an active program as a means for cooperation with interested foreign governments such as the Federal Republic of Germany. To meet these objectives, a new program organization, described in Sect. 1.2.2 was instituted.

1.2 PROGRAM MANAGEMENT — W. H. Pechin*

1.2.1 National Program Plan — W. H. Pechin*

A National Program Plan for HTGR Fuel Recycle Development was prepared. This plan presents the program objectives listed in Sect. 1.1, defines the various tasks, assigns responsibility among the participating contractors for tasks and subtasks, and presents the schedule and resource requirements for the program through the testing of HRDF.

The development program will progress through stages of cold laboratory, hot laboratory, cold engineering, hot engineering, cold prototype, and procedure development. A summary schedule for these activities in reprocessing and refabrication development and design, construction, and testing of HRDF is shown in Fig. 1.1. Similar stages of development for waste treatment will lag those for reprocessing and refabrication by one to two years. The National Program plan also presents a rationale for the timing of HRDF and a discussion of key technical issues and their current status.

---

*Present address, Office of Waste Isolation, Union Carbide Nuclear Co., Oak Ridge, Tennessee 37830.

ORNL-DWG 77-6831

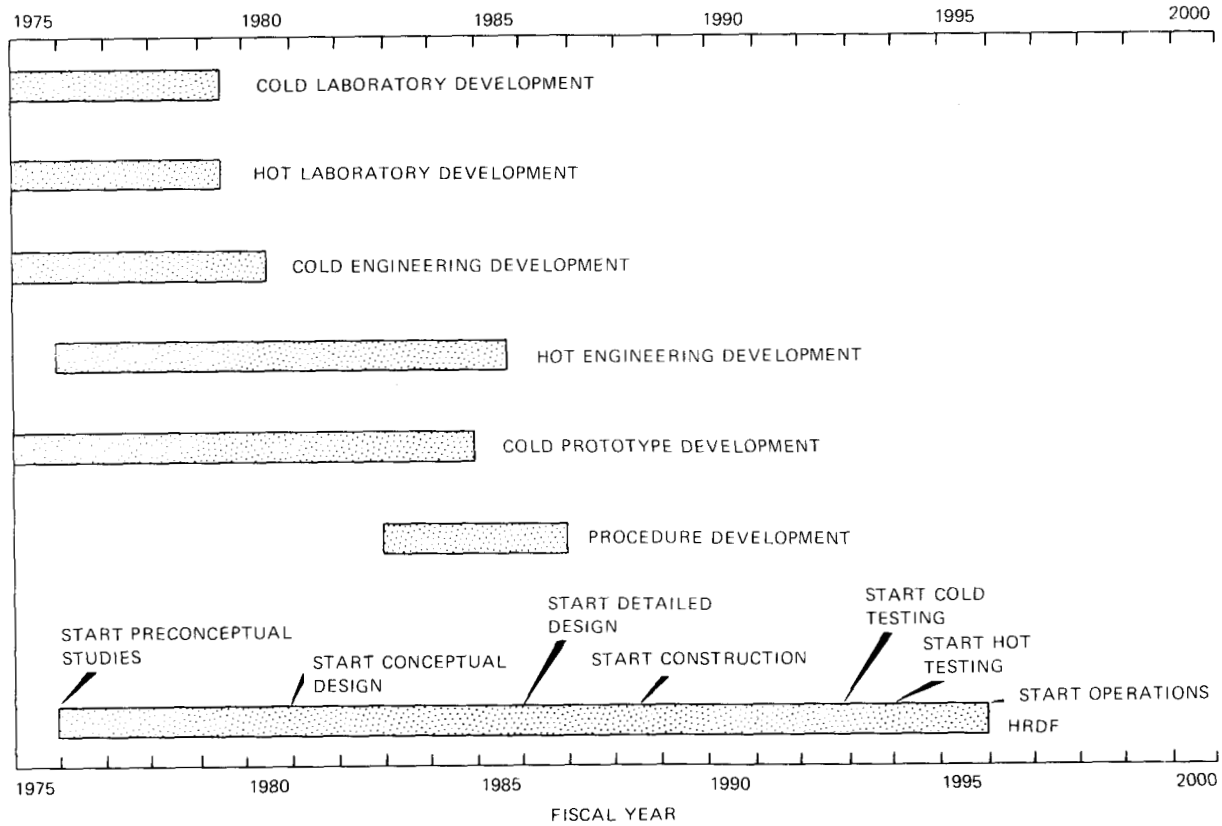

Fig. 1.1. Schedule for Reprocessing and Refabrication Development and HTGR Recycle Demonstration Facility.

1.2.2 Principal Contractor Program Management Plan — T. F. Scanlan

In fulfillment of the ORNL responsibility as principal contractor for the program, a Principal Contractor Program Management Plan was drafted to establish uniform engineering and management practices among the contractors participating in this program.

The plan defines the National program technical organization; assigns responsibilities for programs to participating contractors and personnel; identifies the plans, reports, interface documents, and document control procedures required for programs control and states the essential features of each; and specifies the particular program management procedures or directives that provide detailed instructions for compliance with the management plan requirements.

The National program technical organization is set up in a matrix form, as shown in Fig. 1.2 to provide support for project work, which must draw upon the expertise developed within several diverse tasks.

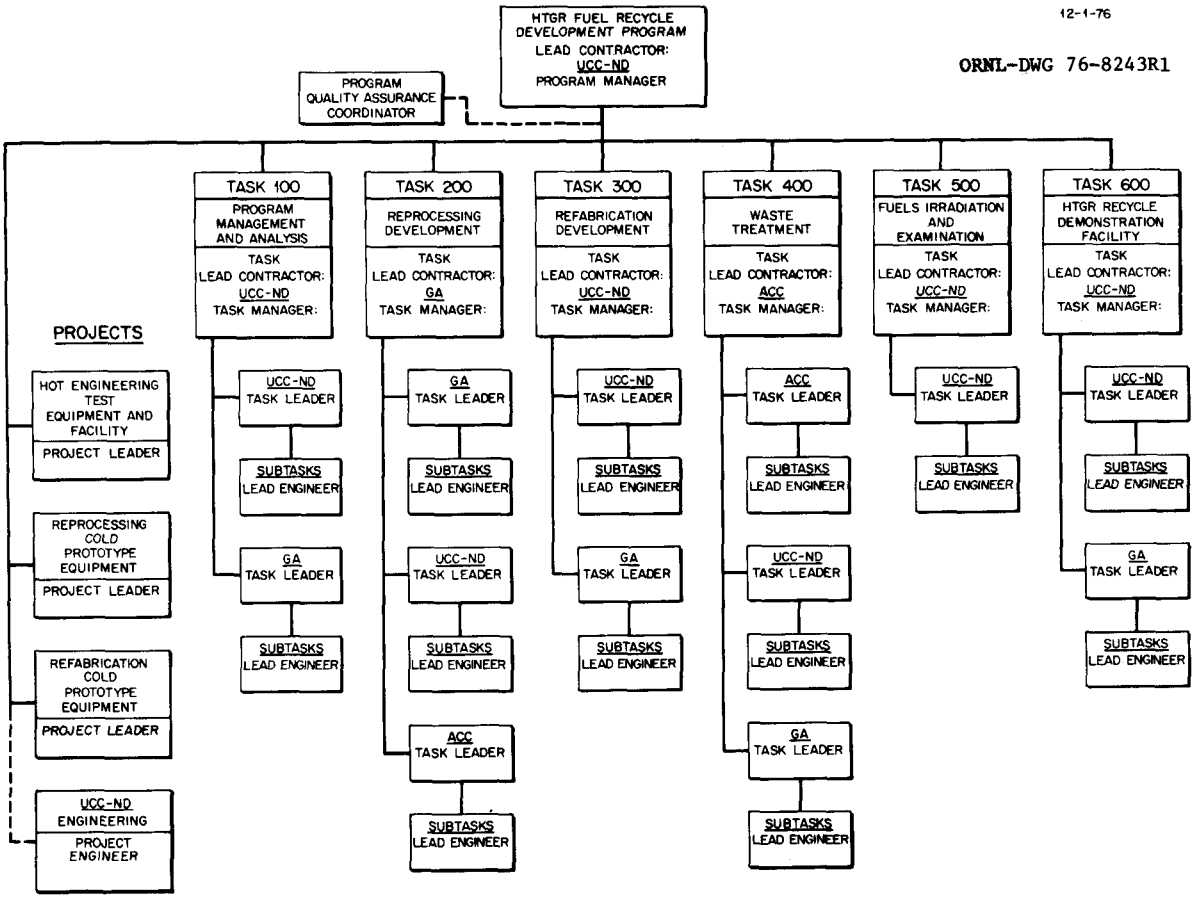

Fig. 1.2. National Program Technical Organization.

1.2.3 Requirements Documents — T. F. Scanlan

A requirements documentation concept was formalized and initiated to provide a mechanism for determining necessary development work and providing design control. The requirements documentation system adopted for the program is a modified form of the system used by the U.S. Air Force, as described in the *Air Force Systems Command Manual*.[1] The requirements documentation system provides the following control features:

1. definition of design requirements at the plant, facility, system, and subsystem levels;
2. allocation of requirements to the appropriate design levels;
3. traceability of requirements both through the design levels and from HRDF to development stage projects (e.g. HET);
4. preparation of functional flow diagrams from which functional requirements, interfaces, and interface requirements may be identified;
5. identification of responsibility for development work related to the defined requirements.

In essence, the requirements documents provide the link between both the HTGR program and UCC-ND engineering division and the program and task development work.

The principal function of the requirements documentation system is to translate the functional requirements defined by the program into design requirements, which are to be satisfied by UCC-ND engineering. Hence, the program defines the design requirements, and UCC-ND engineering proposes design solutions. The requirements documents are then used in design reviews to evaluate the acceptability of the proposed design solutions.

A supplementary function of the requirements documentation system is identification of development work that must be performed to adequately define functional and/or design requirements. Hence, the development work expressed in experimental plans is directly relatable to the program requirements.

1.3 PROGRAM ANALYSIS — J. A. Carpenter, Jr.

This section covers several studies, not specifically addressed elsewhere, that are of general programmatic interest but limited duration. In the previous report[2] most of the topics discussed below were presented in Sect. 3.2 — "HTGR Refabrication Process Development." Under the new program organization the scope of this work has been broadened to

include reprocessing as well as refabrication. In the next period the principal effort in these areas will be HETF Environmental Requirements discussed in Sect. 1.3.2.

1.3.1 ^{14}C Studies — G. G. Killough and S. V. Kaye

The release of ^{14}C to the atmosphere from HTGR fuel reprocessing facilities has long been considered a potential source of difficulty in licensing such facilities. Two scales affect the analysis of environmental transport and dose to man:

1. local (or "first pass"), which in the present context is interpreted to apply to the estimation of dose to individuals and population whose exposure environment lies within 80 km (50 miles) of the point of release;
2. global, which encompasses the estimation of dose to the present and future population of the world.

The first scale was investigated by Environmental Sciences Division (ESD) staff during FY 1975; the conclusions of that work are discussed by Killough et al.[3] During FY 1976, the attention of the ESD staff has been centered on the problem of dose to world population from HTGR releases.

Because of its long radioactive half-life (5730 years) and environmental behavior, ^{14}C has the potential for long-term persistence in those world reservoirs that constitute man's exposure medium. Fundamental to the estimation of population dose from released ^{14}C are models of the global carbon cycle that can predict the specific activities of carbon in these reservoirs as functions of time. Numerous investigators have attempted to understand the global carbon cycle in terms of simple box-compartment models, but such models have failed to explain consistently carbon transport phenomena whose time constants span a wide range (e.g., naturally produced radiocarbon vs CO_2 from the combustion of fossil fuels). Recent analyses by Oeschger et al.[4]

have demonstrated that this deficiency can be overcome by treating the ocean as a diffusive medium with respect to the vertical transport of carbon.

The chief emphasis of the ESD research in FY 1976 has been the assembly of a model of global transport of carbon that reflects the current state of the art and is appropriate for the estimation of population doses corresponding to various scenarios of population growth, production of CO_2 from fossil-fuel combustion, and release of ^{14}C from HTGR fuel reprocessing. While dose estimates based on a variety of global carbon models have appeared in the literature, the supporting models generally have been inadequately described and unavailable for detailed scrutiny, and sensitivity tests have often been lacking in these papers. Moreover, most of these models have been of the simple box variety and therefore subject to the deficiency described earlier. The model that has emerged from the FY 1976 ESD research will be published in a form to facilitate its discussion and computer implementation at other sites. Parameters and scenarios for a reference simulation have been defined, and the sensitivities of population dose estimates to variations from this reference case have been estimated.

1.3.2 HETF Environmental Requirements — J. A. Carpenter

The regulatory environmental requirements for approval of the Hot Engineering Test Facility were determined, and a plan was drawn to meet them in the next period. An Environmental Impact Assessment (EIA) will be written and submitted for approval about January or February of 1977. This document will be a brief review of the expected environmental impacts and will be preliminary to the much more detailed Environmental Impact Statement (EIS). This latter document will be written and submitted for approval by September 30, 1977.

1.3.3 BPNL Criticality Studies — S. R. McNeany

Personnel at Battelle Pacific Northwest Laboratories working under an ORNL subcontract have completed a preliminary program for

criticality safety to support HTGR fuel recycle. The program consisted of studies and calculations necessary to define an experimental plan for performance of "Benchmark" critical experiments on ^{233}U fuels. These experiments are needed to fill gaps in the available data required to validate criticality calculational techniques and neutron cross sections.

The experimental plan is presented in a Battelle report[5] that is currently undergoing distribution. Details found within the report include material form, procurement and processing of the experimental fuel, and currently estimated funding levels.

The results of a series of ^{233}U criticality calculations are being prepared for transmittal to ORNL. These calculations will be compared with identical calculations previously performed at ORNL with the AMPX[6] code system. The objective of this work is to ensure that the cross section processing codes and neutronics codes used at ORNL and BPNL provide consistent results when used in conjunction with a standard nuclear data base[7] (ENDF/B-IV).

1.3.4 Economic Studies — W. E. Thomas

The economic studies applicable to this section have been reported in two ORNL topical reports.[8,9]

The first report[8] described the status of a calculational procedure directed toward costing fresh fuel fabrication, chemical reprocessing, and refabrication of HTGR fuel in a large-scale commercial plant. The decline in commercialization of HTGRs resulted in termination of this effort. In its present state of development, the code is confined principally to calculating annual mainstream and scrap recovery process throughputs in fresh fuel fabrication, chemical reprocessing, and refabrication. The code works from user-supplied reactor build schedules and fuel specifications to approximate changing fuel fabrication requirements over a 20-year (maximum) projection. The availability of a reprocessing facility may be delayed to some

specified date beyond the first year of a projection. Some of the cost routines have also been programmed and are described in the report.

The second report[9] documents a study of enriched-uranium feed costs for the HTGR. The report discusses each of the components that affect the unit cost for enriched uranium; that is, ore costs, U_3O_8-to-UF_6 conversion costs, costs for enriching services, and proposed charges in transaction tails assay. Historical trends and announced changes (before October 1975) are included. Unit costs for highly enriched uranium (93.15% ^{235}U) and for low-enrichment uranium (3.0, 3.2, and 3.5% ^{235}U) are displayed as functions of changes in the above components and compared. The trends in these cost components will probably result in significantly less future cost increase for highly enriched uranium than for low-enrichment uranium — hence favoring the High-Temperature Gas-Cooled Reactor.

1.3.5 Thorium Assessment — F. J. Homan

A brief assessment of the thorium fuel cycle in power reactors was conducted at ORNL in March and April 1976. This study was jointly sponsored by ERDA-DNRA and ERDA-DNFCP. The scope of the assessment was evaluation of the role of the thorium fuel cycle in view of the delay and possible abandonment of the HTGR concept. Several converter systems were considered: light water reactors (LWRs), heavy water reactors (HWRs), high-temperature gas-cooled reactors (HTGRs), and fast reactors, both sodium cooled (LMFBR) and helium cooled (GCFBR). The light water breeder reactor (LWBR) was considered in the initial study, but it was later decided not to consider the LWBR in the thorium assessment report, but rather to consider break-even breeders in a separate report. A draft of the report[10] was widely distributed for review and comments in July 1976, and the final draft is scheduled for publication by the end of December 1976.

Several conclusions and recommendations were reached in the report. These are summarized below.

1.3.5.1 Conclusions

1. Development of the thorium fuel cycle is justified on the basis of better U_3O_8 utilization, improved potential for long-term economics, and additional flexibility with regard to fuel recycle alternatives. Thus, introduction of the thorium fuel cycle provides additional power generation capability in case of delayed introduction of commercial FBRs, or in case a low-gain FBR is introduced on the reference schedule.

2. Of the three thermal reactors considered (LWR, HWR, HTGR), the HTGR employs the thorium fuel cycle most economically. The combination of favorable fuel utilization, high thermal efficiency, a favorable design relative to safety considerations, and flexibility with respect to reactor siting and future high-temperature applications make the HTGR the most useful converter reactor if it were available commercially.

3. The HWR(Th) system appears better suited than the LWR(Th) system for attaining high conversion ratios. However, the capital component of the HWR power cost appears at least as high as that of LWRs, exclusive of the HWR requirement for heavy water, such that total power costs of HWRs appear higher than that of LWRs for U_3O_8 prices less than about \$110/kg (\$50/lb). A decrease in HWR capital costs appears important to HWR application in the U.S. At \$220/kg (\$100/lb) U_3O_8, the HWR(Th) system was more economic than either the LWR(Th) or LWR(U) systems.

4. Use of LWR(Th)s rather than LWR(U)s will increase the amount of energy generated from a given U_3O_8 resource by about 20% above the reference value, considering substitution of thoria for urania in present type LWR designs. Use of LWR(Th)s beginning in 1995 to 2000 increases the energy generation from specified U_3O_8 resources by 12 to 16% relative to complete use of LWR(U)s. However, LWR(Th) systems do not appear economic compared with LWR(U) systems.

5. Use of HTGRs and HWRs with conversion ratios in the 0.8–0.9 range increases energy generation from a given U_3O_8 resource by 20–64%, considering introduction of these reactors by 1995–2000.

[Power growth scenarios used in estimating the above considered nuclear power levels to rise to 400–600 GW(e) by the year 2000.]

6. Operation of thermal reactors on plutonium-thorium fueling appears to be economically attractive when plutonium is recovered from LWRs or enriched-uranium HWRs. However, use of plutonium-thorium fueling does not have a large impact on fuel utilization characteristics because of limited plutonium availability. Further, use of plutonium in this manner would not permit plutonium to be available for startup of FBRs. The plutonium needs of FBRs under reference introduction and growth scenarios are such that reserving plutonium for FBRs would preclude large-scale use of plutonium-thorium fuel cycles.

7. Economic application of the thorium cycle in thermal reactors generally requires establishment of a fuel recycle industry, particularly for LWRs and HWRs (fuel recycle is also required for utilizing product plutonium and uranium from the uranium cycle). Without fuel recycle, the thorium cycle can be used most effectively in HTGRs; however, recycle in HTGRs is desirable to increase fuel utilization performance, and is also economically desirable when U_3O_8 costs rise above about \$88/kg (\$40/lb) for the reference conditions of this study.

8. Converter reactor operation with conversion ratios above $\sim$ 0.9 does not appear economic; the high fuel recycle costs associated with low fuel burnups and the high fissile inventory requirements outweigh the improvement in fuel utilization achieved.

9. The discounted economic benefits from thorium cycle use in the various reference-type reactors, and relative to LWR(U) with plutonium recycle, varied from \$1–3.8 billion for HWRs, and from \$6.4–21.6 billion for HTGRs, based on economic conversion ratios, estimated power growth scenarios, thorium reactor introduction by 1995–2000, and a U_3O_8 price of \$220/kg (\$100/lb). The use of thorium cycles in reference LWRs was not economic relative to LWR(U)s.

10. The HTGR economic benefits given in (9) would be canceled if the unit capital costs of HTGRs were increased by \$95–115/kW(e) above those for LWRs; similarly, the HWR economic benefits would be canceled if the relative HWR capital costs were increased by \$13–18/kW(e).

11. Although the nuclear performance of the thorium fuel cycle in FBRs is generally not as good as that of the uranium cycle, use of mixed cycles in FBRs may be satisfactory and/or desirable. Also, use of metallic thorium fuels might be possible because of the superior properties of thorium metal relative to uranium alloys. Use of metallic thorium fuel would improve the performance of the thorium cycle relative to use of oxide fuel. Further, if plutonium is delayed significantly, but ^{233}U recycle is not, use of the thorium cycle in FBRs would be advantageous. From a safeguards viewpoint, developing a mixed uranium-thorium fuel cycle permits a "denaturing" of recycle fissile fuels, since ^{233}U can be diluted with ^{238}U. This flexibility could be important if fuel feed to certain FBR power stations were limited to about 20%-enriched uranium.

1.3.5.2 Recommendations

Strong support should be given to HTGRs as the best contingency reactor in case there is a significant delay in the introduction of LMFBRs. Primary emphasis should be placed on commercializing the HTGR and introducing it on a time schedule such that it can capture a large share of the nuclear power market by 1995—2000.

In addition to the above, continued studies and evaluations should be carried out on the HWR(Th) and LWR(Th) systems. HWR(Th)s should be considered for commercial introduction into the U.S. as a backup to the HTGR. Associated effort should include an evaluation of the costs and schedules for commercial introduction and licensing of HWRs, of the capital investments required for D_2O separation plants, and an assessment of all costs not expected to be borne by industry. Also, since LWRs are the most direct vehicle for thorium utilization, LWR(Th) systems should be studied more thoroughly to be sure the conclusions of this limited study are valid. Such studies should also consider LWR designs based on a more advanced technology; in the latter case, care must be taken to consider the influence of licensing requirements on design.

Finally, it should be noted that the above considers no limitations on fuel use or on fuel recycle other than those associated with economic

and technical factors. If limitations on fuel recycle are imposed upon the nuclear industry because of safeguards considerations, the use of thorium-uranium mixed cycles in FBRs may be necessary to have a breeder economy and could have implications on thermal reactor fuel cycles. This situation was examined only peripherally in this report; from the results obtained, we recommend that detailed studies be carried out with regard to thorium-uranium fuel cycles in FBRs and their interactions with thermal reactors.

1.4 REFERENCES

1. "Systems Engineering Management Procedures," Sect. 375–5 in *Air Force Systems Command Manual*, U.S. Air Force Systems Command Headquarters, Andrews Air Force Base, Washington, DC, March 10, 1966.
2. A. R. Olsen and J. D. Sease, "General Development," *Thorium Utilization Program Prog. Rep. Jan. 1, 1974–June 30, 1975*, ORNL-5128, pp. 100–8.
3. G. G. Killough, K. R. Dixon, N. T. Edwards, B. D. Murphy, P. S. Rohwer, W. F. Harris, and S. V. Kaye, *Progress Report on Evaluation of Potential Impact of ^{14}C Releases from an HTGR Reprocessing Facility*, ORNL/TM-5284 (July 1976).
4. H. Oeschger, U. Siegenthaler, U. Schotterer, and A. Gulgelmann, "A Box Diffusion Model to Study the Carbon Dioxide Exchange in Nature," *Tellus* 27: 2 (1975).
5. S. R. Bierman and E. D. Clayton, *High-Temperature Gas-Cooled Reactor Criticality Research Program*, Battelle Pacific Northwest Laboratories, report in preparation.
6. N. M. Greene et al., *AMPX: A Modular Code System for Generating Coupled Multigroup Neutron-Gamma Libraries from ENDF/B*, ORNL/TM-3706 (March 1976).
7. D. Garber et al., *Data Formats and Procedures for the Evaluated Nuclear Data File, ENDF*, BNL-NCS-50496 (ENDF-102) (October 1975).
8. W. E. Thomas, *Development of a Procedure for Evaluating the Economics of Process Options in Commercial HTGR Fuel Recycle*, ORNL/TM-5125 (May 1976).

9. W. E. Thomas, *Enriched-Uranium Feed Costs for the High-Temperature Gas-Cooled Reactor: Trends and Comparison with Other Reactor Concepts,* ORNL/TM-5270 (April 1976).

10. P. R. Kasten, F. J. Homan, E. J. Allen, D. E. Bartine, W. L. Carter E. H. Gift, J. D. Jenkins, A. L. Lotts, K. J. Notz, A. R. Olsen, R. H. Rainey, J. E. Rushton, and M. L. Tobias, *Assessment of the Thorium Fuel Cycle in Power Reactors,* ORNL/TM-5565 (January 1977).

2. REPROCESSING DEVELOPMENT (TASK 200)

K. J. Notz

2.1 INTRODUCTION

The purpose of this task is to develop the processes, equipment, and procedures required to design, construct, and operate an HTGR Fuel Recycle Demonstration Facility (HRDF). This will be accomplished by orderly progression through six development stages:

1. cold laboratory development,
2. hot laboratory development,
3. cold engineering development,
4. hot engineering development,
5. cold prototype development,
6. procedure development.

While progression through these stages is nominally sequential, in practice it is entirely feasible to simultaneously conduct stages 2 and 3 after stage 1, likewise stages 4 and 5 after stage 3. Cold and hot laboratory development jointly provide the base-line process flow-sheets, cold engineering provides scalable equipment designs, hot engineering verifies these equipment designs in a radioactive environment, cold prototype provides full-size components including key remote features, and procedure development uses the prototype facilities to develop procedures for the HRDF.

In addition to the vertical subdivision into development stages, this task is also subdivided horizontally into functional subtasks:

Subtask 201 — Task management and coordination
Subtask 205 — Fuel element size reduction
Subtask 210 — Crushed fuel element burning
Subtask 215 — Particle classification, crushing, and crushed particle burning
Subtask 220 — Dissolution, insolubles separation, and drying
Subtask 225 — Solvent extraction including feed adjustment
Subtask 230 — Dry solids handling
Subtask 235 — Krypton separation

Subtask 240 — Semivolatile fission product collection

Subtask 245 — Gaseous effluent treatment

Subtask 250 — Waste processing and scrap recovery

Subtask 255 — Thorium product treatment and storage

Subtask 260 — Plant management

Subtask 265 — Fuel Shipping and storage

These various stages and subtasks are being accomplished in two ERDA national laboratories — ORNL and Idaho National Engineering Laboratory (INEL) — and by a private contractor — General Atomic Company (GA), with ORNL having overall technical responsibility for all tasks and GA having the lead responsibility for Task 200. The assignment of specific responsibilities is shown in Table 2.1. For most subtasks, stage 1 is completed, stages 2 and 3 are being finished, and stages 4 and 5 are getting started. Subtask 250 and 255 are not this far along, but they are not required in the schedule until later.

Table 2.1. Specific Responsibilities Under Task 200

Subtask	Lead Contractor	Principal Contractor For Each Development Stage[a]					
		1	2	3	4	5	6
201	GA	GA	ORNL	GA	ORNL	GA	GA
205	GA	GA	ORNL	GA	ORNL	GA	GA
210	GA	GA	ORNL	GA	ORNL	GA	GA
215	GA	GA	ORNL	GA	ORNL	GA	GA
220	GA	GA	ORNL	GA	ORNL	GA	GA
225	GA	GA	ORNL	GA	ORNL	GA	GA
230	GA	GA	ORNL	GA	ORNL	GA	GA
235	ORNL	ORNL	ORNL	ORNL	ORNL	NA	ORNL
240	INEL	INEL	ORNL	INEL	ORNL	GA	GA
245	GA	INEL	ORNL	GA	ORNL	GA	GA
250	GA	GA	ORNL	GA	ORNL	GA	GA
255	GA	INEL	ORNL	INEL	ORNL	INEL	INEL
260	GA	NA	NA	GA	GA	GA	GA
265	GA	NA	NA	NA	GA	NA	GA

[a]NA - Not applicable

The following sections of Chapter 2 describe work done at ORNL on Task 200 during this 15-month period. The presentation is organized into major headings in terms of development stages, with subheadings based on subtasks. Hot engineering development is reported in Chap. 7, cold prototype development is carried out at GA and hence not reported here, and procedure development is yet to start.

2.2 TASK MANAGEMENT AND COORDINATION (SUBTASK 201) — K. J. Notz

In addition to performing the obvious functions of planning, organizing, controlling, reviewing, commenting, and coordinating, we issued two topical reports. The first[1] was *An Overview of HTGR Fuel Recycle* and the second,[2] prepared as a more detailed backup for a paper given at the AIChE 82nd Annual Meeting, was *Selected Studies in HTGR Reprocessing Development*. Abstracts of these reports follow.

> An overview of HTGR fuel recycle is presented, with emphasis placed on reprocessing and fuel kernel refabrication. Overall recycle operations inlcude (1) shipment and storage, (2) reprocessing, (3) refabrication, (4) waste handling, and (5) accountability and safeguards.

> Recent work at ORNL on hot-cell studies, off-gas cleanup, and waste handling is reviewed. The work includes small-scale burning tests with irradiated fuels to study fission product release, development of the KALC process for the removal of ^{85}Kr from a CO_2 stream, preliminary work on a non-fluidized-bed burner, solvent extraction studies including computer modeling, characterization of reprocessing wastes, and initiation of a development program for the fixation of ^{14}C as $CaCO_3$.

Figure 2.1, taken from these reports, shows the central role of reprocessing in the HTGR fuel cycle.

We also comparatively assessed reprocessing costs for various thorium fuel cycles relative to light water reactors. This was part of an overall assessment,[3] which considered all aspects of the fuel cycles treated, and is reported in Sect. 1.3.5 of this report. These thorium fuel cycles were included: HTGR, LWR, HWR (CANDU), FBR, and LWBR. The reprocessing evaluation, which was based on comparative, semidetailed flow sheets, will also be published separately.[4]

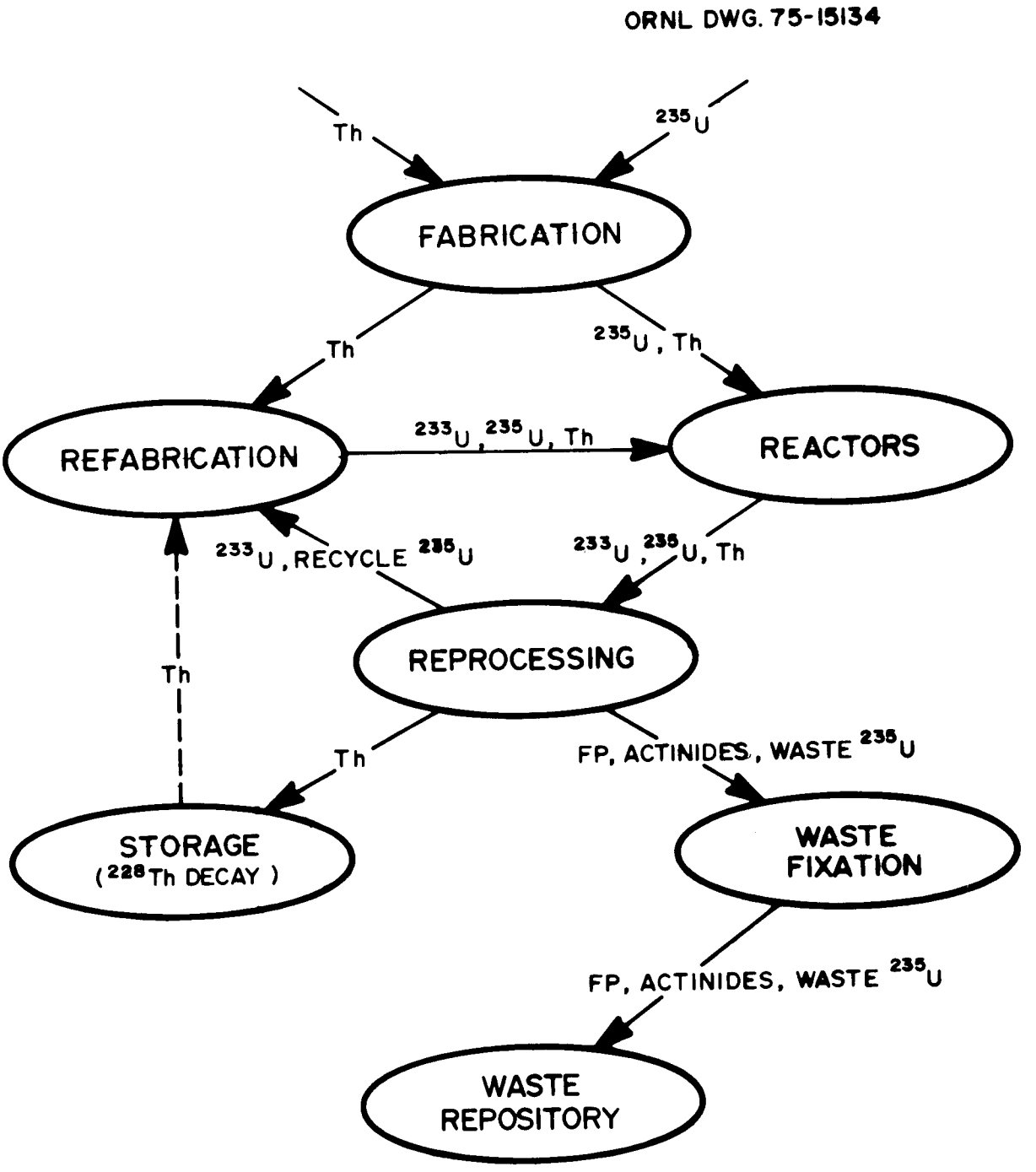

Fig. 2.1. HTGR Fuel Cycle.

2.3 COLD LABORATORY DEVELOPMENT

2.3.1 Crushed Fuel Element Burning (Subtask 210)

2.3.1.1 Small Burner Design Study — J. R. Horton

The concept of burning fuel elements whole, without crushing, in a "whole-block burner" has received attention in the past.[5,6] As part of a study to select and design an intermediate-size burner for in-cell use, a non-fluidized-bed burner using gas recycle (Fig. 2.2) was conceptually designed. This work has been reported internally along with a section by D. W. Langenberg on ejector design. The results may be summarized as follows:

> A preconceptual design study of a nonfluidized burner was initiated following prescribed specifications to achieve a very high burn rate and to see if the required burner and accessories could be fitted into Cell 1 in Building 4507. From preliminary layouts developed, all the major components, with some difficulties, could be designed to fit in the hot cell. Ejectors may be used for recycling the off-gas as determined by calculations. A temperature control system was developed to automatically sustain burning at maximum rate while protecting against overheating. Additional work is recommended in mathematical modeling to establish conditions for burning front stability and thus minimum condition to sustain combustion.

2.3.2 Particle Classification, Crushing, and Crushed Particle Burning (Subtask 215)

2.3.2.1 Particle Classification — V.C.A. Vaughen

A report was published[7] on particle classification. The abstract follows:

> The separation of ^{235}U and ^{233}U in the reprocessing of HTGR fuels is a key feature of the feed-breed fuel cycle. This is attained in the Fort St. Vrain (FSV) reactor by coating the fissile (Th-^{235}U) particles and the fertile (Th-^{233}U) particles separately with silicon carbide (SiC) layers to contain the fission products and to protect the kernels from burning in the head-end reprocessing steps. Pneumatic (gas) classification based on size and density differences is the reference process for separating the SiC-coated particles into fissile and fertile streams for subsequent handling.

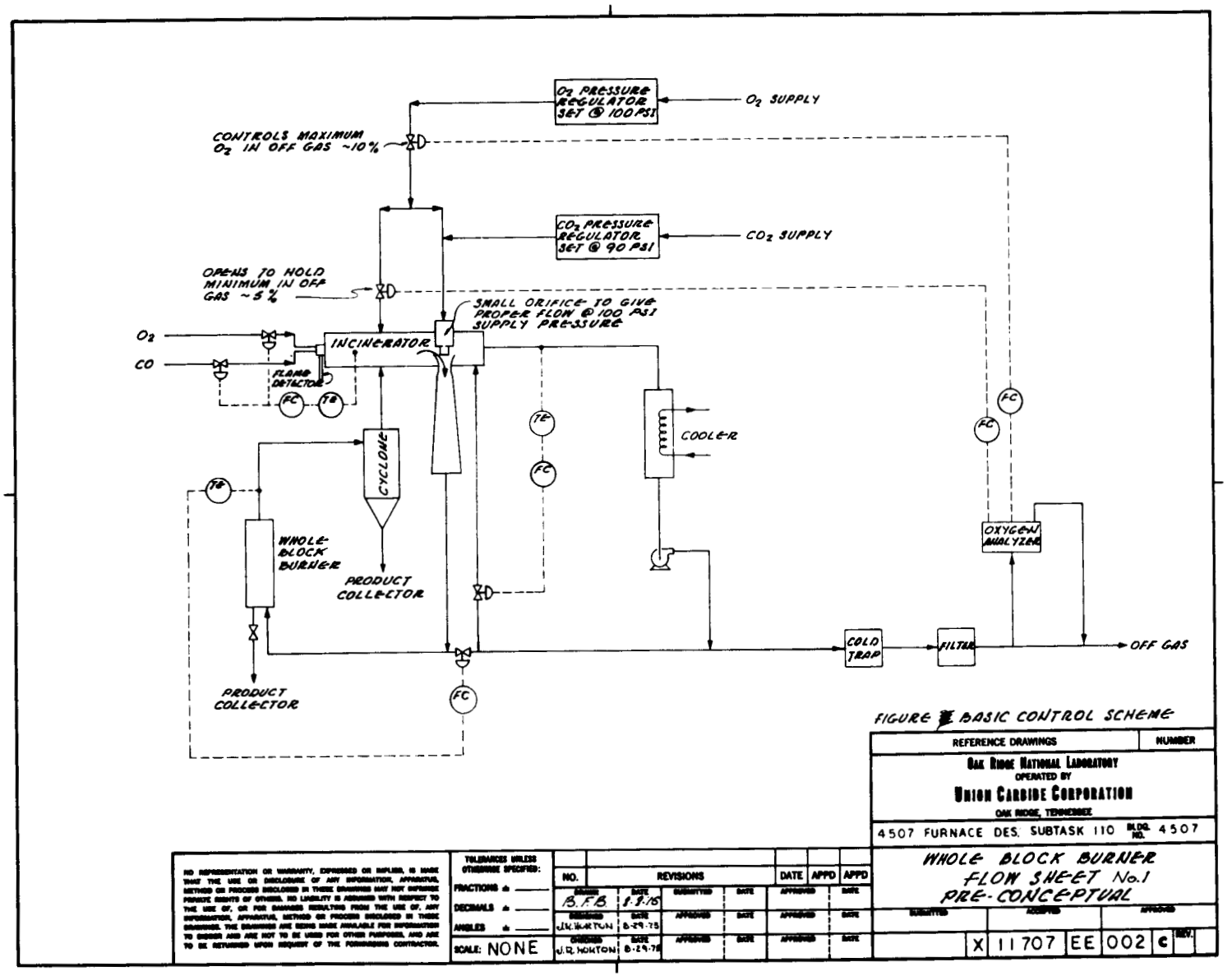

Fig. 2.2. Conceptual Design for Nonfluidized Bed Burner. Pressures indicated are 0.62 and 0.69 MPa.

Terminal velocities have been calculated for the $\pm 2\sigma$ ranges of particle sizes and densities for "Fissile B"—"Fertile A" particles used in the FSV reactor. Because of overlapping particle fractions, a continuous pneumatic separator appears infeasible; however, a batch separation process can be envisioned. Changing the gas from air to CO_2 and/or the temperature to 300°C results in less than 10% change in calculated terminal velocities.

Recently reported work in gas classification is discussed in light of the theoretical calculations. The pneumatic separation of fissile and fertile particles needs more study, specifically with regard to (1) measuring the recoveries and separation efficiencies of actual fissile and fertile fractions in the test of the pneumatic classifiers and (2) improving the contactor design or flowsheet to avoid apparent flow separation or flooding problems at the feed point when using the feed rates required for the pilot plant.

2.3.3 Solvent Extraction Including Feed Adjustment (Task 225)

The major effort under this work unit has been the continued development of the computer program for simulating the Acid Thorex solvent extraction process. Principal advances have been the modification of the program to calculate a complete solvent extraction cycle (i.e., extraction, scrub, partition, and strip); obtaining laboratory data and determining equations for the effect of temperature on the extraction of thorium, including the effects on third-phase formation and the density; and, obtaining laboratory data and determining equations for the effect of fluoride on the extraction of thorium.

2.3.3.1 Computer Code for Simulating the Acid Thorex Solvent Extraction System — R. H. Rainey and S. B. Watson

A computer program "SEPHIS," was previously prepared to simulate the Purex solvent extraction system.[8-10] This program is now being modified to simulate the solvent extraction steps required to recover HTGR fuel. The original SEPHIS program was based on a fitting of the extraction coefficients. In this program the fitting is based on the calculation of the organic phase composition from the aqueous feed.

Empirical equations were obtained for the simultaneous extraction of thorium, uranium and nitric acid in the system $Th(NO_3)_4$-$UO_2(NO_3)_2$-

HNO_3-H_2O-30 vol % TBP in *n*-dodecane* at "room temperature" by statistical analysis of published data. This modification gave a system in which calculations could be made as the organic phase approached saturation (a desirable condition for operating fuel processing plants).[8–11] The profiles for thorium, uranium, and nitric acid concentrations obtained from a countercurrent batch extraction and the values calculated by SEPHIS are compared in Table 2.2.

The SEPHIS code has been modified so that streams could be removed at points other than the first and last stages, and provisions were made for the organic phase to exit the system and reenter at a point other than the next stage. In addition, the number of stages allowed in the computer program was increased from 25 to 100. These modifications allow SEPHIS to simulate a full solvent extraction cycle of either the extraction-costrip or the extraction-partitioning-strip type.

---

*TBP is tri(*n*-butyl) phosphate.

Table 2.2. Comparison of Experimental and Calculated Results of Acid Thorex Solvent Extraction System

Flowsheet Conditions

Feed: 278 g/liter Th, 17.6 g/liter U, 0.21 *M* acid-deficient, 1 volume at stage 1E

Scrub 1: H_2O, 0.8 volume at stage 6S

Scrub 2: 5 *M* HNO_3, 0.2 volume at stage 3S

Salting acid: 13 *M* HNO_3, 0.5 volume at stage 4E

Solvent: 30 vol % TBP in *n*-dodecane, 7 volumes at stage 5E

Stage	Thorium Concentration, g/liter				Uranium Concentration, g/liter				Acid Concentration, *M*			
	Aqueous		Organic		Aqueous		Organic		Aqueous		Organic	
	Exptl	Calcd	Exptl	Calcd	Exptl	Calcd	Exptl	Calcd	Exptl	Calcd	Exptl	Calcd
6S	85.9	86.0	40.2	39.5	0.31	0.32	2.64	2.51	0.42	0.46	0.07	0.08
5S		95.7		49.3		0.30		2.57		0.88		0.13
4S	103	90.9	50.4	50.5	0.28	0.28	2.69	2.55	1.26	1.31	0.19	0.18
3S		85.4		49.8		0.26		2.53		1.81		0.2
2S	90.6	96.9	52.6	51.6	0.28	0.27	2.74	2.55	1.60	1.60	0.23	0.19
1S		109		53.2		0.28		2.55		1.38		0.16
1E	126	117	55.8	55.1	0.30	0.29	2.54	2.55	1.03	1.10	0.13	0.13
2E		40.9		33.2		0.016		0.08		1.85		0.28
3E	1.46	8.2	11.6	11.6	0.0001	0.0016	0.002	0.004	2.36	4.65	0.50	0.49
4E		0.50		2.3		<0.0001		0.0005		4.40		0.72
5E	0.27	0.09	0.27	0.15	<0.0001	<0.0001	0.0005	<0.0001	1.85	2.71	0.47	0.60

2.3.3.2 Effect of Temperature on the Extraction of Thorium — R. H. Rainey, S. B. Watson, and A. J. Weinberger

New data are being obtained on the extraction behavior of thorium and nitric acid in 30% TBP—70% *n*-dodecane as a funtion of temperature over a range of conditions expected in actual plant operation. The extractions are being made with extensive cross-checking, and the preliminary data appear quite reproducible (Tables 2.3—2.5). The new thorium distribution coefficients are slightly lower than the averages currently calculated in the SEPHIS program (Fig. 2.3). Increasing the temperature from 30 to 40 or 60°C reduced the extraction of thorium slightly. The current SEPHIS-Thorex work consists of fitting equations to the data.

Conditions at which a third phase (second organic phase) formed are also being measured in these experiments. At 30°C the third phase was observed when the organic contained 0.20 to 0.23 *M* thorium and the acid was between 0.1 to 0.004 *M*. At 40°C the third phase was observed when the thorium concentration reached 0.21 to 0.26 *M* over this range of acidities (Fig. 2.4). Data at 60°C are not complete.

The densities of the solutions are also being measured (Tables 2.3—2.5).

2.3.3.3 Effect of Fluoride on the Extraction of Thorium — R. H. Rainey, S. B. Watson, and R. J. Shannon

The complexing of the thorium by fluoride decreases the thorium extraction under conditions present at the bottom of the Acid Thorex extraction column. Experimental data are now being obtained to evaluate the magnitude of the effect. The data show no appreciable effect when the fluoride-to-thorium mole ratio is less than about 0.5. As the ratio increases, thorium is increasingly retained in the aqueous until at high ratios ($> \sim 4$) the distribution coefficient of the thorium is depressed by about a factor of 4 to 10 (Fig. 2.5). In this figure the experimental effects of the fluoride are compared with SEPHIS calculations based on no fluoride in the system. A major problem with this program has been obtaining reproducible analytical data. The program is continuing.

Table 2.3. Extraction, Third-Phase Formation, and Density in the System $Th(NO_3)_4$-HNO_3-30 vol % TBP in *n*-Dodecane at 30°C

Concentration, *M*, in Aqueous Solution Before Equilibration		Concentration After Equilibration, *M*				Density After Equilibration, g/cm³		Distribution Coefficient Organic/Aqueous	
		Thorium		Free Acid					
Thorium	Free Acid	Aqueous	Organic	Aqueous	Organic	Aqueous	Organic	Thorium	HNO_3
0.0500	0.000	0.0496	0.0003	0.0000	0.0004	1.0162	0.8076	0.0061	
0.0500	0.100	0.0490	0.0014	0.0931	0.0081	1.0187	0.8081	0.0286	0.087
0.0500	0.500	0.0420	0.0080	0.429	0.066		0.8125	0.190	0.154
0.0500	1.000	0.0336	0.0167	0.841	0.167	1.0366	0.8185	0.497	0.198
0.0500	3.000	0.0160	0.0320	2.538	0.497	1.0840	0.8342	2.00	0.196
0.1000	0.050	0.0944	0.0052	0.0449	0.0054	1.0360	0.8094	0.0551	0.120
0.1000	1.500	0.0544	0.0449	1.268	0.236	1.0590	0.8316	0.825	0.186
0.2000	0.000	0.1734	0.0239	−0.0003	0.0016	1.0677	0.8164	0.138	
0.2000	0.100	0.1661	0.0308	0.0863	0.0142	1.0677	0.8192	0.185	0.165
0.2000	0.500	0.1478	0.0517	0.424	0.0771	1.0701	0.8289	0.350	0.182
0.2000	0.996	0.1275	0.0700	0.846	0.148	1.0754	0.8385	0.550	0.175
0.200	2.991	0.0872	0.1074	2.604	0.395	1.1145	0.8609	1.23	0.152
0.300	0.250	0.2224	0.0706	0.214	0.0378	1.0951	0.8360	0.317	0.177
2.500	0.000	0.3323	0.1228	−0.0060	0.0016	1.1472	0.8550	0.370	
0.500	0.100	0.3690	0.1327	0.0869	0.0149	1.1475	0.8580	0.360	0.171
0.500	0.500	0.3510	0.1503	0.431	0.068	1.1512	0.8661	0.428	0.158
0.500	1.000	0.3224	0.1610	0.864	0.127	1.1579	0.8743	0.499	0.147
0.500	3.000	0.2112	0.1940[a]	2.443	0.314	1.1623	0.882	0.918	0.128
0.750	0.750	0.475	0.208[a]	0.623	0.0891	1.2083	0.889	0.438	0.143
0.999	0.000	0.624	0.226[a]	−0.0131	0.0035	1.2461	0.891	0.362	
1.000	0.100	0.596	0.223[a]	0.0797	0.0118	1.2391	0.892	0.374	0.148
1.000	0.500	0.532	0.216[a]	0.380	0.539	1.2215	0.889	0.406	0.142
1.000	1.000	0.453	0.208[a]	0.743	0.1018	1.2030	0.890	0.459	0.137
1.250	0.050	0.613	0.224[a]	0.0272	0.0061	1.2421	0.884	0.365	0.224
1.250	1.500	0.409	0.201[a]	1.007	0.1343	1.190	0.888	0.490	0.133

[a]Boundary for third phase.

Table 2.4. Extraction, Third-Phase Formation, and Density in the System $Th(NO_3)_4$-HNO_3-30 vol % TBP in *n*-dodecane at 40°C

Concentration, *M*, in Aqueous Solution Before Equilibration		Concentration After Equilibration, *M*				Density After Equilibration, g/cm³		Distribution Coefficient Organic/Aqueous	
		Thorium		Free Acid					
Thorium	Free Acid	Aqueous	Organic	Aqueous	Organic	Aqueous	Organic	Thorium	HNO_3
0.0500	0.0000	0.0496	0.00066	0.0006	0.0006	1.0123	0.7996	0.0133	
0.0500	0.1000	0.0491	0.00133	0.0955	0.00682	1.0149	0.8002	0.0270	0.0714
0.0500	0.5000	0.0431	0.00710	0.438	0.0597	1.0235	0.8040	0.165	0.136
0.0500	1.0000	0.0347	0.0155	0.844	0.1452	1.0332	0.8098	0.447	0.172
0.0500	3.0001	0.0177	0.0322	2.483	0.489	1.0789	0.8257	1.82	0.197
0.1000	0.0500	0.0950	0.00440	0.0458	0.00439	1.0326	0.8012	0.0463	0.0959
0.1000	1.5000	0.0575	0.0431	1.256	0.229	1.0554	0.8226	0.750	0.182
0.2000	0.0000	0.181	0.0200	−0.00135	0.00159	1.0653	0.8069	0.110	
0.2000	0.1000	0.174	0.0263	0.0885	0.01264	1.0656	0.8097	0.151	0.143
0.2000	0.5000	0.155	0.0473	0.427	0.0708	1.0679	0.8192	0.305	0.166
0.2000	0.9956	0.134	0.0670	0.845	0.1434	1.0726	0.8289	0.500	0.170
0.2000	2.9905	0.0921	0.1065	2.580	0.414	1.1106	0.8512	1.16	0.160
0.3000	0.2500	0.238	0.0670	0.2146	0.0357	1.0934	0.8257	0.280	0.166
0.5000	0.0000	0.388	0.1240	−0.00574	0.00266	1.1461	0.8438	0.319	
0.5000	0.1000	0.384	0.1300	0.0792	0.01314	1.1461	0.8474	0.338	0.166
0.5000	0.5000	0.365	0.1470	0.422	0.0670	1.1487	0.8557	0.403	0.159
0.5000	1.0000	0.349	0.1655	0.854	0.1290	1.1551	0.8639	0.474	0.151
0.5000	3.0000	0.312	0.2031	2.648	0.318	1.1968	0.898	0.651	0.120
0.7502	0.7500	0.547	0.2119	0.642	0.0888	1.2268	0.8829	0.387	0.138
0.9992	0.0000	0.761	0.2552[a]	−0.0136	0.00439	1.2862	0.892	0.335	
1.0000	0.1000	0.738	0.2549[a]	0.0769	0.0126	1.2787	0.892	0.345	0.164
0.9996	0.5000	0.660	0.2412[a]	0.418	0.0575	1.2635	0.890	0.365	0.137
0.9998	1.0000	0.598	0.2373[a]	0.815	0.1075	1.2471	0.890	0.397	0.132
1.0000	3.0010	0.383	0.2153[a]	2.275	0.282	1.2104	0.886	0.562	0.124
1.2498	0.0500	0.751	0.2546[a]	0.0280	0.00697	1.2827	0.894	0.339	0.249
1.2501	1.5000	0.553	0.2318[a]	1.085	0.1395	1.2369	0.889	0.419	0.129

[a]Boundary for third phase.

Table 2.5. Extraction and Density in the System $Th(NO_3)_4$-HNO_3-30 vol % TBP in *n*-Dodecane at 60°C

Concentration, *M*, in Aqueous Solution Before Equilibration		Concentration After Equilibration, *M*				Density After Equilibration, g/cm³		Distribution Coefficient Organic/Aqueous	
		Thorium		Free Acid					
Thorium	Free Acid	Aqueous	Organic	Aqueous	Organic	Aqueous	Organic	Thorium	HNO_3
0.0500	0.0000	0.0499	0.000608	0.00093	0.000572	1.0030	0.7838	0.0122	
0.0500	0.1000	0.0494	0.00113	0.0981	0.00558	1.0055	0.7842	0.0229	0.0569
0.0500	0.5000	0.0443	0.00603	0.451	0.0523	1.0145	0.7873	0.136	0.116
0.0500	1.0000	0.0368	0.0137	0.866	0.138	1.0241	0.7928	0.372	0.159
0.0500	3.0001	0.0202	0.0293	2.516	0.525	1.0676	0.8087	1.45	0.209
0.1000	0.0500	0.0970	0.00334	0.0475	0.00357	1.0233	0.7852	0.0344	0.075
0.1000	1.5000	0.0615	0.0392	1.265	0.230	1.0463	0.8047	0.637	0.182
0.2000	0.0000	0.1875	0.0150	−0.00176	0.00238	1.0570	0.7892	0.080	
0.2000	0.1000	0.1832	0.0212	0.0912	0.01127	1.0573	0.7918	0.116	0.124
0.2000	0.5000	0.163	0.0410	0.431	0.0654	1.0600	0.8005	0.252	0.152
0.2000	0.9956	0.142	0.0605	0.852	0.1390	1.0645	0.8102	0.426	0.163
0.2000	2.9905	0.103	0.0980	2.564	0.427	1.1009	0.8319	0.951	0.166
0.3000	0.2500	0.248	0.0580	0.217	0.0332	1.0863	0.8060	0.234	0.153
0.5000	0.0000	0.405	0.1055	−0.0066	0.00483	1.1399	0.8224	0.260	
0.5000	0.1000	0.395	0.1145	0.0843	0.01561	1.1396	0.8261	0.290	0.185
0.5000	0.5000	0.377	0.1340	0.434	0.0710	1.1413	0.8350	0.355	0.164
0.5000	1.0000	0.358	0.1530	0.868	0.1370	1.1468	0.8438	0.427	0.158
0.5000	3.000	0.325	0.1798	2.656	0.366	1.1874	0.8606	0.553	0.138
0.7502	0.7500	0.551	0.2056	0.654	0.0966	1.2170	0.8626	0.373	0.148
0.9992	0.0000	0.775	0.2409	−0.0127	0.0068	1.2825	0.8726	0.311	
1.0000	0.1000	0.764	0.2456	0.0750	0.0152	1.2838	0.8757	0.321	0.203
0.9996	0.5000	0.755	0.2529	0.429	0.0651	1.2907	0.8809	0.335	0.152

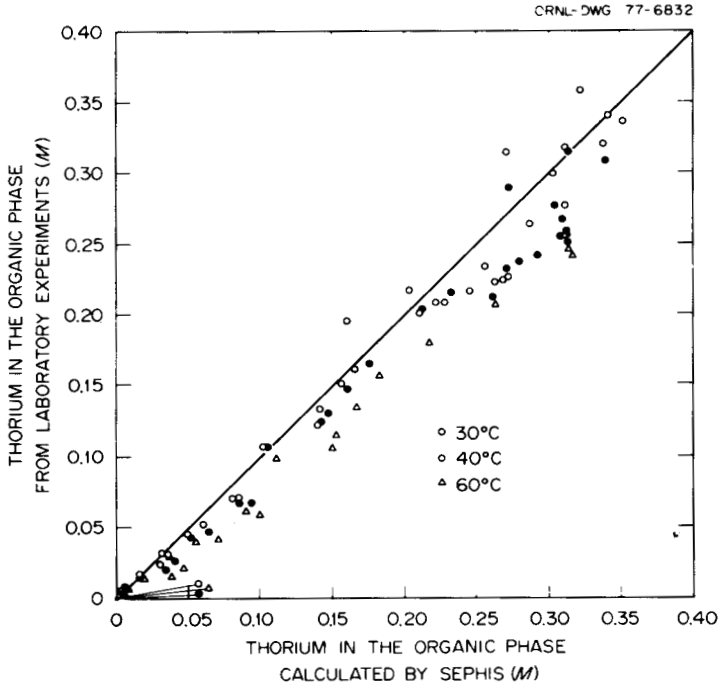

Fig. 2.3. The Effect of Temperature on the Extraction of Thorium in the System $Th(NO_3)_4$-HNO_3-H_2O-30 vol % TBP in *n*-dodecane.

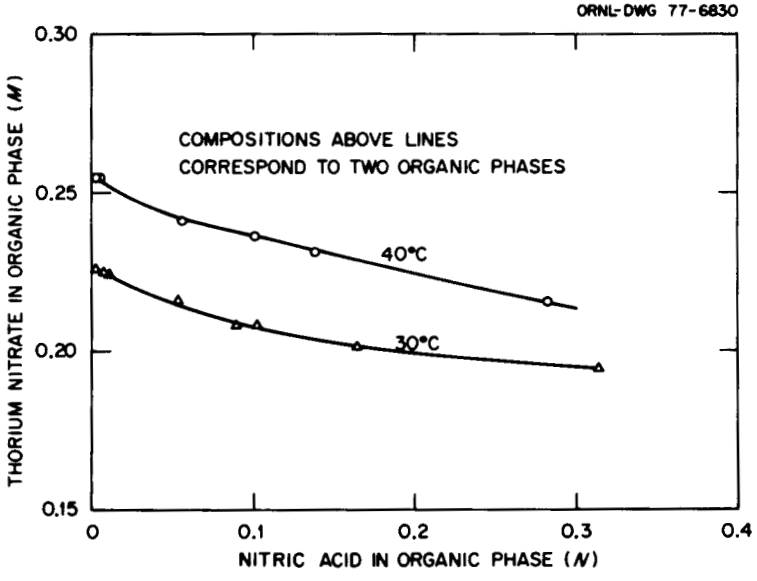

Fig. 2.4. Extraction Conditions Resulting in a Second Organic Phase (Third Phase) in the System $Th(NO_3)_4$-HNO_3-H_2O-30 vol % TBP in *n*-dodecane at 30 and 40°C.

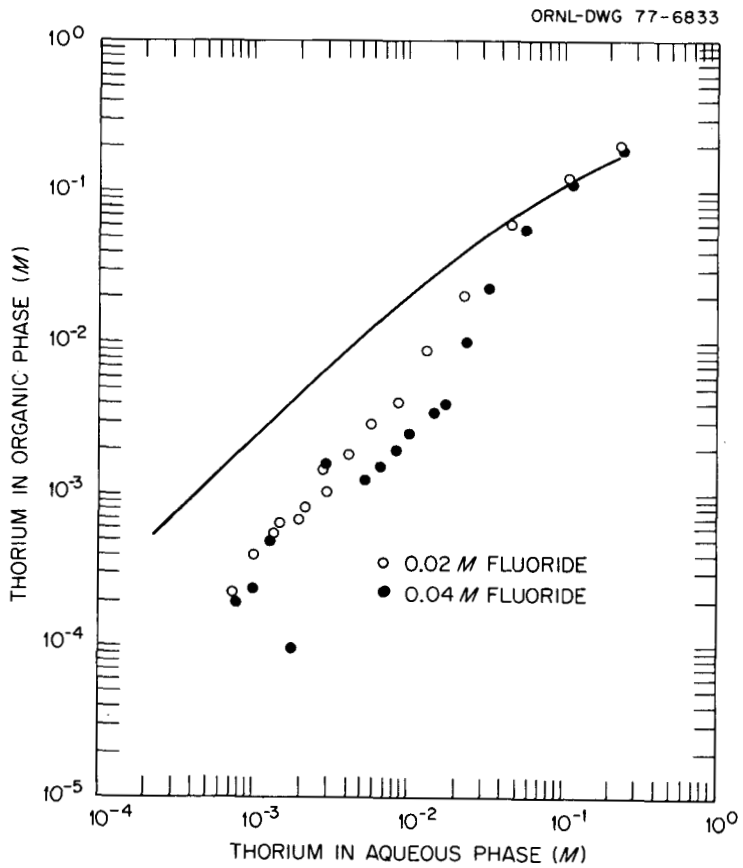

Fig. 2.5. The Effect of Fluoride on the Extraction of Thorium in the Acid Thorex Flowsheet. [(Extraction conditions: 2.5 *N* HNO_3, NaF complexed with 2 mole ratios of $Al(NO_3)_3$.]

2.3.4 Krypton Separation (Subtask 235)

2.3.4.1 Sorption of Tritiated Water from Flowing Liquid CO_2 — R. D. Ackley and J. H. Shaffer

The burner off-gas generated in the head-end reprocessing of HTGR fuel will contain CO_2 as the major component and ^{3}H (as H_2O), ^{85}Kr, $^{129,131}I$ (as I_2), and ^{220}Rn as low-concentration radioactive contaminants. As presently planned, the ^{3}H, $^{129,131}I$, and ^{220}Rn will be removed from the off-gas (while it is in the gaseous state) by using solid sorbents. Then, following compression and partial liquefaction of the CO_2, the ^{85}Kr will be removed by the KALC process. No provision for liquid-phase removal of H_2O or I_2 by solid sorbents is included in the current flowsheet for off-gas treatment. However, should it prove feasible to trap H_2O and/or I_2 from flowing liquid CO_2, provision for

such trapping of one or both of these substances could readily be incorporated in a modified design of the KALC system. This addition would then serve two purposes: (1) to protect the KALC equipment against plugging by ice and/or corrosion by I_2 and (2) to provide supplemental capability for off-gas decontamination. Accordingly, an experimental investigation to examine the feasibility of trapping tritiated water and elemental iodine from flowing liquid CO_2 has been initiated.[12] The first phase of this work, which consisted of the survey testing of possible sorbents for removing tritiated water from flowing liquid CO_2, has been completed.

In this first phase, 13 survey tests were performed. The more important test conditions were as follows: approximately 0°C and 3.9 MPa (570 psia) for the test bed section; a liquid CO_2 flow rate of 0.6 kg/sec per square meter of bed cross section; and a 4-hr injection period during which tritiated water was introduced upstream of the test bed section to provide calculated loadings in the range of 5 to 11 kg tritiated water per cubic meter of sorbent in a 51-mm (2-in.) depth. Sorbents investigated were an activated alumina, a silica gel, and several types of molecular sieves. All sorbents were at least moderately effective under the test conditions. For a 51-mm (2-in.) depth of sorbent and a loading in the above range, the lowest decontamination factor obtained was at least 7 and the highest was at least 3000. Molecular sieve types 4A, 4A-50, 5A-50, and 13X [all in the form of 1.6-mm (1/16-in.) pellets] were the more promising of the sorbents tested.

2.3.4.2 The Systems Kr-CO_2 and Xe-CO_2 — R. D. Ackley, A. B. Meservey, and K. J. Notz

The KALC (Krypton Absorption in Liquid CO_2) process has been developed on an engineering scale for removing ^{85}Kr from the burner off-gas generated in the head-end reprocessing of HTGR fuel. To provide basic data for KALC design calculations, the distribution of krypton and xenon between gaseous and liquid CO_2 has been investigated in the laboratory as reported previously,[13–15] and final reports covering this work have now been issued.[16,17]

The results were expressed in terms of a distribution ratio, Y_{Kr}/X_{Kr} or Y_{Xe}/X_{Xe}, which is defined as the ratio of the mole fraction of krypton or xenon in the gaseous phase to that in the liquid phase. For the Kr-CO_2 system, the distribution ratio decreased from 29.4 at −52.8°C to 1.44 at 29.1°C; for the Xe-CO_2 system, the distribution ratio decreased from 7.53 at −54.8°C to 1.10 at 30.5°C.

2.3.4.3 The CO_2-I_2-CH_3I-H_2O System — L. M. Toth, S. R. Buxton, J. T. Bell, H. A. Friedman, D. W. Fuller, and M. R. Billings

Since fission product iodine and tritiated water are likely impurities in the KALC process, the chemistry of the CO_2-I_2-CH_3I-H_2O system in stainless steel was investigated with respect to the probable reactions of these impurities in the process equipment.[18] Most of the work was performed with a high-pressure spectrophotometer cell fabricated from type 304 stainless steel. Absorption spectra were measured from 200 to 2500 mm on a Cary 14 recording spectrophotometer.

Distribution coefficients for I_2 and CH_3I between gaseous and liquid CO_2 were measured from −26 to +30°C and illustrated in Fig. 2.6. The solutes favor the liquid phase as the temperature is lowered.

Iodine was stable in dry liquid CO_2 contained in stainless steel. However, the addition of 3 ppm H_2O (or more) produced a corrosion reaction, which caused the loss of I_2 and H_2O from solution as an insoluble product and considerable etching of the metal surfaces. No corrosion reaction was observed for CH_3I from −30 to 30°C, even in the presence of 500 ppm added water. Methyl iodide invariably produced stable solutions in CO_2, whether or not water was present.

2.3.4.4 Radon-220 Control in Off-Gas Streams — W. L. Carter

Reprocessing operations produce off-gas streams that contain volatile radioactive components such as iodine, krypton, xenon, tritium, and radon; refabrication produces radon-contaminated off-gases. The hazards associated with iodine, krypton, and xenon have been recognized for a number of years, and considerable research has been directed toward their removal from carrier gases and their subsequent containment.

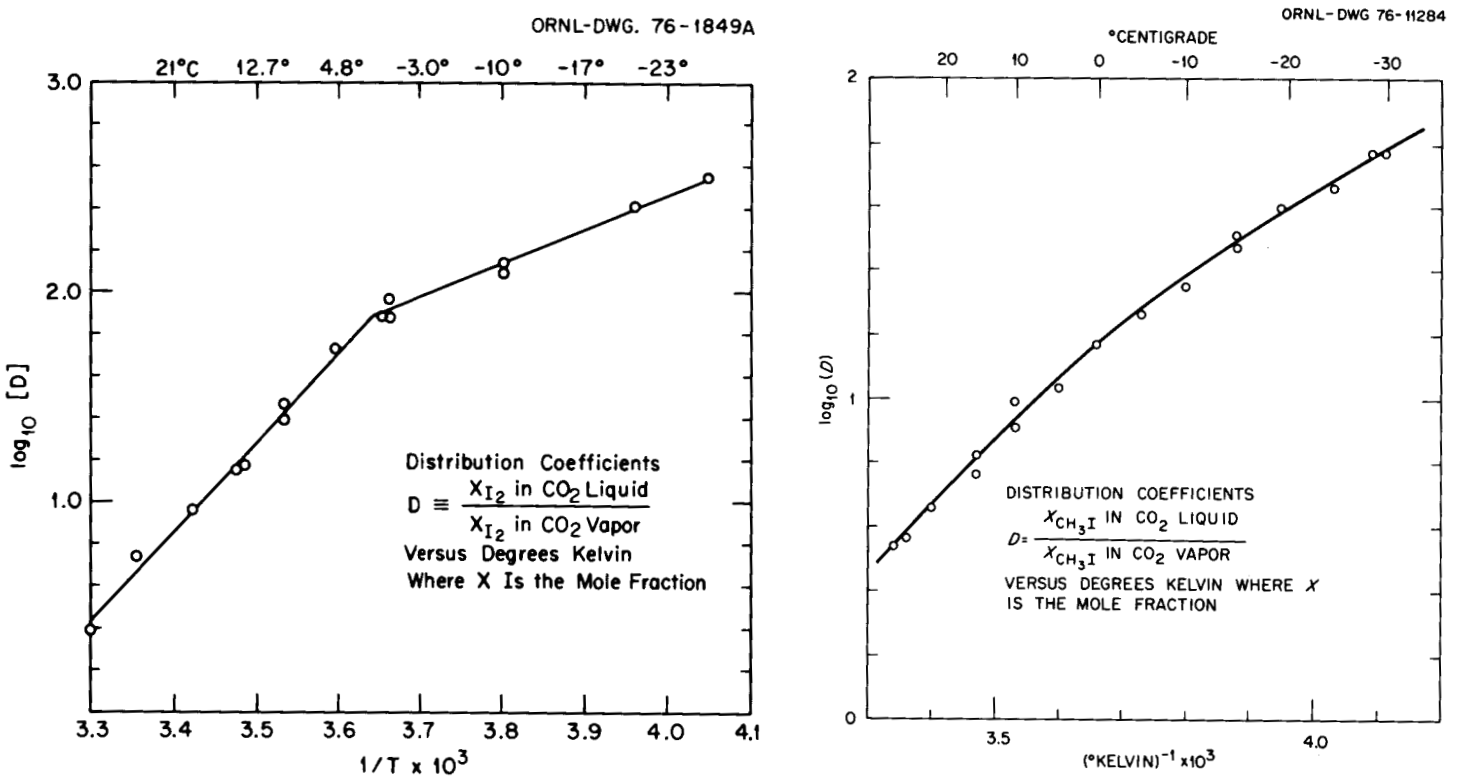

Fig. 2.6. Temperature Dependence of the Distribution Coefficients of I_2 and CH_3I Between Liquid and Gaseous Carbon Dioxide.

The radon isotope of importance is ^{220}Rn, which is a decay product of ^{232}U, which in turn, has been formed by nuclear reactions involving ^{233}U, ^{232}Th, and ^{230}Th when HTGR fuel is irradiated. The decay scheme for ^{232}U is shown in Fig. 2.7, and some of the more significant gamma emissions are given in Table 2.6. The hazards associated with radon are not from the ^{220}Rn *per se* but from its longer lived decay products that have energetic gamma emissions, particularly ^{208}Tl. Inside the reprocessing system, carrier gases transport radon and daughter products to areas that would not normally be radioactive, making equipment maintenance and replacement more difficult. If the carrier gas is released via the plant stack, the radioactive particles can settle and contaminate the environs.

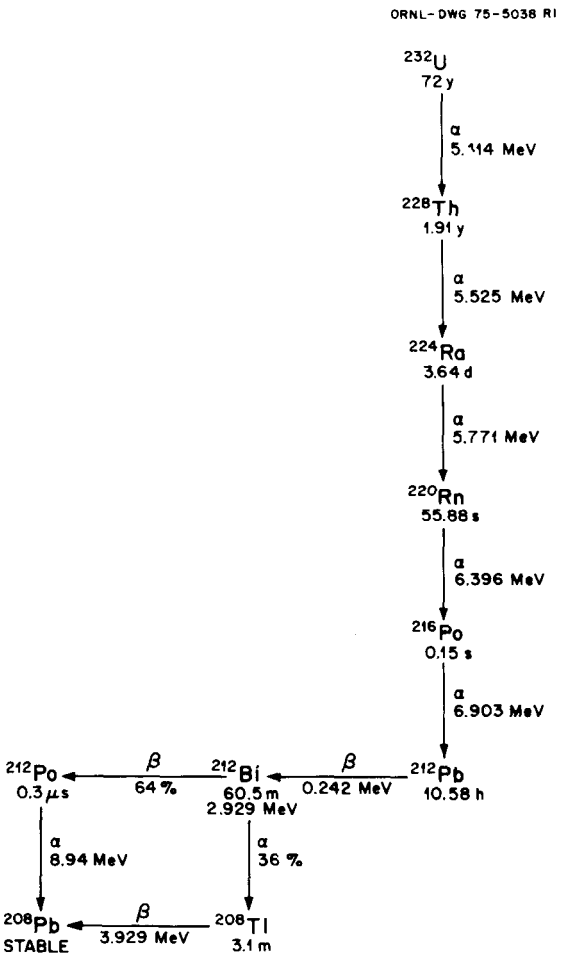

Fig. 2.7. Decay Chain of ^{232}U.

Table 2.6. Significant Gamma Emissions in the ^{232}U Decay Chain

Nuclide	Half-Life	Fraction of Decays	Gamma Energy (MeV)
^{212}Pb	10.58 hr	0.81	0.238
		0.05	0.3
^{212}Bi	60.5 min	0.022	1.62
		0.014	1.51
		0.05	0.727
		0.7	0.04
^{208}Tl	3.1 min	0.97	2.61

The amount of ^{232}U in recycled fuel depends rather strongly on the ^{230}Th content of the thorium ore. Some ores, particularly those that are by-products of phosphate manufacture, may contain less than 10 ppm ^{230}Th, whereas ores that are found in uranium-bearing regions may contain up to 100 ppm ^{230}Th. The steady-state ^{232}U content of recycled HTGR fuel has been calculated to be 309 ppm for a thorium feed that contained no ^{230}Th, 370 ppm for feed that was 10 ppm ^{230}Th, 625 ppm for feed that was 50 ppm ^{230}Th, and 944 ppm for feed that was 100 ppm ^{230}Th. Hence, the radon production might be as much as three times larger in recycled fuel from a high-^{230}Th ore as from a low-^{230}Th ore.

The carbon coating on HTGR ThC_2-UC_2 fuel kernels retains solid and gaseous fission products and higher molecular-weight nuclides formed during irradiation. However, when the spent fuel is reprocessed, this protective coating is destroyed and the confined gases are released. Confined gases are released in seven distinct process operations: fuel element crushing, burning, kernel classification and crushing, fuel kernel dissolution and solvent extraction, carbonization of resin beads, conversion, and inspection and analytical operations. The composition of the off-gases from several of these process operations is estimated in Tables 2.7 and 2.8. The first four steps are concerned with reprocessing and release of the major portion of the gases; this is particularly true of the burning step. After the initial four operations

Table 2.7. Off-Gases from HTGR Fuel Reprocessing and Refabrication

Process Operation	Off-Gas Components		Flow	
	Bulk	Trace	(std liters/sec	(scfm)
Crushing	CO_2 or air	^3H,Kr,Xe,^{220}Rn	24	50
Primary burning	CO, CO_2, air	^3H,Kr,Xe,^{220}Rn,semivolatiles	24	50
Secondary burning	CO, CO_2, air	^3H,Kr,Xe,^{220}Rn,semivolatiles	5.7	12
Classification and kernel crushing		^3H,Kr,Xe,^{220}Rn	14	30
Dissolution	air, NO_x	I,Kr,Xe,^{220}Rn	2.4	5
Carbonization	Ar, hydrocarbons	^{220}Rn	24	50
Conversion	Ar, hydrocarbons	^{220}Rn	24	50
Inspection and analysis	air	^{220}Rn	140[a]	300[a]

[a]Maximum rate. Normally the flow rate is much less.

Table 2.8. Composition of Off Gas from HTGR Fuel Reprocessing and Refabrication[a]

Bulk Component	Content (%)	Trace Component	Content	
			(g/day)	(Ci/day)
CO_2	90	^3H	0.05	504
CO	1	I	59.8	0.198
$N_2 + O_2$	9–10	Kr	780	20,442
		Xe	4226	0.221
		^{220}Rn	5×10^{-7}	38.8

[a]Stored from the various process steps and intermittently processed through the off-gas system at 180 std liters/sec (380 scfm).

there is little concern for iodine, krypton, and xenon because the precursors of these nuclides are short-lived compared with the 180-day cooling time or have been removed by solvent extraction. However, the last three steps, which are refabrication operations, must contend with radon that is continuously formed from ^{232}U (half-life = 72 yr) and ^{228}Th (half-life = 1.91 yr) that are present in all recycle operations with thorium-uranium fuels.

2.3.4.5 Final Krypton Concentration — C. W. Forsberg

Molecular sieves were investigated[19] to separate krypton from carbon dioxide and oxygen. This separation is required to concentrate radioactive krypton from the KALC (Krypton Adsorption in Liquid Carbon dioxide) process before bottling it for final radioactive waste disposal. The KALC process removes radioactive and nonradioactive krypton from the off-gas stream of an HTGR fuel reprocessing plant and concentrates the krypton by a factor of 1000 to produce a krypton-rich gas stream of 1.5% Kr, 95+% CO_2, and varying amounts of O_2 and Xe. A second process is then required to remove CO_2 and preferably other gases from this krypton product stream. Because of the simplicity, reliability, and low costs projected for selective adsorbants, particularly molecular sieves, for this separation, molecular sieves were chosen as the separation medium for this task.

The proposed separation of Kr, O_2, and CO_2 is accomplished by feeding the feed gas into a long clean molecular sieve bed at 0°C. All three gases are adsorbed; however, krypton is more strongly adsorbed than O_2 and hence will replace O_2 on the bed. Similarly, CO_2 is more strongly adsorbed than O_2, and Kr and will displace both gases on the bed. As the feed gas is fed into one end of the bed, the bed acts as a frontal analysis chromatograph, and pure oxygen initially exits from the bed, followed by a concentrated krypton gas stream containing some oxygen followed by the feed gas breaking through the bed. Separation is accomplished by simply valving the concentrated krypton to the bottling station when it exits from the bed. The molecular sieve bed is regenerated by heating to a high temperature and desorbing the CO_2.

Oxygen that leaves the bed during adsorption and CO_2 that leaves the bed during desorption (regeneration) are both recycled to the front end of the KALC process so that any residual krypton may be recovered. In effect, krypton is the product and all other gases are recycled to earlier processes in the fuel reprocessing plant off-gas stream. With the use of two columns the process can be continuous.

A series of experiments to investigate molecular sieves for separating Kr from CO_2 and O_2 was conducted. The experimental variables investigated included gas flow rate, gas composition, temperature, pressure, and type of molecular sieve. Most experiments used a feed gas of 93.09% CO_2, 1.48% Kr, and 5.43% O_2. The following results of experimental work were obtained.

1. Optimum bed temperature for adsorption is near 0°C. Little is gained by going to lower temperatures, for the adsorption saturates out.

2. Pressure is not a highly important variable. Operation near 0.1 MPa (1 atm) will probably be the most economical.

3. Linde 5A, 4A, and 3A molecular sieves were investigated. The 5A molecular sieve offers the best performance.

4. Krypton product concentrations always exceeded 50%. The impurity in the krypton was oxygen, which can be easily removed.

5. The CO_2 content of the krypton product gas is less than 10 ppm.

6. Rates of gas flow in the molecular sieve bed are limited by heat transfer, not mass transfer. Adsorption of Kr and CO_2 releases large amounts of heat, which must be removed. Failure to cool the bed increases the bed temperature and stops the adsorption. Mass transfer is sufficiently fast that it is not a limiting characteristic with any reasonable design.

For the expected conditions in an HTGR fuel reprocessing plant, molecular sieves will provide the required separation of krypton from carbon dioxide and oxygen in a reliable, low-cost system that is easy to design and scale.

2.3.5 Semivolatile Fission Product Collection (Subtask 240)

2.3.5.1 Vapor Transport of Fission Products — E. E. McCombs and J. H. Shaffer

In the head-end reprocessing of spent HTGR fuel elements, the fuel blocks, graphite matrix, and particle coating materials will be burned with oxygen, and the residual ash processed for the recovery of uranium and thorium and the isolation of fission products. The gaseous effluent from the graphite burner will likely contain prohibitive quantities of radionuclides and must, therefore, be processed to achieve suitable decontamination before discharge into the atmosphere. Expected contamination consists of known gaseous fission products — xenon, krypton, tritium, and iodine — and certain other semivolatile and particulate fission products and actinides, which may be present as vapor or entrained as aerosols in the burner effluent stream. Investigative programs are currently in progress to develop effective separations processes for these materials; condensation of volatiles is an important part of this developemnt. This experimental program will examine the vapor transport of a number of elements and compounds selected from Table 2.9 under conditions applicable to burner technology.

The graphite will be burned under controlled conditions to regulate maximum temperatures below 950°C. This control can be achieved by a balance of graphite and oxygen feed rates into the fluidized bed of the burner. However, the manner by which this control is achieved may affect fission product transport in the system. Conceivably, excess oxygen in the feed stream could promote oxidation of certain fission products and actinides and enhance their volatility. Similarly, a deficiency in oxygen would impose more reducing conditions by the formation of carbon monoxide. This condition may promote the formation of volatile suboxide or metallic species and possibly the production of volatile carbonyl compounds. This experimental program will survey the behavior of fission products and actinides under simulated burner conditions to evaluate these transport processes. Fundamental studies will also be conducted to determine the vapor pressures of the oxides of these elements, or the elements themselves, in controlled atmospheres

Table 2.9. Fission Products and Actinides

Element	Isotope[a]	"Hazard index"[b] (ft^3/metric ton)
Ac	225	6.2×10^{14}
Ag	110m	1.4×10^{13}
Am	243	4.2×10^{15}
Ba	137m	3.6×10^{14}
Bi	211	1.6×10^{14}
Ce	144	1.8×10^{17}
Cm	244	4.7×10^{17}
Cs	134	6.6×10^{16}
Eu	154	4.5×10^{15}
Fr	221	1.6×10^{14}
Nb	95	8.4×10^{15}
Np	237	2.3×10^{14}
Pa	233	4.1×10^{15}
Pm	147	2.1×10^{15}
Pr	144	1.2×10^{15}
Pu	238	6.4×10^{18}
Ra	224	2.3×10^{14}
Ru	106	1.5×10^{16}
Sb	125	7.5×10^{14}
Sm	151	1.0×10^{13}
Sn	123m	2.3×10^{14}
Sr	90	3.6×10^{17}
Tc	99	6.0×10^{11}
Te	127m	5.4×10^{14}
Th	228	2.3×10^{16}
U	232	8.7×10^{15}
Y	91	1.1×10^{16}
Zr	95	1.4×10^{16}

[a]Isotope of greatest potential hazard.

[b]Dilution required per metric ton of heavy metal from six-year-irradiated FSVR fuel cooled 150 days. To convert to cubic meters, multiply by 0.0283. From J. W. Snider and R. E. Leuze, pp. 501–26 in *Proc. 12th AEC Air Cleaning Conf., Oak Ridge, Tennessee, Aug. 28–31, 1972,* CONF-720823 vol II.

of argon (neutral), CO_2-O_2 (oxidizing), and CO_2-CO (reducing). Such investigations will yield data that are independent of chemical reactions involving graphite.

Under actual burner conditions the temperature in localized zones might exceed the average bed temperature by several hundred degrees. Consequently, vapor pressure will be measured at temperatures up to 1300°C.

Where feasible, these experiments will be performed with stable isotopes of the elements listed in Table 2.9; however, the apparatus and procedure have been designed for eventual adaptation to glove-box operation for the study of actinides. Although a versatile program has been designed for these volatility experiments, some modifications may be required by the singular nature of a number of the elements, and we anticipate that investigation of some of them may not be practical.

Silver was selected from Table 2.9 as the element with which to perform the initial shakedown runs, because its vapor pressure is sufficiently high [approximately 0.13 Pa (10^{-3} torr) at 920°C] to yield definitely measurable amounts of condensed silver. Furthermore, the vapor pressure values calculated from these runs may be compared with the considerable data in the literature. All runs reported herein were conducted at approximately 918°C and used argon as the carrier gas.

Since vapor pressures and vapor transport rates are to be examined in various dynamic atmospheres, a transpiration method was selected as the most versatile way of conducting these investigations. This technique is well described in the literature,[20-23] is applicable over a wide range of vapor pressures, and permits the determination of very low vapor pressures in the presence of high concentrations of other gases. Pardue and Keller[24] employed this technique for the determination of vapor pressures of PuO_2 in oxygen atmospheres, and some details of their procedure and apparatus have been adopted.

In this initial series of experiments natural silver metal was heated at 918°C. A flow of argon was directed over this material and out through a tube in which the vaporized silver condensed. Downstream, the volume of argon gas was measured. The natural silver condensate

was dissolved from the tube and spiked with a known amount of silver isotopically enriched in ^{109}Ag. From the resultant change in mass assay, the amount of natural silver vaporized was determined. Knowing this and the volume of argon carrier gas, the vapor pressure of silver at 918°C was calculated. The apparatus and general procedure have been described previously.[25]

This initial series of tests consisted of 38 runs, all made at 918 ± 1°C using argon carrier gas at various flow rates. A number of procedural and equipment changes were made during the course of these runs, and only the results from the 17 runs that were conducted under the final conditions are presented in Table 2.10. As indicated by these data, the apparent vapor pressure determinations over a wide range of gas flow rates compare very favorably with values cited[26–28] in the literature.

Table 2.10. Vapor Pressure of Silver at 918°C and Various Flow Rates

Run	Flow Rate (cm^3/min)[a]	Apparent Vapor Pressure of Ag[b] (Pa)	(torr)
18	10.5	0.1184	8.88×10^{-4}
20	16.8	0.1216	9.12
21	24.6	0.1227	9.20
23	34.2	0.1276	9.57
24	13.8	0.1244	9.33
25	49.9	0.1263	9.47
26	57.8	0.1312	9.84
29	105.5	0.1308	9.81
30	78.9	0.1291	9.74
31	151.0	0.1316	9.87
32	244.3	0.1292	9.69
33	30.2	0.1388	10.41
34	29.9	0.1366	10.24
35	31.3	0.1296	9.72
36	30.7	0.1289	9.67
37	360.8	0.1097	8.23
38	540.4	0.0944	7.08

[a]Volume at 0°C, 0.102 MPa (1 atm).

[b]Vapor pressure values at 918°C from three independent sources in the literature are 0.121, 0.129, and 0.131 Pa (9.1×10^{-4}, 9.7×10^{-4}, and 9.8×10^{-4} torr).

The investigation of the volatility of U_3O_8 in atmospheres of CO_2-CO, CO_2-O_2, and argon is contemplated as the next phase of this activity.

2.4 HOT LABORATORY DEVELOPMENT

2.4.1 Fuel Element Size Reduction (Subtask 205)

2.4.1.1 Properties of Irradiated Graphite — C. L. Fitzgerald

The reprocessing of HTGR fuel elements necessitates the storage and transport of crushed graphite and fuel elements in the head-end flowsheet.[1] Knowledge of the flow properties of these granular materials needs to be determined to assure that they can be moved when and where needed. The Jenike Method[29] was selected by General Atomic Company (GA) to measure the flow properties of these materials, and preliminary results have been obtained.[30] These studies were done with unirradiated materials, so the question remains as to whether irradiated materials will behave similarly. A joint program with GA is in progress at ORNL to repeat selected tests with irradiated graphite. These tests will be done with Recycle Test Element fuel bodies[31] that have been irradiated for 701 effective full power days (EFPD). The steps involved in completing these tests are: (1) reduce the fuel bodies to a size suitable for testing (<1 mm), (2) perform the tests with a unit that has been calibrated with unirradiated material, and (3) reduce the data to a usable form. The first two operations will be done at ORNL and the data will be transmitted to GA to complete the third step.

The RTE fuel bodies about 380 mm long by 95 mm in diameter (15 by 3.75 in.), will be crushed in the commercially available jaw crusher shown in Fig. 2.8. The unit is a laboratory model, 0.10 by 0.15 m (4 by 6 in.), purchased from Morse Brothers Machining Company, Denver, Colorado. It was tested with unirradiated rough-cut RTE fuel bodies made of H-327 graphite. The bodies (Fig. 2.8) were passed through the crusher once with the jaws in the fully open position and twice with the jaws in

Fig. 2.8. Jaw Crusher.

the fully closed position. The material was scalped of all particles larger than 1 mm for the tests described below. The results are shown in Fig. 2.9 with the results obtained in the crushing system used at GA. The various fractions obtained with our jaw crusher were recombined in the proportions necessary to approximate the particle size distribution given[32] by GA. The unit has been operated enough to give reasonable assurance that it is ready for installation in the hot cell for the tests with irradiated material.

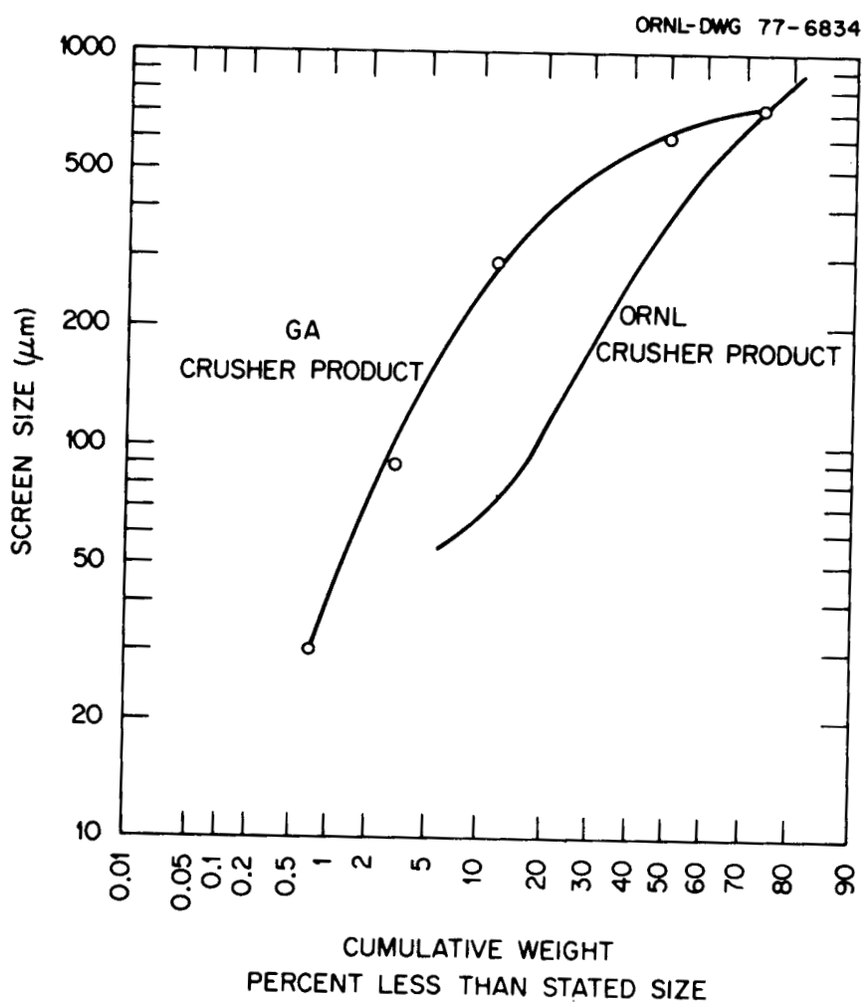

Fig. 2.9. Particle Size Distribution of ORNL and GA Crusher Product.

The Jenike test basically consists of measuring the forces necessary to slide a material over itself (or another surface) while under different vertical loads. The commercially available equipment to perform these tests has never been operated remotely. A remotely operated Jenike-type apparatus was built and used in Germany,[33] but it does not conform to the standard system, and the results can not be guaranteed to compare with data taken on the standard system. We felt the difficulties of performing the various operations remotely warranted the design and fabrication of a unit at ORNL. The shear cell and electronics (containing the load cell and signal conditioner) were purchased; all other associated hardware has been designed at ORNL. The basic measuring unit, as used for calibration, is shown in Fig. 2.10. Material used for these initial tests was the product from the crusher tests described above (<1 mm).

Fig. 2.10. Shear Cell and Electronics for Jenike Test.

Each test consists of the following steps: (1) preconsolidation: load the shear cell [0.1 m (4 in.) diam] with the crushed material and compact under a given load with the top ring off-center forward about 1.6 mm (1/16-in.); (2) first shear force measurement: push the material across itself under a given vertical load until a constant force is obtained (the retaining ring is essentially centered); (3) second shear force measurement: reduce the vertical load a given amount and push the material across itself until the force goes through a maximum. If the material does not perform reproducibly, the preconsolidation procedure is adjusted until it does. The procedure is repeated with different reduced weights to give a total of three points. Then the shearing force is plotted against vertical load to establish the "flow function" for that preconsolidation force and time. This should be constant for a given material under the same conditions. The measurements are repeated to attain statistical confidence and extended to other conditions as needed.

Three series of tests have been done in our equipment with unirradiated material. The first series was done with a powder sent to ORNL by GA. The test results and powder were returned to GA. The material was also tested in GA's unit. The results were significantly different. An ORNL representative went to GA to observe their methodology. A number of precedural changes were suggested. The changes were made and a second series of tests was done with a powder system prepared from our crusher product. The same powder was sent to GA and the tests were repeated in their unit. The results were still significantly different (Test 2, Table 2.11) and a GA representative visited ORNL to observe our methodology. Additional changes were suggested and these have been made. The tests were repeated with a similar powder system and the results show improved agreement but still some disparity (Test 3, Table 2.11). The disagreement will be resolved before the hot-cell tests begin.

The above tests were made with the isolated hot-cell shear cell and remotized electronics. The hardware ancillary to the shear cell (which permits remote powder loading and handling) is in the late stages of design.

Table 2.11. Comparison of ORNL and GA Jenike Test Results

Force Measured	Ratio, ORNL to GA Results	
	Test 2	Test 3
F, Unconfined yield force	0.09	0.33
V_1, Major Consolidating force	0.34	0.83

2.4.2 Crushed Fuel Element Burning (Subtask 210)

2.4.2.1 Component Tests — C. C. Fitzgerald and V.C.A. Vaughen

Head-end reprocessing studies with irradiated fuels historically have been limited at ORNL by the quantities of fuel available for use. Sufficient quantites now are becoming available to allow us to scale up our studies from one to four fuel rods [13 mm diam by 50 mm each (1/2 by 2 in.)] to about 50 fuel rods per experiment. The reasons for increasing the size of our experiments are to increase the confidence in our data by providing a larger source term, larger amounts of residues and precipitates, and larger volumes of dissolver solutions for solvent extraction studies (Subtask 225). The system being assembled to do these studies consists of (1) fuel rod crusher, (2) fluidized bed burner, (3) cyclone, (4) micrometallic filters, (5) fission product condenser, (6) absolute filters, and (7) associated instrumentation. The status of the system is described below.

The design goals were to be able to (1) crush 50 fuel rods to less than 4.8 mm (3/16 in.), load the burner, and leak test the system in one day, and (2) complete the burning operation within an 8-hr work day. A fuel rod crusher concept was suggested by D. C. Watkin, and a prototype unit was built and tested in the laboratory. The crushing results were satisfactory [i.e., the product size was $\leq$4.8 mm (3/16 in.)], and the speed of operation was such that 50 fuel rods could be crushed within about 1 hr. A unit suitable for remote operation was designed and is being fabricated. The unit is simple, is easy to operate, and should perform its function adequately.

Operating conditions and material of construction for the primary burner were selected accoring to the conditions currently in use[34] at GA. These are a burning temperature of 875°C at a fluidizing velocity of 0.76 m/sec (2.5 fps) in a Hastelloy X burner tube. A 76-mm-ID by 0.51-m (3 by 20-in.) burner tube with the lower 76 mm (3 in.) in a 30°-included-angle cone was constructed of Pyrex so the fluidizing characteristics could be observed. The unit performed well at 0.76 m/sec (2.5 fps) [calculated at 76 mm (3 in.)] fluidizing velocity, and a hot-cell unit was constructed of Hastelloy X (Fig. 2.11).

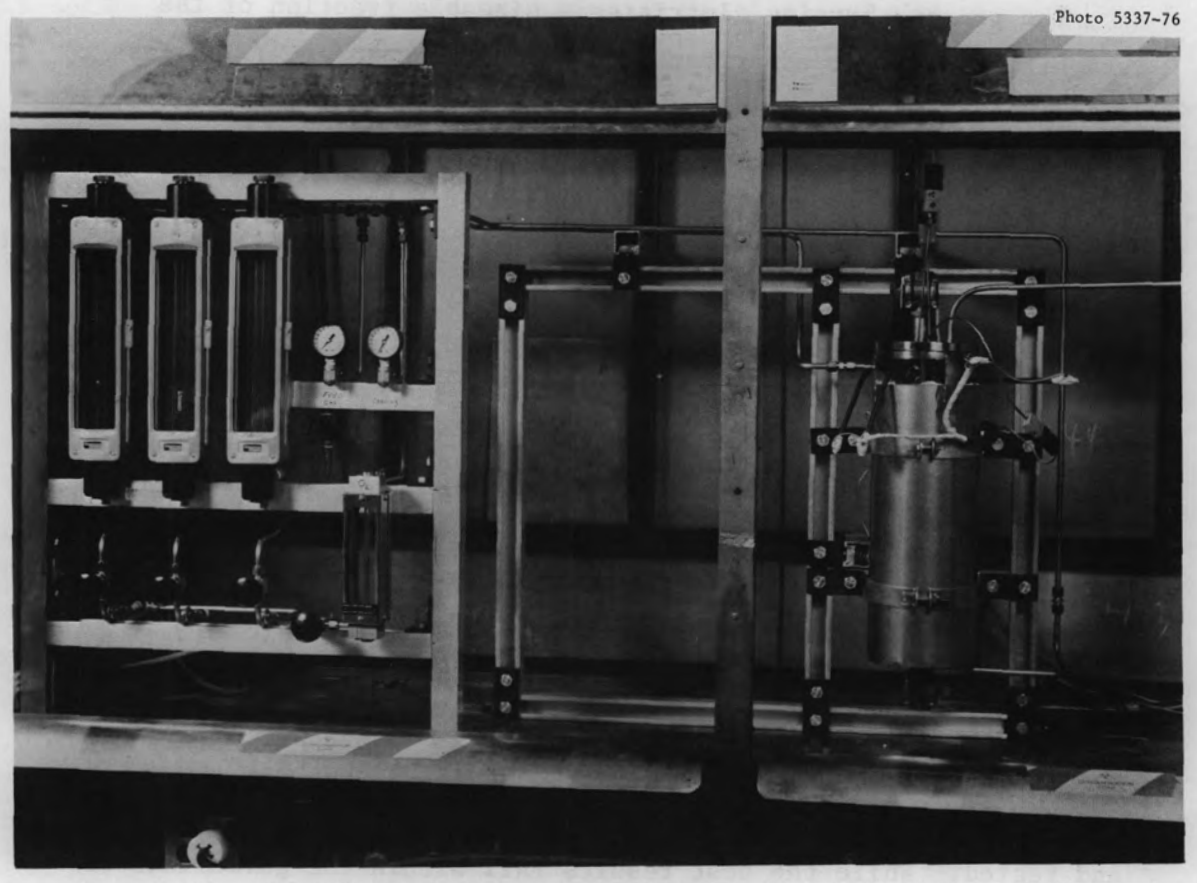

Fig. 2.11. Fluidized-Bed Burner to Handle 50 Crushed Fuel Rods.

A cooling gas jacket was included to assure adequate control at the burning rates desired. Standard ball valves [19 mm (3/4 in.)] for use in loading and dumping the burner were modified by replacing Teflon gaskets with annealed copper and valve seats with Grafoil. Resistance heating for start-up is provided by two 3-kW Calrod units. The unit has been operated in the laboratory and performs satisfactorily at a carbon burning rate of 375 g/hr (including blow-out) in air at 875°C with about 50% of the cooling capacity in use. This is well within our original specification. The burner will be tested again when the entire system is assembled.

The primary burning elutriates a sizeable fraction of the graphite fines (our experience indicates about 30 wt %). A gas-solids separation unit is specified before micrometallic filtration of the burner off-gases to prevent too rapid a plugging of the filter units. A cyclone based on Stairmand's high efficiency model[35] was miniaturized by Vaughen and used in his studies while on assignment at KFA, Jülich. The unit has an efficiency exceeding 98% at 15-μm particle size and above[33] and was selected for use in our system. The cyclone currently is being fabricated, and delivery is expected soon.

The porosity and material of construction for the micrometallic filter units were selected to match ones in use at Allied Chemical Company (ACC) and GA. The average pore size is reported as 10 μm, and material of construction is Hastelloy X. Each unit is 38 mm diam by 150 mm long (1.5 by 6 in.) We plan to operate up to two lines of filters containing two filters each. Provisions will be made to operate one line while the other is "blown back" to avoid excessive pressure build-up. Ten of the units have been received and tested. While the test results fall within the guidelines for checking the average porosity grade given by the manufacturer,[36] the <u>maximum</u> pore diameters ranged from 32 to 50 μm according to the ASTM procedure for laboratory sintered filters. The filters have been accepted as suitable for experimental test use. The filters will be used in the hot-cell operation and scanned periodically

to monitor fission product build-up as a function of operating time until failure or destructive analysis. We hope to use these results to help predict the useful life of micrometallic filters in reprocessing plants.

The fate of fission products that pass through the micrometallic filters is a matter of concern since plateout in lines could cause operational difficulties. A fission product "condenser" was designed and constructed to measure deposition as a function of off-gas temperature. The unit consists of two concentric tubes 3.66 m (12 ft) long coiled in a spiral to take less room. The inner tube is for the burner gases and the outer for cooling gas; flows are countercurrent. A mockup of the hot-cell cooler (uncoiled) was tested with hot gases to determine the temperatures along the length. These results are shown in Fig. 2.12. The temperature gradient is not linear, but appears to be predictable. The condenser is suitable for our early tests. We expect to use this unit for several experiments, and the fission product deposition will be measured after each experiment.

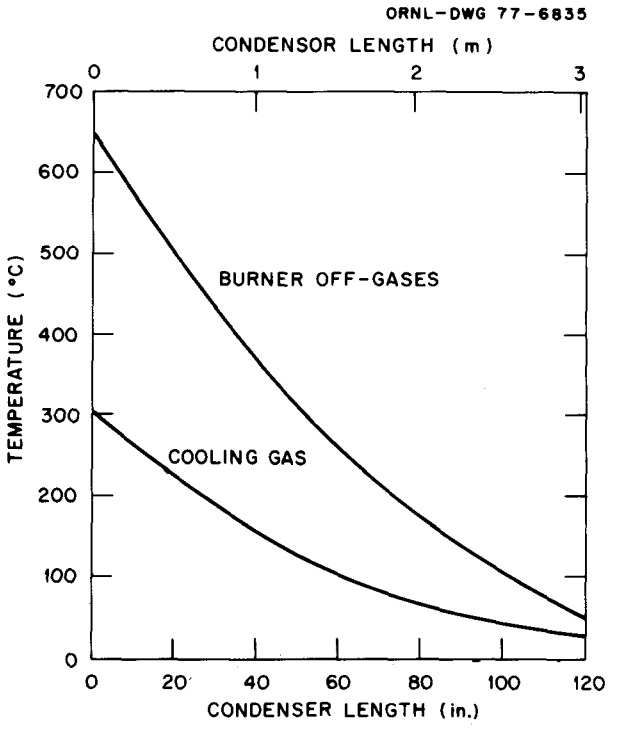

Fig. 2.12. Temperature Profiles for Fission Product Condenser.

The off-gases from the condenser will pass through an absolute filter, a portion will be bled off for in-line analyses, and the remainder will be discharged to the cell environment. The absolute filter unit is a disposable off-the-shelf item,* and several will be used in parallel as dictated by the back pressure. This assembly will be replaced after each experiment so that the used filters can be analyzed for fission product content.

In-line instrumentation consists of inlet and outlet O_2 analyzers, CO and CO_2 analyzers, a multichannel analyzer for ^{85}Kr, inlet and outlet mass flowmeters, and inlet and outlet flow totalizers. All instrumentation has been installed and tested. Final assembly and testing of the system is anticipated by early 1977.

2.4.3 Particle Classification, Crushing, and Burning (Subtask 215)

2.4.3.1 Studies With FTE-4 Irradiated Fuel — C. L. Fitzgerald C. E. Lamb, and V.C.A. Vaughen

These experiments are part of a continuing study of the combustion of irradiated HTGR fuel test specimens and behavior of the heavy metals and fission products in head-end reprocessing steps. Specially fabricated Recycle Test Elements (RTE) with fuel rods of known composition[31] have been irradiated under controlled conditions in the Peach Bottom reactor. Additional Fuel Test Elements (FTE) were also irradiated by GA. In these experiments, the major goal was to compare material balances by three independent means: (1) the normal method using "wet analytical chemistry" techniques, (2) calculation of materials using the ORIGEN code,[37,38] and (3) nondestructive gamma spectrometry. The need for this comparison grows out of a concern for knowing the degree of surface deposition ("plateout") of materials on the walls of the processing equipment (burner, filters, lines, etc.), which may be obtained by material balance.

---

*Filter assembly, MBY 3001 URA, Pall Trinity Micro Crop.

A complete FTE-4 fuel rod was used in each experiment to minimize the number of processing steps and, hence, losses. The fuel rods were ground to a fine powder before burning. After burning, the ashes were leached and the residues were fused for analysis. The equipment, except for the burner, was disassembled for destructive analysis. As usual, throughout the run precautions were taken to minimize losses and avoid cross-contamination of the sample during handling.

The data, after extensive ORIGEN and chemical analysis (and reanalysis) is presented in Tables 2.12 and 2.13 for two FTE Rods. Quantities of materials from ORIGEN, chemical analysis, and gamma scanning are presented by isotope. (ORIGEN predicts many isotopes that are not listed in the table.) With the exception of ^{234}U the results of chemical analysis were within about ±15% of the ORIGEN predictions for heavy metals in both samples.

Table 2.12. Comparison of ORIGEN Calculations with Chemical Analysis of Heavy Metals in FTE Fuel Rods

Nuclide	Content, g		CA/OC
	ORIGEN, OC[a]	Chemical Analysis, CA	
	Rod FTE-4-3-5-7		
^{233}U	0.034	0.032	0.94
^{234}U	0.008	0.004	0.50[b]
^{235}U	0.340	0.284	0.84
^{236}U	0.037	0.031	0.84
^{238}U	0.025	0.028	1.12
Total U	0.444	0.379	0.85
Average Ratio			0.94
^{232}Th	2.336	2.149	0.92
	Rod FTE-4-3-1-8		
^{233}U	0.072	0.057	0.79
^{234}U	0.010	0.007	0.70
^{235}U	0.348	0.326	0.94
^{236}U	0.035	0.033	0.94
^{238}U	0.025	0.027	1.08
Total U	0.490	0.450	0.92
Average ratio			0.89
^{232}Th	5.094	4.534	0.89

[a]ORIGEN, (564 days cooling, Aug. 5, 1976) for rod 4-3-5-7; Aug. 4 for 4-3-1-8.

[b]Omitted from the average.

Table 2.13. Comparison of ORIGEN Calculations with Chemical Analysis and Gamma Scan of Fission Products in FTE Fuel Rods

Nuclide	Activity, dis/min[a]			Ratios	
	ORIGEN, OC[b]	Chemical Analysis, CA	Gamma Scan, NDA	CA/OC	NDA/OC
		Rod FTE-4-3-5-7			
^{85}Kr	1.18E11	1.30E11		1.10	
^{90}Sr	1.00E12	6.71E11		0.67	
^{95}Zr	7.68E10	5.15E10	9.32E10	0.67	1.21
^{95}Nb	1.65E11	≤1.37E09		0.01[c]	
^{106}Ru	3.93E11	5.97E10	4.57E11	0.15	1.16
^{110}Ag	6.96E09	1.33E08		0.02[c]	
^{125}Sb	3.33E10	1.19E10	2.66E10	0.36	0.80
^{134}Cs	5.82E11	2.10E11	4.66E11	0.36	0.80
^{137}Cs	9.96E11	4.92E11	1.09E12	0.49	1.09
^{144}Ce	4.39E12	3.52E12	4.57E12	0.80	1.04
^{152}Eu	9.83E07	≤1.07E10	8.88E09	109.[c]	90.3[c]
^{154}Eu	3.10E10	1.30E10	3.11E10	0.42	1.00
^{155}Eu	6.90E09	5.14E09	1.89E11	0.74	27.4[c]
Average ratio				0.62	1.01
		Rod FTE-4-3-1-8			
^{85}Kr	1.26E11	3.68E10		0.29	
^{90}Sr	1.01E12	7.78E11		0.77	
^{95}Zr	8.10E10	≤6.88E10	4.88E10	0.85	0.60
^{95}Nb	1.74E11	≤2.01E09		0.01[c]	
^{106}Ru	3.91E11	8.12E11	1.80E11	2.08[c]	0.46
^{110}Ag	6.62E09	≤4.40E08		0.07[c]	
^{125}Sb	3.66E10	≤1.67E10	2.66E10	0.46	0.73
^{134}Cs	5.43E11	2.61E11	1.67E11	0.48	0.31
^{137}Cs	1.00E12	6.61E11	5.00E11	0.66	0.50
^{144}Ce	4.47E12	3.63E12	1.81E12	0.81	0.40
^{152}Eu	1.03E08	≤7.92E09	6.66E09	76.9[c]	64.6[c]
^{154}Eu	2.84E10	≤1.37E10	2.66E10	0.48	0.94
^{155}Eu	6.67E09	≤5.74E09	1.73E11	0.86	25.9[c]
Average ratio				0.67	0.56

[a]Read 1.26E11 as 1.26×10^{11}.

[b]ORIGEN, (564 days cooling), Aug. 5, 1976, for rod 4-3-4-7; Aug. 4 for 4-3-1-8.

[c]Omitted from the average.

The results of chemical analysis (CA) for the other materials, principally gamma-emitters, were not the same for both fuel rods. Four isotopes — ^{95}Nb, ^{106}Ru, ^{110}Ag, and ^{152}Eu — diverged widely from the ORIGEN (OC) predictions. Omitting these, the range of ratios CA/OC was about 36 to 109% for FTE-4-3-5-7 and about 29 to 86% for FTE-4-3-1-8.

In like manner, comparing the results of nondestructive gamma-scan analysis (NDA) to ORIGEN (OC), the range of the ratios NDA/OC was about 80 to 121% for FTE-4-3-5-7 and 31 to 94% for FTE-4-3-1-8.

The main purpose of these experiments was to select a suitable means for establishing a credible total inventory of materials in the oncoming fuel, for use in material balances and as an indirect measure of plateout losses to surfaces of the equipment in future runs. We have had only limited success in reaching this goal.

Feedback from this work has improved ORIGEN results for HTGR fuels. The two fuel rods were separated by only inches in the reactor. Adding better estimates of reactor operating times (and decay periods), as well as focusing on the influence of the ORIGEN inputs has resulted in calculations agreeing between the two rods within ±10% (or less); see Table 2.14. Further work is indicated:[38] (1) to obtain more detailed reactor flux-time histories and (2) to improve the performance in predicting activation products by improving the ORIGEN input term RES.

While gamma scanning has great potential in allowing an independent estimate of certain isotopes, and assists in tuning ORIGEN so that all isotopes may be estimated more precisely, the early promise in FTE-4-3-5-7 of ±20% correspondence to ORIGEN was not sustained with FTE-4-3-1-8 (Table 2.14). It appears that the broken fuel rod with its inhomogeneity may not have been adequately corrected by the methods used. Therefore, to establish the usefulness of gamma scanning, one should repeat the comparisons with other fuels, and develop better methods to correct for fuel rod breakage and nonhomogeneities.

As mentioned above (Tables 2.12 and 2.13) the comparisons of the chemical analysis with ORIGEN calculations indicate that these summations of inventories from many solutions and solids give apparent

Table 2.14. Ratio of Estimates of Inventories in FTE 4-3-1-8 to Those in 4-3-5-7 by Several Methods

Nuclide	ORIGEN[a] Calculations	NDA Results	Chemical Analysis
^{233}U	2.1[b,c]		1.78[b,c]
^{234}U	1.25		1.75[b]
^{235}U	1.02		1.15
^{236}U	0.95		1.06
^{238}U	1.00		0.96
Total	1.10		1.19
Average ratio	1.06		1.09
^{232}Th	2.18		2.11
^{85}Kr	1.07		1.00
^{90}Sr	1.01		1.16
^{95}Zr	1.05	0.52	∿1.3
^{95}Nb	1.05		∿1.5
^{106}Ru	0.99	0.39	13.6[b]
^{110}Ag	0.94		3.31[b]
^{125}Sb	1.10	1.00	∿1.4
^{134}Cs	0.93	0.36	1.25
^{137}Cs	1.00	0.46	1.34
^{144}Ce	1.02	0.40	1.03
^{152}Eu	1.05	0.75	∿0.74[b]
^{154}Eu	0.92	0.86	∿1.0
^{155}Eu	0.97	0.92	∿1.1
Average ratio	1.01	0.63	1.21

[a]ORIGEN, (564-day cooling), Aug. 5, 1976, for Rod 4-3-5-7; Aug. 4 for 4-3-1-8.

[b]Omitted from the average.

[c]Due to larger amount of thorium.

yields from about 36% to about 80% (excluding ^{85}Kr, ^{95}Nb, ^{106}Ru, ^{110}Ag, and ^{152}Eu). However, when the chemical analysis results of the two runs are compared with each other, the range of ratios of inventories by chemical analysis of 4-3-1-8 to 4-3-5-7 was only about 1.25 ± 0.25, excluding ^{106}Ru, ^{110}Ag, and ^{152}Eu (Table 2.14). This indicates a consistency of results, even though they are not in agreement with ORIGEN, and may, on repetition, attain some more basic significance. However, as mentioned above, the results in Tables 2.12 and 2.13 are the product of many recheck analyses, some rechecked more than once. A number of values remain faulty or indeterminate because of decay,

low concentrations, gamma peak overlap, handling losses, or cross-contamination. Thus, at this stage one cannot draw conclusions about plateout or the loss by other mechanisms.

With more detailed reactor operating parameters, better calculation of the ORIGEN input parameter RES, and better gamma-scan interpretation, close agreement between ORIGEN predictions and actual inventories determined by gamma scanning may be routinely possible in future runs. The chemical analysis for uranium isotopic composition already agrees within about 15% of the ORIGEN values. For other isotopes, the chemical analysis in general gave low values ($\sim$50% ± 20%) when compared with ORIGEN. This has brought attention to several problems in the separation and analysis of materials having high radiation levels.

Analytical procedures needing improvement are: (1) preparing storable aliquots of sample solutions very soon after preparation, (2) increasing the capability for analyzing minor components, and (3) improving the capability to analyze undissolved solids and precipitates. Some isotopes — especially ^{106}Ru, ^{110}Ag, and ^{234}U — appear to give problems in analysis. Isotopes that have decayed to essentially zero quantities are, of course, lost to analysis.

The continued improvements in hot-cell techniques and the extensive use of experimental run sheets has allowed a sharper focus to be drawn on which in-cell areas still require improvment. The problem areas found and suggested improvements are: (1) sampling procedures — to test in-cell dilutions to reduce the chances for error due to changes in solutions on aging, (2) material balances — gamma scanning of incoming fuel to obtain more reliable estimates of fission product inventories for use in guiding ORIGEN calculations to "fill in the gaps," and (3) particulate collection — a better system to collect particulates from off-gases. In addition, a new technique should be developed to periodically analyze our hot-cell equipment nondestructively to detect and account for fission product buildup.

2.4.3.2 Material Balances — W. Davis, Jr., C. W. Kee, V.C.A. Vaughen, and M. L. Tobias

A report on obtaining estimates of fission product inventories in Peach Bottom FTE-4 fuel rods has been prepared.[38] The abstract follows:

> Nondestructive gamma-ray analyses (NDA) for fission products and mass-spectrometric analyses for five uranium isotopes in two samples of fuel removed from the Peach Bottom reactor have been compared with corresponding quantities calculated from reactor operating data using the ORIGEN code, to form the basis for material balance calculations in head-end reprocessing steps. Satisfactory agreement between ORIGEN results and measured uranium isotopic distributions was found with the standard ORIGEN inputs.
>
> Many fission products of interest, including ^{89}Sr, ^{91}Y, ^{95}Zr, ^{95}Nb, ^{103}Ru, ^{106}Ru, $^{127}Te^*$, $^{129}Te^*$, ^{131}I, ^{134}Cs, and ^{144}Ce, have half-lives that are less than about 2 years. Comparisons of ORIGEN calculations and NDA values for ^{95}Zr, ^{106}Ru, ^{125}Sb, ^{134}Cs, ^{144}Ce, and ^{154}Eu demonstrated the need to include realistic reactor operating data, including shutdown times, in the ORIGEN input parameters

2.4.3.3 Head-End Studies — C. L. Fitzgerald, V.C.A. Vaughen, K. J. Notz, and R. S. Lowrie

A report was published[39] on the head-end reprocessing studies with RTE-7. The abstract follows:

> Head-end reprocessing studies on irradiated Fort St. Vrain type HTGR fuel (Triso coated UC_2- Triso coated ThC_2) have been performed. Fuel sticks were burned quiescently in oxygen at 750°C, the ash was screened to separate the fissile SiC-coated particles from the fertile SiC-coated particles. Each particle fraction was crushed and burned separately in oxygen, and the secondary burner ash products were leached.
>
> These studies concentrated on the release of radionuclides to the burner off-gases after passing through a 20-μm sintered metal frit held at 500°C. Fission product and heavy metal inventories were made on the process gaseous, liquid, and solid streams. Experimental results are compared with pre-irradiation average fuel stick compositions and with calculated fission product inventories.

2.4.4 Solvent Extraction, Including Feed Adjustment (Subtask 225)

2.4.4.1 Feed Adjustment and Solvent Extraction of Irradiated Thoria — R. H. Rainey and R. H. Shannon

In scouting studies a solution of irradiated thoria was adjusted to acid-deficient conditions, then batch extracted with 30% TBP. The amount of feed for this study was too small (∿15 ml) for a comprehensive study. We were able to follow the path of the plutonium in the solvent extraction and the carry-over of fission products during the feed adjustment.

The feed adjustment consisted of concentrating the dissolver solution to a boiling point of 135°C, steam stripping until the solution became acid deficient, then diluting with water to the concentration desired for solvent extraction feed. The distillate contained about 10^{-4} of the total ^{106}Ru and 10^{-6} of the ^{144}Ce, ^{134}Cs, and ^{137}Cs. The adjusted feed was then batch extracted eight times with equal volumes of 30% TBP. The thorium extracted slightly better than the plutonium, but both were nearly completely extracted in the eight contacts (Fig. 2.13). There was no indication that the plutonium [which was determined by analysis to be Pu(IV)] had polymerized in the acid-deficient thorium nitrate solution.

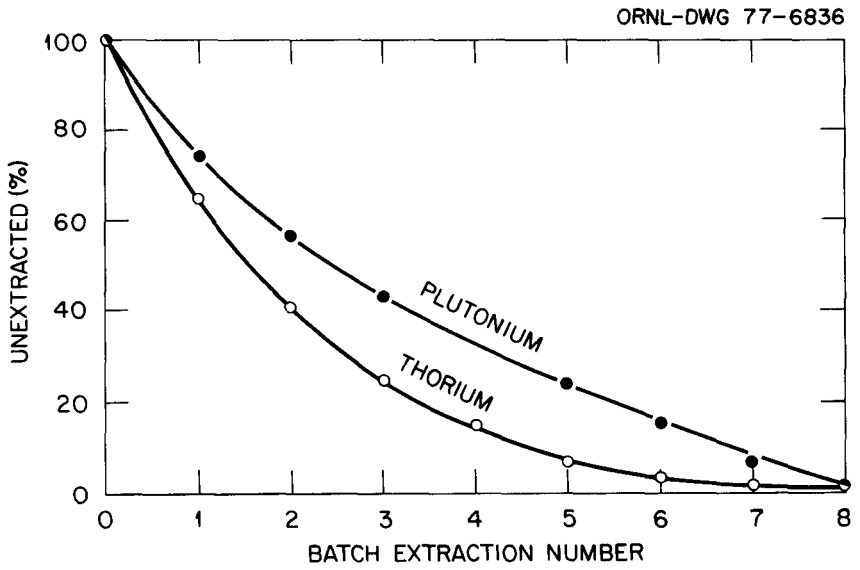

Fig. 2.13. Extraction of Thorium and Plutonium from Acid-Deficient Feed Solution.

2.4.5 Gaseous Effluent (Subtask 245)

2.4.5.1 Fuel Storage Test — C. L. Fitzgerald and C. E. Lamb

A consideration of the environmental impact of releases on the requirements for cleanup of the storage vault cooling gas and the cost of specification fuel storage containers prompted the request from GA to measure the releases of ^{85}Kr, ^{3}H, and other isotopes from a stored fuel element and determine the release patterns at several storage temperatures. Fuel body RTE-2-5 was available for these tests. It consists of a cylindrical graphite body about 76 mm diam by 0.38 m long (3 by 15 in.) containing a central hole and eight smaller holes arranged like a telephone dial. Seven of the holes still have the original loading of loose Biso-coated $(4Th,U)O_2$ and Biso ThC_2 (Type a) fuel.[31] The fuel in the other hole had been removed for postirradiation examination. Experimental work described here began on January 27, 1975, and is continuing.

The amount of ^{85}Kr in RTE-2-5 has been estimated by analogy to RTE-2-3 with the assistance of the ORIGEN code. About 0.38 Ci ^{85}Kr per fuel channel was predicted for RTE-2-3. We measured 0.31 Ci ^{85}Kr (about 80% of the calculated amount) in the experiment with fuel channel RTE-2-3-2. The neutron flux at the RTE-2-5 position was about 75% of the flux at RTE-2-3; RTE-2-5 had only seven fuel channels filled with fuel; RTE-2-5 was loaded with more uranium and thorium than RTE-2-3. By adjusting the ORIGEN yield of ^{85}Kr for RTE-2-3 by simple factors, we have estimated an inventory of 2.6 Ci ^{85}Kr in RTE-2-5. In like manner, we estimated the ^{3}H inventory to be 56 mCi.

The fueled body was placed into a closed system as shown in Fig. 2.14. The element was purged with moist air, continuously at first. After the daily release rates fell to levels approaching the analytical limits, the system was sealed and purged weekly. The filtering units were added after the ambient-temperature run was finished.

The measured releases of ^{85}Kr in this experiment are shown in Fig. 2.15 and in Table 2.15. Almost any change resulted in an increased release rate temporarily. The integrated amounts released, the initial

ORNL DWG 75-8360

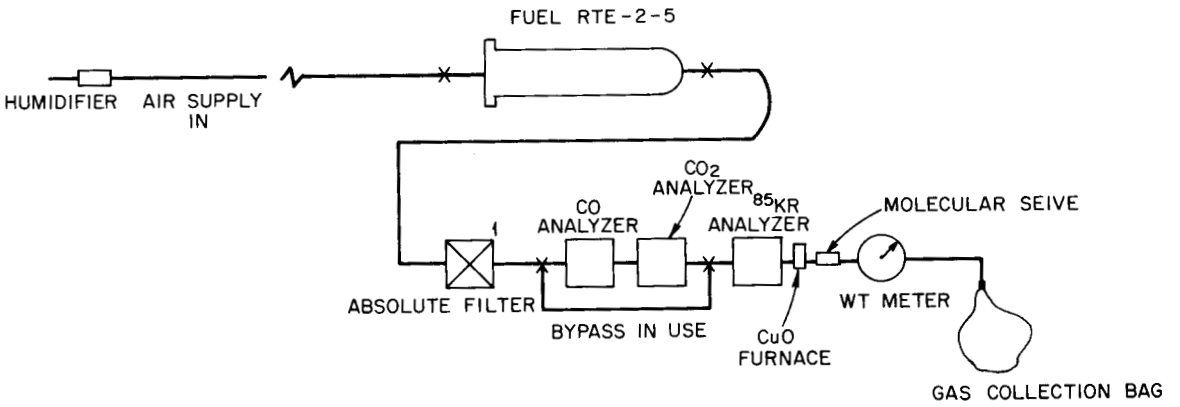

STORAGE EXPERIMENT RTE-2-5

1– NOT IN LINE AT AMBIENT TEMPERATURE

Fig. 2.14. Equipment Flowsheet for the Long-term Fuel Element Storage Experiment.

ORNL DWG 76-14504

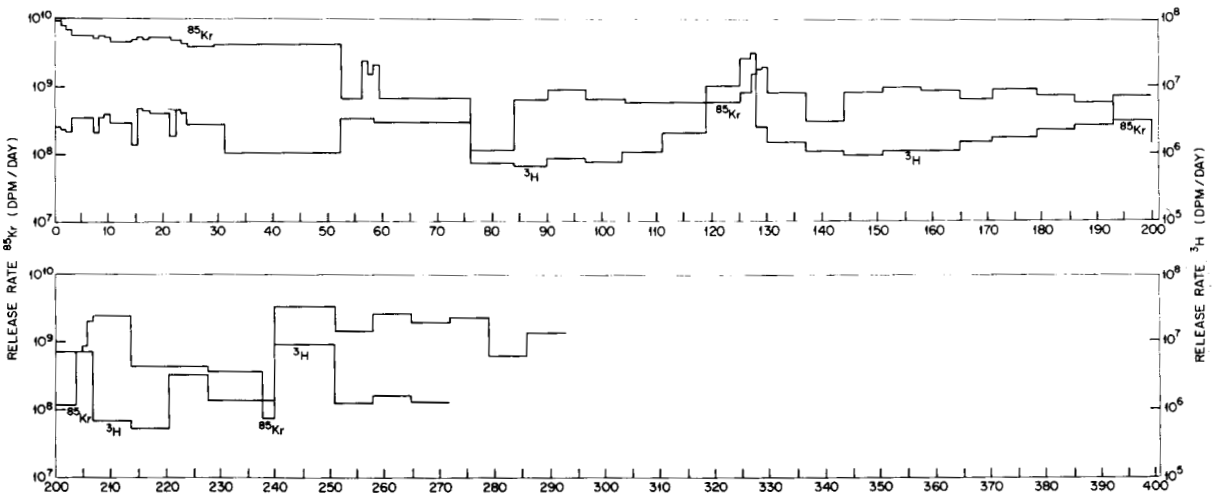

Fig. 2.15. Release of ^{3}H and ^{85}Kr from a Stored Fuel Element.

Table 2.15. Release of ^{85}Kr and ^{3}H from RTE-2-5 in Storage

Temperature (°C)	Exposure (days)	Total Release at Temperature (mCi)	Rate, μCi/day	
			Initial	Final
		Release of ^{85}Kr		
25 ± 5[a]	67	15.7	9180	81
100	73	66.6	6510	53
150	114	40.1	1110	114
200	295	167.5	4230	52.1
		Release of ^{3}H		
Ambient	67	0.0085	3.01	0.014
100	75	0.0085	0.33	0.016
150	113	0.0935	0.01	0.056
200	280	0.371	1.21	0.748

[a]The temperature of the cell varied.

release rates, and the final release rates are given in the table. The release rate of about 570 μCi/day corresponds to less than about 0.3%/day.

Tritium release rates are also listed in Table 2.15. Approximately 0.9% of the calculated total ^{3}H has been released to date.

2.4.5.2 Data on ^{85}Kr and ^{14}C Releases — V.C.A. Vaughen and C. L. Fitzgerald

The purge and burner off-gases from the FTE 4 (Sect. 2.4.3) were collected and analyzed for ^{85}Kr and ^{14}C. The distribution of ^{85}Kr found is given in Table 2.16. More ^{85}Kr was released during the grinding and leaching of FTE-4-3-1-8 than for the other rod, and a substantially lower total amount of ^{85}Kr was detected (16 vs 59 mCi). One explanation is that the value from FTE-4-3-1-8 burner off-gas is low. The yields of ^{85}Kr predicted by ORIGEN are 53 mCi for FTE-4-3-5-7 and 57 mCi for FTE-4-3-1-8.

We determined ^{14}C in samples of the burner off-gas for both runs and for the leach of the run with carbide fuel (Table 2.17).

Table 2.16. Distribution of ^{85}Kr in Off-gas System for FTE Fuel Rods

Operation	Off-gas Volume (Std liters)	^{85}Kr Content		
		dis/min[a]	(mCi)	(%)
		Rod FTE 4-3-5-7		
Grind	14.8	6.65E09	3.0	5.1
Burn	27.4	1.23E11	55.4	94.4
Leach	33.8	6.13E08	0.3	0.5
Total	76.0	1.30E11	58.7	100.0
		Rod FTE 4-3-1-8		
Grind	10.4	1.79E10	8.06	48.7
Burn	31.7	1.42E10	6.40	38.6
Leach	82.0	4.68E09	2.11	12.7
Total	124.1	3.68E10	16.57	100.0

[a]Read 6.65E09 as 6.65×10^9.

Table 2.17. Determinations of ^{14}C in FTE Fuel Rods

Operation	Volume (Std liters)	Sample Code	^{14}C		CO_2 (%)
			(dis/min)	(mCi)	
		Rod FTE 4-3-5-7			
Burn	27.4	GB-1	6.17×10^7	0.027	
		GB-2			56.3
		GB-3	6.27	0.028	
		GB-4			42.0
		GB-5	6.54	0.029	
		GB-6			51.1
		Av	6.33	0.028	49.8
Leach	33.8	GB-7	0.13106	<0.001	
		GB-8	0.11206	<0.001	
		GB-9			2.4
		Av	0.12206[a]	<0.001[a]	
		Rod FTE 4-3-1-8			
Burn	31.7	GB-1	3.91×10^7	0.018	43.5
		GB-2	Sample bulb leaked		
		GB-3	3.38	0.015	
		GB-4	3.04	0.014	40.6
		GB-5	4.22	0.019	
		GB-6	3.20	0.014	
		Av	3.55	0.016	42.1

[a]Corrected for carbon added as flushes.

Since the carbon in the off-gas included flush carbon, the ratio of ^{14}C to total carbon measured was multiplied by the calculated ratio of total carbon to carbon in the fuel to correct back to the fuel-based carbon. These ratios correspond to about 1600 and 450 g N per metric ton heavy metal in the fuel, respectively.[38] The ^{14}C and CO_2 in the leacher purge off-gas are assumed to have come from a residual amount of burner off-gases since special steps to avoid this contingency were not taken. (It could conceivably also have come from unburned carbides during leaching.)

2.4.6 Waste Processing and Scrap Recovery (Subtask 250) — K. H. Lin

The work was started to develop methods for processing solid wastes from the head-end system, consisting of SiC hulls, insoluble noble metals, and semivolatile radionuclides, which are trapped in the sintered metal filters and cold traps in the burner off-gas line. The objectives of the program are: (1) to determine whether or not the wastes will contain enough fissionable material to require a recovery step, (2) to determine from the distribution of various radionuclides whether or not it may be justified to separate and concentrate the residual actinides and fission products from the wastes so that the secondary wastes resulting from the separation can be handled as non-high-level wastes, and (3) to develop methods for incorporating these wastes into nonleachable solid materials suitable for transport and long-term storage.

Major efforts in the hot-cell experimental work have been directed toward characterization of SiC hulls and sintered metal filters contaminated with semivolatile and particluate radionuclides. Some scoping studies have also been performed on the decomposition of nonradioactive SiC hulls. No definite conclusion can be made at this time pertaining to trends in the distribution of different radionuclides in these wastes.

2.4.6.1 SiC Hulls and Insoluble Residues — W. E. Clark and K. H. Lin

Residues from six hot-cell experiments were examined for the distribution of U, Th, Pu, and selected fission products after the crush-burn-leach processing of four different types of irradiated fuels. The experiment designations and the fuel descriptions follow:

RTE 2-3-3 UC_2 Triso, ThC_2 Biso

RTE 2-3-76 UC_2 Triso, ThC_2 Biso

FTE 4-279-1 UO_2 Triso, ThO_2 Biso

FTE 4-279-2 UC_2 Triso, ThC_2 Biso

FTE 4-279-3 $(Th,U)C_2$ Triso, ThC_2 Biso

FTE 4-279-4 $(Th,U)C_2$ Triso, ThC_2 Biso

In all cases, individual batches of residues were separated by gravity in diiodomethane into the light fraction (predominantly SiC hulls) and the heavy fraction (assumed to be mostly noble metals). Each fraction was analyzed for U, Th, Pu, and fission products that were sufficiently abundant to be quantitatively determined by common inexpensive procedures.

The preliminary results of analyses for SiC hulls and heavy residues are inconclusive concerning the necessity for uranium recovery. The uranium found in these solids varied from less than 0.001% for FTE 4-279-3 to about 3% for FTE 4-279-2. For FTE 4-279-4, supposedly of the same fuel type as FTE 4-279-3, the uranium content of the residues was about 0.8% by weight. Among major radionuclides other than U and Th found in SiC hulls and heavy residues were Pu, ^{90}Sr, ^{106}Ru, ^{134}Cs, ^{137}Cs, ^{144}Ce, and ^{154}Eu (10—100 ppm each).

We briefly investigated the decomposition of SiC hulls in various media. The most satisfactory media appeared to be mixtures of either KNO_3 and Na_2CO_3 or KOH and Na_2O_2.

2.4.6.2 Semivolatile Radionuclides — K. H. Lin and W. E. Clark

Six sets of sintered metal filters (either nickel or type 316 stainless steel) individually exposed to off-gas streams from burning of the fuels described above were analyzed for U, Th, Pu, and selected fission products. Three sets of these filters were analyzed "as is"

after dissolution in aqua regia. The other three were first leached in HNO_3 (1 or 6 *M*), and samples of leachate solutions and filters were analyzed separately. The latter procedure was to investigate feasibility of removing the bulk of radionuclides present in the filter to the extent that the filter itself could be processed as a low-level solid waste. The leachate solution could presumably be concentrated and combined with the high-level liquid waste.

According to the preliminary analytical results, up to about 1 wt % of the uranium in the original fuel may be found on the sintered metal filter. Also present in appreciable quantities were ^{137}Cs, Th, ^{129}I, ^{134}Cs, and ^{90}Sr (approximately in the order of abundance). Leaching of the filter with HNO_3 for about 30 min at ambient temperature removed substantial fractions of the radionuclides, including uranium. However, much less than 50% of that present in the filter was removed.

2.5 COLD ENGINEERING DEVELOPMENT

2.5.1 Krypton Separation (Subtask 235) — A. D. Ryon

Reprocessing of HTGR fuel involves burning of the graphite-matrix elements to release the fuel for recovery. The resulting off-gas is primarily CO_2, with residual amounts of N_2, O_2, and CO, together with fission products. Trace quantities of ^{85}Kr must be recovered in a concentrated form from the gas stream, but processes commonly employed for rare gas removal and concentration are not suitable for use with off-gas from graphite burning. The KALC process employs liquid CO_2 as a volatile solvent for the krypton and is, therefore, uniquely suited to the task.

Engineering development of the KALC process[40] is currently under way using facilities at both the Oak Ridge National Laboratory (ORNL) and the Oak Ridge Gaseous Diffusion Plant (ORGDP). The ORNL system[41] is designed for close study of the individual separation operations involved in the KALC process, while the ORGDP system[42] provides a complete pilot facility for demonstrating combined operations on a

somewhat larger scale. Packed column performance and process control procedures have been of prime importance in the initial studies.

Previous studies of the KALC process have been summarized in the preceding Thorium Utilization Program Progress Report.[43] The flooding capacity and mass transfer of krypton in the absorber column have been measured in the ORNL facility. The ORGDP pilot plant has been run to shake down the equipment and make necessary revisions. During this report period, both facilities were operated to obtain overall process performance and individual component data for the absorption, fractionation, and stripping functions required for KALC. Computer programs have been prepared to analyze and model the KALC process.

2.5.1.1 Experiments in the ORGDP Pilot Plant — A. D. Ryon, M. J. Stevenson,* and R. S. Eby*

Additional tests of the KALC process were made during Campaign II in the ORGDP LMFBR-HTGR Fuel Reprocessing Off-Gas Pilot Plant in May, June, July, and August 1975.[44] The primary goal of Campaign II was to operate the KALC process in the three-column array of absorber, fractionator, and stripper with the system CO_2-O_2-Kr to demonstrate simultaneous decontamination of feed gas and concentration of krypton. Target values are 100 for the process decontamination factor (DF) of krypton and 1000 for the process concentration factor (CF). The separation of krypton from O_2 is an integral part of KALC; thus, to permit an additional CF of 100 on the krypton stream leaving KALC, an O_2 concentration in the krypton stream of less than 1% is desirable. This becomes essential if the additional CF is obtained by freezeout of CO_2, but it may not be necessary if other methods are used (e.g., the use of molecular sieves).

Secondary objectives of Campaign II were to determine component performance, particularly absorber and fractionator column efficiency, as a function of flow rate and flow ratio; to test effects of transients of feed composition and flow rate on performance; and to explore methods of control.

---

*Oak Ridge Gaseous Diffusion Plant.

The general performance of the pilot plant was good considering that the malfunction of only one of the many components can cause shutdown. The changes that were made between Campaigns I and II improved the performance significantly. The installation of gamma counters was essential to measuring ^{85}Kr concentration in the process streams. The addition of recording rate meters near the end of the campaign permitted measurement of the effects of transients on krypton concentration. The installation of a set point control for liquid level control in the columns resulted in easy and reliable control of the liquid flow throughout the system. All the major equipment items such as liquid metering pump, gas compressor, condensers, refrigeration systems, reboilers, packed columns, and controllers operated smoothly with only a few exceptions.

The data from over 30 runs in which the krypton CF was greater than 100 were analyzed. The process feed gas rate, which is equal to the absorber feed rate less the recycle rate from the fractionator, ranged from 1.98 to 4.9 std liters/sec (4.2—10.3 scfm). The CF depends directly on the ratio of flow rate of process feed gas to stripper off-gas. It was varied by manually setting the stripper off-gas rate, which ranged to as low as 1.1 std ml/sec (0.0023 scfm), to give the maximum CF (4080) demonstrated. At this very low off-gas rate, a large fraction of the krypton inventory was in the stripper condenser, and small leaks in the piping from the condenser could cause large losses of krypton. Most of the runs were made at higher flow rates to give CF values less than 1000; however, CF values exceeded 1000 in 14 runs.

One of the primary objectives of the campaign was to demonstrate simultaneous process DF > 100 and CF > 1000. This was achieved on six occasions. The flow ratios (L/V) in the absorber and fractionator for these runs ranged from 11 to 13. It may be assumed that any L/V within this "window" would produce DF > 100 and CF > 1000. Although satisfactory flow ratios may also occur outside this range, this was not demonstrated mainly because most of the runs were made at stripper off-gas rates to give CF < 1000.

In addition, the O_2 concentration in the stripper off-gas is important because it may limit further concentration of the krypton, especially if a CO_2 freezeout technique is used. The O_2 concentration was normalized to a CF value of 1000 to permit better evaluation. The normalized O_2 concentration ranged from 0.2 to 11% for runs in which the absorber feed gas ranged from 6.6 to 19.5% O_2. In seven runs, the O_2 was less than 1% at CF = 1000 and DF > 100. The flow ratios in the absorber and fractionator for these runs are shown in Fig. 2.16. The range of L/V is 11.9 to 12.6 in the absorber and 11.8 to 13.4 in the fractionator. Although these ranges give satisfactory DF and O_2 concentrations at CF = 1000, they are not defined enough to exclude other flow ratios.

ORNL DWG 76-503

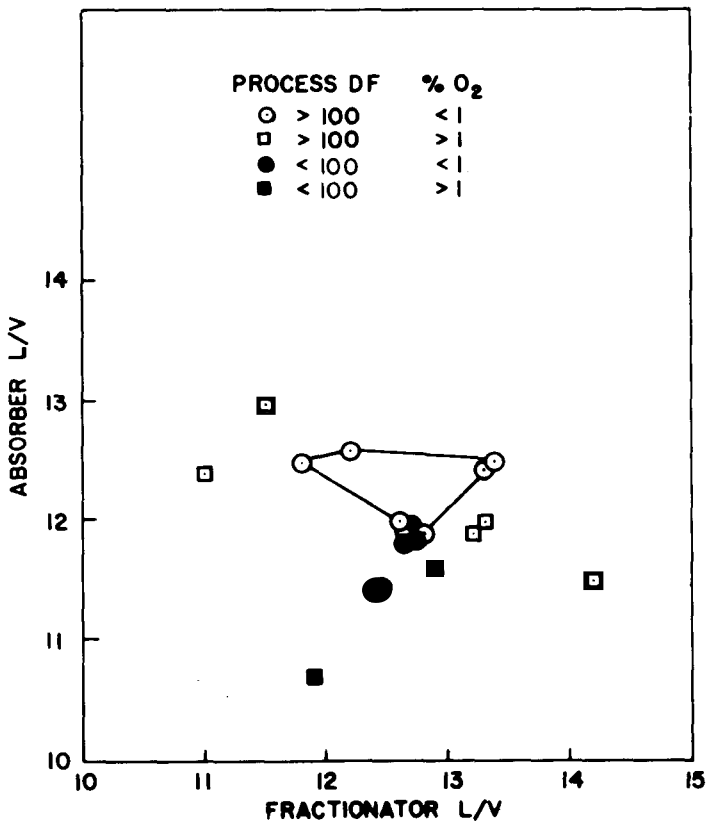

Fig. 2.16. Effect of Flow Ratio in Absorber and Fractionator on Process DF and Oxygen Content of Stripper Off-gas at CF = 1000.

2.5.1.2 Data From Experimental Engineering Facility at ORNL — T. M. Gilliam, C. W. Forsberg and A. D. Ryon

The experiments performed during the period covered by this report are collectively referred to as Campaign III.[45] Flooding and absorber mass transfer data were obtained and compared with previously reported values. Fractionation and stripper mass transfer data were obtained to quantify the height-of-a-transfer unit (HTU) values for each of the two operations.

The flooding studies were performed on two 38 and 76-mm (1 1/2- and 3-in.) stainless steel columns packed with Goodloe wire mesh packing. These experiments involved a liquid phase of CO_2 and a vapor phase of CO_2 saturated with O_2. The resulting flooding data, as well as the previously reported data,[46] were then presented (Fig. 2.17) in a modified Sherwood correlation of the following form:

$$y' = A + BX' + CX'^2$$

where*

y' = $\log U_m^2 \rho_G \mu_L^{0.2} / g \rho_L$

X' = $2.0 + \log \frac{L}{G}\sqrt{\rho_G/\rho_L}$

L = liquid flow rate, lb/hr ft^2,

G = gas flow rate, lb/hr ft^2,

ρ_G = gas phase density, lb/ft^3,

ρ_L = liquid phase density, lb/ft^3,

μ_L = liquid phase viscosity, cP,

U_m = gas velocity at flooding, fps,

g = 32.2 ft/sec^2 = 9.81 m/sec^2,

A = −3.6035,

B = 0.5317, and

C = −0.3488.

---

*1 lb/hr ft^2 = 1.356 g/sec m^2; 1 lb/ft^3 = 16.02 kg/m^3; 1 cP = 1 mPa sec; 1 fps = 0.305 m/sec.

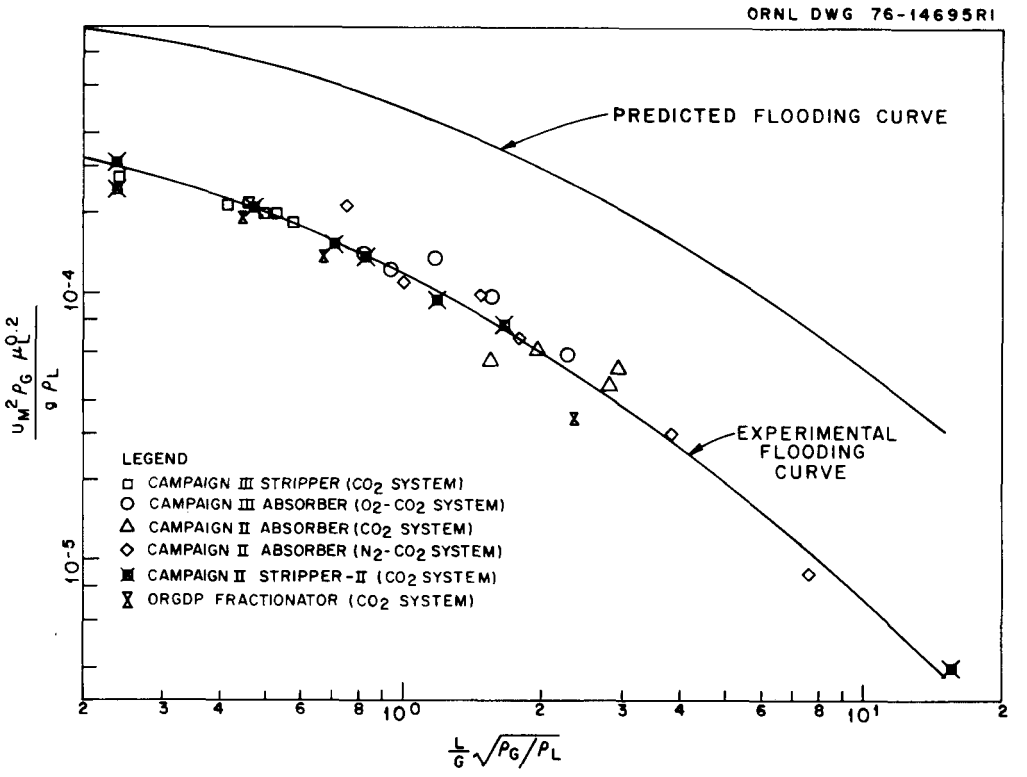

Fig. 2.17. Flooding Curve.

The flooding data was found to be consistent between the 38- and 76-mm (1 1/2- and 3-in.) columns. The experimentally determined throughput was approximately half that predicted by the manufacturer.

Absorber mass transfer experiments were performed at liquid flow rates approximately half that of experiments in Campaign II. The range of liquid rate, as well as other variables, is shown below.

Variable	Range
pressure, MPa gage (psig)	2.139–2.672 (310.2–387.5)
temperature, °C	−11.3 to −18.0
feed gas O_2 concentration, %	5.2–11.0
liquid rate, std liters/sec (scfm)	11.17–21.2 (23.67–44.87)
vapor rate, std liters/sec (scfm)	1.35–2.46 (2.86–5.22)

Decontamination factors (DF) and HTUs obtained in Campaign III agree quite favorably with previously reported data (Figs. 2.18 and 2.19),

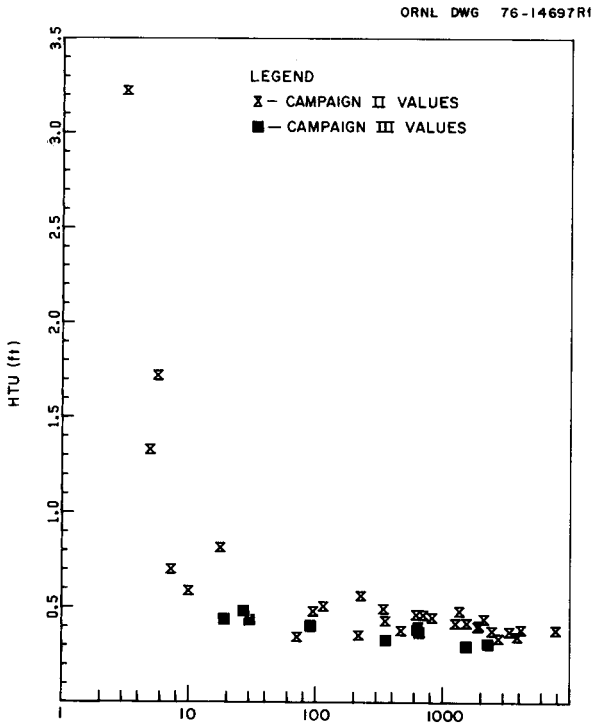

Fig. 2.18. HTU versus Decontamination Factor for Absorber Column. 1 ft = 0.305 m.

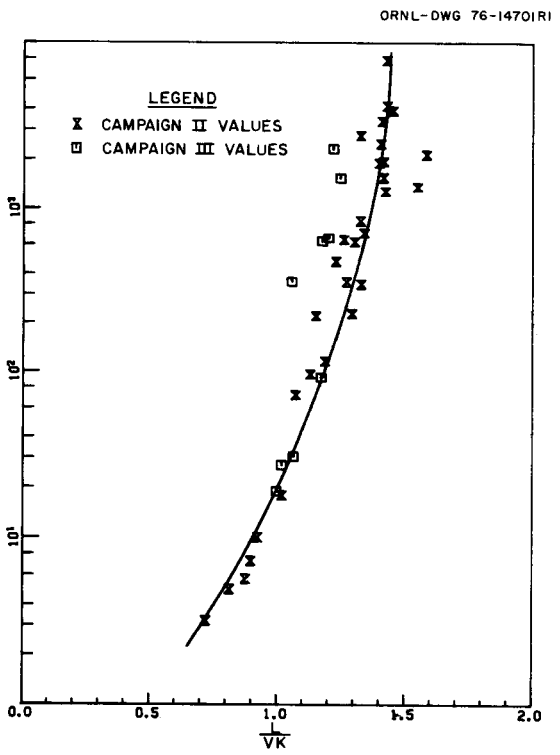

Fig. 2.19. Absorber Decontamination Factor versus Absorption Factor.

indicating that HTU_G is not a strong function of liquid flow rate. The collective mass transfer data produced an average HTU value (based on krypton) of 0.12 m (0.4 ft). In one experiment the height of the column was shortend from 2.512 m to 1.673 (8.24 ft to 5.49) with no visible effect on HTU, indicating that column end effects are negligible.

Fractionation studies were performed over the following range of operating conditions:

Variable	Range
pressure MPa gage (psig)	1.727–1.944 (250.5–282.0)
temperature, °C	−19.3 to −23.4
liquid flow rate, std liters/sec (scfm)	24.1–26.7 (51.1–56.6)
vapor flow rate, std liters/sec (scfm)	1.38–1.91 (2.93–4.06)

The average HTU_L value (based on O_2) from the data obtained was 0.15 m (0.5 ft). Figure 2.20 presents the fractionator decontamination factor (based on O_2) versus stripping factor.

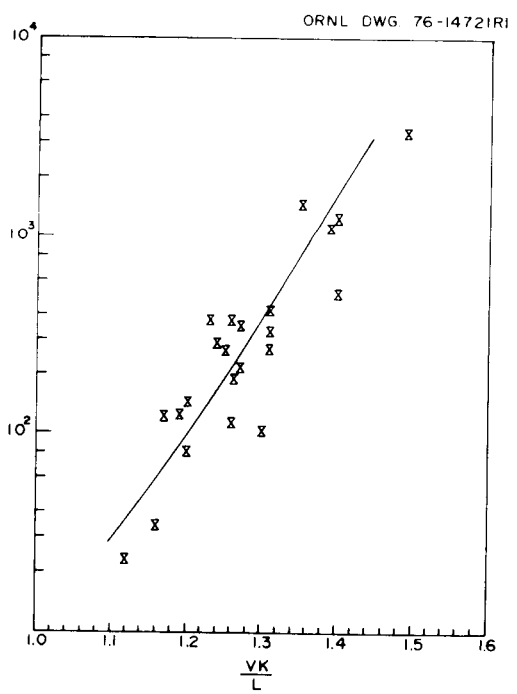

Fig. 2.20. Fractionator Decontamination Factor for Oxygen versus Stripping Factor.

Stripping studies were performed over the following range of operating conditions:

Variable	Range
pressure, MPa (psig)	1.520–1.928 (220.5–279.7)
temperature, °C	−18.6 to −28.1
vapor flow rate, std liters/sec (scfm)	2.44–4.09 (5.18–8.67)
liquid flow rate, std liters/sec (scfm)	22.6–29.3 (47.9–62.1

The average HTU_L value (based on krypton) obtained from these data was 0.21 m (0.7 ft). An empirical correlation relating HTU with pertinent operating variables was found:

$$HTU_L = AL^B / V^C K^D$$

where*

HTU_L = height of a transfer unit based on resistance in the liquid phase, ft,

L = average liquid rate, scfm,

V = average vapor rate, scfm,

K = average Kr equilibrium constant,

A = 1.798,

B = 2.877,

C = 2.138,

D = 3.643.

The resulting correlation had a determination coefficient of 0.88. Figures 2.21 and 2.22 present the pertinent mass transfer information obtained during stripper experiments.

---

*1 ft = 0.305 m; 1 scfm = 0.472 std liters/sec.

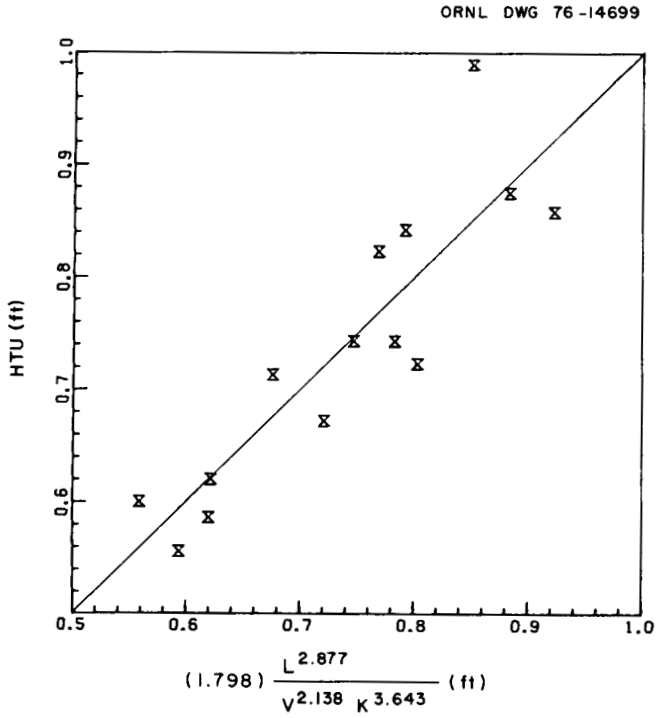

Fig. 2.21. Fit of Experimental HTU Values by Empirical Equation. 1 ft = 0.305 m.

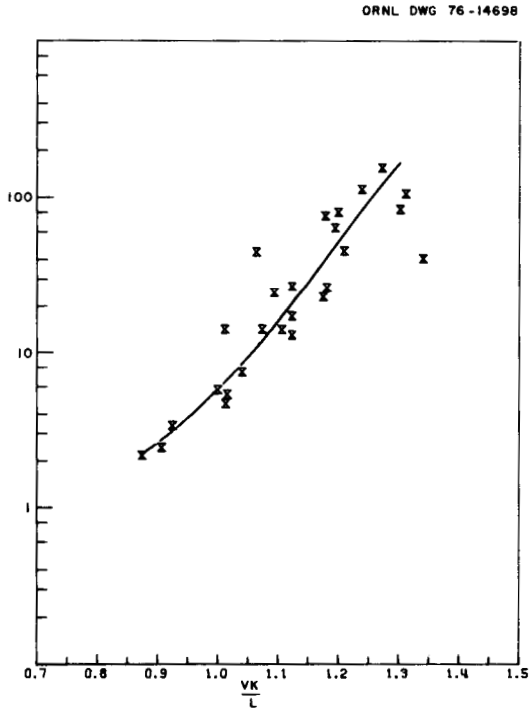

Fig. 2.22. Stripper Decontamination Factor for Krypton versus Stripping Factor.

2.5.1.3 Computer Modeling Studies of KALC — R. W. Glass, R. E. Barker, and J. C. Mullins*

Recent computer studies of the KALC process are in fact the culmination of several related activities. Early models[47] for the KALC system focused on equilibria *per se* and attempted to provide reasonably accurate representation of the known data for CO_2-O_2, CO_2-Kr, and CO_2-Xe binary systems. The early model for use with experimental operations[46] relied on the infinitely dilute attribute for Kr and Xe, and consequently represented the CO_2-O_2 system as per T, P, x, and y and simply "superimposed" the Kr and Xe behavior. Within the accuracy of available data, this model proved extremely valuable for easy and rapid equilibrium calculations. Phase enthalpies, again based on the CO_2-O_2 system primarily, were an integral part of the model, but little use was made of this aspect since column-type calculations were not intended for the model.

Following closely the equilibrium model just described, another model more inclusive and thermodynamically sound was developed to permit multicomponent, multicolumn calculations.[48,49] Thus, in addition to a comprehensive treatment of available data for CO_2-Xe, CO_2-O_2, CO_2-CO, CO_2-N_2, and CO_2-Kr systems, the model included a state-of-the-art method for multicolumn stagewise calculations. Again, phase enthalpies are an integral part of this new model and coupled with the column calculations afford very realistic performances to be studied for different system configurations and operating conditions.

By allowing relativily easy manipulations of feed and side streams and variation in the number of stages for respective KALC columns, and requiring only input that is physically associated with a typical KALC system, the model is both usable and instructive. Little mathematical or theoretical understanding is required. Associated with the column model, a plotting package has been developed to allow McCabe-Thiel type plots for selected components and columns, thus providing a visual interpretation in addition to the numerical results.

---

*Research Participant from Clemson University.

To date, the primary use of the column model has been in the trial association of experimental three-column operations with selected models. In this manner, approximate theoretical stage heights can be determined, and, moreover, once the parameters for simulation have been determined vis-a-vis actual operation, the model can be tested with selected feed rates, feed concentrations, etc. to determine feasible operations for the more costly and time-consuming equipment operations.

Considerable effort has been expended to produce a realistic KALC model, both as regards equilibria and column performance. Just as the earlier equilibrium model proved valuable in interpreting experimental data, the equilibrium portion of the column model has been excised for use in data analyses.[50]

2.6 REFERENCES

1. K. J. Notz, *An Overview of HTGR Fuel Recycle*, ORNL/TM-4747 (January 1976).
2. K. J. Notz, *Selected Studies in HTGR Reprocessing Development*, ORNL/TM-5328 (March 1976).
3. P. R. Kasten, F. J. Homan, E. J. Allen, D. E. Bartine, W. L. Carter, E. H. Gift, J. D. Jenkins, A. L. Lotts, K. J. Notz, A. R. Olsen, R. H. Rainey, J. E. Rushton, and M. L. Tobias, *Assessment of the Thorium Fuel Cycle in Power Reactors*, ORNL/TM-5565 (January 1977).
4. W. L. Carter, K. J. Notz, and R. H. Rainey, *A Comparative Evaluation of Reprocessing Costs for Various Thorium Fuel Cycles*, ORNL/TM-5790 (in preparation).
5. J. W. Snider, D. C. Watkin, and H. Barnert-Wiemer, *An Evaluation of HTGR Primary Burning*, ORNL/TM-4520 (November 1974).
6. P. A. Haas, *HTGR Fuel Reprocessing: A Whole-Block Burner with Recycle of Cooled Gas for Temperature Control*, ORNL/TM-4519 (August 1974).
7. V.C.A. Vaughen, *On the Separation of Silicon Carbide-Coated Fertile and Fissile Particles by Gas Classification*, ORNL/TM-5091 (July 1976).

8. W. S. Groenier, *Calculation of the Transient Behavior of a Dilute-Purex Solvent Extraction Process Having Application to the Reprocessing of LMFBR Fuels*, ORNL-4746 (April 1972).

9. G. L. Richardson and J. L. Swanson, *Plutonium Partitioning in the Purex Process with Hydrazine-Stablized Hydroxylamine Nitrate*, HEDL-75-31 (June 1975).

10. S. B. Watson and R. H. Rainey, *Modifications of the SEPHIS Computer Code for Calculating the Purex Solvent Extraction System*, ORNL/TM-5123 (December 1975).

11. R. H. Rainey and D. B. Watson, "Modifications of the SEPHIS Computer Program for Calculations of the Acid Thorex Solvent Extraction System," *Trans. Am. Nucl. Soc.* 22: 315–17 (1975).

12. R. D. Ackley, J. H. Shaffer, and D. C. Watkin, "Sorption of Tritiated Water and Elemental Iodine from Flowing Liquid CO_2," *Thorium Utilization Program Prog. Rep. Jan. 1, 1974–June 30, 1975*, ORNL-5128, p. 50.

13. A. B. Meservey and K. J. Notz, "Krypton-CO_2 System," *Gas-Cooled Reactor Programs Annu. Prog. Rep. Dec. 31, 1972*, ORNL-4911, pp. 7–8.

14. R. D. Ackley, K. J. Notz, A. B. Meservey, J. T. Bell, and S. R. Buxton, "Laboratory Development," *Gas-Cooled Reactor Programs Annu. Prog. Rep. Dec. 31, 1973*, ORNL-4975, pp. 11–14.

15. R. D. Ackley and J. H. Shaffer, "The Systems Kr-CO_2 and Xe-CO_2," *Thorium Utilization Program Prog. Rep. Jan. 1, 1974–June 30, 1975*, ORNL-5128, pp. 48–9.

16. K. J. Notz and A. B. Meservey, *The Solubility of Krypton in Liquid CO_2*, ORNL-5121 (June 1976).

17. R. D. Ackley and K. J. Notz, *The Distribution of Xenon Between Gaseous and Liquid CO_2*, ORNL-5122 (October 1976).

18. L. M. Toth, J. T. Bell, D. W. Fuller, S. R. Buxton, H. A. Friedman, and M. R. Billings, *Chemistry of the KALC Process. The CO_2-I_2-CH_3I-H_2O System*, ORNL/TM-5656 (November 1976).

19. C. W. Forsberg, "Separation of Krypton from Carbon Dioxide and Oxygen with Molecular Sieves," paper presented at 14th ERDA Air Cleaning Conference, Aug. 2–4, 1976, Sun Valley, Idaho.

20. U. Merten and W. E. Bell, "The Transpiration Method," pp. 91–114 in *The Characterization of High-Temperature Vapors,* ed. by J. L. Margrave, Wiley, New York, 1967.

21. C. B. Alcock and G. W. Hooper, "Measurement of Vapor Pressures at High Temperatures by the Transpiration Method," pp. 325–39 in *Physical Chemistry of Process Metallurgy,* Part 1, ed. by G. R. St. Pierre, Interscience, New York, 1961.

22. U. Merten, "Diffusion Effects in the Transpiration Method of Vapor Pressure Measurement," *J. Phys. Chem.* 63: 443 (1959).

23. J. V. Lepore and J. R. Van Wazer, *A Discussion of the Transpiration Method for Determining Vapor Pressure,* MDDC-1188.

24. W. M. Pardue and D. L. Keller, "Volatility of PuO_2 in Nonreducing Atmospheres," *J. Am. Ceram. Soc.* 47: 610–14 (1964).

25. E. E. McCombs and J. H. Shaffer, "Vapor Transport of Fission Products," *Thorium Utilization Program Prog. Rep. Jan. 1, 1974–June 30, 1975,* ORNL-5128, pp. 35–8.

26. C. L. McCabe and C. E. Birchenall, "Vapor Pressure of Silver," *J. Met.* 5: 707–9 (1953).

27. R. Hultgren et al., *Selected Values of Thermodynamic Properties of Metals and Alloys,* p. 30, Wiley, New York, 1963.

28. R. E. Honig, "Vapor Pressure Data for the Elements," pp. 475–94 in *The Characterization of High-Temperature Vapors,* ed. by J. L. Margrave, Wiley, New York, 1967.

29. A. W. Jenike, *Storage and Flow of Solids,* Bull. 123 of the Utah Experiment Station, Vol. 53, No. 26 (November 1964).

30. B. J. Baxter, General Atomic Co., unpublished results.

31. R. P. Morissette and K. P. Steward, *Recycle Test Element Program Design, Fabrication, and Assembly,* GA-10109 (September 1971).

32. B. J. Baxter, personal communication to V.C.A. Vaughen, Aug. 4, 1975.

33. *Wiederaufarbeitung Thoriumhaltiger Kernbrennstoffe, Jahres-Tätigkeitsbericht 1 Juli 1972 bis 30 Juni 1973,* Kenrforschungs-anlage, Jülich, (August 1973).

34. D. T. Young, *The Use of Fluidized Bed Combustion in HTGR Fuel Reprocessing,* GA-A-13748 (November 1975).

35. C. J. Stairmand, *Trans. Inst. Chem. Eng.* 29: 356 (1951).

36. Pall-Trinity Corp., personal communication to V.C.A. Vaughen.

37. M. J. Bell, *ORIGEN — The ONRL Isotope and Generation Depletion Code*, ORNL-4628 (May 1973).

38. W. Davis, Jr., C. W. Kee, V.C.A. Vaughen, and M. L. Tobias, *Calculating Fission Product Inventories in Peach Bottom FTE-4 Fuel Rods Using the ORIGEN Code*, ORNL/TM-5691 (November 1976).

39. C. L. Fitzgerald, V.C.A. Vaughen, K. J. Notz, and R. S. Lowrie, *Head-End Reprocessing Studies with Irradiated HTGR-Type Fuels: III. Studies with RTE-7: TRISO UC_2-TRISO ThC_2*, ORNL-5090 (November 1975).

40. R. W. Glass, H.W.R. Beaujean, H. D. Cochran, Jr., P. A. Haas, D. M. Levins, and W. M. Woods, "Development of the Krypton Absorption in Liquid Carbon Dioxide (KALC) Process for HTGR Off-Gas Reprocessing," pp. 232-45 in *Proceedings of the Thirteenth AEC Air Cleaning Conference*, San Francisco, August 12—15, 1974, CONF-740807 (March 1975).

41. R. W. Glass, H. D. Cochran, Jr., D. M. Levins, J. W. Snider, D. C. Watkin, W. M. Woods, and M. E. Whatley, *System Features and Component Descriptions for the Unit Operations Off-Gas Decontamination Facility*, ORNL/TM-4596 (February 1975).

42. M. J. Stephenson et al., *System Design Description of the ORGDP LMFBR-HTGR Fuel Reprocessing Off-Gas Decontamination Pilot Plant*, K-GD-873 (September 1973).

43. H.W.R. Beaujean, H. D. Cochran, Jr., V. L. Fowler, T. M. Gilliam, R. W. Glass, D. J. Inman, D. M. Levins, J. C. Mullins, A. D. Ryon, F. H. Wilson, and W. M. Woods, "Engineering Development," *Thorium Utilization Program Prog. Rep. Jan. 1, 1974—June 30, 1975*, ORNL-5128, pp. 55—62.

44. A. D. Ryon, *Demonstration of the KALC (Krypton Absorption in Liquid CO_2) Process: Campaign II at the ORGDP Off-Gas Pilot Plant*, ORNL/TM-5298 (July 1976).

45. T. M. Gilliam et al., *Krypton Absorption in Liquid CO_2 (KALC): Campaign III in the Experimental Engineering Section Off-Gas Decontamination Facility*, ORNL/TM-5655 (in publication).

46. R. W. Glass, H.W.R. Beaujean, V. L. Fowler, T. M. Gilliam, D. J. Inman, and D. M. Levins, *Krypton Absorption in Liquid CO_2 (KALC): Campaign II in the Experimental Engineering Section Off-Gas Decontamination Facility*, ORNL/TM-5095 (February 1976).

47. R. W. Glass, T. M. Gilliam, and V. L. Fowler, *An Empirical Model for Calculating Vapor-Liquid Equilibrium and Associated Phase Enthalpy for the CO_2-O_2-Kr-Xe System for Application to the KALC Process*, ORNL/TM-4947 (January 1976).

48. J. C. Mullins and R. W. Glass, *An Equilibrium Stage Model of the KALC Process*, ORNL/TM-5099 (August 1976).

49. R. W. Glass and R. E. Barker, *A Computer Model for the KALC Process Studies in the ORGDP Off-Gas Decontamination Pilot Plant*, ORNL/TM-5457 (September 1976).

50. R. W. Glass, R. E. Barker, and J. C. Mullins, *A Computer Program for the Calculation of Gas-Liquid Equilibrium in the KALC System CO_2-N_2-CO-O_2-Xe-Kr*, ORNL/TM-5275 (December 1976).

3. REFABRICATION DEVELOPMENT (TASK 300)

R. A. Bradley, W. J. Lackey, K. J. Notz, and J. D. Sease

3.1 INTRODUCTION

Refabrication is that portion of the HTGR fuel cycle that begins with nitrate solution containing recovered ^{233}U and produces quality-assured fuel elements for use in an HTGR. The basic steps in refabrication are similar to those in fresh fuel manufacture and consist of preparation of fuel kernels, application of multiple layers of pyrolytic carbon and SiC, preparation of fuel rods, and assembly of fuel rods into fuel elements. The major difference between the manufacture of fresh fuel and recycle fuel is that the recycle fuel must be fabricated remotely in hot-cell facilities. The HTGR fuel refabrication development program is therefore directed toward the development of processes and equipment for remote application.

The refabrication development task is subdivided into five phases leading to the design, construction, and operation of the HRDF. These development phases are: (1) cold laboratory development, (2) hot laboratory development, (3) cold engineering development, (4) hot engineering development, and (5) cold prototype development. The term cold development refers to work not requiring the presence of radioactivity, while hot development requires the presence of radioactivity. The objective of cold and hot laboratory development is to prove process feasibility. The purpose of cold engineering development is to develop equipment concepts and to demonstrate that acceptable fuel can be produced in reasonably large batches. Hot engineering development will be performed only in those areas where the presence of radioactivity is expected to affect the process, equipment, or product. The objectives for cold prototype development are to establish in-cell equipment configuration and to develop process procedures. The phases will not necessarily be accomplished sequentially. Work during this report period has primarily been in cold engineering development. Work in waste and scrap handling is in the cold laboratory development phase.

The work in refabrication development is subdivided into 11 subtasks parallel to the major systems of the refabrication portion of the HRDF. These are:

1. Subtask 301 — General Development,
2. Subtask 310 — Uranium Feed Preparation,
3. Subtask 320 — Resin Loading,
4. Subtask 330 — Resin Carbonization,
5. Subtask 340 — Microsphere Coating,
6. Subtask 350 — Fuel Rod Fabrication,
7. Subtask 360 — Fuel Element Assembly,
8. Subtask 370 — Sample Inspection,
9. Subtask 380 — Plant Management,
10. Subtask 390 — Waste and Scrap Handling, and
11. Subtask 395 — Material Handling.

The Hot Engineering Development phase of the Refabrication Development Task is reported in Chap. 7. The Cold Prototype Development phase of the Refabrication Development Task is reported in Chap. 8.

3.2 GENERAL DEVELOPMENT (SUBTASK 301) — R. A. Bradley and A. R. Olsen

This subtask is responsible for the coordination and review of all functions of Task 300, providing criteria and technical guidance for the refabrication development activities. In addition, this subtask coordinates the preparation of specifications, Quality Control procedures, material accountability techniques, nuclear material safeguards, criticality control procedures, and safety requirements for all phases of refabrication development as well as coordinating work done in Task 300 in support of recycle fuel irradiation testing.

3.2.1 General Coordination — R. A. Bradley, J. D. Sease, and A. R. Olsen

At the start of this reporting period changes in the National Program Plan were under consideration. The evolution of this program with the end objective of designing, constructing, and operating an HTGR Recycle Demonstration Facility (HRDF) required considerable support. This support included the drafting, review, and distribution of a new phased generic development program outline ["HTGR Fuel Recycle Development

Program — Definition of Development Program Activities and Stages" approved Dec. 5, 1975 (HTGR Program internal document T-11387-TV-Y02-W-0)] and a preliminary document identifying common terminology to be used throughout the program ["HTGR Fuel Recycle Development Program — HRDF Terminology" approved Oct. 24, 1975 (HTGR Program internal document D-11387-TV-Y03-Y-0)]. These were incorporated into the management system.

One phase of the development involves Hot Engineering tests. With the removal of hot pilot plants from the program we analyzed the minimum hot engineering test requirements. This analysis and proposal evolved into the Hot Engineering Test Facility (HETF) Project discussed in Chap. 7. Coordination of the criteria preparation and continuing support of the conceptual design were provided by this subtask.

The fabrication of fuel for the proposed irradiation experiment "Early Validation Test 1" was monitored. Details of this effort are discussed in Sect. 3.5.4.5 of this report. Future work including the irradiation and postirradiation testing will be monitored to ensure incorporation of significant findings in the various subtask development activities.

In keeping with the changes in the National program, revisions have been made in the Summary Work Plans and Schedules for Task 300. At the end of this period new detailed experimental programs for each subtask were under review.

3.2.1.1 Reference Recycle Resin Loading Flowsheet Determination — J. A. Carpenter, Jr., and J. D. Sease

A joint ORNL-GA committee met at ORNL June 7—9, 1976, to weigh the relative merits of the two methods developed for loading of uranium onto weak-acid resin microspheres from which fissile fuel kernels are produced. The committee recommended the selection of the amine extraction method over the ammonia neutralization process as the reference for recycle fuel fabrication.

Before the meeting, a series of carbonization and conversion tests was given batches of resin prepared by both methods. Using the results of the tests and other data, the committee reviewed all aspects

of process, waste, effluents, fuel performance, and equipment complexity and costs. Each method was judged according to a list of 32 criteria. The following differences were established.

1. The residual nitrogen content is higher in the ammonia neutralization particle.

2. The ammonia neutralization particles tend to vary more in the content of uranium per unit volume.

3. More ammonia neutralization particles are cracked in the converted state.

4. The ammonia neutralization particle has a lower crushing strength in both the carbonized and converted states.

5. The ammonia neutralization particle is denser after conversion.

6. The amine extraction method is slightly more complicated and as a result the capital costs are higher.

7. To date, kernels made with the amine extraction flowsheet using Duolite C-464 resin have too low a density to meet 3000-MW(t) HTGR loading requirements.

The recommendation of the amine extraction method was based primarily on a modest superiority of this process in minimizing rejection caused by particle breakage and maximizing interparticle loading uniformity. The ammonia neutralization process was judged to be slightly superior to the amine extraction process with respect to space requirements and process complexity, but these differences were too small to overcome the superiority of the amine extraction process in product quality.

An internal distribution report detailing the deliberations of the committee was written.

3.2.2 Specification and Quality Control Development

3.2.2.1 Specification Development — A. R. Olsen and W. H. Pechin*

Specification development is a primary function of this subtask in that it combines both functional requirements and practical process limitations to define development goals. In the past the HTGR Recycle Fuel Product Specifications were emphasized. Interim I specifications[1] were issued in January 1975. Resolution of review comments was to result in issuance of Interim II specifications. However, because of the close relationship between fresh fuel specifications and recycle fuel specifications an agreement was reached whereby future modifications will be issued by GA after review and concurrence by ORNL and ERDA. Detailed reviews have continued throughout this reporting period, together with the preparation of an HTGR Fuel Product Specification Support document. Publication of both the support document and revised product specifications is currently scheduled for calendar year 1977.

In the meantime Interim II specifications for uranyl nitrate feed solutions have been drafted, reviewed, revised, and issued: S-001, "Interim II Specifications for ^{233}Uranyl Nitrate Feed Solution to the Resin Loading Process," and S-002, "Interim II Specifications for Recycle ^{235}Uranyl Nitrate Feed Solution to the Resin Loading Process." The broad influence of the specifications is borne out in two examples: they impose purity goals for the reprocessing portion of the recycle plant and may impose accuracy limitations on the nondestructive homogeneity analysis of the fabricated fuel rods. Although the Interim II specifications are satisfactory for current development program plans, they do contain values still to be verified with further development.

3.2.2.2 Quality Control Development — F. L. Layton and D. A. Costanzo

A cooperative effort has been under way with GA to develop standardized quality control procedures. As part of this effort a manual entitled "Laboratory Procedures for the Analysis of HTGR Fuels

---

*Present address, Office of Waste Isolation, Union Carbide Nuclear Co., Oak Ridge.

and Materials" has been compiled. This manual provides information concerning some analytical methods used by the Analytical Chemistry Division of ORNL in the chemical characterization of various HTGR fuel materials. As new methods pertaining to HTGR-type samples are developed and demonstrated to be reliable, they will be included in this manual.

3.2.3 Safety and Safeguards Evaluation

3.2.3.1 Environmental, Safety, and Safeguards Evaluation — Refabrication Effluents — M. S. Judd*, A. R. Olsen, and J. E. Till

Initial work aimed at identifying the types and quantities of chemical and radioactive effluents that would be released from a reference fuel refabrication facility was concluded and a report[2] issued. This work identified many questions concerning effluents to be answered by further refabrication development work. Much of that latter work was done in this period and is discussed in detail in Sect. 3.5 under the various subtasks.

Work by the Environmental Sciences Division to assess the potential radiological impacts of released ^{233}U with ^{232}U and its decay products from a model HTGR fuel recycle plant and the radiotoxicity of HTGR recycle fuel relative to recycle LMFBR fuel or freshly reprocessed LWR fuel was continued. Three new reports on these topics were published;[3—5] the findings were essentially those discussed previously.[6]

Work along the lines above will be broadened in the next period to a generic study of the potential environmental impacts of effluents from a large HTGR fuel recycle plant, including both reprocessing and refabrication. This work will focus on the HRDF as the model plant and will be done in anticipation of the Environmental Impact Statement that will be needed for that facility.

The needed environmental assessment for the hot engineering test phase of the refabrication development program is being done in the program management and analysis task (Sect. 1.3.2 of this report) to combine it with the reprocessing activities in the same facility.

---

*Present address, U.S. Steel Corp., Monroeville, PA.

3.2.3.2 Polynuclear Aromatic Hydrocarbon Emissions from HTGR Fuel Production — W. H. Griest, H. Kubota, and D. A. Costanzo

A cooperative program involving Industrial Hygiene, Analytical Chemistry, and Metals and Ceramics has been initiated to evaluate the hazard associated with the potential release of carcinogens from fuel fabrication processes. Certain steps in the process for fabrication of HTGR fuel elements produce large quantities of hydrocarbons. These hydrocarbon emissions most likely contain appreciable quantities of polynuclear aromatic hydrocarbons (PAH), some of which may possess undesirable biological activities. Samples were collected at points posing the greatest potential for fugitive PAH emissions such as during furnace operation and on disassembly. The samples are screened by measurement of the fluorescence of the gross sample at the benzo-a-pyrene (BaP) emission wavelength. At most sampling points, the results suggested that emissions were below 0.2 μg BaP/m^3, an unofficial guideline. Other samples are being collected and analyzed as the production operation permits.

3.2.3.3 Criticality Analysis — S. R. McNeany

The criticality of a resin carbonization furnace containing moist resin beads loaded with ^{233}U was studied. The effective neutron multiplication factor (k_{eff}) was calculated for three different sized resin carbonization furnace designs. The purpose of these calculations is to illustrate the effect of furnace diameter and particle-bed water content on k_{eff}. It is important to note that these calculations show only the sensitivity of k_{eff} to various system changes; they do not give k_{eff} for the worst possible criticality condition.

A description of the system calculated is given below.

1. The furnace contains 7.0 kg ^{233}U in the form of loaded resin particles (i.e., size of two batches in a 22.9-cm furnace).

2. The loaded resin beads have not been dried and consequently contain 30 wt % H_2O.

3. The wet resin particle density is 1.88 g/cm^3 with uranium weight fraction at 0.329.

4. The particles are in a close-packed bed with a 62% volume packing fraction.

5. A neutron reflector consisting of a particle container, insulating fire brick, and a perchloroethylene cooling jacket surrounds the particle bed.

Table 3.1 gives the calculated k_{eff} for systems that contain void or H_2O in the interstitial spaces of the particle bed for three furnace diameters. In the case where H_2O fills the interstitial volume, 6.93 liters (1.83 gal) of H_2O is needed.

Table 3.1. Criticality of ^{233}U-Loaded Resin Carbonization Furnace

Particle Bed Dimensions			Calculated k_{eff}	
Diameter		Height (mm)	Interstitial Void	Interstitial H_2O
(mm)	(in.)			
127	5.0	1441	0.437 ± 0.005	0.772 ± 0.006
178	7.0	735	0.643 ± 0.005	1.030 ± 0.007
229	9.0	445	0.785 ± 0.007	1.176 ± 0.006

Two additional calculations were performed on a 178-mm-diam furnace to examine the effect on criticality due to particle bed saturation with perchloroethylene. In one case, the interstitial spaces were filled with pure C_2Cl_4, while the other contained C_2Cl_4 mixed with 10 wt % kerosene (13,200 ppm H in mixture). The results of these calculations yielded system k_{eff} of 0.583 ± 0.005 and 0.637 ± 0.004 respectively.

The calculations were performed with the KENO IV Monte Carlo criticality code[7] using the 16-group Hansen-Roach[8] cross section set. For comparison, the calculations were also done with a 123-group ENDF/B-IV derived set of cross sections.[9] The ENDF set generally gave results that were 10% higher than the Hansen-Roach results for all cases.

Conclusions arrived at from this work include the facts that the furnace k_{eff} is highly sensitive to the furnace diameter and the hydrogen

content of the particle bed, and that a large double-batched furnace can be easily made critical by the addition of water to the particle bed. Also, particle bed saturation with perchloroethylene has a poisoning effect on the system, even when the perchloroethylene is homogeneously mixed with 10 wt % kerosene.

Note that the above calculations were performed to provide general guidance for conceptual design decisions and that they do not necessarily represent situations that will be encountered in an operating facility. For instance, the assumption of a double batch size of 7.0 kg ^{233}U may be realistic for a 22.9-cm furnace, but it is excessively large for a smaller furnace.

A report describing all the criticality work done at ORNL in the past two years in the area of HTGR fuel refabrication is currently being prepared. This report will describe in detail the calculations that have been performed.

3.2.3.4 Material Flow Modeling — S. R. McNeany

The HTGR Fuel Refabrication Task includes the development of material flow modeling capability to aid in the design of a refabrication demonstration plant. The goals of this modeling capability are first to generate the average relative flow streams within a plant for the purpose of equipment design and plant layout and second to aid in the development of an efficient material accountability system. As previously reported,[10] a computer program named NOMUF was written to estimate time-averaged uranium and thorium flow rates through a generalized model of a fuel refabrication facility. The program fulfills in part the goals of the material flow modeling development. Building upon this base, a new computer program named WATCHDOG has been written to extend the treatment of NOMUF to a more generalized model that examines the time-dependency of material locations. Currently this dynamic model simulates the transport of a single material through a batch-operated process of a user-specified system. For example, a model of a proposed HTGR fuel refabrication facility has been constructed and run on the ORNL

computers. The primary output of the code consists of a table listing the history of material transfers.

One possible application of the simulation model could be as a monitor for material diversion or errors in material transfer. Another use could be as an estimator of material quantities in unmeasured areas.

As both NOMUF and WATCHDOG have been written in a generalized manner, they could be used for analysis of material flows through other types of facilities in different fuel cycles.

3.2.3.5 Radiation Level Analysis — R. M. Young

Work related to radiation level analysis focused on the development of an analytical tool for computing gamma-ray dose rates and the shield effectiveness for certain nuclear materials. Such tasks precede the formulation of a calculational method to determine radiation guidelines for the design of fuel fabrication equipment. Activity included the following:

1. modification of the PUSHLD atomic-nuclear data library,[11]
2. application of USHLD, the revised PUSHLD to Thorium-Uranium fuel, and
3. the determination of gamma-ray shield effectiveness.

The computer code PUSHLD has three-dimensional capability and the capacity to calculate gamma dose rates from plutonium for various source and shield geometries. The program also treats varying source composition, shield thicknesses, and isotopic ages following chemical purification. Shield materials include those typically required for hot-cell and glove box construction.

The modifications to the PUSHLD library included the substitution of basic uranium shielding data for the plutonium data that was incorporated in the code, and the assembly of gamma-ray energies and intensities for all heavy nuclides associated with ^{233}U-Th fuels.

Dose rates computed with USHLD for a typical ^{233}U-Th fuel rod compared favorably with results obtained by other methods.

As illustrated in Fig. 3.1, the shield effectiveness of several materials was also examined. In order of increasing gamma-ray attenuation, the shields include the following: (1) Lucite, (2) safety glass, (3) steel, (4) lead glass, and (5) lead.

To demonstrate application of the methodology being developed, ^{233}U-Th radiation levels within the Hot Engineering Test Resin Carbonization System are to be determined.

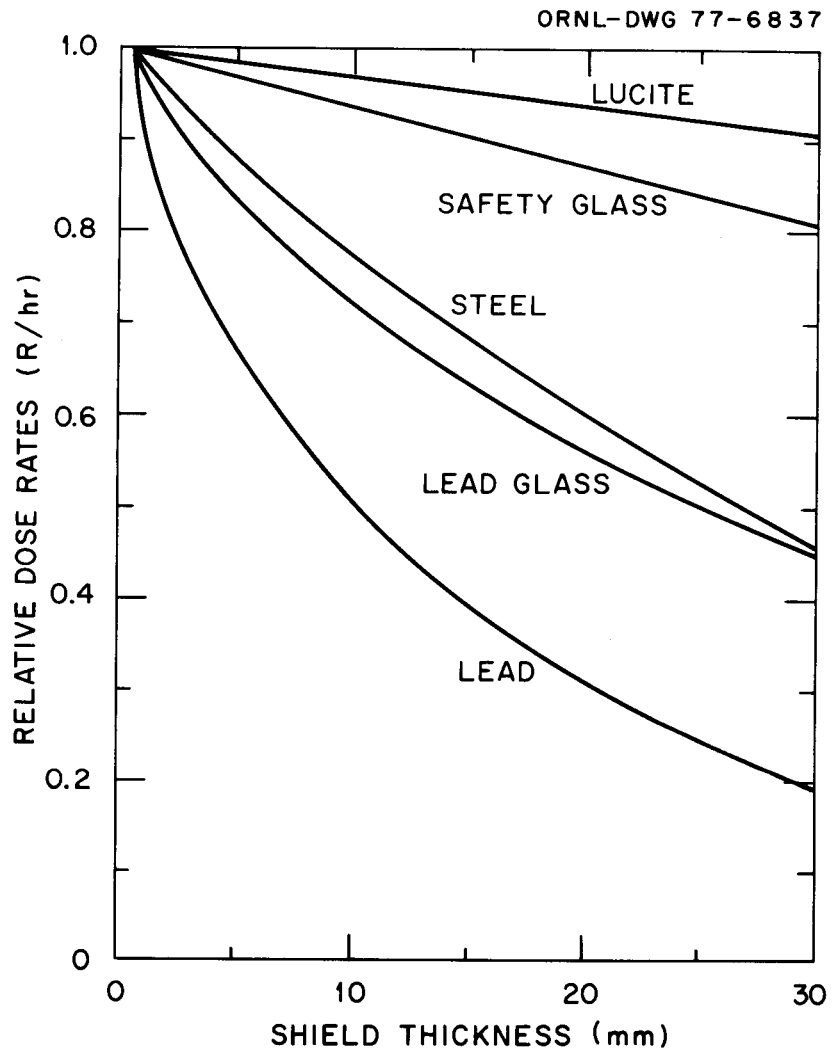

Fig. 3.1. Gamma-Ray Attenuation of a ^{233}U-Th Source for Various Shield Materials.

3.3 COLD LABORATORY DEVELOPMENT

3.3.1 Resin Loading — J. H. Shaffer

As developed by the Thorium Utilization Program, microsphere fuel kernels for refabricated HTGR fuel elements will be prepared from spherical cation exchange resins that have been fully loaded with ^{233}U. Engineering development of the resin loading process is based on contacting weak acid resin, in its hydrogen form, with acid-deficient uranyl nitrate (ADUN) in a recirculating system. Side-stream loops from the uranyl nitrate feed tank will be concentrated by evaporation and contacted with an immiscible amine extractant for partial removal of nitrate ion.[12] Laboratory development, in support of this engineering process, has been directed toward evaluations of associated reaction equilibria and of process parameters that affect the relative rate at which full resin loading can be achieved. Two resins, Amberlite IRC-72 and Duolite C-464, have been used in these studies.

3.3.1.1 Resin-Uranyl Nitrate Reaction Equilibria — J. H. Shaffer

Chemical development for the resin loading process has been based on a systematic study of the reaction of the two commercially available weak acid resins, in hydrogen form, with uranyl nitrate solutions under equilibrium conditions at various fractional resin loadings. Although the resin loading reaction may be complicated by the hydrolysis of uranyl ion, it was treated in this study as the simple metathesis,

$$UO_2^{2+} + 2HR \rightleftharpoons UO_2R_2 + 2H^+ , \qquad (1)$$

where R denotes the anionic resin group in the solid phase. Equilibrium quotients were calculated from the equation,

$$K_Q = [UO_2R_2][H^+]^2/[HR]^2[UO_2^{2+}] . \qquad (2)$$

The concentrations in the resin phase were expressed as molar quantities based on the solid volume of resin in its hydrogen form; however, these

may be expressed as bulk quantities by use of a measured 60% packing fraction for the resin. Hydrogen ion concentrations were calculated from pH measurements over the range from about 0.1 to 3.5 pH units. The molar concentration of uranyl ion in solution was assumed equivalent to the total uranium concentration. Each test series was conducted at a constant nitrate concentration, and the respective value of K_Q was determined by linear regression analysis of Eq. (2) in its logarithmic form. These experimental values for K_Q obtained for each resin at 30 and 40°C at nitrate concentrations of 0.2 to 2.5 *N* are shown in Table 3.2. As noted, values for K_Q show a significant dependence on the nitrate ion concentration in solution and probably reflect the hydrolysis in the uranyl nitrate system.[13]

Table 3.2. Equilibrium Quotients Calculated for the Uranium Loading of Weak-Acid Resins from Uranyl Nitrate Solution

Temperature (°C)	Nitrate (*N*)	K_Q, Equilibrium Quotient, × 10^4		
		Best Value	95% Confidence Limits	
		Amberlite IR-72		
30	0.2	3.0	5.0	1.8
	0.6	4.3	5.3	3.3
	1.0	6.7	8.3	5.3
	1.6	23	30	17
	2.0	48	77	30
40	0.2	5.0	9.0	2.8
	0.5	6.0	8.2	4.5
	0.9	12	18	7.3
	1.5	33	75	14
	1.8	43	130	15
		Duolite C-464		
30	0.2	5.0	8.0	3.2
	0.6	9.3	22	4.0
	1.0	16	33	7.7
	1.5	48	140	17
	2.0	77	160	38
	2.3	280	530	150
40	0.2	6.5	12	3.7
	0.6	11	18	6.2
	0.9	16	25	11
	1.5	50	120	20
	1.8	57	130	23

3.3.1.2 Thorium Distribution — J. H. Shaffer

Since ^{233}U originates by neutron irradiation of thorium as the fertile component of the HTGR core loading, the uranyl nitrate product stream from the fuel reprocessing plant will likely contain thorium as an impurity. Although this event will not have a deleterious effect on the refabricated fuel, the distribution of thorium relative to that of uranium on the resin is an important process consideration. An experimental program, similar to that used for uranium equilibrium studies, was begun to investigate the behavior of thorium as an impurity in uranyl nitrate solutions under conditions that would yield essentially full loading of the resin with uranium. Tests at constant uranium and nitrate concentrations having thorium concentrations of 0.15 to 1.5 wt % with respect to uranium have been conducted at 30 and 40°C with Amberlite IRC-72 resin.

The effect of hydrolysis on the exchange reaction with thorium[14] is probably more pronounced than that observed with uranium. However, this effect may require more extensive examination of the uranium-thorium nitrate system for solution. Data obtained thus far in this program were treated according to the reaction,

$$Th^{4+} + 2UO_2R_2 \rightleftharpoons ThR_4 + 2UO_2^{2+} , \qquad (3)$$

where R denotes the solid resin phase. Values for the equilibrium quotient for this reaction were calculated from the expression,

$$K_Q = \frac{[ThR_4]}{[Th^{4+}]} \cdot \frac{[UO_2^{2+}]^2}{[UO_2R_2]^2} , \qquad (4)$$

using molar quantities for thorium and uranium on the resin phase that were based on the solid volume of resin (60% of bulk volume) in its hydrogen form. Aqueous phase concentrations were expressed as molar quantities. Equilibrium quotients calculated from data obtained at 30 and 40°C at nitrate ion concentrations of 0.2 to 2.0 *N* are given in Table 3.3. The magnitude of these constants by comparison with

Table 3.3. Equilibrium Quotients Calculated for the Replacement of Uranium by Thorium on Amberlite IRC-72 Cation Exchange Resin that had Been Fully Loaded with Uranyl Ion from Nitrate Solution

Temperature (°C)	Nitrate ion (N)	K_Q
30	0.2	53 ± 9
	0.6	73 ± 16
	0.9	32 ± 2
	1.6	6.7 ± 2.5
	1.9	3.4 ± 1.3
40	0.2	18 ± 3
	0.6	22 ± 6
	1.0	16 ± 4
	1.7	5.2 ± 0.9
	2.0	5.2 ± 0.2

those obtained for uranium alone illustrates that thorium as an impurity in the uranyl nitrate feed stream of the resin loading process will be preferentially loaded onto the resin.

3.3.1.3 Resin Loading Rates — J. H. Shaffer and R. B. Evans III

The resin loading process must be located within a hot cell enclosure for attenuation of energetic gamma rays associated with decay products of the ^{232}U impurity (∿1000 ppm) in the ^{233}U obtained from the fuel reprocessing plant. Quality control of the resin loading process will be aggravated by the remote control procedures necessary for plant operation. Consequently, an experimental program was conducted as a quality assurance measure to examine the effects of process parameters on the relative rate of resin loading as a means of predicting process time requirement.

The experimental assembly consisted of a small jacketed column fitted with a porous glass plate to retain the resin. The column was loaded with selected volumes of sized Amberlite IRC-72 in its

hydrogen form. For experimental expedience the tests were conducted with downflow of uranyl nitrate feed solution in place of upflow conditions proposed for the pilot plant process. Heated water was circulated through the column jacket and through a heat exchanger in the feed stream to maintain a constant reaction temperature of 30°C. Fifteen experiments were conducted, in which resin volumes varied from 50 to 125 cm^3, feed flow rates ranged from 3 to 40 cm^3/min, and feed solutions had nitrate ion concentrations of 0.5 to 2.0 *N*, with overall compositions that would yield full resin loading. The resin beds had length-to-diameter ratios of 2.2, 3.4, and 5.6.

The results of a preliminary experiment in which a small quantity of resin was contacted with uranyl nitrate solution under constant chemical driving force revealed that the distribution of uranium within the resin particle corresponded to a diffusional process. For simplicity, the data from the flow experiments were analyzed for film resistance and for first-order reversible reaction to approximate the diffusion process.

The rate of resin loading, dC_τ/dt, where C_τ is the molar concentration of uranium in the solid resin, was suitably described by the equation

$$\frac{dC_\tau}{dt} = \frac{kQ}{V_2}\left(C_1 - \frac{C_\tau}{K}\right) \tag{5}$$

for each experimental run and yielded a value for the relative reaction velocity constant, k, of 0.56 ± 0.07/min. For this evaluation the feed flow rate, Q, had units of liters/min and the solid resin volume, V_2 (liters), was 60% of the bulk resin volume. Uranium in the aqueous phase, C_1, was expressed as moles U per liter solution. The unique feature of Eq. (5) is that the constant, K, is defined by the distribution C_τ^*/C_0, where C_τ^* is the concentration of uranium on the resin that will be in equilibrium with the feed concentration, C_0, and may be calculated from the equilibrium quotient defined by Eq. (2). The kinetic description of the flow system was obtained by putting Eq. (5) into the general equation,

$$V_1 \frac{dC_1}{dt} = Q(C_0 - C_1) - V_2 \frac{dC_\tau}{dt} \tag{6}$$

where V_1 (liters) is the volume of the aqueous phase. The integrated rate equation,

$$C_1(t) = C_0 + \alpha_1 e^{S_1 t} + \alpha_1 e^{S_1 t} + \alpha_2 e^{S_2 t} \ , \tag{7}$$

describes the concentration of uranium in the aqueous effluent stream as a function of time. The roots S_1 and S_2 can be calculated from the equation

$$S_{1,2} = \frac{-(\beta_1 + \beta_2 + \beta_3) \pm \sqrt{(\beta_1 + \beta_2 + \beta_3)^2 - 4\beta_1\beta_2}}{2} \ . \tag{8}$$

The $\alpha_{1,2}$ values are:

$$\alpha_1 = \frac{\beta_1 C_0}{S_1 - S_2}\left(1 + \frac{\beta_2}{S^1}\right) \ ,$$

and

$$\alpha_1 = \frac{\beta_1 C_0}{S_1 - S_2}\left(1 + \frac{\beta_2}{S^1}\right) \ .$$

The definitions of β_1, β_2, and β_3 in terms of system parameters are:

$\beta_1 = Q/V_1$

$\beta_2 = kQ/V_2K$

$\beta_3 = kQ/V_1$.

The values for the beta terms applicable for a 4-kg U/day pilot plant are well within the range of those calculated from the experimental data. For reactions approaching instantaneous equilibrium, $C_\tau \rightarrow C_\tau^*$ as $C_1 \rightarrow C_0$ and the time required for full resin loading may be calculated from Eq. (7). However, values for $C_\tau(t)$ may be developed through substitution of Eq. (7) into Eq. (5) and integration over the time interval, 0 to t.

The mathematical evaluation of the experimental data for film resistance yielded coefficients that were lower by a factor of 100 than those that could be predicted for the system. Nevertheless, the quickly attained equilibrium of the aqueous and resin phases together with the relatively low value of the equilibrium quotients, *K*, for this system had the net result of a pseudo-film resistance on the loading process. However, maximum experimental flow rates could have been advanced by a factor of 10 without significant effect from true film resistance.

3.3.1.4 Slurry Loading of Weak-Acid Resin with Uranium in a Continuous Column — K. J. Notz and J. H. Shaffer

Full loading of weak acid resin with uranium from a suspension of UO_3 in uranyl nitrate solution was demonstrated in a countercurrent, continuous resin column of the Higgins type. Also, a gross excess of UO_3 in the suspension did not adversely affect the operation of the column.

There are numerous ways of loading weak-acid (carboxylate) ion exchange resins with uranium,[15] all of which are based on neutralization or removal of acidity, since protons compete strongly for exchange sites in the loading equilibrium:

$$2RH + UO_2^{2+} \rightleftharpoons R_2UO_2 + 2H^+ .$$

The original method,[16] using UO_3 to neutralize acid, is a batch operation, which starts with a slurry of UO_3 in uranyl nitrate solution and finishes with a clear liquor with a NO_3^-/U ratio of approximately 1.5. It has been shown that this method could be applied to column loading by reacting UO_3 and uranyl nitrate solution in a separate vessel to produce liquor with a NO_3^-/U ratio of about 1.5, then circulating this liquor through the column, and returning the effluent to the UO_3 contactor.

Another loading method, which has much potential incentive, is based on partial thermal denitration to yield directly a product with a NO_3^-/U ratio of about 1.5, without going through complete denitration to UO_3. Laboratory and bench-scale experiments showed, however, that

under the conditions of temperature and concentration required to attain the necessary NO_3^-/U ratio, a two-phase system resulted. The product was a suspension of a hydrated UO_3 in molten uranyl nitrate, which on cooling and dilution in water yielded a suspension of hydrated UO_3 in a nitrate solution. If the overall NO_3^-/U ratio exceeded 1.5, the suspension would eventually dissolve. By analogy with the direct UO_3 method, such a suspension could also be used for batch loading of weak-acid resin.

The objective of this work was to determine if slurries or suspensions of the type described above could be used to load weak-acid resin in a continuous, countercurrent column. Two experiments were conducted: one to load the resin with a small amount of suspended UO_3 in the slurry, and one to operate with a large amount of suspended solids present. The 25-mm-diam (1-in.) laboratory column and the general procedures have been described previously, including the loading of weak-acid resin from a pre-equilibrated solution of acid-deficient uranyl nitrate.[15] The effective loading length of the column is 1.8 m (6 ft).

The objective of the first run was to use a moderate to light suspension of solids (UO_3 in uranyl nitrate solution) to demonstrate the principle. A loading rate of 100 g U/hr was desired; this rate is equivalent to 120 kg U/day in a 0.13-m-diam (5-in.) column with 3.7 m (12 ft) of effective loading length. Since the resin (in its H^+ form) has a capacity of 400 g U/liter, the corresponding resin pulse rate in the laborabory column is 250 ml/hr; this gives a residence time of almost 4 hr.

Before starting the test run, the column of resin (Amberlite IRC-72) was brought to a steady-state operating condition with acid-deficient uranyl nitrate, as described previously.[15] This was done so that the test run could be evaluated under steady-state conditions. Start-up differs from steady state only in that the resin is not pulsed for 2 hr to allow the front to load before it is pulsed out of the loading region. The feed suspension was made up by stirring UO_3 hydrate with about 1.1 *M* $UO_2(NO_3)_2$ solution. Two batches were made, with these analyses:

	U(g/liter)	NO_3^-(g/liter)	U(*M*)	NO_3^-/U ratio
1st Feed	360	133	1.51	1.42
2nd Feed	374	147	1.57	1.51

These feed batches were stirred overnight at ambient temperature, during which about half the UO_3 went into solution. The feed was thus a solution about 1.3 *M* in U with a NO_3^-/U ratio of about 1.7, containing a suspension of UO_3 that was about 0.2 *M*. During the loading run the feed was stirred constantly to keep the UO_3 in suspension.

The test run was carried out over a 4-hr period; it was continued until the feed ran out. The column was warmed to about 50°C (with heating tapes) to simulate standard procudure as practiced with both amine extraction and UO_3 batch loading. Feed was introduced at 14 to 17 ml/min, wash water was fed at 24 to 40 ml/min, and resin was pulsed at 300 to 330 ml/hr. During the run, conductivity measurements indicated that the exchange front remained fairly stationary within the column. Uranium utilization was about 37%. During the run, the washed, loaded resin product was almost free of suspended uranium; analysis of the pulse water, which carried the loaded resin out of the column, showed only 0.63 g U/liter.

After the run was completed, all residual liquor and suspension was washed out, and the resin was sampled every 0.15 m (6 in.). The resin samples were dried and analyzed for uranium content, with the results shown in Table 3.4 and Fig. 3.2. This profile is essentially identical to the one obtained previously with pre-equilibrated feed.[15] Two product samples obtained during loading analyzed 46.64 and 47.18 wt % U (normalized to zero % loss on drying). For Amberlite IRC-72, full loading (i.e., utilization of all available exchange sites) yields 47.0 ± 0.5% U.

Properly operated, a continuous column with slurry or suspension feed will yield a clear effluent, as shown above, since acid released during loading will dissolve any UO_3 still present. In case of extreme unbalance between uranium feed rate and resin pulse rate, excess UO_3 could work its way to the effluent point. A second run demonstrated that such a condition could be handled physically. In this run, the resin pulse rate was decreased to about 200 ml/hr, while the uranium

Table 3.4. Analysis of Slurry-Loaded Resin

Sample[a]	U content (%)[b]	Remarks
1	47.15	In washing section
2	47.20	In washing section
3	47.43	In washing section
4	47.40	Feed inlet point
5	47.22	
6	46.55	
7	46.28	
8	45.55	
9	44.16	
10	42.18	On either side of U-bend at bottom;
11	29.95	0.30 m (12 in.) apart
12	17.91	
13	15.28	
14	12.15	
15	9.47	Effluent outlet point

[a]Samples taken every 0.15 m (6 in.), except as noted.

[b]Normalized to zero % LOD (loss on drying at 110°C), where the LODs ranged between 0.21 and 2.15%. This is our standard procedure, to compensate for variations in drying before actual analysis.

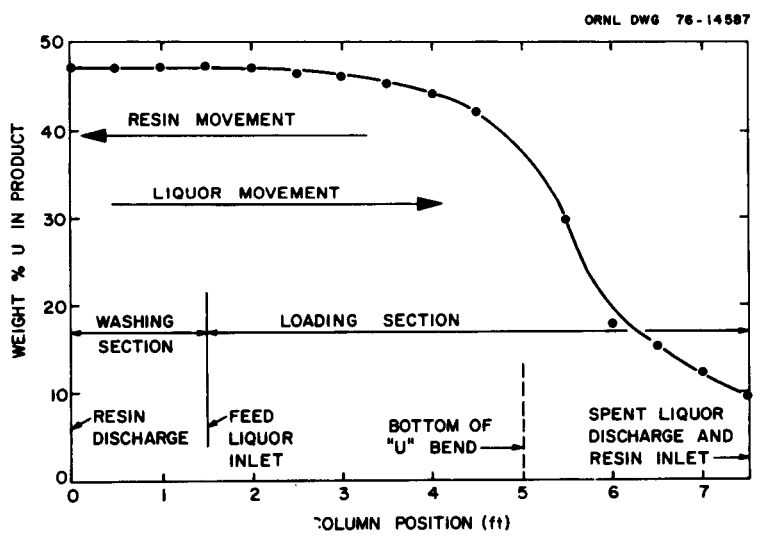

Fig. 3.2. Uranium Content of Resin as a Function of Column Location. 1 ft = 0.305 m.

feed rate was kept about the same. In 1.5 hr UO_3 suspension appeared in the effluent and continued for the balance of the run (another 1.5 hr). There was no adverse effect during the run, and the product showed a normal content of 47.07 wt % U.

3.3.1.5 Resin Loading With ^{235}U — J. H. Shaffer

Facilities for resin loading with fully enriched ^{235}U (650 g U batch size) have been maintained for support of in-reactor tests of the HTGR base program. Approximately 3 kg of resin was prepared for this program during this report period.

3.3.1.6 Density, Acidity, and Conductivity Measurements of Uranyl Nitrate-Nitric Acid Solutions — J. L. Botts and D. A. Costanzo

The reference kernel of HTGR recycle fuel particles is prepared by loading a weak-acid resin (carboxylic acid exchange groups) with uranium from an acid-deficient nitrate solution, by the exchange reaction: $UO_2{}^{2+} + 2HR \rightleftharpoons UO_2R_2 + 2H^+$. The degree of loading of the uranium on the resin depends primarily on the acidity of the solutions.[12] The measurement of the acidity and the uranium content of these solutions is important to the process control of the resin loading. Therefore, it is desirable to continuously monitor solution properties — such as acidity, density, or conductivity — which can be used to control the process to obtain maximum loading efficiency.

Two experiments were conducted. In the first, measurements were obtained from a wide range of uranium (0.05—1.0 *M*) and nitrate (0.1—2.0 *M*) concentrations under acid-deficient and acid-excess conditions. A second set of measurements more closely simulated process conditions of uranium concentration (0.1—0.5 *M*), nitrate concentration (0.15—1.0 *M*), and solution acid deficiency NO_3/U ratio (1.56—2.00).

Computer techniques were used to obtain least squares fits of the acidity, density, and conductivity as functions of temperature, and two programs were written to relate these solution properties to the uranium and nitrate concentrations. The conditions of these experiments

together with the data accumulated and the conclusions are given in detail elsewhere.[17] Representative data for the above quantities are shown in Fig. 3.3.

3.3.2 Sample Inspection (Subtask 370) — D. A. Costanzo

The Sample Inspection System must provide the facilities and techniques for adequately characterizing the refabricated fuel particles and rods. During this period the development of methods to determine the entire heavy metal content of samples as well as the defective particle fraction was pursued. Also developed were procedures for determining the sulfur content of fuel rods and the thorium carbide content of partially converted thorium oxide fuel particles. Procedures for 25 analyses were included in an HTGR Procedure Manual.

3.3.2.1 Determination of Defective Particle Fraction — D. E. LaValle and F. L. Layton

At the beginning of this reporting period the number of particles with defective coatings was determined routinely on unirradiated fuel specimens by chlorination for 2 hr at 1500°C. Irradiated specimens were chlorinated in a hot cell at 1000°C for unspecified periods of time. Both methods have been described.[18]

The chlorination method has also been applied experimentally during this period to study the influence of carbon monoxide on the leach rate. The rate of removal of fuel from the defective particles progressively increased with increasing carbon monoxide concentration until two-thirds of the total amount was removed in 7 hr compared with overnight runs previously required.

Also under study was the reaction of chlorine with the SiC coating of Triso-coated fuel particles. At 1050°C the silicon was driven off as $SiCl_4$, leaving an intact porous layer of elemental carbon.

Experiments on the permeability of the carbon coatings and possible damage to the coatings by chlorination at 1500°C demonstrated that

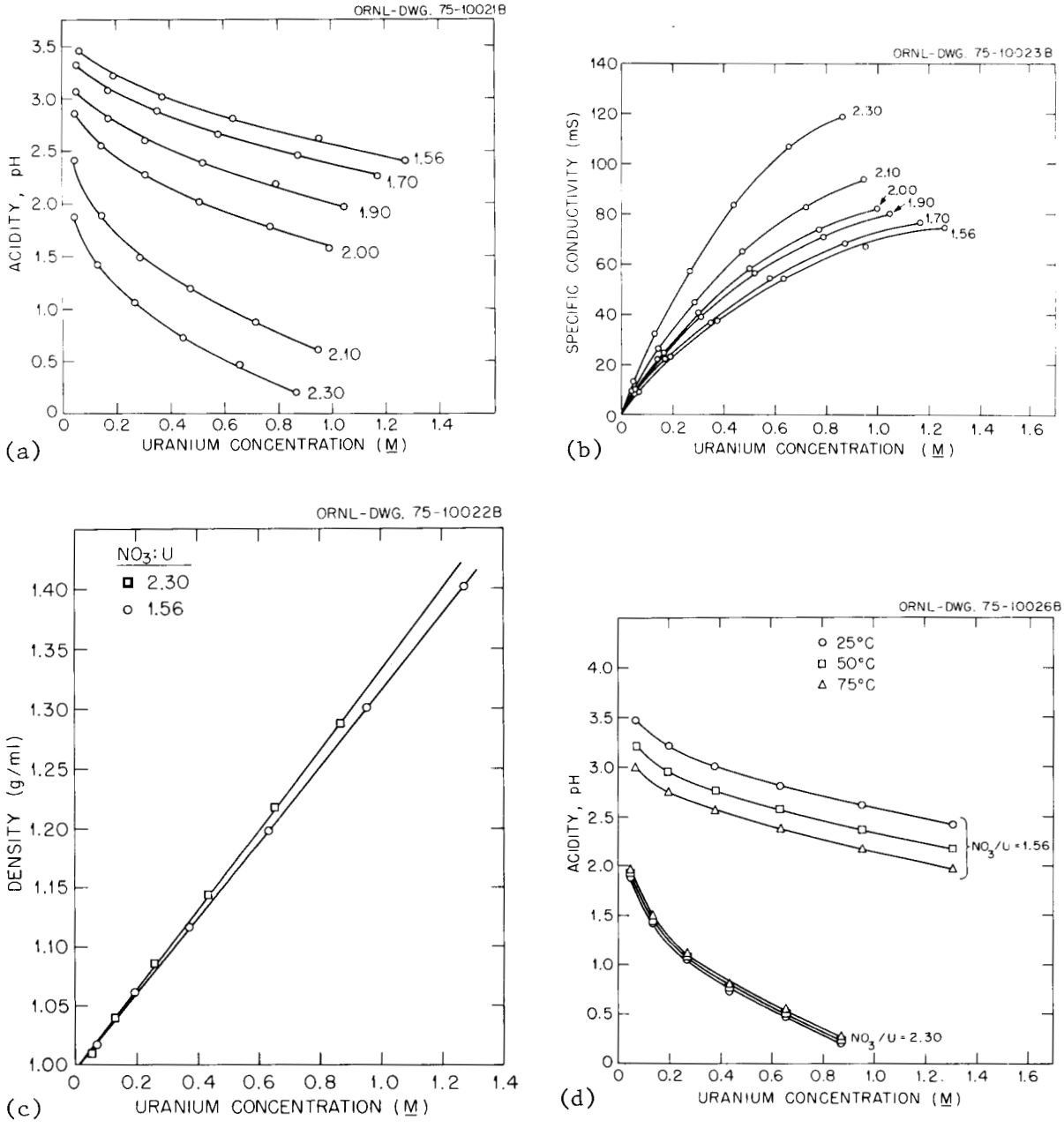

Fig. 3.3. Relationship Between Various Properties of Uranyl Nitrate Solutions and Uranium Concentration at Various Nitrate-to-Uranium Ratios. (a) Acidity at 25°C. (b) Conductivity at 25°C. (c) Density at 25°C. (d) Acidity at various temperatures.

particles fabricated under optimum coating conditions show no permeability or significant removal of fuel, even after extended chlorination runs.

The chlorination technique was successfully applied to the determination of the defective particle fraction in Peach Bottom archive fuel compacts. Sectioned samples were deconsolidated to remove any particle that had been damaged in the cutting operation. Chlorination at 1000 and 1500°C for 23-hr and 2-hr periods, respectively, showed 97% (∿3.5 mg) of the thorium in the defective particles was removed during the first time period.

During this period, the defective particle fraction for SiC-coated particles was determined by a mercury intrusion method, which involves submersion of the sample in mercury with subsequent pressurization to force the liquid through existing cracks in the outer coating into the porous carbon layers. The sample is then radiographed, and the number of defective particles is readily observed. Figure 3.4 illustrates the effects of this technique in revealing a hairline fracture in the SiC coating of the particle pictured. Because of its higher degree of accuracy, this technique has replaced the burn and aqueous leach procedure used previously.

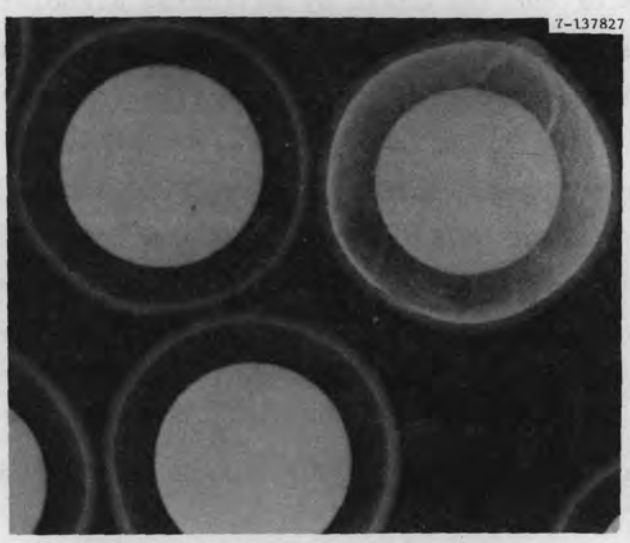

Fig. 3.4. Defective SiC Coating Shown Among Triso-Coated Particles Exposed to Mercury at 103 MPa (15,000 psi). 120×. The shadow (white) of the defective particle shows mercury in the pores of the carbon coating and in the hairline crack in the SiC coating.

3.3.2.2 Heavy Metal Assay — D. E. LaValle

A second application of the chlorination technique mentioned above is the determination of the total fuel content in a given sample of particles. A method had been developed[19] to remove the pyrocarbon and SiC coatings using oxygen and chlorine in preference to mechanical crushing. Dissolution of the ThO_2 by alkali or borate fusion has proven unsatisfactory. Conversion of ThO_2 to water-soluble $ThCl_4$ by high-temperature chlorination was attempted with only moderate success until the proper apparatus was designed. A series of chlorination runs at 1300°C on 2.5-g samples of ThO_2 kernels from previous decoating runs yielded 97 to 99% of theoretical conversion in 4.5 hr. These results compare favorably with those of the burn-grind-acid-leach method, which requires up to 44 hr for completion. We noted that fabrication stresses arising during coating may make the particles more amenable to reaction, since chlorination of virgin kernels rarely yielded conversions greater than 95% in 7 hr.

3.3.2.3 Determination of Thorium Carbide in Partically Converted Biso-Coated Thorium Oxide Fuel Particles — F. L. Layton

A procedure was developed for the determination of thorium carbide in the presence of thorium oxide by selective dissolution of the thorium carbide in HNO_3 and subsequent thorium determination by titration with EDTA using standard solutions of thorium as a reference.

3.3.2.4 Determination of Sulfur in Fired Fuel Rods — F. L. Layton

The sulfur content of fired fuel rods was determined by igniting the rods in a stream of oxygen and determining the evolved SO_2 iodometrically. Analysis of sulfur standards indicated an average sulfur recovery of 98 ± 3%

3.3.3 Waste and Scrap (Subtask 390) — J. E. Van Cleve, Jr., and S. M. Tiegs

Our goal is to develop waste and scrap handling technology for HTGR refabrication. During the past year, work has focused on the perchloroethylene reclamation system, with additional effort on uranium

recovery from the perchloroethylene distillation bottoms and from uncarbonized fuel sticks.

Perchloroethylene is the solvent used in the off-gas scrubber systems attached to the particle carbonization and coating furnaces as well as the cure-in-place furnace. During scrubber operation, the perchloroethylene traps soot, tars, and various hydrocarbon compounds from the furnace off-gases. To maintain scrubbing efficiency, the dirty perchloroethylene must be replaced by fresh solvent. This dirty perchloroethylene can be reclaimed by distillation, and thereby the volume of waste from the scrubbing operation can be reduced.

To determine the distillation characteristics of the dirty perchloroethylene, a glassware still was constructed and operated. Presently, an engineering-scale still is being used for solvent reclamation, and the glassware still is being used for analytical sample preparation and for quickly checking the dirty perchloroethylene composition. A distillation performed in this small-scale equipment rapidly yields information such as solids content, water content, and acidity. Each of these values can be used to monitor scrubber operation and to detect any malfunctions.

Distallation bottoms, the by-product of perchloroethylene reclamation, may contain recoverable uranium in the form of fissile particles blown over from the furnace and uranium vaporized during furnace operation. To recover this uranium, a burn-leach flowsheet has been proposed. Preliminary burning experiments have been performed on the perchloroethylene still bottoms. They will burn, but while burning they produce copious fumes. Various burning methods are presently being studied to determine if an incineration system is available or might be developed that does not release these fumes and will render any uranium present in an easily recoverable form.

Another form of refabrication scrap is reject green (uncarbonized) fuel rods. One proposed flowsheet for uranium recovery from the fissile particles contained in these rods involves a burning step. Since the fuel rod matrix contains approximately 40% volatiles, a large quantity of off-gas fumes would be expected during conventional burning of the

fuel rods. Preliminary burning trials confirmed this. Various burners are being evaluated — such as fluidized-bed burners, standard combustion chambers, and a molten salt burner — to determine an incineration method that would minimize the off-gas cleanup problems associated with the combustion of both green fuel rods and perchloroethylene still bottoms and would also allow uranium recovery. A coincident evaluation of crushing and grinding techniques for green fuel rods is under way to coordinate with the various burning options.

3.4 HOT LABORATORY DEVELOPMENT

3.4.1 Resin Loading (Subtask 320)

3.4.1.1 Radiolysis Effects in Loaded Resin — J. H. Shaffer, C. D. Bopp, and W. L. Carter

According to literature surveys, radiation-induced oxidative degradation of ion exchange resins may be appreciable if the resin salt is held for as long as several days in the water-swollen condition. Although such long delays are not anticipated for the resin loading process, an experimental study has been initiated to examine the effects of this contingency on the resin carbonization phase of the HTGR fuel refabrication process.

The principal component of the radiation dose is from the alpha decay of ^{232}U impurity in ^{233}U if its content is as high as 1000 ppm. The dose rate at this level is about 0.1 megarad per hour. Experimental facilities for handling material of this radiation level through the resin loading and carbonization cycles are not presently available. However, the dose rate from ^{233}U alone is about 0.02 megarads/hr. Consequently, an experimental program based on extended contact periods using ^{233}U with 10 ppm ^{232}U should provide valid conditions for examining the effects of self-radioysis on the preparation of resin-based microsphere fuel kernels.

The experimental program will examine both Amberlite IRC-72 and Duolite C-464 resins fully loaded with ^{233}U from nitrate solution. The loaded resins will be maintained at three levels of hydration —

about 10% moisture content, about 20% moisture content, and fully saturated with water. These resin batches will be sampled periodically during a six-months storage period for examination.

Although the chemical assessment of radiation damage in ion exchange resins requires interpretation of complex reactions, the primary objective of this program is to assess radiolytic effects on the carbonized product during manufacture of coated fuel kernels. Consequently, the primary evaluation of radiation damage to material examined by this program will be based on the results of a comprehensive study of the resin carbonization procedure and the variation in product quality as a function of sample age and moisture content.

3.4.1.2 Laboratory-Scale Test of Reference Process with ^{233}U — P. A. Haas, J. P. Drago, and W. D. Simpson

For all radiation test material prepared to date, the ADUN for resin loading has been prepared by reacting UO_3 with nitrate solutions. The chemical compositions of the solution and resin during resin loading can be identical independent of how the ADUN is prepared. However, a facility to prepare irradiation test materials using the amine extraction of nitric acid is needed for several reasons. First, the product would be more representative of possible secondary effects. As examples, entrainments in the amine regeneration system or residues of undissolved UO_3 when UO_3 is used might have unrecognized effects. (We have not seen any significant effects with natural uranium.) Second, the high alpha activity for ^{233}U as compared with natural uranium might degrade the solvent or resin and result in operating problems. This might affect the product characteristics. Finally, the preparation of loaded resin, including waste handling, could be more efficient and safe than the past preparations in laboratory equipment. The conversion of purified $^{233}UO_2(NO_3)_2$ solution to $^{233}UO_3$ is a troublesome process.

A hot laboratory facility is planned to load resin with ^{233}U using the reference process for HTGR recycle fuel. The amine extraction of nitric acid was applied for preparation of sols from $^{233}UO_2(NO_3)_2$ solutions in a Building 3019 facility at ORNL.[20] The containment and

waste handling requirements for resin loading are almost identical to those for the sol-gel processes. About one-half of the sol-gel process equipment can be used for resin loading after minor changes to piping and pumps. The sol-gel solvent extration enclosure will allow amine regeneration with little modification. The nitrate extraction contactor, in-line pH indicators, and the resin loading-drying contactor will be installed new in the other sol-gel enclosure. Flowsheet conditions and flow rates have been specified for loading 500 g U per batch. Equipment design and operating procedures were also specified, and the resulting flowsheets were checked and approved so that installation of this resin loading facility can proceed.

3.5 COLD ENGINEERING DEVELOPMENT

3.5.1 Resin Loading (Subtask 320) — P. A. Haas, J. P. Drago, D. L. Million, R. D. Spence, R. D. Arthur, T. V. Dinsmore, and J. R. Parrott, Jr.

The reference fuel kernel for recycle of ^{233}U to high-temperature gas-cooled reactors (HTGRs) is prepared by loading carboxylic acid cation exchange resins with uranium and carbonizing at controlled conditions. The carbonized products must be spheres with high uranium contents containing only U, C, and O as major constituents.

A resin and process condition to give acceptable loaded spheres was initially developed using the hydrogen form of the cation resin and UO_3 to maintain acid-deficient uranyl nitrate.[16,21] The purified $^{233}UO_2(NO_3)_2$ solution from a fuel reprocessing plant contains excess HNO_3 (NO_3^-/U ratio of about 2.2). Considering the requirements for remote operation, accountability, and control of nuclear criticality, the usual processes for preparing UO_3 and the in-cell use of UO_3 did not seem acceptable. Therefore, an amine extraction process was developed for resin loading.

The reference flowsheet for a ^{233}U recycle fuel facility at Oak Ridge uses solvent extraction of nitrate by a 0.4 *M* secondary amine in a hydrocarbon diluent to prepare acid-deficient uranyl nitrate. This nitrate extraction, along with resin loading and amine regeneration

steps, was demonstrated[12] in 14 runs using components and procedures originally developed as part of sol-gel studies, and modified as necessary for resin loading.

Continued development of resin-based fuels has involved: (1) preparation of resin feed to supply resin with properties adequate to meet the product specifications; (2) installation, testing, and operation of an integrated engineering-scale resin loading system with natural uranium; and (3) preparation of materials as a service to development of subsequent process operations. All three of these major areas have required the development of new equipment or flowsheet conditions for individual operations.

3.5.1.1 Preparation of Feed Resin

This includes both the procurement and evaluation of commercial ion exchange resins and the processing of the commercial resins to meet the specifications for size, shape, composition, and quality assurance. Amberlite IRC-72* is the reference weak-acid resin. Duolite C-464† has about equally suitable properties but shows significant differences from the Amberlite IRC-72. Both resins cost in the range of $50 to $100/kg U, depending on the allowable range of sphere diameter.

Both manufacturers have modified their preparation procedures to increase the size and shape yields for our requirements. Therefore, the size and shape results reported are for specific batches only and are not typical of the commercial resins. For the Amberlite IRC-72, the changes have been to narrow the size distribution and minimize the amount of very small spheres. Apparently these are accomplished by small process variations and do not result in any increase in price. For the Duolite C-464, the size and shape yields are greatly improved and appear to meet the current product specifications without any further resin feed treatments. Since the size

---

*Trademark of the Rohm and Haas Company.

†Trademark of Diamond Shamrock Chemical Company.

yields for standard commercial resins are 15 to 20%, the six-times-higher unit price of the specially prepared Duolite C-464 is equivalent to the same cost per gram of uranium. These two resins do not have large commercial uses, and the reproducibility of the best (most recent) lots will have to be confirmed for future orders.

Size classification by wet screening

Commercial −20 +50 mesh Amberlite IRC-72 resin is now size classified by wet screening using a 0.76-m-diam (30-in.) commercial* vibrating screen unit. The unit is operated with three screens producing four size fractions. Each lot is processed with two sets of screens. The first series removes the oversize and most of the fines from the desired fraction and produces one product fraction of large resin. The second screening reprocesses the other fraction from the first screening to provide the desired −26 +30 mesh fraction (730 ± 50 μm) as well as cuts for other experimental work. The size distribution for a recent lot of material (Lot 2-6681) is shown in Fig. 3.5. The size distribution

*SWECO, Inc., Los Angeles, Calif.

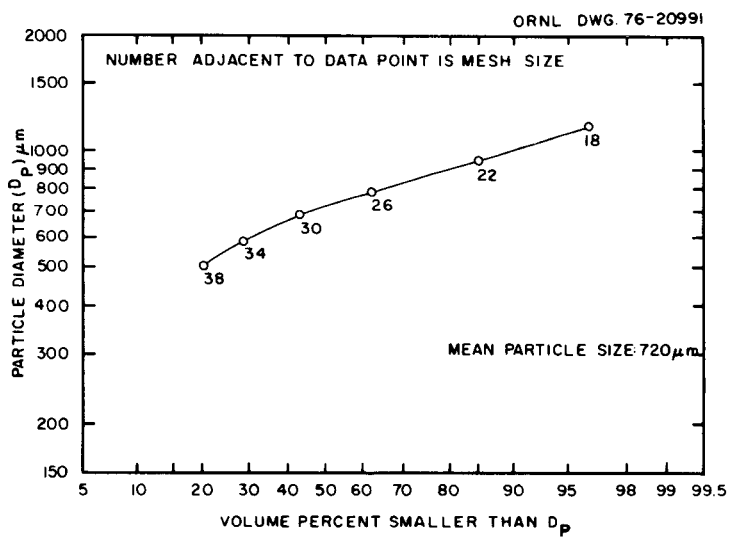

Fig. 3.5. Size Distribution of Amberlite IRC-72, Lot 2-6681.

indicates about 18 vol % yield for the desired fraction. The mean particle size obtained from this plot agrees well with manufacturer's specification of 715 μm. The Duolite C-464 resin is purchased to be over 90% in a ±50-μm diameter range and is not size classified after delivery.

A schematic flowsheet of the resin size and shape classification process is shown as Fig. 3.6 Resin to be size classified is fed to the 0.76-m screen from the resin holding tank through a hydraulic jet ejector. An additional water stream to the screen is used in order to obtain a high water-to-resin volume flow ratio of 40. A high water-to-resin ratio assures removal of the fines and minimizes overloading the screen. A typical feed rate to the screening unit is 50 liters (1.7 ft^3) of resin per hour.

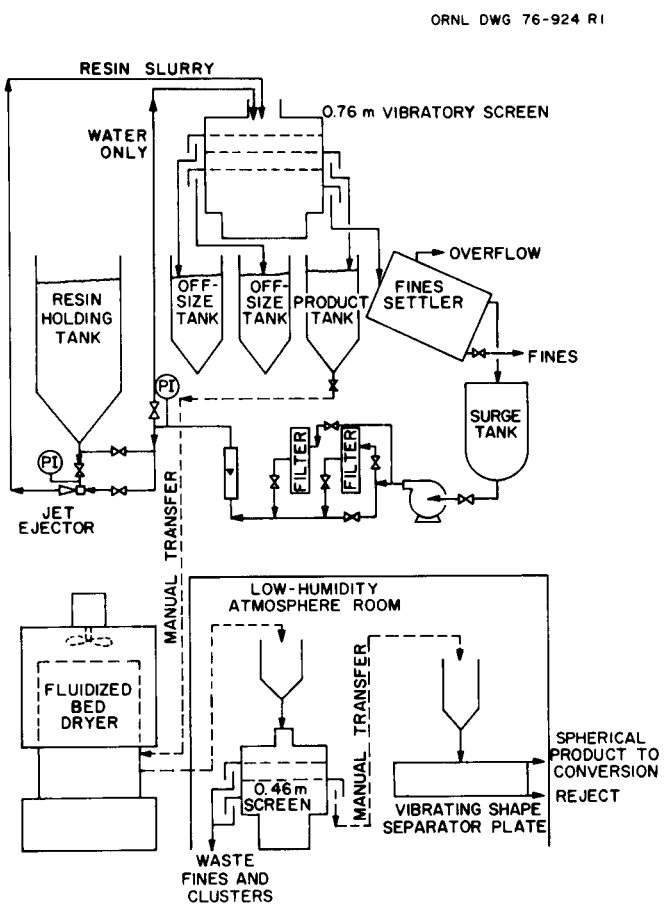

Fig. 3.6. Resin Size and Shape Classification Equipment Flowsheet.

Drying of sodium-form resin

The wet sized resin must be dried to give free-flowing individual beads for the shape separation described in the next section. Damp resin is sticky, but completely dried resin shows static charge effects, which result in unacceptable shape separator operations. Therefore, the dryer must give acceptable control of the amount and uniformity of drying. Sticking together or clustering of two or more spheres is also troublesome if the resin is not agitated. The maximum temperature must be limited to prevent thermal degradation. As a result of these requirements, drying in a rotary drum vacuum drier, with microwave heating, and in a fixed bed were all unacceptable.

Based on small-scale tests, a commercial, packaged fluidized bed dryer* was purchased and tested[22] for drying sodium-form resin. The dryer is operated routinely and has satisfied our product requirements. A schematic of the dryer is shown as Fig. 3.7. The product container

*Fitzpatrick model FA-75, Fitzpatrick Co., Elmhurst, Ill.

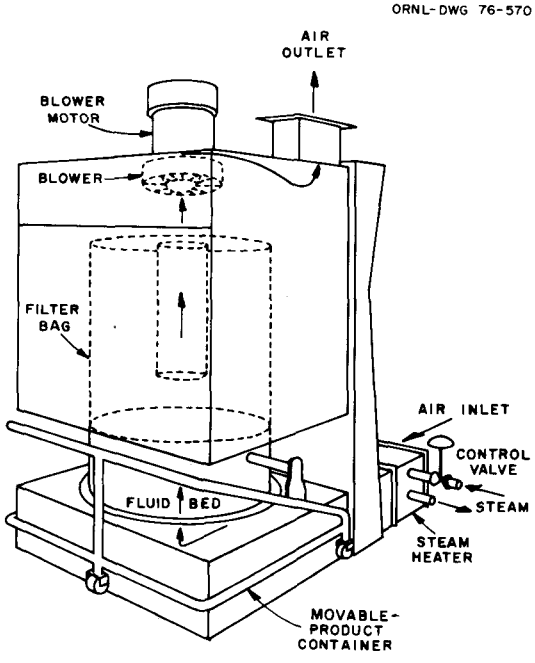

Fig. 3.7. Fluidized-Bed Dryer Used for Ion Exchange Resin.

has a maximum charge capacity of 82 liters (2.9 ft^3). An electrically driven blower pulls room air through a steam heater. The inlet air temperature is set at 65°C (150°F). This temperature was selected as a compromise between long drying cycles and clustering or thermal damage to the resin. The drying cycle is complete when the temperature of the gas leaving the bed is within 11°C (20°F) of the inlet temperature. For a full charge, the drying cycle is approximately 2.5 hr. The dry resin has a loss on drying (LOD) of 13 to 15 wt %; this is an acceptable residual moisture content for shape separation.

Size Classification and Shape Separation

After the resin is dried, it is dry screened in a 0.46-m-diam (18-in.) vibratory unit* to remove any clusters formed or fines released during drying. The dried resin is fed to the screening equipment at about 0.5 kg/min. Dry screening results of a recent batch of sodium form, wet-screened −26 +30 mesh, then dried are: 94.5 wt % accept, 5 wt % oversize, and the remainder fines. These fractions are shown in Fig. 3.8.

The screened resin is then passed over a shape separator to remove nonspherical particles. A shape separator is a highly polished vibrating plate that allows the spherical particles to roll while the nonspherical material moves only by vibration. The plate is tilted (<2°) in two directions such that the spherical beads roll at approximately 45° with respect to the nonspherical material. This type of shape separator has been used with coated particles.[23]

A five-nozzle stainless steel feeder plate [0.18 by 0.76 m (7 by 30 in.)] with a 0.4-μm (16-microinch) finish is used for shape separating dry sodium-form resin. The spherical particles are seen traveling diagonally across the plate (Fig. 3.9). The plate is tilted to the left and to the front face of the unit. The unit is adjusted to obtain the minimum angles and vibration necessary to remove the reject particles from the plate surface. The reject particles move along the long axis of the plate; the spherical beads roll at

*Kason Corp. model K18-E-SS.

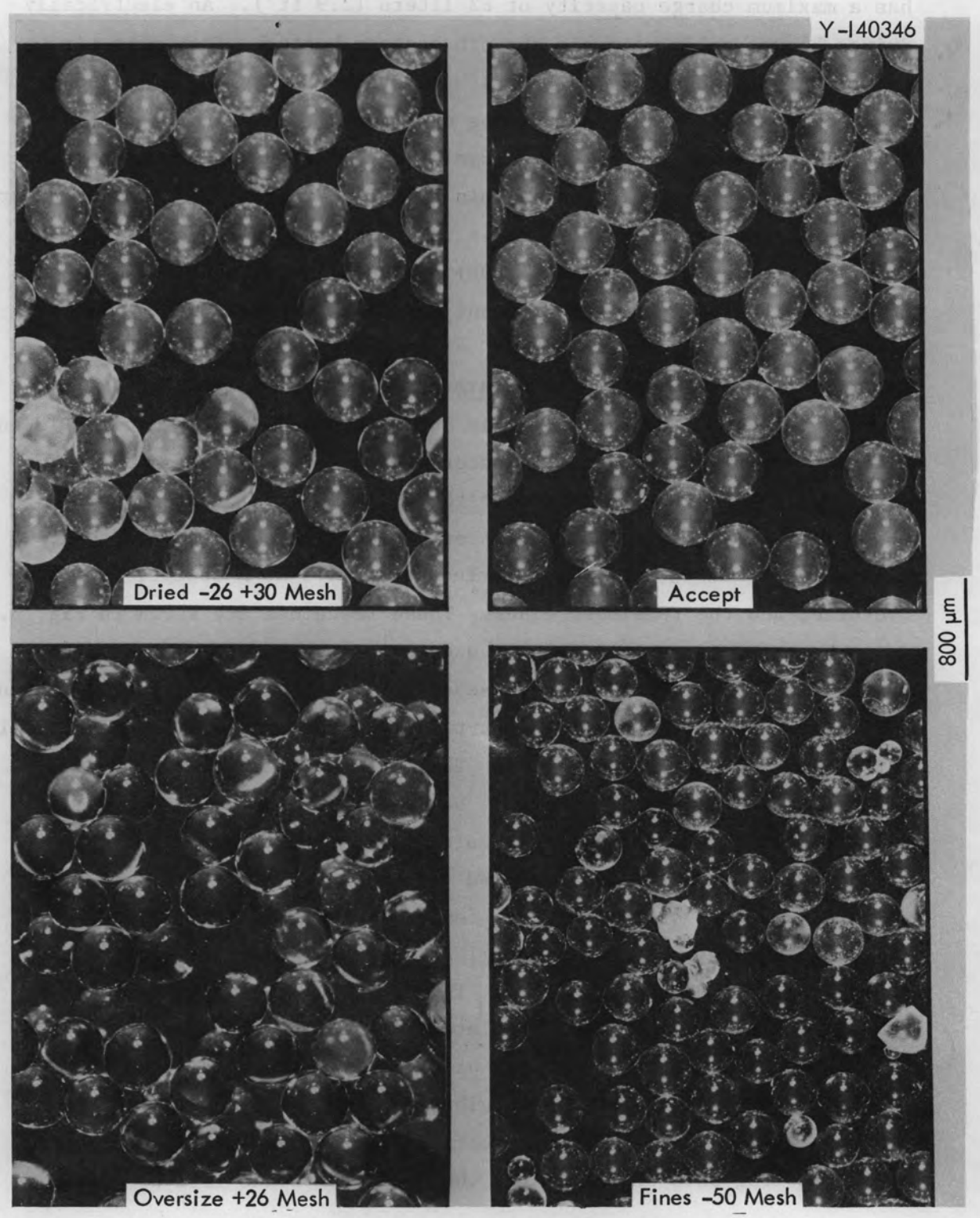

Fig. 3.8. Dry-Screened Samples of Amberlite IRC-72.

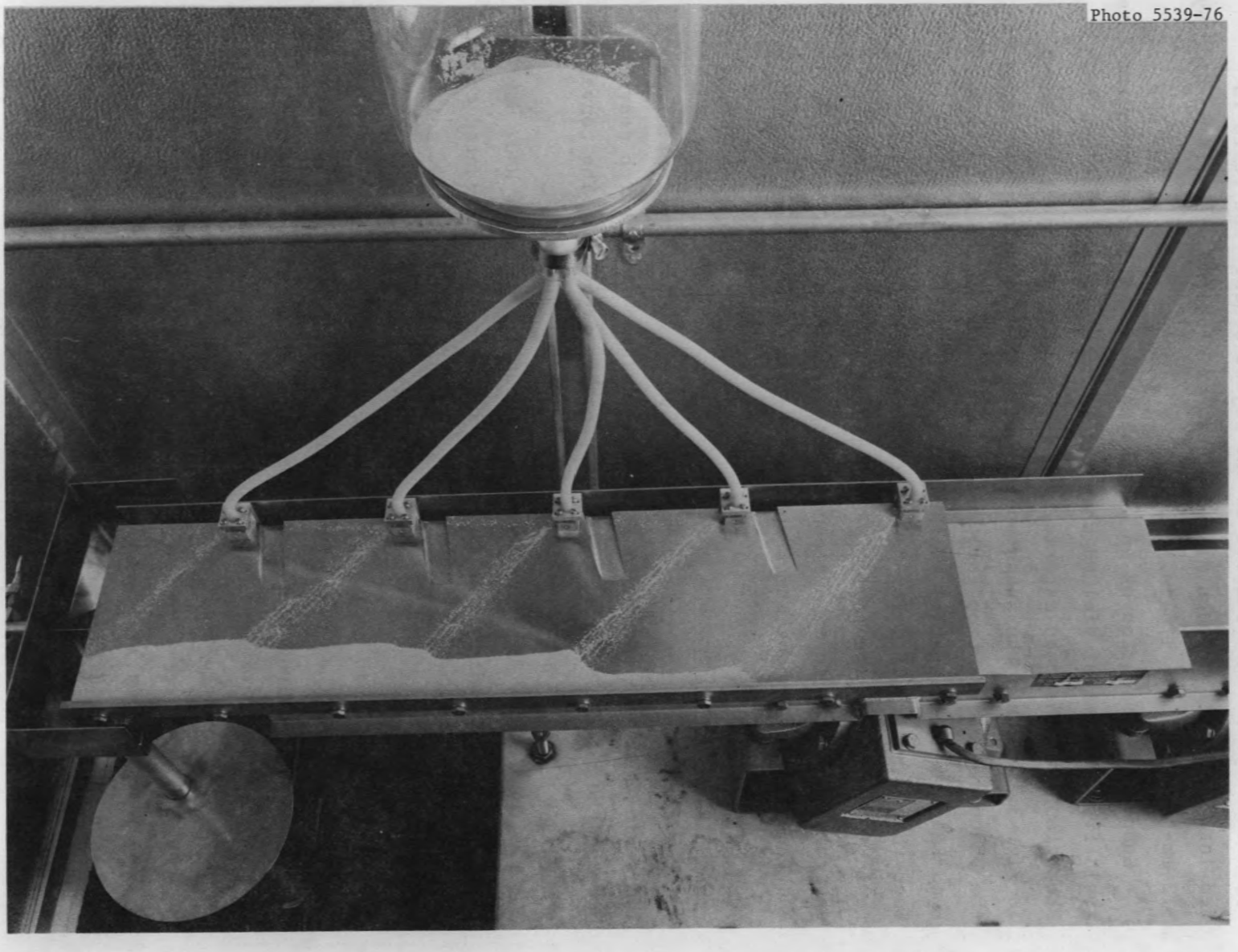

Fig. 3.9. Five-Unit Shape Separator Operating with Resin.

approximately 45° with respect to the reject beads. The resin is fed into the plate through milled blocks of aluminum with 1.6-mm-wide by 3.2-mm-high (1/16 by 1/8-in.) slots.

Shape classification of an 8-kg batch of dried, screened sodium-form resin from lot 2-6681 yielded shape acceptance 99.5 wt % of the feed. Photographs of the feed material, shape accept, and reject are shown in Fig. 3.10. When the shape-accept material was again shape separated, the shape reject fraction for the second separation was 0.05 wt %. Feed rate of this material was approximately 1 kg/hr per plate. Lower feed rates are required for feed with more off-shape particles. The resin feed preparation facility in Building 3503 uses three shape separators located in an air-conditioned room to control the humidity and thus the water content of the resin during shape separation.

Sodium-to-acid form conversion

The conditions for this conversion step have not been optimized. The resin feed preparation facility was designed for a batch conversion because the remainder of the feed preparation is batch. The conversion is done in three steps:

1. The resin volume is measured. About 1.8 moles of HNO_3 per liter of resin is circulated for about 30 min and then decanted to waste. For routine operation, this acid would be the stored acid from the second step of a previous conversion.

2. A second acid addition is made with circulation for more than 3 hr with pH less than 0.5. For routine operation, this batch of acid is stored for use in the first step of the next conversion; then a large excess of acid can be used without being wasted.

3. The converted resin is washed with demineralized water to a pH above 2.7.

A 51-mm-ID (2-in.) Higgins contactor was tested for continuous resin conversions in place of the reference batch conversions. Results for the conversion of Amberlite IRC-72 from the sodium to the hydrogen form are excellent. An in-line pH measurement for the effluent $NaNO_3$ solution allows easy adjustment and control of the resin/HNO_3 ratio.

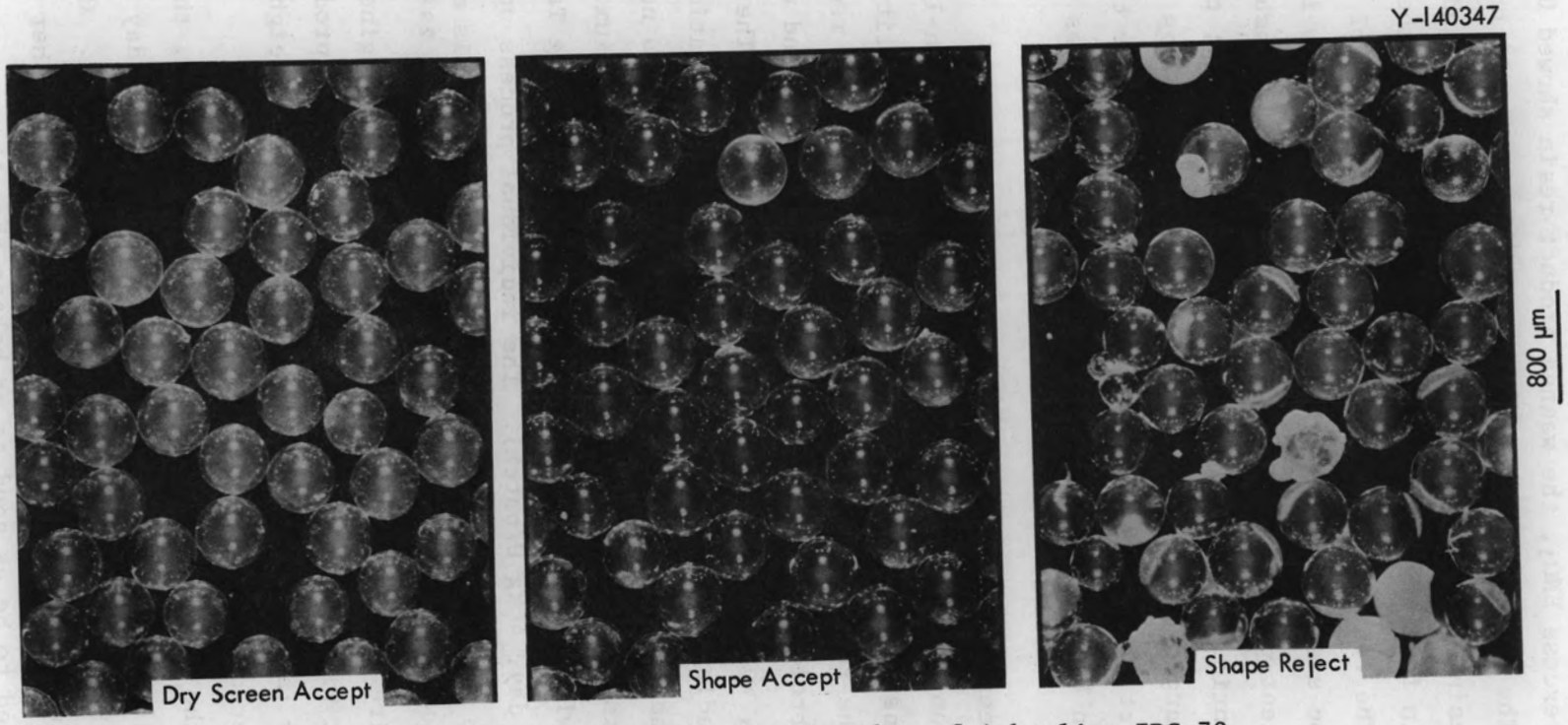

Fig. 3.10. Shape Classification Samples of Amberlite IRC-72.

For about 10% excess HNO_3, the washed product resin showed 0.6 to 5.0 ppm Na. The best initial charge procedure is to fill the column with sodium resin, then start the normal acid feed rate, and finally start the resin feed when the solution effluent drops to the selected control pH. The resin in the column when all of a batch of resin has been fed can be easily processed to completion. Acid flow is stopped when the effluent pH indicates low utilization of acid; wash water is continued until the effluent pH indicates good washing; then the resin is discharged completely by use of the valve settings for the resin-pulse part of the operating cycle. The large volume change (hydrogen resin has half the volume of sodium resin) causes no difficulty.

3.5.1.2 Engineering-Scale Resin Loading System

Results from operation of a complete, integrated resin-loading system were considered necessary to design a recycle facility for HTGR fuels. The recycle of ^{233}U imposes requirements for remote operation, control of criticality, treatment of wastes, and material accountability, which do not occur for natural uranium. The engineering-scale resin-loading system was intended to provide information on concepts necessary to meet these requirements, but it does not meet the requirements in detail and is limited to natural uranium. It is full-scale with respect to the proposed Hot Engineering Test Facility (one batch per day, 4 kg U/batch). The individual process operations are intended to require a maximum of 4 to 6 hr/batch. This means that the commercial recycle plant capacity of about 20 kg ^{233}U/day would not require any increase in equipment size. The engineering-scale equipment with two loading contactors could easily produce six batches per day (at 4 kg U/batch) or, with optimization, eight or more batches per day.

After all the major process components were installed, the engineering-scale system was operated on a one shift per day basis to prepare one batch per day for six successive work days. Operation was good throughout. The loading, uranium losses, and other performance criteria appeared to be as good as or better than those expected from

previous operation of individual components. The uranium contents were 47.1 ± 0.4 wt % U (0% LOD basis).

Process selection

The product from a fuel reprocessing plant is $^{233}UO_2(NO_3)_2$ solution containing some excess HNO_3. The preparation of uranium-loaded resin requires the exchange of uranyl for the cation in the feed resin. When the carboxylic acid resin equivalent to one exchange site is indicated by R and the resin is in the hydrogen (HR) form, the exchange reaction is:

$$UO_2^{2+} + 2HR \rightleftharpoons UO_2R_2 + 2H^+ \ . \qquad (1)$$

The exchange of UO_2^{2+} is limited by the back reaction as H^+ accumulates in solution.

When uranyl nitrate is dissolved, part of it hydrolyzes as follows:

$$UO_2(NO_3)_2 + H_2O \rightleftharpoons UO_2(OH)^+ + H^+ + 2NO_3^- \ . \qquad (2)$$

As a result of the hydrolysis represented by Eq. (2), stoichiometric uranyl nitrate has too high a H^+ concentration to give high exchanges of UO_2^{2+} for H^+ on the weak acid resins. Eq. (1) can be driven to the right, that is, high uranium loadings are possible, if the H^+ concentrations are reduced by removing HNO_3 from the uranyl nitrate solution. The uranium will remain in solution for NO_3^-/U ratios as low as 1.5. Such solutions are termed "acid deficient" and have average compositions equivalent to $UO_2(OH)_{0.5}(NO_3)_{1.5}$.

The reference process for ^{233}U recycle uses the extraction of HNO_3 by a liquid organic amine to supply acid-deficient uranyl nitrate (ADUN). Where X_2NH represents the Amberlite LA-2 secondary amine (N-lauryl-N-trialkylmethylamine), the extraction is:

$$X_2NH + HNO_3 \rightarrow X_2NH_2NO_3 \ . \qquad (3)$$

The regeneration of the amine with NaOH (other bases would be similar) takes place as follows:

$$NaOH + X_2NH_2NO_3 \rightarrow X_2NH + NaNO_3 + H_2O \qquad (4)$$

By addition of an evaporator, the operations can be integrated into an efficient system (Fig. 3.11) for conversion of the uranyl nitrate solution into loaded dried resin. The uranyl nitrate feed including the excess HNO_3 is introduced into a central surge tank (Fig. 3.11). One stream of solution is pumped to the resin loading operation, where part of the uranium exchanges for H^+ in the resin. Another stream is pumped to the evaporator, where water is removed and a concentrated solution is returned. A third stream is pumped to the nitrate extraction system and returns as a more acid-deficient solution.

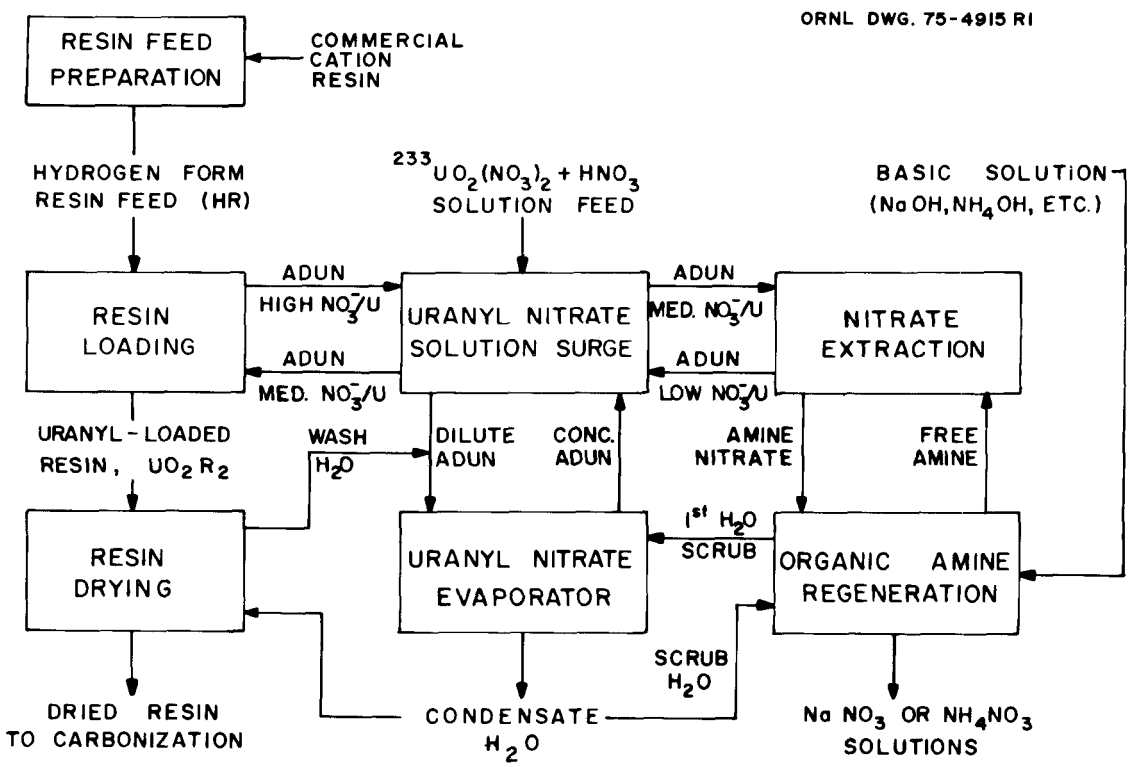

Fig. 3.11. Reference Process for Resin Loading in a ^{233}U Recycle Facility. ADUN Indicates Acid-Defieient Uranyl Nitrate ($NO_3/U < 2$).

The resin loading process for the carboxylic acid resins was developed by using UO_3 to prepare ADUN.[16,21] The dissolution of UO_3 may be described by either of the following:

$$UO_3 + 2H^+ \rightleftharpoons UO_2^{2+} + H_2O \tag{5a}$$

$$UO_3 + 2HNO_3 \rightleftharpoons UO_2^{2+} + 2NO_3^- + H_2O \tag{5b}$$

The net effect of adding Eqs. (1) and (5a) or (1) and (5b) and subtracting HNO_3, which is not consumed) is:

$$UO_3 + 2HR \rightarrow UO_2R_2 + H_2O \tag{6}$$

This net reaction can be easily carried out in the presence of a small amount of uranyl nitrate solution, which is reused. But the conventional processes for conversion of uranyl nitrate to UO_3 are very troublesome and undesirable for remote operation with ^{233}U.

The H^+ concentration can be reduced or HNO_3 removed by addition of bases [NH_4OH, NaOH, $Mg(OH)_2$]. The same net effect results if the resin is initially in the corresponding salt form instead of the acid form. All of these result in cations that compete with UO_2^{2+} for exchange sites on the resin. All the metals result in unacceptable impurities in the product resin, but ammonium is more acceptable as it can be volatilized during carbonization. The amine extraction process was compared with an ammonia neutralization process developed by the General Atomic Compnay for fresh fuel fabrication. A joint ORNL-GA review committee met at ORNL on June 7—9, 1976. The recommendation from the committee report is:

> The recommendation of the WAR (weak-acid resin) review team is to adopt the reference amine extraction HTGR refabrication recycle kernel flowsheet. All aspects of process, waste, effluents, fuel performance, and equipment complexity and costs were reviewed.
>
> The recommendation was based primarily on a modest superiority of the amine extraction WAR product with regards to minimizing rejection caused by particle breakage and maximizing interparticle loading uniformity.

The ammonia neutralization process was judged to be slightly superior to the amine extraction process with regards to space requirements and process complexity, but these differences were not of sufficient magnitude to overcome the superiority of the amine extraction product noted in the second paragraph.

Other approaches to removal of HNO_3 are less promising or less well developed. Chemical decomposition of HNO_3 using reducing agents such as formaldehyde are chemically complicated and are of doubtful practicality for the ADUN. The use of permselective membranes to remove HNO_3 by dialysis is an untested approach. The preparation of ADUN by a steam stripping or partial thermal denitration process was tested experimentally and is not as simple as had been hoped. High uranium concentrations and boiling points above 140°C are required to give useful acid deficiencies. As the temperature is increased, UO_3 precipitates at higher NO_3^-/U ratios and the process produces a slurry of UO_3 in uranyl nitrate. The conditions that result in precipitation are uncertain; however, no precipitation was observed for a NO_3^-/U ratio of 2.0, while precipitate was present in solutions with NO_3^-/U ratios of 1.9 or slightly lower at denitration temperatures of about 150°C. While the UO_3 dissolves easily when agitated in diluted uranyl nitrate solutions at 50 to 80°C, it can settle and be difficult to resuspend. Because HNO_3 is a preferred form of nitrate waste for either reuse or disposal, this steam stripping process remains attractive for long-term development.

Solvent extraction to prepare ADUN

The nitrate extraction system consists of a series of five cocurrent contactors (one theoretical stage of contact each). A single solvent stream (0.4 *M* Amberlite LA-2 in diethylbenzene) is pumped once and flows by gravity through all five contactors back to the solvent surge tank. The mixing sections are organic continuous and are also heated to 40 to 50°C to improve the phase separation.

The two initial regeneration system contactors are water scrubs to minimize the losses of uranium to the nitrate solution wastes. The scrub water is returned to the ADUN tank. The organic leaving the

nitrate extraction system contains 200 ppm U for typical operating conditions and will have higher uranium concentrations for high NO_3^-/U ratios or high uranium concentrations in the ADUN. About 70% of the uranium is recovered by the first water scrub and 80% of that remaining by the second scrub. The loss is less than 0.05% of the uranium loaded on the resin and is equivalent to about 50 ppm U in the nitrate waste solution. For NH_4NO_3 solution at pH = 6, part of the uranium precipitates and can be removed by filtration, leaving about 10 ppm U in solution. Little of the uranium precipitates for 50 ppm U in $NaNO_3$, and the uranium solubility is even higher if the $NaNO_3$ waste contains $NaHCO_3$ and Na_2CO_3. The 50 ppm U losses are reasonable with respect to the economic value of the ^{233}U. The radioactivity hazard of ^{233}U is controlled by the ^{232}U content. Conversion of the nitrate solutions to low-level waste solids is not practical because less than 1 ppm ^{233}U would be allowed in the solutions.

The third contactor in the regeneration system reacts the amine nitrate with aqueous solutions of base to regenerate the free amine. Excess NaOH results in formation of emulsions and is not allowable. The initial demonstration of amine extraction[12] used equimolar mixtures of NaOH and Na_2CO_3. The solvent/aqueous ratio was selected to give complete regeneration of the amine with complete utilization of the NaOH, but only partial conversion of the Na_2CO_3 to $NaHCO_3$. The typical Na/NO_3^- ratio in this waste was 1.7. Partial regeneration of the amine using NaOH (or NH_4OH) only and a NaOH/amine ratio of about 0.7 is an important process improvement. The amount of waste salt is greatly reduced; the Na/NO_3^- ratio is 1.0. The waste is almost neutral (pH $\sim$ 6) and phase separation is improved. The solubility of uranium is minimized, so any large losses can be recovered by filtration. These improvements for partial regeneration were demonstrated by using both NaOH and NH_4OH for regeneration. The advantages were realized and no difficulties were observed.

For an in-cell system, detection and feedback control of the regeneration system interfaces would be troublesome and undesirable. Overflow weirs are simple, cheap, and less likely to malfunction than

a control valve system. The solvent extraction system as initially adapted[12] required large changes in weir heights to compensate for liquid density variations. The largest variations were from uranium concentration changes in the ADUN and from temperature changes for the organic solvent. The liquid-liquid interface position results from a pressure balance as follows:

$$H_O \rho_O = H_A \rho_A \tag{7a}$$

where

H is height above interface
ρ is density
subscript O indicates organic
subscript A indicates aqueous.

This can be rearranged to give:

$$H_A = (H_O - H_A) \frac{\rho_O}{\rho_A - \rho_O} \tag{7b}$$

$$H_O = (H_O - H_A) \frac{\rho_A}{\rho_A - \rho_O}$$

For fixed interface positions, $H_O - H_A$ is fixed. For the original arrangement as shown by Fig. 3.12 on the left the H_A was about 0.7 m and interface variations would be as large as 0.15 m for fixed weirs. Such large variations would not be tolerable. For the arrangement shown on the right in Fig. 3.12, the H_A is about 0.10 m and the resulting interface variations (up to 20 mm) are acceptable. This modification was demonstrated for both the nitrate extraction and the caustic regeneration contactors. Results were as expected with no difficulties.

The mixing requirements and the effects of temperature initially reported[12] were confirmed. The phase separation is adequate at 25°C but is visibly faster at 40°C. Since radiochemical processing cells are usually warmer than 25°C, the higher temperature is easier to maintain than 25°C. The effects of temperature in the 40 to 60°C range are not important.

ORNL DWG. 76-20992

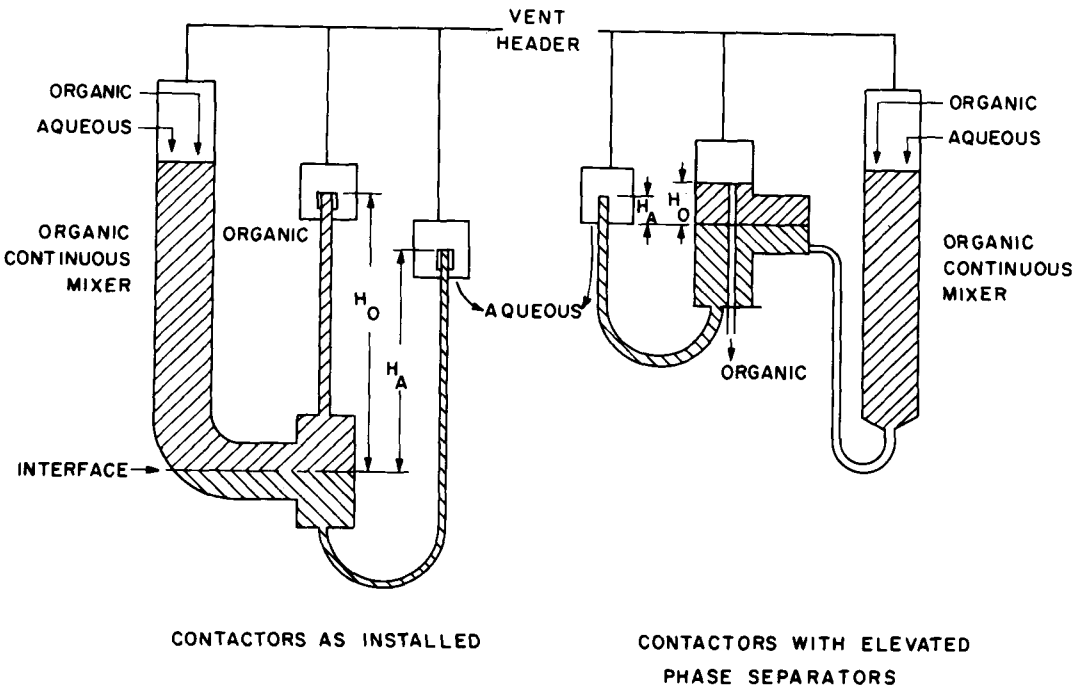

Fig. 3.12. Interfaces in Nitrate Extraction and Amine Regeneration Contactors for Resin Loading.

The details of the contactor designs have been reported.[20] The contactors have six stages with cocurrent flow using a common agitator with a 44-mm-diam by 13-mm-high (1 3/4 by 1/2-in.) impeller in each stage. For the resin loading flowsheet, the optimum agitation requires 350 to 500 rpm for these agitators.

A 76-mm-ID by 1.8-m-long (3 in. by 6 ft) packed column [9.5-mm (3/8-in.) Raschig ring packing] were fabricated, installed, and tested to replace the two cocurrent mixer-settler stages for uranium recovery from the nitrate extraction solvent. The packed column would be simpler mechanically and a countercurrent contactor might provide more than two theoretical stages, thereby reducing the uranium content of the nitrate waste. During two test runs, the 1.8 m (6 ft) of packed column gave only a fraction of a theoretical stage. The uranium losses were about 0.5%, as compared with less than 0.05% for the two cocurrent mixer-settler stages. The aqueous scrub does not disperse into small

drops in the packed column. A pulsed column contactor could probably be an efficient countercurrent scrubbing contactor.

ADUN evaporator

One essential component for an efficient resin loading system is an evaporator to remove water and concentrate the ADUN. A thermosiphon evaporator (Fig. 3.13) designed to produce 60 liters/hr condensate of less than 1 ppm U (Fig. 3.14) was fabricated, installed and tested. The results have been reported[24] in detail; the conclusions were as follows: Operation of the thermosiphon evaporator was simple and easy to control. The fixed jackleg maintains a constant liquid level in the evaporator and allows continuous circulation through the evaporator. The evaporation rate (and thus the uranium concentration in the resin loading system) was controlled by regulating the steam pressure while maintaining the feed flow rate to the evaporator constant. Using a tangential vapor entry to the large vapor disengaging

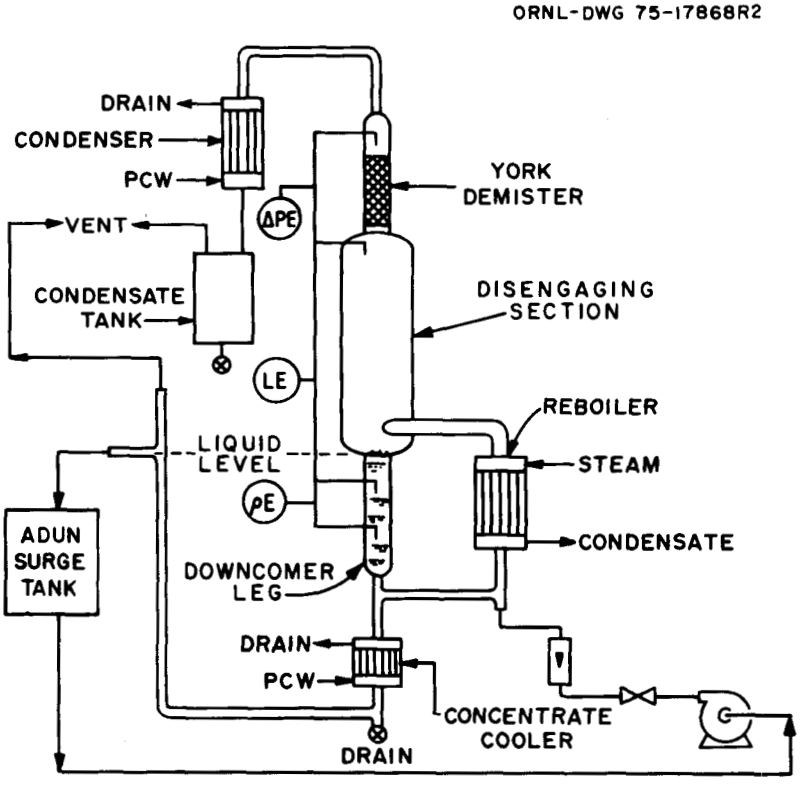

Fig. 3.13. Vertical Thermosiphon Evaporator for Uranyl Nitrate.

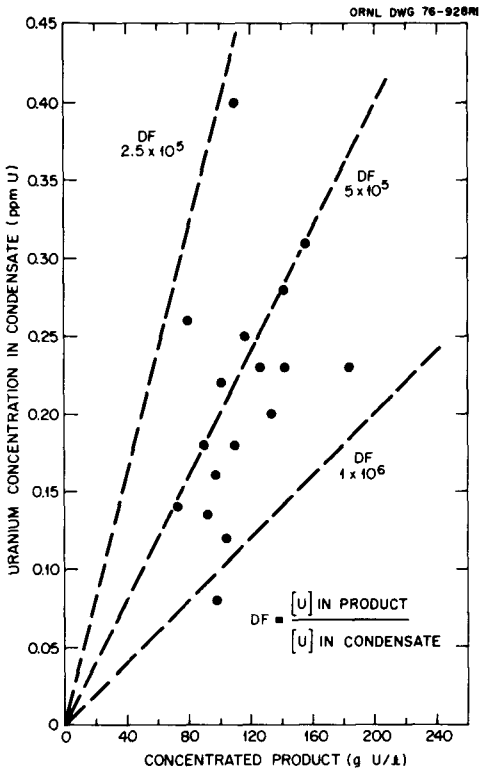

Fig. 3.14. Decontaimination Factor For Uranyl Nitrate Evaporator.

section and a wire mesh mist separator gave a high quality condensate containing less than 0.5 ppm U for an overall decontamination factor exceeding 5×10^5. The decontamination factor was not a consistent function of the condensate rate in the range 17 to 79 liters/hr. This evaporator design is acceptable for meeting the HTGR fuel recycle pilot plant requirements.

During tests of a new loading contactor, the evaporator plugged because of precipitation of UO_3. Apparently large amounts of UO_3 precipitate at 105°C if the ADUN feed has a NO_3^-/U ratio of 1.6. This problem was solved by feeding the more acidic exit solution from the loading column to the evaporator. Plugging had never occurred during use of the batch loading contactor because the evaporator was not operated for long periods at maximum acid deficiency.

Uranium loading of resin

The resin loading contactor design and procedures used for early demonstration runs[12] were used with only minor modifications. The contactor body was a 0.13-m-ID by 1.5-m-long (5 × 60 in.) plastic cylinder with a cone bottom and a 120 mesh stainless steel screen top. Commercial instrumentation continuously indicated the pH of the feed and exit ADUN solutions.

Transfers of feed resin and uranium-loaded resin through 13-mm-OD (1/2-in.) tubing lines were completed without significant difficulty. Pressures of 34 to 55 kPa gage (5–8 psig) were usually used, and an additional 1 to 2 liters of slip water or solution was required in addition to the volume of the settled resin bed. Although flowing resin never shows any tendency to plug, tight settling or packing of resin into a line without flow should be avoided. The tightly packed resin may limit the solution flow to a low value, which will not initiate resin flow.

During loading, the batch contactor shows several mixing cells over a 0.9 to 1.2-m (3–4 ft) length. The bottom cell appears to be a spouting bed as a result of the central solution inlet and the conical bottom. Above this are two or more mixing cells with downflow at the column wall. The volumes of the fluidized resin bed relative to the settled bed volumes are 150% maximum a few minutes after start-up, about 110% just before the flow increase, 125% immediately after, and 115% at the end of the loading.

The reliability of the in-line pH instrumentation has been good. These instruments are standardized by sampling the ADUN solution and measuring the sample pH with a standardized laboratory meter. The ADUN is a buffered solution, and use of the process solution for standardization is much less troublesome than introducing a standard solution into the process system. One of the commercial in-line units has shown more drift or changes than the other two, and the two more stable units will be preferred for in-cell use.

The rate of uranium loading is limited by different factors as loading proceeds. At the start, 20% or more of the uranium in the solution is removed rapidly and the exit solution is in equilibrium with resin of low uranium content. The rate of uranium loading during this period is determined by how fast the ADUN is supplied. Since the resin has a low density, both the uranium concentration and the solution flow rate must be limited to avoid forming a packed bed of resin against the exit screen. As the resin becomes heavy with uranium, the solution flow rate can be increased. For the last 20% of the loading, the rate of loading is much lower as a result of mass transfer and/or kinetic limitations inside the resin particle. Further increases in uranium solution flow rates then only have small effects on the rate of loading. The ADUN must have a favorable acid deficiency before loading can be completed. If the rate of nitrate extraction is low, then the loading time required is increased; that is, the resin loading cannot be completed until the acid deficiency is favorable. If the rate of nitrate extraction is high, the nitrate extraction will have to be stopped to avoid precipitation of UO_3 and then resumed after more uranium is loaded. We have selected conditions that minimize the number of flow changes required. The ADUN flow to resin loading is 1.6 liters/min initially and 4.8 liters/min for the remainder of the run. The flow can be changed when the exit ADUN pH exceeds 1.6 or at a preset time at about 80 min for normal run conditions. The evaporator is operated until the ADUN surge tank reaches a preselected value of either volume or density. The nitrate extraction system is operated until the ADUN reaches the correct pH for the uranium concentration present. The approximate nitrate extraction rate is calculated for removing the required amount of nitrate in about 150 min. Thus the flow through the resin loading contactor is normally continued at least 1.5 hr after the nitrate extraction and evaporator are turned off.

Two loading runs were made to test the procedure for end-of-uranium-feed batches. The objective is to end with a low uranium inventory as the ^{233}U of different isotopic compositions would be processed as separate campaigns. For both tests, the uranium remaining

was concentrated to about 8 liters in the evaporator after the loading was completed. The first batch showed a high loading of uranium (48.4% dry basis) and the uranium remaining in solution was about 800 g or one-fifth of a batch. For the second batch, the loading was slightly low (46.2 wt %) and the uranium remaining was 450 g. With this small heel, the NO_3^-/U increased to a less favorable value after the nitrate extraction was shut off. A higher loading would probably have been achieved by using a second short period of nitrate extraction.

The two requirements for assuring high and reproducible loadings are a favorable pH for more than a minimum time. The uranium concentrations are determined from density measurements. An in-line density cell has been purchased and is being installed for testing. Measurements by Botts[17] for conditions used in the engineering-scale resin loading system can be adequately represented by:

$$\rho(\text{ADUN}) = \rho(H_2O) + 0.324[U] \tag{8a}$$

$$[U] = 3.10[\rho(\text{ADUN}) - \rho(H_2O)] \tag{8b}$$

where

ρ(ADUN) is density of acid-deficient uranyl nitrate in g/cm^3,
$\rho(H_2O)$ is density of water at the same temperature.
[U] is the uranium molarity.

The data reported by Botts[17] for ADUN pH are shown with a log scale for U *M* (Fig. 3.15) to allow easier interpolation at the lower uranium concentrations. These data agree reasonably with those used previously,[12] and are believed to be more accurate. The data of Shaffer and Greene[25] for pH versus present uranium loading can be combined with the data of Fig. 3.15 to give the NO_3^-/U ratios versus percent resin loadings shown as Fig. 3.16. For 0.2, 0.6, and 1.0 *N* NO_3^-, there were no significant differences between the two resins nor between temperatures of 30 and 40°C. For the controlling region of above 70% loading, all the conditions of importance to the engineering-scale resin loading

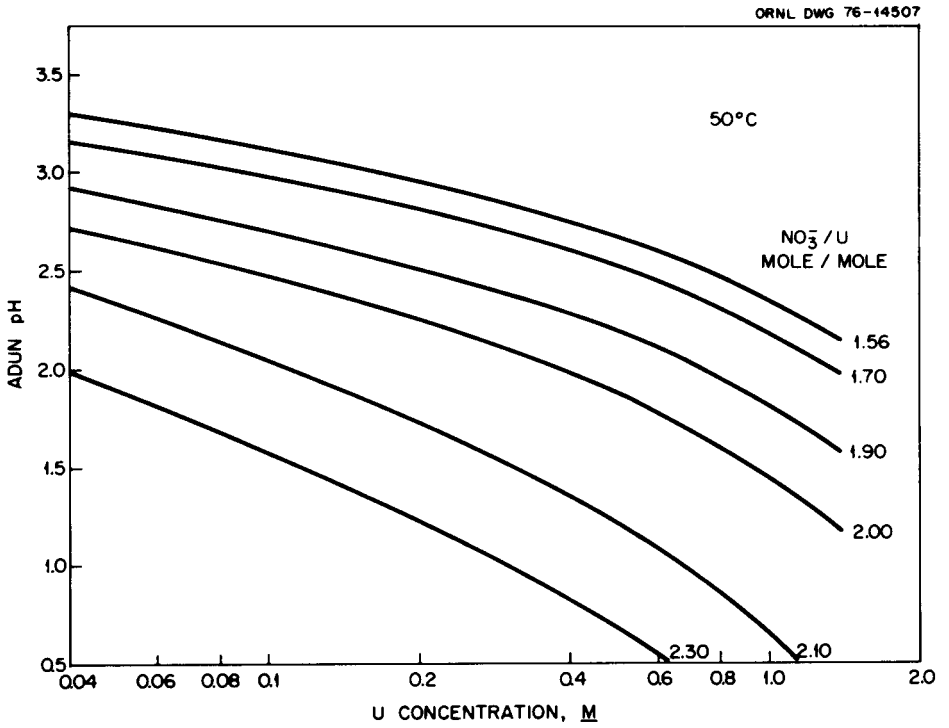

Fig. 3.15. The pH of Acid-Deficient Uranyl Nitrate (ADUN) at 50°C Versus Uranium Concentration and NO_3^-/U Mole Ratio.

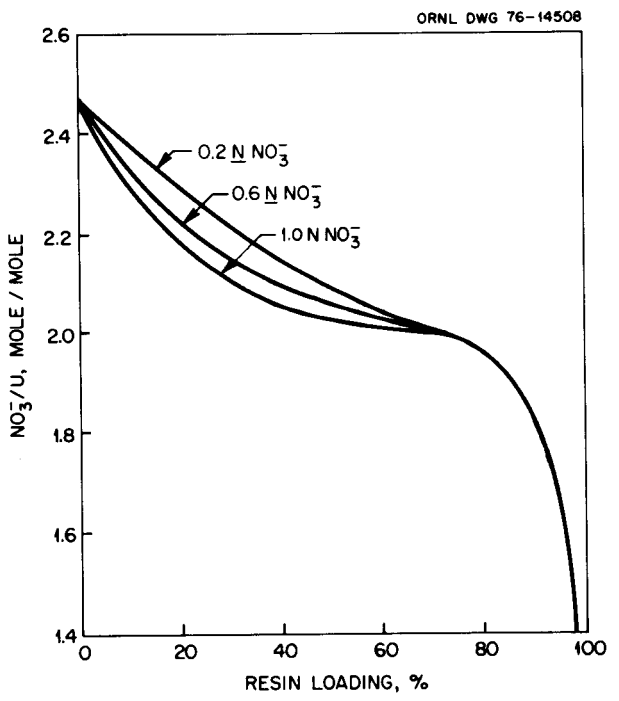

Fig. 3.16. The Equilibrium Conversions of Amberlite IRC-72 or Duolite C-464 to the Uranium Form in Uranyl Nitrate Solutions at 30 or 40°C.

are represented by a single curve of percent loading versus NO_3^-/U ratio. The criterion for the batch loadings is that the pH of the exit ADUN indicates NO_3^-/U ratio less than 1.7 for at least 1 hr, and a longer time is preferred. Data on the uranium contents are reported in Sect. 3.5.1.4.

Tests with a 51-mm-ID (2-in.) Higgins column in place of the batch resin loading contactor were started at the end of this report period. The Higgins column gives the effect of continuous loading of uranium on the resin to match the high capacity of the continuous nitrate extraction system. By use of timers and electrically operated valves, periods of solution flow through the resin are alternated with shorter periods of hydraulic movement of the resin. Thus, the solution and resin move countercurrent to each other, but the movements alternate rather than being truly continuous. This technique has been tested sucessfully on a laboratory scale.[15]

The preliminary results are encouraging. Over 100 liters of resin was discharged at conditions of engineering-scale tests adequate for good loading; analyses are in progress. The only major problems were with the hydraulic pulsing of the resin, and these were controlled by minor column modifications. Control of the uranium, nitrate, and water inventories has been excellent. Tests will be continued to test a range of operating conditions and to determine the column capacity.

3.5.1.3 Drying of Uranium-Loaded Resin with Microwave Heating

The primary requirement of the dryer is to produce dried resin of acceptable moisture content consistently, to allow pneumatic transfer of the material to the next processing step. The individual requirements for the drying process are not exceptional. But the combination of requirements for controlled and uniform drying, remote operation in a radiochemical cell, control of nuclear criticality, and limited drying time are difficult to meet. Microwave heating has several advantages over conventional heating, which relies primarily on conduction-convection. These advantages include instant on-off capability, moisture leveling (i.e., preferential heating of the wettest material), and shorter drying cycle without high temperatures. For this application with geometry restrictions, poor thermal conductivity

of the resin, and uniformity requirement, microwave heating has satisfied our requirements better than any other methods considered.

The optimum water content for uranium-loaded Amberlite IRC-72 appears to be 10 to 16 wt % water. Above 20 wt %, resin particles stick together. Resin dried to less than 9 wt % shows detectable static charge effects.

A microwave energy system for drying uranium-loaded resin was purchased from a commercial manufacturer* and tested (Figs. 3.17 and 3.18). Reproducibility and control of the moisture content were satisfactory (Table 3.5). Detailed results were reported[26,27] and the conclusions are as follows:

> Microwave heating was sucessfully demonstrated to give controlled and reproducible drying of 11-liter batches of uranium-loaded (4 kg of uranium) resin in a vessel of safe dimensions for nuclear criticality (12.4 cm ID). The dried resin must have a water content of 10 to 16 wt % to minimize handling problems. The microwave heating evaporates water throughout the resin bed, with preferential heating of the wettest resin, and allows short drying cycles.

---

*Gerling Moore, Palo Alto, Calif.

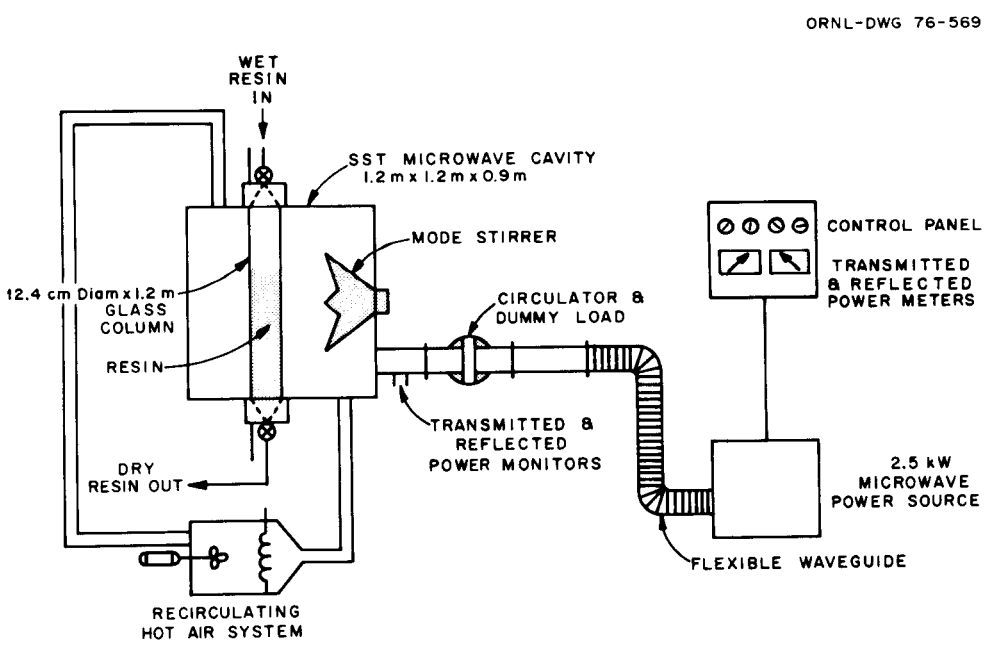

Fig. 3.17. Microwave Dryer for Uranium-Loaded Ion Exchange Resin.

Fig. 3.18. Microwave Dryer System.

Table 3.5. Microwave Drying of Uranium-Loaded Amberlite IRC-72

Dried Resin LOD[a], wt % for Each Sample Location in Column				Wet Resin Volume (liters)	Microwave Exposure	
Bottom	Middle	Top	Average		(min)	(kW)
14.7	15.2	14.8	14.9	11.1	44.5	2.0
7.7	15.6	13.2	14.4	11.5	46.0	2.0
15.5	16.2	15.1	15.6	11.5	37.0	2.5
14.8	14.8	14.4	14.7	11.25	38.5	2.5
14.2	15.4	15.4	15.0	9.65	34.0	2.5
9.6	14.2	13.4	13.8	10.95	39.5	2.5
13.7	13.3	13.2	13.4	11.1	40.0	2.5
14.0	14.5	12.3	13.6	11.4	41.0	2.5
12.5	13.4	13.4	13.1	11.7	42.0	2.5
15.0	15.1	15.0	15.1	7.3	26.5	2.5
13.6	14.6	13.6	13.9	9.65	36.0	2.5
13.8	14.2	11.6	13.2	12.0	46.0	2.5
10.2	12.7	12.4	11.8	10.25	39.0	2.5
17.6[b]	16.2	16.9	16.9	10.5	40.0	2.5

[a]Loss On Drying.

[b]Duolite C-464 resin.

A standard drying procedure and methods for determining the duration of microwave heating, in order to obtain the desired water content, were developed. Using an experimentally derived drying factor or monitoring the amount of water removed from the wet resin has been found to provide reproducibly acceptable dried product. Temperature or reflected power were not very reliable in obtaining resin of the preferred moisture content.

A heat balance on the resin dryer system and the coupling efficiencies of the microwave energy with the wet resin is calculated and found to agree well with experimental results and the manufacturers literature, respectively. The minimum fluidization velocity was also calculated and compared favorably with experimental observations. Mixing of the material was found to be required in order to ensure a uniform moisture content. No significant operating difficulties were encountered.

3.5.1.4 Material Preparation

The development of subsequent fuel refabrication operations (carbonization, conversion to $UC_{2-x}O_x$, coating, etc.) requires large batches of resin loaded with natural or depleted uranium. Other compositions of resin are needed to meet special requirements. Information from preparation of these materials is briefly reported.

Uranium-loaded resin

All preparation of resin loaded with natural or depleted uranium during this period has been by use of the engineering-scale resin loading system. Operation of this system has included over 50 loading runs to prepare over 400 kg of dried resin. The uranium contents in the dried resin (corrected for LOD) reproduce well with significant differences between Amberlite IRC-72 and Duolite C-464 (Table 3.6). Shorter times or less acid deficiency than those recommended will result in lower uranium contents. End-of-batch runs with low uranium concentrations in the ADUN and extended loading times can give normal loadings of uranium. The amounts of uranium loaded per unit bulk volume (meq/cm^3) are less reproducible than the wt % uranium. As compared with a resin that meets specification, resin containing off-shape particles packs to a lower density, while resin with a wider range of sizes packs to a higher density.

The composition of the UO_2^{2+}-loaded and dried resin ready for carbonization will depend on the completeness of loading, the drying conditions, and the presence of impurities. Information on this composition is important to quality control, to selection of carbonization conditions, and to the interpretation of carbonization results. It has been compiled in an internal document. The Amberlite IRC-72 carboxylic acid cation exchange resin in the hydrogen form has a capacity of about 11 meq/g, which is in close agreement with that calculated for the polymerization of 82 wt % pure acrylic acid with 18 wt % of a divinylbenzene-ethylvinylbenzene mixture. The loaded resin has carbon/uranium ratios of about 9, in agreement with about 95% exchange of uranyl for hydrogen. Other analyses indicate about 2 moles

Table 3.6. Effects of Run Conditions on Uranium Contents for Engineering-Scale Resin Loading

Resin Feed		End-of-run Conditions			U 0% LOD Basis (wt %)	U Loaded (meq/cm^3)	Run	Remarks
Type and Lot	Mean Size (μm)	U (*N*)	Final NO_3/U	Time at NO_3^-/U <1.7 (hr)				
IRC-72	690	0.42	1.50	2.0	46.84	3.09	S32	
2-3947	690	0.42	1.50	1.8	46.79	3.04	S33	
	690	0.32	1.50	2.2	47.48	3.14	S34	
	690	0.31	1.50	1.8	47.08	3.03	S35	
	580	0.34	1.55	2.0	46.41	2.87	S38	
	580	0.44	1.50	2.0	46.51	2.87	S39	
	690	0.39	1.45	2.6	48.76	3.28	S40	
	580	0.34	1.45	2.6	48.68	3.16	S43	
	580	0.19	1.45	3.6	48.36	3.05	S41	Low U *N*
	690	0.50	1.45	2.0	48.39	3.28	S42	High U *N*
	580	0.36	1.55	1.6	45.98	2.78	S37	Short Time
	580	0.24	1.65	2.0	44.45	2.61	S36	High NO_3^-/U
	580	0.11	1.55	3.2	46.20	2.81	S44	High NO_3^-/U Low U *N*
	690	0.28	1.50	2.2	47.40	3.00	S46	Feed resin
IRC-72	580	0.21	1.45	2.6	48.22	3.14	S47	was dried and
2-6681	580	0.40	1.45	3.0	48.51	3.21	S50	shape separated
C-464	600	0.34	1.55	1.5	44.35	2.30	S05	Duolite resin
1-45	600	0.34	1.50	1.8	43.93	2.30	S06	Duolite resin
C-464	650	0.26	1.40	2.0	43.29	2.41	S45	Duolite resin
2-66	650	0.47	1.40	3.0	43.40	2.49	S48	Duolite resin
	650	0.41	1.45	3.6	43.60	2.49	S49	Duolite resin

H_2O per mole U at the standard LOD conditions of 100°C. The average composition might be represented by:

$$UO_2(H_2O)_2H_{0.1}(C_{4.6}H_{4.7}O_2)_{2.1}$$

The hydrogen- and sodium-form resins do not retain water at these LOD conditions; the water with the uranyl-loaded resin is probably bound with the cation as $U(OH)_4^{2+}$, $UO_2(H_2O)_2^{2+}$ or some similar structure. This would agree with indications of two peaks for water evolution during carbonization. The 10 to 15% LOD preferred (to minimize static charge problems for the uranium-loaded resin) would represent an additional 4 H_2O/U. The nitrate extraction solvent, the sodium from caustic regeneration of the solvent, and metallic impurities from the resin or uranium feed do not appear to result in significant problems as impurities. From the information presently available, the reference flowsheet should give reproducible and acceptable compositions of uranium-loaded Amberlite IRC-72.

Nickel-loaded resin

Most of the process development work for resin loading, carbonization, conversion, coating, and the subsequent process operations is done with natural or depleted uranium. For some tests of particle handling and carbonization, a nonradioactive stand-in resin is needed to avoid radioactive contamination. The hydrogen and sodium forms of the carboxylic acid resins cake or fuse excessively and do not give representative behavior of products during carbonization. Sulfonic acid cation exchange resins do not show the caking and fusing, but the carbonization behavior and products are not representative. A nonradioactive stand-in for resin-based uranium fuel kernels was prepared by loading Amberlite IRC-72 carboxylic acid cation exchange resin with nickel. A two-stage batch-loading procedure was used with addition of NH_4OH solution to hydrogen-form resin in $Ni(NO_3)_2$ solution. The optimum end points for NH_4OH additions were about pH = 6 to give 19 to 20 wt % Ni in the product (dry basis). Higher pH results in formation of ammonia complexes of

nickel without any precipitation of hydroxides. Six batches totaling 175 kg of dried nickel-loaded resin were prepared.

Special compositions

Our experience with resin handling and loading has been applied to provide batches of resin of special compositions for program and nonprogram uses. These results will be briefly listed without details as to the process conditions used.

1. Dowex 50W-X8 sulfonate (strong acid) resin in the hydrogen form was dried in large quantities for Metals and Ceramics Division use. The commercial resin gives spheres of approximately the correct size and density, but not the same chemical behavior, as uranium-loaded resin for HTGR handling and carbonization development studies. The Dowex 50W-X8 resin was dried without difficulty in the fluidized bed (see Fig. 3.7) and in fixed-bed units initially used for uranium-loaded resin.

2. Amberlite IRC-72 was batch loaded to 30.5 wt % Ba from $Ba(OH)_2$. The chemical behavior during carbonization was different than for uranium-loaded resin, and nickel-loaded resin was a more suitable nonradioactive stand-in.

3. Doped resin beads were supplied for synchrotron radiation experiments concerning superheavy elements. Dowex 50W-X8 resin was sized, treated, and dried to provide two samples of about 80-μm-diam shperes with calculated compositions of 10^{-5} and 10^{-7} atoms each of U, Ce, and Cd per atom of (Na + S + O + C). This is equivalent to 10^{11} and 10^{9} atoms of U, Ce, or Cd per sphere.

4. Weak-acid resins loaded with Mo or Hf alone or in combination with other metals might meet special requirements for reactor uses. Both Mo and Hf hydrolyze easily so that Mo and Hf cations exist only at pH very unfavorable for exchange with weak acid resins. Both loaded to about 3% of the resin capacity. Loading with other metals could then be carried out at higher pH to give mixed compositions of cations.

3.5.2 Resin Carbonization (Subtask 330) — R. R. Suchomel

The objective of this task is to develop equipment and processes for carbonizing weak-acid resin microspheres. The carbonization process consists of controlled heating of resin previously loaded with uranium. Such heating is performed in the absence of oxygen and causes evolution of volatile constituents. After heating to about 600°C, the carbonized microspheres consist of UO_2 finely dispersed in a carbon matrix. This material can then be heated to 1600 to 1800°C to convert the desired fraction of UO_2 to UC_2. This later operation is referred to as conversion. Both operations are conducted in fluidized beds using argon as the levitating gas.

3.5.2.1 Equipment Development — J. A. Carpenter, Jr., J. E. Mack, and B. J. Bolfing

The construction, assembly, and initial testing of a 0.23-m-diam (9-in.) furnace system capable of carbonizing batches of up to 8 kg of loaded resin (approximately 4 kg of uranium) was completed. Though not prototypic for hot-cell operation, this system was designed to provide long-term cold operating experience with the resin carbonization process using full-scale equipment.

The furnace consists of a water-cooled steel outer jacket containing a cylindrical clamshell ceramic furnace body within which is suspended the Inconel muffle reaction chamber. Argon is introduced into the bottom of a 60° cone to fluidize the bed. The argon and carbonization effluents flow up the 0.23-m-diam cylindrical muffle to an inverted-cone top, which connects the muffle via an insulated crossover pipe to a perchloroethylene spray-scrubber provided to remove condensables. About halfway up the cylindrical section of the muffle, a fine-mesh particle-retention screen prevents microspheres from being carried over into the scrubber. Past the scrubber, the gases flow through a demister, a cooler, and two absolute filters before discharge. A sheathed thermocouple, which extends horizontally through the furnace body into the center of the bed, monitors temperature in the bed. Argon flow can be set or programmed to that needed to maintain good fluidization at all temperatures. The furnace body has three separately controlled

heating zones: the gas inlet area, the particle bed, and the area above the particle retention screen.

An important adjunct to this furnace was the construction and operation of the particle transfer loop (Fig. 3.19), which transfers particles into and out of the 0.23-m-diam carbonization furnace. The uncarbonized batch of loaded resin is manually loaded into a transfer hopper (left of figure), pneumatically transferred to a receiving hopper above the furnace, and then gravity-fed into the reaction chamber. Upon completion of carbonization, the fluidizing gas is turned off and the bed of carbonized particles drains by gravity into a transfer hopper below the furnace. From here, the particles are pneumatically transferred with argon to a collection hopper above an argon-atmosphere glove box, where they are allowed to cool. They are then drained by gravity into the box for inspection, sampling, upgrading, and subdivision into smaller batches before being forwarded to other furnaces for conversion and coating.

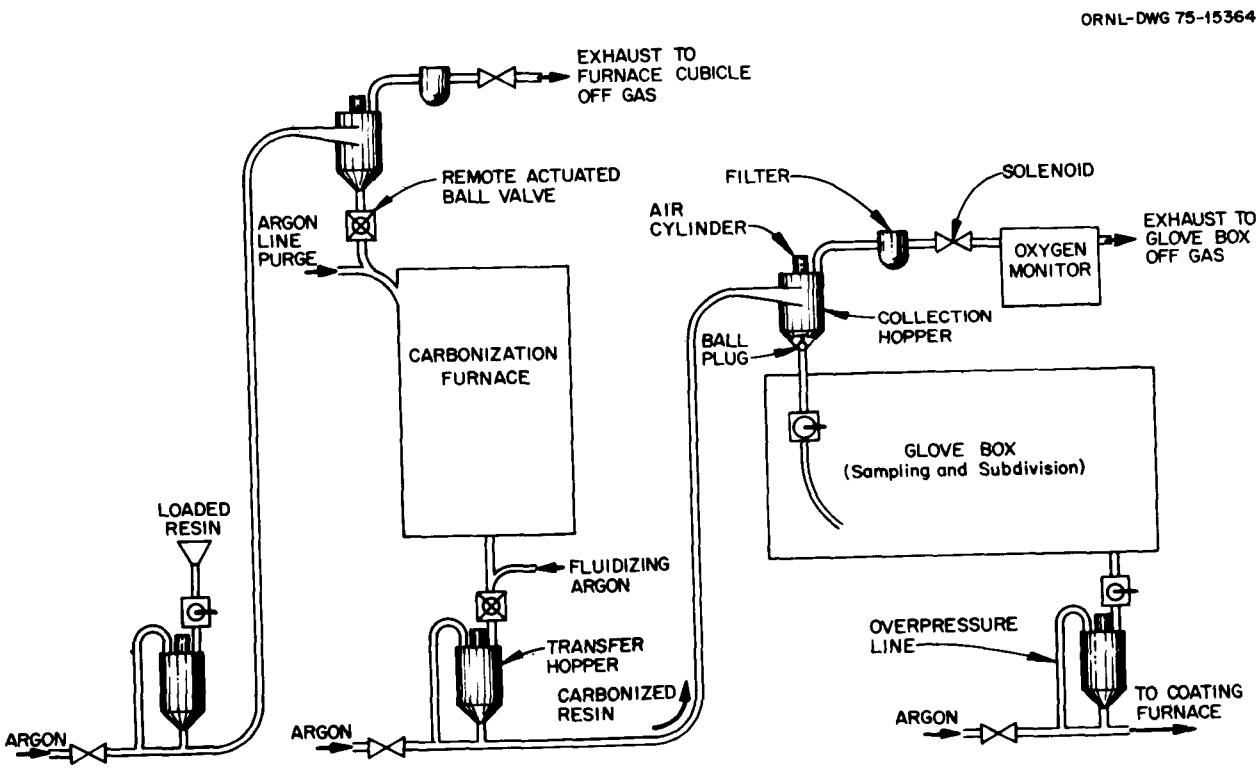

Fig. 3.19. Resin Carbonization Furance Loop.

Tests of the system indicate that particles are transfered with little or no retention or damage. Resin is typically unloaded from the furnace and transferred at temperatures of 400 to 600°C. A special particle-level indicator capable of withstanding such high temperatures was designed, built, and successfully tested in the transfer hopper below the furnace. This level indicator ensures complete transfer of a batch of particles. While each step in the transfer process is manually actuated by a switch, the actual sequencing of the steps is controlled by a programmable logic controller (PLC), which continuously monitors the system and provides sufficient interlocks to virtually eliminate operator error.

A device for size classifying large quantities of resin (a Sweco Turbo-Screen classifier) was purchased and performance tested. Something of a cross between a true air classifier and a standard screening device, this machine essentially consists of an impeller-type fan mounted behind a vertically oriented screen. The fan creates a swirling suction action through the screen. Particles small enough pass through the screen and are directed out by the impeller vanes through a duct and disentrained in a cyclone separator, while the oversize particles fall through a chute in front of the screen. In operation, an "air wand" rotates between the screen and fan continuously directing a blast of air back through the screen to prevent blinding. Pneumatic tests with substitute nickel-loaded Amberlite IRC-72 weak-acid resin showed the device to be capable of quite high throughput with high cut efficiency, negligible screen blinding, and minimal particle breakage. A major disadvantage for possible hot-cell use of the present unit is that it uses only one screen at a time; nevertheless, the utility of the principal of operation seems to have been demonstrated.

Work also continued with the 0.10-m-diam (4-in.) laboratory-scale carbonization furnace. The possible use of pressure transducers for measuring the pressure within the reaction chamber muffle was investigated and proved feasible. A special sampling system was built and used to connect the TOF (Time of Flight) mass spectrometer to the crossover pipe between the furnace system's muffle and scrubber. Cold traps

provided in this sampling system showed that they might be used instead of a perchloroethylene spray scrubber to remove condensables (water and condensable aromatic hydrocarbons) produced during carbonization. A system for withdrawing small samples of particles from the reaction chamber during operation was designed and constructed. It will be tested in the next period.

3.5.2.2 Process Development — J. A. Carpenter, Jr., and D. P. Stinton

The production of fissile fuel kernels via resin carbonization is a relatively new development. The first process development work in large-scale equipment[28] took a generally phonomenological approach, as did extensive laboratory-scale studies by the Base Technology Program.[29] This work provided a workable carbonization cycle; 2°C/min to 600°C, 7.5°C/min to 800°C, and a 30-min hold at 800°C, all under argon flow conditions suitable to maintain adequate fluidization at each temperature.

Work conducted in this period was aimed at providing process optimization and a better understanding of the mechanisms of the decomposition of the resin. The studies included TGA, DTA, and quadrupole mass spectrometer investigations of vacuum and inert-gas pyrolyses of small quantities of resin in laboratory-scale equipment, and simple tests of resin drying in air. Also in-line time-of-flight (TOF) mass spectrometer studies of effluents from carbonizations in the 0.13-m-diam coating furnace and the 0.10-m-diam Inconel muffle carbonization furnace were conducted. Results of the carbonization in the 0.13-m-diam furnace were reported.[30]

From these studies, the following understanding has emerged of the decomposition in an inert atmosphere of the uranium-loaded acrylic acid divinylbenzene cross-linked resins presently used, Amberlite IRC-72 and Duolite C-464.

The first reaction to occur in carbonization is the evolution of water absorbed in the pores of the resin. This occurs in reasonable times between about 80 and 150°C.

Between about 280 and 290°C, true decomposition begins. A major endotherm appears and is probably due to the loss of hydrate water associated with the uranyl ion, perhaps the breaking of carbon-carbon bonds, and a possible rearrangement of the polymer structure.

Between about 300 and 340°C, CO_2 and a lesser amount of CO are evolved. We believe that this is from the carboxyl radical weakly bound to the uranyl ion. Probably from a more strongly bound carboxyl radical, CO_2 and CO are also evolved between about 350 and 400°C. The kinetics of these reactions were also determined.

Between about 400 and 440°C, condensable aromatic hydrocarbons are given off as a fine aerosol. These were collected in the cold-trap of the sampling system attached to the 0.10-m-diam furnace, analyzed by a gas chromotagraph mass spectrometer, and identified as predominantly substituted benzenes with three and four carbon atoms in the side chains. It is thought that these compounds are the decomposition products of what were the divinylbenzene cross-links of the polymer. We also feel that these light aromatic hydrocarbons are precursors to the heavy tars observed in the crossover pipes.

Another endotherm occurs between about 450 and 500°C; it is probably due to another structural rearrangement. Between about 500 and 650°C, copious quantities of hydrogen and lesser amounts of methane are liberated, and the carbonization process is essentially complete. In addition, a slight evolution of CO occurs and may be due to reduction of hyperstoichiometric UO_2.

Based on this information, carbonizations were performed in isothermal steps (as opposed to the dynamic heating typically used) designed to allow the completion of a given reaction at some given temperature before starting another reaction at a higher temperature. Dynamic heating through a "critical" range of about 360 to 400°C at high rates produces a final carbonized particle with a low carbon-to-uranium ratio. Such low ratios seem to be associated with difficulties of bed sticking during conversion. The present understanding suggests that the effect of the fast heating may be to overlap the CO_2 evolution in the 350 to 400°C range with the reaction that evolves the aromatic hydrocarbon aerosol, causing loss of free matrix carbon as CO by

reaction with the CO_2. Isothermal step carbonizations in which the bed was held between 350 and 400°C long enough to drive off the CO_2 before proceeding to higher temperatures have produced particles with carbon-to-uranium ratios as high as those produced by slow dynamic heating through the "critical" range.

Some attention has been paid to identifying the properties and quality typical of the resin microspheres both before and after carbonization and conversion. As of October 1976, 130 carbonization runs using large-scale equipment had been performed. A brief resumé of properties of carbonized resin from typical runs is presented in Table 3.7. Some properties of a few batches converted to approximately the same degree are presented in Table 3.8. It must be remembered that, while it is possible to speak of properties typical of carbonized resin, the properties of converted resin depend strongly on the degree of conversion.[31]

Quality parameters investigated included shape reject proportions and interparticle variation of the uranium content per unit volume. A shaking table shape separator was set up in an inert-atmosphere glove box to permit shape analyses of the pyrophoric carbonized and converted resin. The results showed that rejections of about 0.5 wt % have been typical after carbonization, whereas 0.2% is more typical after conversion. Neutron activation of individual particles was used to determine the uranium content per unit volume. Variations of ±2.6% were found for Duolite C-464 and ±1.4% for Amberlite IRC-72, both loaded by the amine extraction method.

Previously, weak-acid resin microspheres were converted with a conical gas distributor. Use of the porous plate gas distributor (frit) for all conversion and coating operations is now desired, Thus, a series of conversion runs was performed to determine suitable conditions for use with the frit.

This experiment taught that material could be converted in the frit without sticking provided sufficiently high argon flows were used. Batches of 0.5 kg U were sucessfully converted by increasing the argon flow rate from 0.5 to 1.4 std liters/sec (1 to 3 scfm).

Table 3.7. Summary of Some Results for Carbonization of Uranium-Loaded Weak-Acid Resin in the 0.10-m (4-in.) Inconel Furnace

Run	Uranium Content[a] (wt % dry)	Water Content (wt %)	Cycle	Argon Flow[b]	Final Analysis, wt %			Density (g/cm^3)	Diametral Shrinkage (%)	Weight Loss (%)	Crushing Strength	
					Uranium	Carbon	Oxygen				(N)	(lb)
				Duolite C-464 Loaded with UO_3[c]								
C-27	46.0	3.19	Dried in air 110°C, 7.5°C/min to 800°C, hold 30 min	constant	72.26	17.525	8.263		31.17	34.59[d]	12.6	2.83
C-28	46.0	3.19	75°C/min to 800°C, hold 30 min	program	70.81	19.11	9.655	2.77	31.87	35.74	13.9	3.12
				Amberlite IRC-72 Loaded by Amine Extraction[e]								
C-33	48.7	9.58	2°C/min to 600°C, 75°C/min to 800°C, hold 30 min	program	70.61	19.66	8.92	3.41	∿3.5	41.43	35.2	7.91
C-34	48.7	9.58	2°C/min to 600°C, 75°C/min to 800°C, hold 30 min	program	71.02	19.32	9.86	3.52	∿37.0	43.09	15.6	3.50
C-45	49.3	10.74	2°C/min to 600°C, 7.5°C/min to 800°C, hold 1 hr	constant	72.535	17.44	9.64	3.48	33.97	38.25		
C-46	49.3	10.74	2°C/min to 600°C, 7.5°C/min to 800°C, hold 1 hr	program	72.95	16.97	9.76	3.63	34.23	39.39	23.9	5.37
C-47	49.3	10.74	2°C/min 59 600°C, 7.5°C/min to 800°C, hold 1 hr	constant	72.405	17.48	9.39	3.50	33.37	39.02		
C-85	49.9	12.89	2°C/min to 600°C, 7.5°C/min to 800°C, hold 30 min	program	70.52	19.59		3.12		39.96		

[a]Approximate; calculated from water content shown and uranium content of undried resin determined from analyses of resin loading solutions.

[b]Rate 0.47 std liter/sec (1 scfm).

[c]P. A. Haas, *HTGR Fuel Development: Use of UO_3 to Load Cation-Exchange Resin for Microsphere Preparation*, ORNL/TM-3817 (September 1972).

[d]With respect to batch weight after drying.

[e]P. A. Haas, *HTGR Fuel Development: Loading of Uranium on Carboxylic Acid Cation-Exchange Resins Using Solvent Extraction of Nitrate*, ORNL/TM-4955 (September 1975).

Table 3.8. Data for Carbonization and Conversion of Amberlite and Duolite Resins

Furnace: 0.13-m-diam (5-in.) multipurpose furnace employing 30° cone, graphite muffle

Heat cycle: resin dried at 110°C in air at least 16 hr; 2°C/min to 600°C, hold 15 min, ∿240°C/min to 1712°C, hold 30 min; constant argon flow at 0.47 std liter/sec (1 scfm)

	Value for Each Run			
	V 54	V 55	V 47	V 48
	Resin Feed Data			
Resin	Duolite C-464	Amberlite IRC-72	Amberlite IRC-72	Duolite C-464
Loading Method	Ammonium	UO_3	$UO_2(NO_3)_2$[a]	UO_3
U, % by weight of undried resin	45.5	43.5	46.3	46.0
Water, % by weight of undried resin	10.79	9.24	3.78	1.72
U, % by weight of resin dried at 110°C	51.0	47.9	48.0	46.8
Radiograph size of undried resin, μm	490	530[b]	524	530[b]
Size range by screening undried resin, μm	400–600	480–580	480–580	480–580
	Carbonized and Converted Resin Data			
U, % by weight	82.6	81.935	82.14	80.595
C, % by weight	14.28	16.14	15.925	16.94
O, % by weight (by analysis)	3.94	2.93	2.87	3.51
O, % by weight (by difference)	3.12	1.925	1.935	2.465
Conversion (by analysis), %	64.5	73.4	74.0	67.6
Conversion (by difference), %	71.9	82.5	82.5	77.3
Excess Carbon (by analysis), %	62.4	62.4	61.5	67.5
Excess Carbon (by difference), %	58.1	47.8	57.1	62.9
Radiograph Size, μm	315	339	354	382
Diametral Shrinkage, %	35.7	36.0	32.4	27.9
Density, g/cm^3	3.20	3.38	3.23	2.59

[a]With solvent extraction of nitrate.

[b]Assumed.

Also, 0.85 and 1.2-kg-U batches could be converted without sticking if the argon flow rate was 1 or 1.4 std liters/sec (2 or 3 scfm).

Particles adhered to the furnace walls at low flows. A visual examination of the fluidized bed at elevated temperatures revealed that the cone produced much more violent fluidization than the frit when equal flow rates of argon were used. Using Plexiglas models of the frit and cone at room temperature showed that 2 or 3 times the flow rate of argon was required for the frit to produce similar fluidization. When higher flow rates were used in the frit, particles no longer adhered to the furnace liner.

The TOF mass spectrometer was also used to study the conversion process. It recorded the levels of H_2, CO, CO_2, H_2O, and O_2 present throughout the run. The amounts of H_2, CO_2, H_2O, and O_2 were similar for every run. The peaks reached a maximum at about 1200°C and tailed off for the remainder of the run. The major constituent of the off-gas was CO. It yielded two separate peaks during heating from room temperature to 1700°C. There was a small peak at about 1150°C and the major peak during the isothermal heat treatment at 1700°C. The large peak continues until nearly 100% conversion and then drops off very sharply. Classical thermodynamics does not predict that the conversion reaction would occur at 1150°C. The suspected explanation for the small CO peak is further reduction of hyperstoichiometric UO_2. These results have also been reported.[30]

3.5.3 Microsphere Coating (Subtask 340) — D. P. Stinton

The microsphere coating subtask has as its objective the development of equipment and processes necessary for the remote coating of HTGR fuel particles. We will obtain the data necessary to design and operate a commercial-scale remote coating system. Microsphere coating is separated into the following areas:

1. particle coating, which consists of the conversion of the desired fraction of the UO_2 in the kernel to UC_2 followed by the deposition of porous and dense carbon coatings as well as very high-density silicon carbide coatings;

2. effluent treatment, which renders the effluent from carbon and silicon carbide coating operations into forms suitable for disposal;
3. particle handling, which includes weighing, batching, transferring, classifying, sampling, and storing of kernels and coated particle batches.

The equipment being developed to remotely coat recycled HTGR fuel includes a fluidized bed to deposit the carbon and silicon carbide coatings. The reference fissile particle coatings consist of low-density buffer and dense (LTI) carbon layers, a layer of silicon carbide, and an outer LTI coating. The fissile kernel is obtained by loading uranium onto a resin bead (Sect. 3.5.1), carbonizing at a rate of ∿2°C/min up to about 600°C to remove volatiles (Sect. 3.5.2), and converting the desired fraction of UO_2 in the carbon matrix of the kernel to UC_2. Conversion requires high temperatures (1600–1800°C), and therefore it is performed in the same furnace as that used for coating. However, since the carbonization and conversion operations are interrelated, the results of our conversion studies are presented in Sect. 3.5.2.2. Our 0.13-m-diam (5-in.) coating furnace used for conversion and coating has been described previously.[23,32] Major efforts during the year included modifying several components of the coating equipment, procuring and testing new equipment for remotely loading and unloading the furnace, and developing a better understanding of the deposition of the carbon and silicon carbide layers.

3.5.3.1 Equipment Development — R. R. Suchomel, D. P. Stinton, J. L. Heck, M. K. Preston, W. R. Hamel, and B. J. Bolfing

The main emphasis of equipment development has been on completion of the remote coater loop. As an addition to be incorporated into the existing 0.13-m (5-in.) coating system, this equipment will automatically unload a batch of coated particles. It also will weigh the batch with an accuracy of 0.1% and extract a sample. In addition, a used coating crucible can be replaced. All the coater loop operations will be controlled through a PLC (programmable logic controller). This equipment is illustrated in Fig. 3.20.

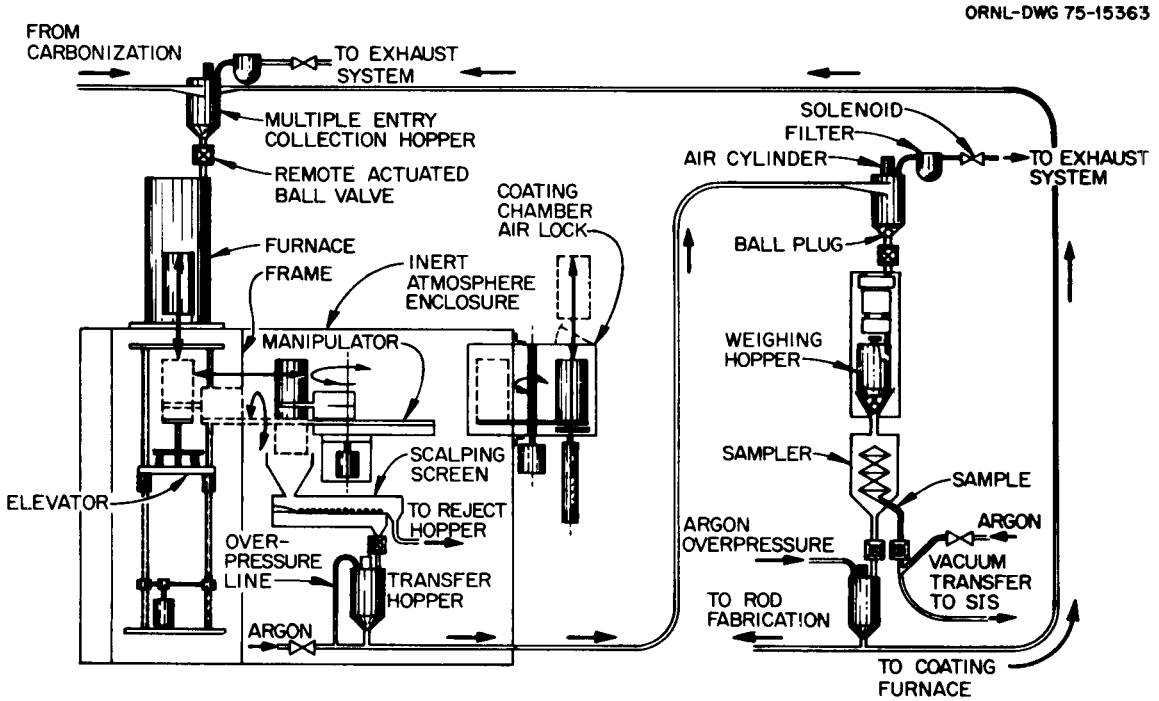

Fig. 3.20. Remote Coating Furnace Loop.

The coater loop has been designed to meet requirements anticipated for future full-scale systems. The equipment will be contained under an inert atmosphere because the kernels and buffer-coated particles are pyrophoric, and the system will have the capability of handling particles as hot as 600°C. Also, the gas injector assembly is to be cooled with perchloroethylene (C_2Cl_4) to demonstrate the use of a nonhydrogenous coolant. During this reporting period, all active components of the loop were procured or fabricated. Once received, each was tested to assure reliability and good performance. This mockup testing resulted in a number of small modifications to the crucible unloading equipment: the elevator, manipulator, scalping screen, and airlock. These components now perform acceptably and are ready for operation. The inert-atmosphere enclosure that will surround these components is currently being fabricated.

An equipment column, which will support the weigher, sampler, and transfer hoppers, has also been erected to test equipment operation and alignment. The hoppers and the shell and mechanical portions of the precision weigher were received and mounted. The electronic package

for the weigher was returned to the vendor and is being modified because the load cell did not meet the required precision.

The sampler is also ready for installation on the column. Samplers of two different designs were tested to determine the most suitable one for inclusion in the coater loop. A ten-stage sampler design, which yields a sample-to-input mass ratio of $1/2^{10}$ or 1/1024, was chosen over a three-stage design, which produced a $1/10^3$ or 1/1000 ratio, because of the consistency of its sampling ratio, its light weight, and its elimination of particle holdup. The two devices, their operation, and the results of comparative testing are described in a topical report.[33]

Another equipment innovation has been development of a self-cleaning connecting pipe between the 0.13-m coating furnace and its effluent scrubber. This connecting pipe is actually made of two concentric tubes, with the inner tube being made of porous metal. Argon is forced radially inward through the porous tube, preventing soot from depositing on the wall. This technique has been used successfully to eliminate the need for periodic removal and cleaning of the crossover pipe. In conjunction with normal furnace operation, experimentation continues to determine the minimum argon flow required. Because of the success of this technique, an entire disentrainment section of the coater is being fabricated with the expectation that more of the cumbersome maintenance can be eliminated.

A new temperature measuring device has been installed on the 0.13-m-diam coating furnace. Previously, the furnace temperature was determined with a manual optical pyrometer. The new system consists of an automatic optical pyrometer with a digital readout. This system is used to automatically heat the furnace to set temperature and hold it there.

A final area of equipment development is the perchloroethylene (C_2Cl_4) scrubber[34] used to remove soot and hydrocarbon vapors from the coater off-gas. This scrubber has performed very satisfactorily since installation more than two years ago. The scrubber has been modified slightly to use a conical-bottom reservoir so that the scrubbing liquid can be circulated through a strainer. The strainer removes any particles

or coating fragments that could damage the recirculation pump. The new system is presently being tested and evaluated.

Internal baffles were added to the C_2Cl_4 reservoir to reduce the carryover of C_2Cl_4 vapors and soot. Preliminary results indicate that the carryover has been significantly reduced. Perchloroethylene level, density, and flow measuring instrumentation have also been added to the scrubber reservoir for remote indication and inspection.

A transfer line has been installed between the scrubber reservoir and the C_2Cl_4 reclamation area. This line permits remote addition of clean C_2Cl_4 and transfer of used C_2Cl_4 to be distilled. The reclamation of used C_2Cl_4 is described in Sect. 3.5.8.

3.5.3.2 Process Development: 0.13-m Coater — D. P. Stinton and J. E. Mack

The first coating applied to both fertile and fissile particles is the buffer layer. Improvements in the buffer coating process have been described in several previous progress reports.[35,36]

The second layer applied to both fissile and fertile particles is the low-temperature isotropic (LTI) coating. All recent coating development has used a contoured porous-plate gas distributor referred to as a frit.[37] Figure 3.21 shows the frit that has been used during

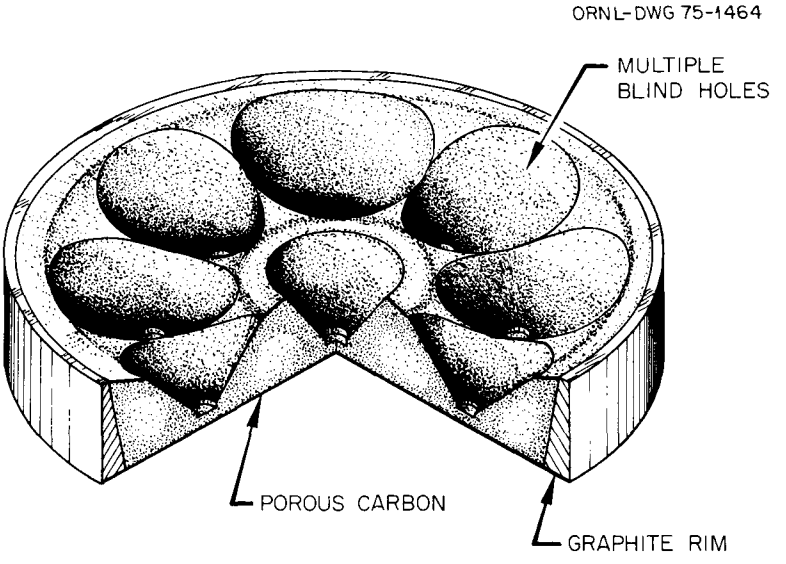

Fig. 3.21. Porous Plate Gas Distributor.

this reporting period. Several previous reports have described the development of the frit in greater detail.[38,39]

Considerable information has been gathered comparing the anisotropy of LTI coatings deposited by using the cone and frit type gas distributors.[39] The coatings that were examined are from statistically designed experiments conducted in 1974 with the 0.13-m-diam coater. The Bacon anisotropy factor as determined optically (BAF_o) was measured by General Atomic Company for all the coatings. The BAF_o depended on the coating rate, in agreement with other investigations.[40] Anistropy values for coatings applied with the cone and frit are compared in Fig. 3.22. The BAF_o values of all the coatings applied with the frit are lower than any values for coatings applied with the cone. The anisotropy difference is more striking if one compares coatings deposited

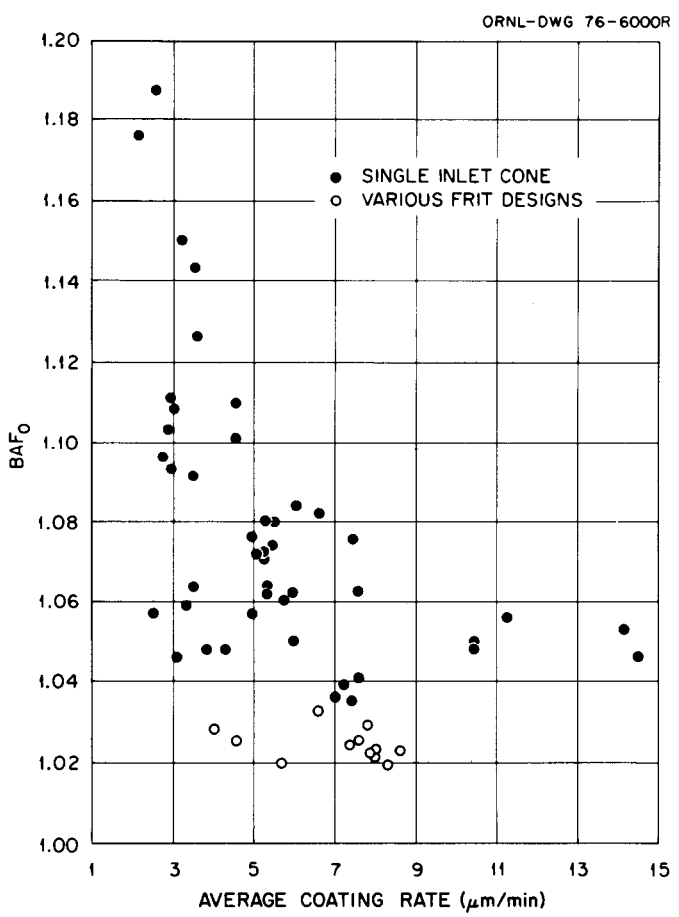

Fig. 3.22. Influence of Coating Rate on BAF_o.

at the same deposition temperature and rate. The curves of Fig. 3.23 were found by a multiple regression analysis for the 45 coating runs made with the cone. They show that the large amount of the scatter in the data of Fig. 3.22 for the cone runs is accounted for by the effect of deposition temperature, which was shown to be statistically significant at the 99% confidence level. The points in Fig. 3.23 are for coatings deposited at 1375°C by use of the frit. Comparison of these points with the line labeled 1375°C shows that the frit produces coatings having BAF_o values about 0.02 to 0.04 units lower than coatings similarly deposited with a cone. This is potentially a significant effect when viewed in terms of the ability of the coatings to survive irradiation to high neutron fluences. The reason for the lower BAF_o values obtained with the frit is unknown but may be related to the more uniform distribution of coating gas.

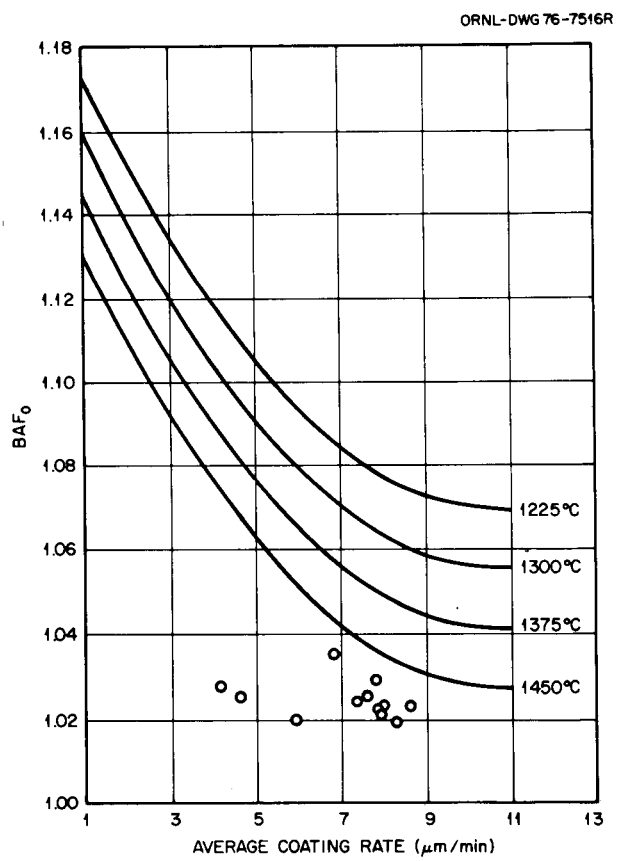

Fig. 3.23. Correlation of BAF_o with Coating Rate and Temperature.

Perhaps a more important factor than the average BAF_o value for a particle batch is the fraction of the particles that have a BAF_o value greater than some critical value above which an appreciable fraction of coatings would fail during irradiation. Thus the particle-to-particle variation in BAF_o within the batch as measured by the standard deviation is important. Particles coated in a 0.13-m-diam cone under typical coating conditions had a standard deviation of 0.011, while particles coated with a 0.13-m or 0.24-m-diam frit had a standard deviation of about 0.004. The lower standard deviation for particles coated with the frit implies greater uniformity of the coating conditions from place to place within the fluidized bed.

For both the cone and frit, the within-batch standard deviation of BAF_o is correlated with the average BAF_o for the batch; standard deviation decreases with decreasing values of mean BAF_o, as shown in Fig. 3.24. Note that coatings deposited with the 0.24-m-diam frit have low values for both the mean BAF_o and the standard deviation of BAF_o.

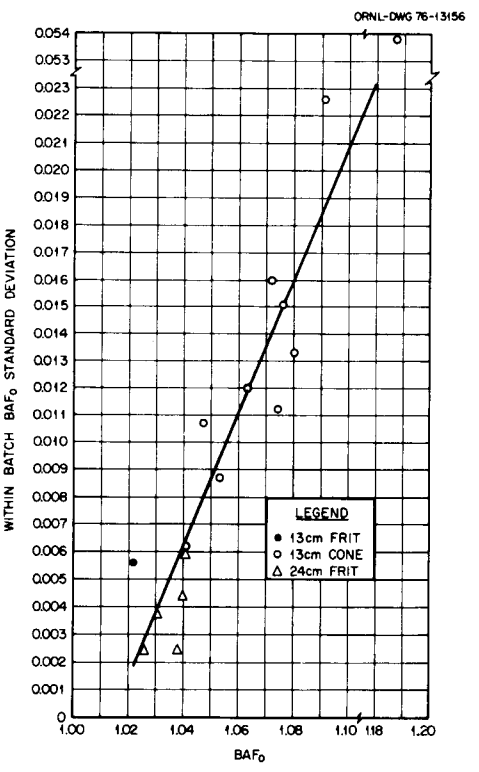

Fig. 3.24. Correlation of BAF_o and Standard Deviation of BAF_o

The importance of the particle-to-particle variation in BAF_o is shown in Fig. 3.25. Here the within-batch distribution of BAF_o values is given for typical frit and cone batches. For the frit batch, note that only 0.6 and 0.01% of the particles have BAF_o values that exceed 1.04 and 1.045, respectively. In comparison, about 3% of the particles coated with a cone have BAF_o values exceeding 1.08. The line labeled "hypothetical" shows the importance of standard deviation. For this line, the average BAF_o value is low (1.03), but because of the high standard deviation (0.011) the fraction of particles having high BAF_o values is much larger than for the particles coated with the frit.

The amount of fuel dispersion has been measured on approximately 50 Biso-coated WAR batches. We examined 200 particles along random horizontal and vertical passes across each x radiograph. Particles showing dispersion were classified into three groups, which are described briefly below and more completely elsewhere.[41]

A: gross fuel dispersion, continuous throughout the buffer;

B: gross fuel dispersion, discontinuous throughout the buffer; and

C: isolated globular regions of fuel dispersion in the buffer, with these regions not physically attached to the kernel.

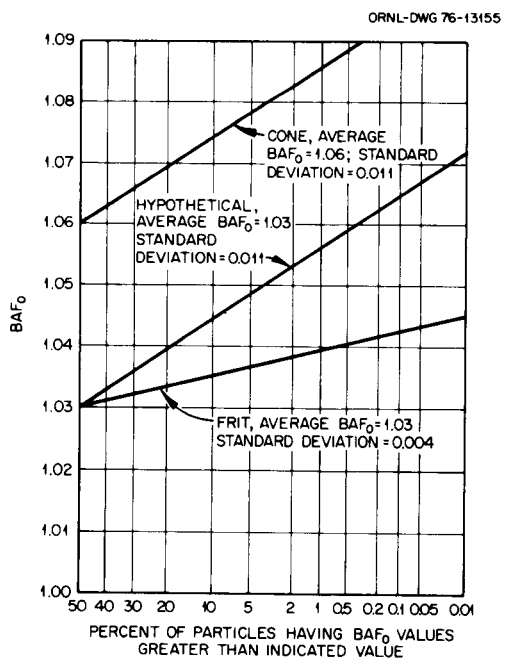

Fig. 3.25. Particle-to-Particle Variation in LTI Anisotropy.

A quantitative value of dispersion was defined by assuming that A-type dispersion had 30% of the uranium in the buffer, B-type had 15%, and C-type had 5%. With these numbers, which are only relative, the total percent of uranium dispersed in the buffer was calculated.

Several conclusions were drawn from this investigation. First, annealed coatings showed more fuel dispersion than identical unannealed ones. The second conclusion involved the installation of a new crossover pipe connecting the coating furnace to the C_2Cl_4 scrubber. The new pipe quadrupled the linear gas velocity in the crossover pipe and decreased the back diffusion of C_2Cl_4 vapors, which aggravates fuel dispersion. The average amount and frequency of fuel dispersion were halved after the crossover pipe was installed. No correlation was found between the percent of fuel dispersion and any of the following coating variables: coating gas flow rate, diluent flow rate, total gas flow rate, or coating rate. The physical properties of LTI immersion density and failure fraction were also unrelated to fuel dispersion.

The fraction of defective LTI coatings on Biso-coated ThO_2 kernels has been reported previously.[42] An experiment concerning the permeability of inner LTI coatings deposited over buffer-coated, uranium-loaded WAR has recently been completed. The experimental variables were: (1) type of hydrocarbon — propylene vs a mixture of propylene and acetylene, (2) percent helium diluent — 0, 50, 67, (3) hydrocarbon flow — 0.94 vs 1.7 std liters/sec (2.0 vs 3.6 scfm), and (4) unannealed vs annealed (1800°C, 30 min) coatings.

Analysis of the permeability data for LTI coatings applied at 1350°C showed that propylene coatings were much less permeable than mixed-gas coatings. A 2-hr chlorine leach removed from 10 to 75% of the uranium from particles coated with 50% mixed gas and 50% helium diluent. Mixed-gas coatings applied with 67% helium diluent behaved slightly better but were still permeable. All the mixed-gas coatings were slightly less dense than the propylene coatings. In an attempt to decrease the permeability, mixed-gas coatings were applied at a lower temperature, 1275°C. These coatings had higher densities but were still quite permeable except for coatings applied at a low flow

rate of mixed gas [1 std liter/sec (2 scfm)], which allowed only 0.5 to 3 % of the uranium to be leached by chlorine.

Coatings applied with propylene were much less permeable than mixed-gas coatings. These coatings had defective fractions ranging from 0.03 to 0.7%. The defective fraction depended on hydrocarbon flow rate and whether the coating was annealed. Surprisingly, the defective fraction could not be correlated with the diluent flow rate. Low hydrocarbon flows [1 std liter/sec (2 scfm) C_3H_6] produced coatings with lower permeabilities than coatings produced with high flow rates [1.7 liters/sec (3.6 cfm) C_3H_6]. Coatings that had not been annealed also showed lower defective fractions than annealed coatings.

Obtaining a high-density silicon carbide coating is an important objective of the silicon carbide coating operation. Densities in excess of 99% of theoretical (3.18 g/cm^3) are likely required to achieve good irradiation performance. An experiment examined the effect of methyltrichlorosilane (MTS) flux, the H_2/MTS ratio, and temperature on density and several other coating properties. The coating densities from this experiment ranged from 3.137 to 3.200 g/cm^3. A multiple regression analysis of the data showed that density depended on the H_2/MTS ratio and on the deposition temperature. The H_2/MTS ratio was significant at the 90% confidence level, while temperature was significant at the 95% confidence level. Curves in Fig. 3.26 show the general effect that temperature and the H_2/MTS ratio have on the silicon carbide density. These curves were plotted by use of the equation predicted by the multiple regression analysis. This figure shows that density increases from 3.15 g/cm^3 at 1400°C to 3.195 g/cm^3 at 1625°C. It then decreases to 3.17 g/cm^3 by 1800°C. The effect of H_2/MTS ratio is also shown in Fig. 3.26. Higher H_2/MTS ratios produce denser coatings. Increasing the H_2/MTS ratio from 25 to 45 or from 45 to 65 increased the coating density by about 0.005 g/cm^3. These results agree very well with a study done in a smaller coater.[43]

In examining the density results, it is important to note that the deposition rate does not affect the coating density for the equipment and process conditions employed.[44] Coatings with densities of 3.195 g/cm^3

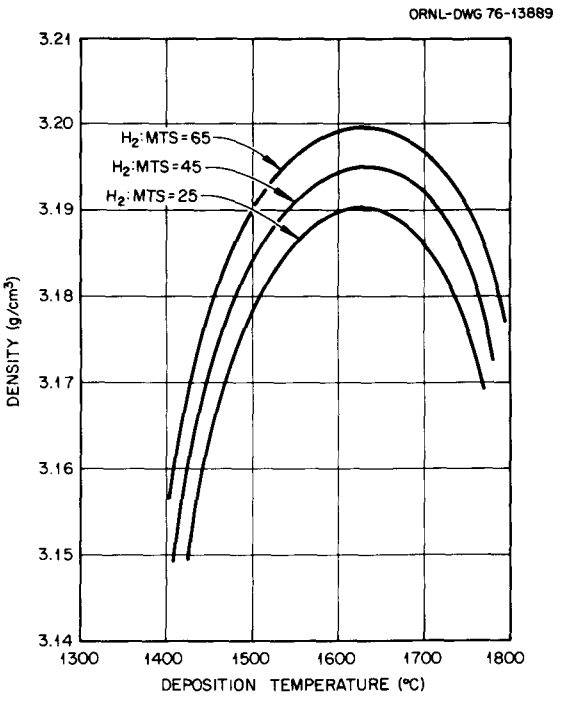

Fig. 3.26. Correlation of Density with Temperature and H_2/MTS Ratio.

or greater were deposited at rates of 0.07, 0.14, 0.26, 0.37, and 0.46 μm/min. An additional coating run was recently made after completion of the designed experiment to verify that high-density coatings could be deposited at high rates provided suitable process conditions were used. For this extra run, the deposition rate was 0.48 μm/min and a density of 3.191 g/cm^3 was obtained. From these results, it appears that high-density coatings can now be produced in the 0.13-m-diam coater at about 0.50 μm/min. Previously, similarly depositing silicon carbide with this furnace using a single-inlet cone to distribute the gas rather than the frit had given unacceptably low-density coatings at deposition rates exceeding 0.15 to 0.20 μm/min. It appears that use of the frit gas distributor is responsible for the attainment of high coating densities at high deposition rates.

The average standard deviation of the coating density for these batches was quite low (0.005). Specifications for silicon carbide might require, for example, that 99% of the silicon carbide coatings have a density greater than 3.17 g/cm^3. Figure 3.27 shows a typical batch having a mean silicon carbide density of 3.195 and a standard

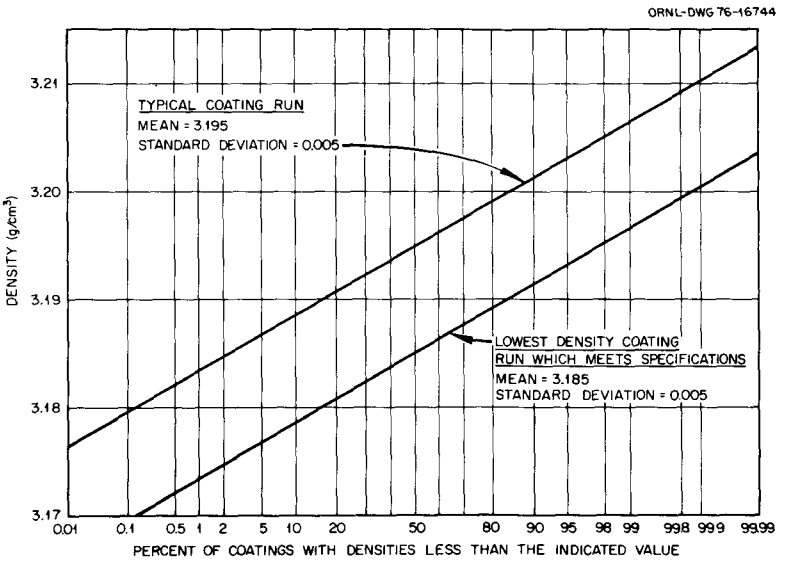

Fig. 3. 27. Particle-to-Particle Variation in SiC Density.

deviation of 0.005 has 99% of the coatings with a density greater than 3.183. With this low standard deviation, the mean can drop to 3.185 and still 99% of the coatings will have densities above about 3.173 g/cm^3.

The whole-particle crushing strengths of silicon carbide coated particles were measured in this study. Silicon carbide strength is important to irradiation performance since the silicon carbide must be strong enough to retain the fission product gases. Crushing strengths are important because the particles must withstand considerable stresses generated during pneumatic particle transfer and fuel rod fabrication. Crushing strenghts are measured by placing a particle between two flat plates and determining the load required to initiate failure. Crushing strengths have been measured on each batch of particles coated in the silicon carbide experiment. An analysis of all the data showed that crushing strength depended strongly on the deposition temperature.[44] Figure 3.28 shows that the maximum crushing strength is produced at a temperature near 1500°C. These results are consistent with results[31] that show the crushing strength of silicon carbide coated particles decreases on annealing at 1800°C.

The microstructures of the coating runs made in this study have been examined by standard metallographic techniques. The etchant[45] used to delineate the grain structure was a mixture of NaOH and $K_3Fe(CN)_6$.

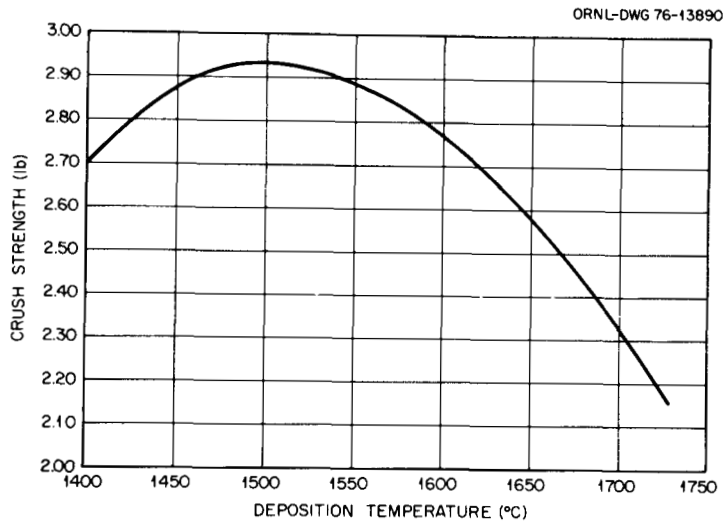

Fig. 3.28. Correlation of Crushing Strength and Temperature.

Several coating variables had very marked effects on the microstructure of the SiC. The H_2/MTS ratio had a drastic effect. Figure 3.29 shows two microstructures produced with very low H_2/MTS ratios (25). The highly banded fine grain structure is typical of low H_2/MTS ratios. Higher fluxes caused wider bands and slightly larger grains as shown in Fig. 3.29(b). These coatings typically have a low density of about 3.18 g/cm^3. Coatings produced with H_2/MTS ratios of 45 or greater do not have as many bands, as shown in Fig. 3.30.

Temperature is another variable that had a very noticeable effect on the microstructure. Very low temperatures (1400°C) produced highly banded structures, in which the bands were very convoluted, as shown in Fig. 3.31. The convoluted bands and fine grain sizes are typical of low-temperature deposits regardless of the H_2/MTS ratio. Coatings deposited at higher temperature (∿1575°C) with an H_2/MTS ratio of 45 show an intermediate grain size as seen in Fig. 3.30. These coatings show only a small number of bands and have a high density of 3.195 g/cm^3. Coatings produced at higher temperatures (∿1675°C) show much larger grains; for example, the coatings in Fig. 3.32 show large columnar grains and have a high density of 3.195 g/cm^3.

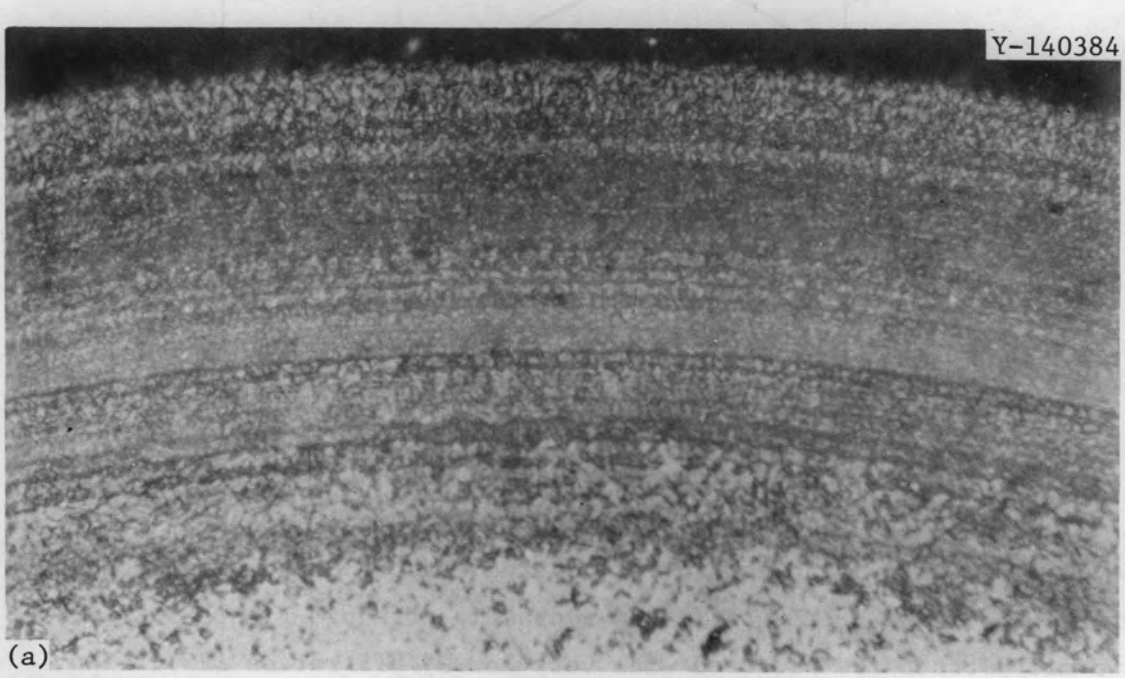

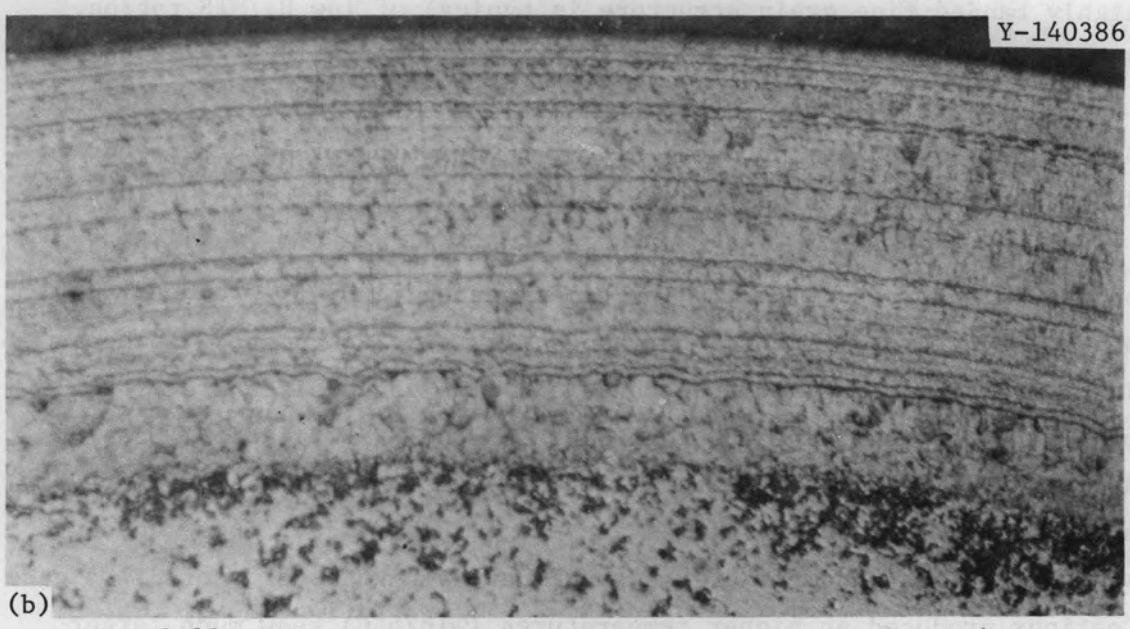

Fig. 3.29. Microstructures of Coatings Made with Low H_2/MTS Ratio (25) at 1475°C. 1500×. (a) A-732, flux = 0.035. (b) A-734, flux = 0.085.

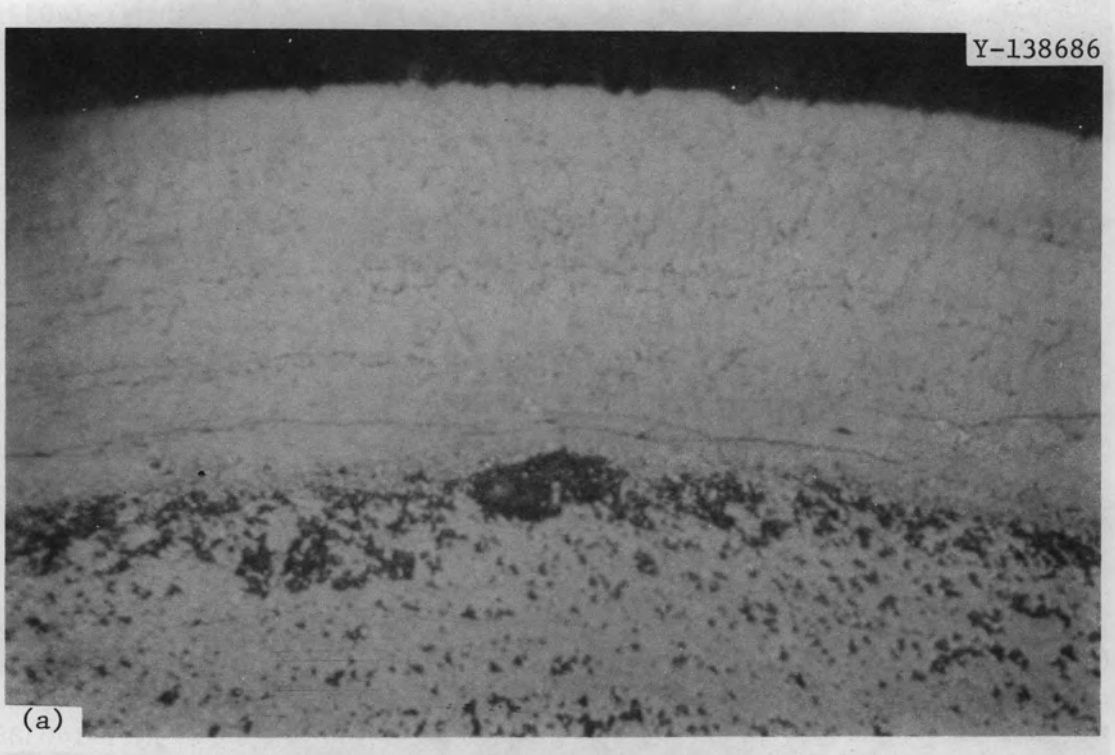

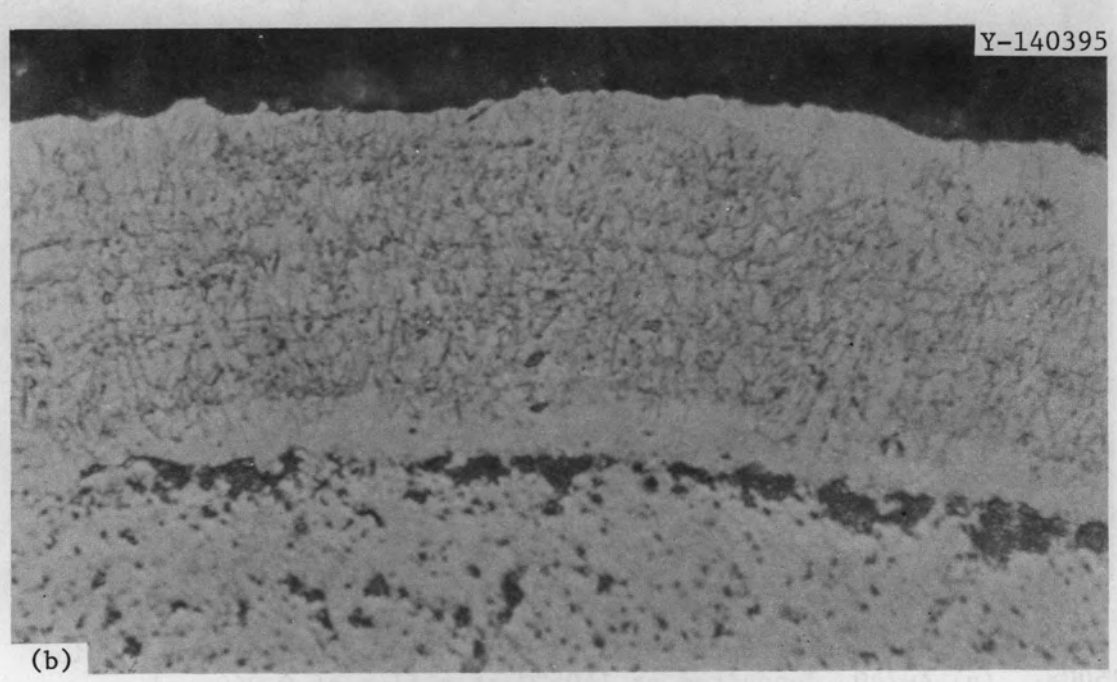

Fig. 3.30. Coatings Deposited at 1575°C Showing Intermediate Grain Size. 1500×. (a) A-737, flux = 0.060, H_2/MTS = 45; (b) A-743, flux = 0.102, H_2/MTS = 45.

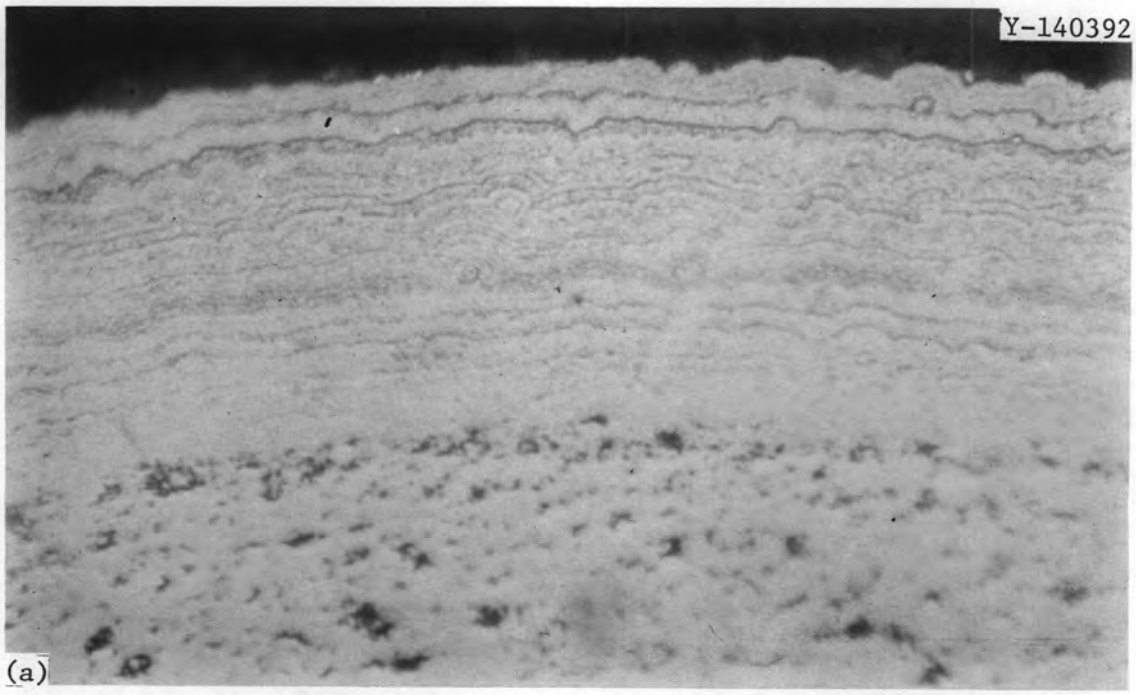

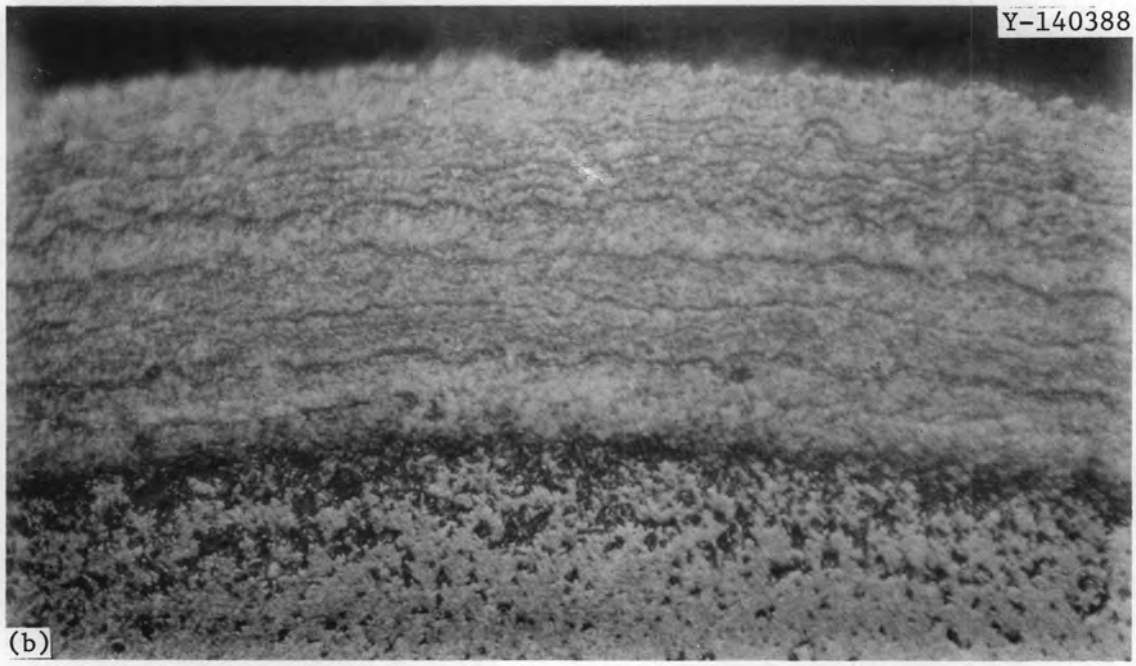

Fig. 3.31. Low-Temperature Deposits Showing Convoluted Banding. 1500×. (a) A-740, deposited at 1405°C at a flux of 0.060 and an H_2/MTS ratio of 45. (b) A-736, deposited at 1475°C at a flux of 0.085 and an H_2/MTS ratio of 65. The actual bed temperature of this run is lower than 1475°C because of high gas flow rate.

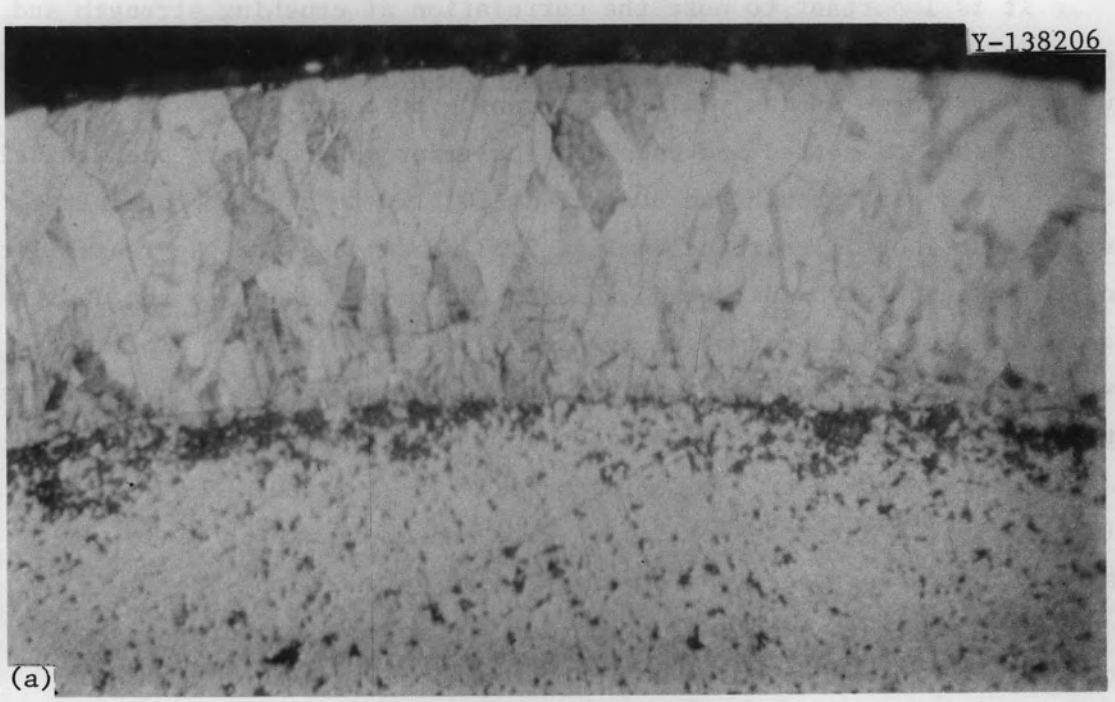

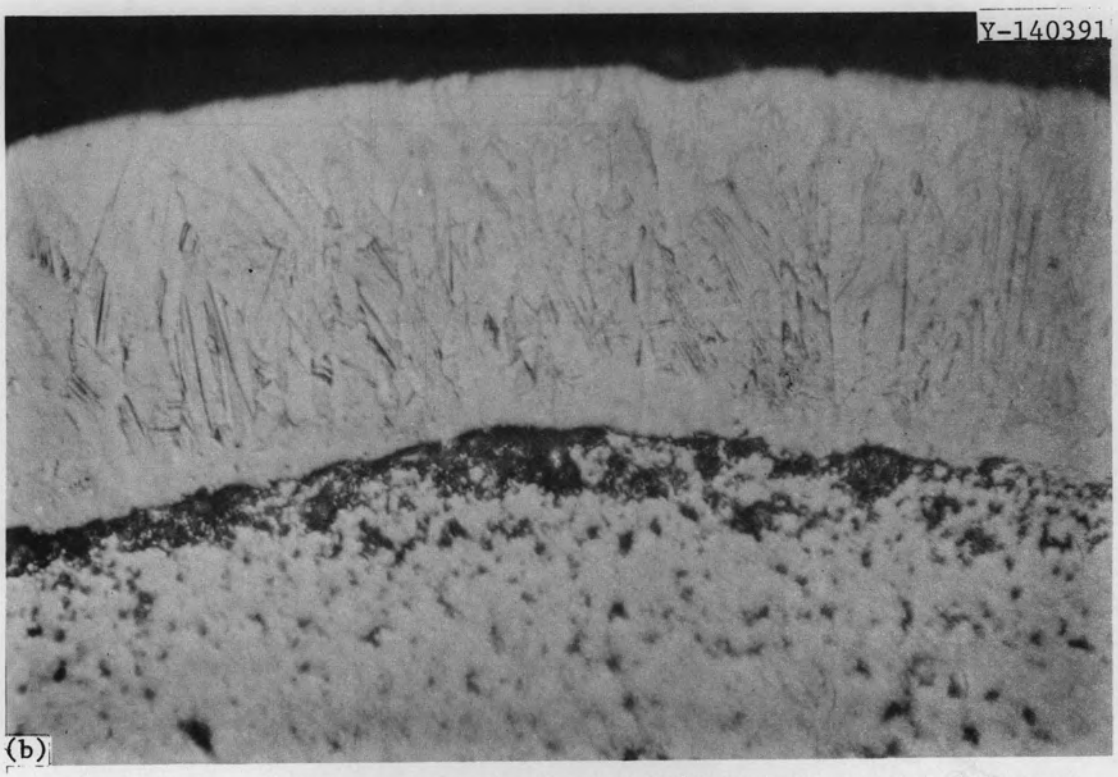

Fig. 3.32. Coatings Deposited at 1675°C Showing Large Columnar Grains. 1500×. (a) A-730, flux - 0.035, H_2/MTS = 65. (b) A-739, flux = 0.085, H_2/MTS = 65.

It is important to note the correlation of crushing strength and grain size. As would be expected, small grain size gives high strength, while very large grains yield low crushing strength.

Batches of coated and uncoated fuel microspheres were pneumatically conveyed in air through the 30-m 16-mm-OD (100-ft 5/8-in.) stainless steel test loop illustrated in Fig. 3.33 to demonstrate the feasibility of this method of handling and to obtain data pertinent to the design and operation of a prototypic system. Data and operating experience were obtained for particles of 500 to 800-μm mean diameter over a density range of 1.5 to 4.4 g/cm^3. Batches of 1 to 2 kg were transferred at air flow rates of 1 to 3 std liters/sec (7.6–23 m/sec) [2–6 scfm (25–75 fps)]. Particle velocities were measured with photoelectric sensors over short sections of translucent polyethylene tubing in conjunction with a high-speed recorder. Screened pressure taps in the line were used to measure line pressure and pressure drops.

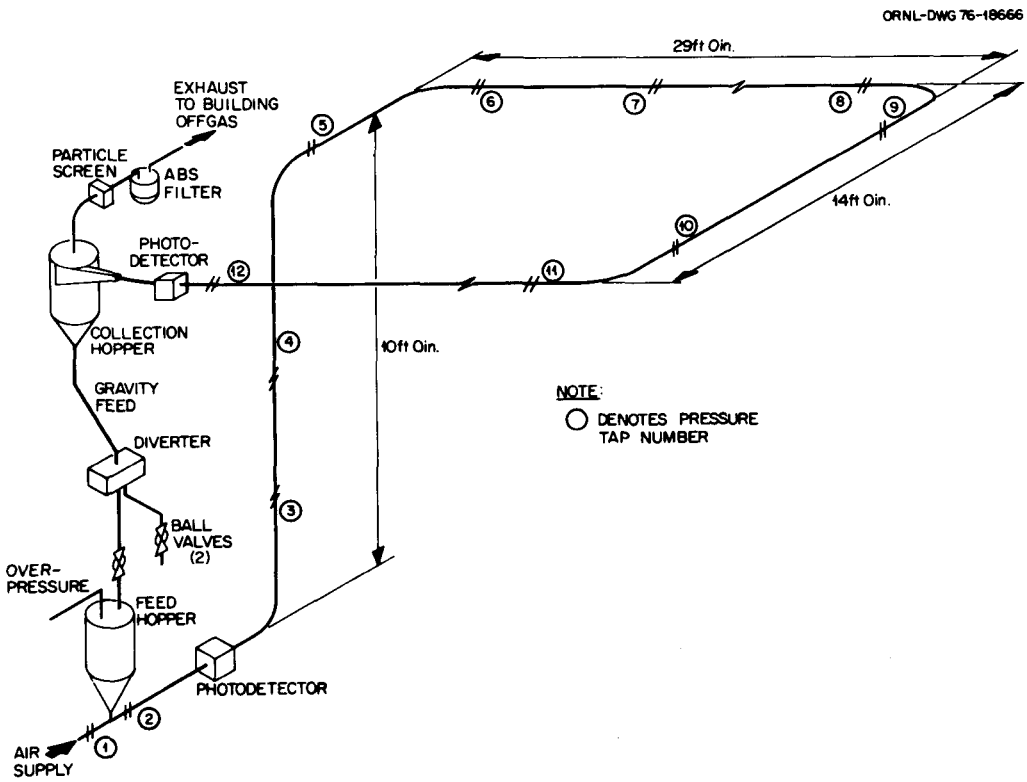

Fig. 3.33. Batch Transfer Test Loop. Dimensions shown are 8.84, 4.27, and 3.05 m.

Multiple regression analysis of the data on pressure drops in horizontal and vertical straight sections permitted the formulation of mathematical equations useful in predicting total pressure drop for any design configuration. Data on the transfer characteristics of six particle types were used to obtain the equation plotted in Fig. 3.34 for two particle types. Correlation of pressure drops in bends of different radii is under way. Current interest involves application of these equations to particle types whose diameters or densities are outside the range tested, such as the pyrophoric carbonized and converted resin kernels.

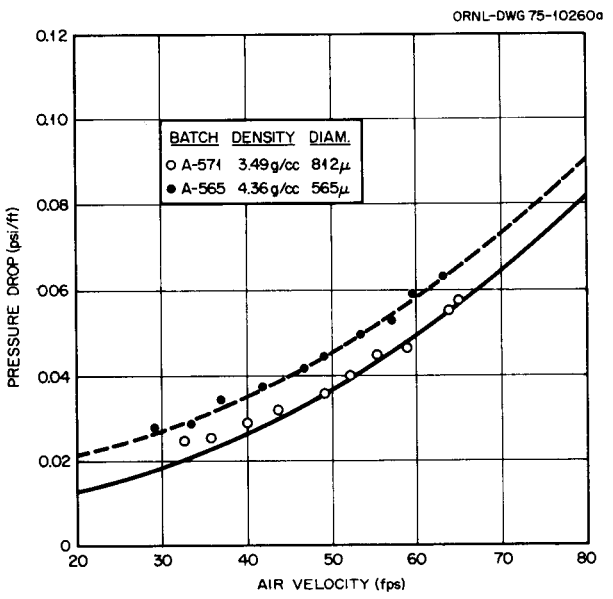

Fig. 3.34. Data and Predicted Curve for Pressure in a Horizontal Conveyor as a Function of Air Velocity, Particle Diameter, and Particle Density. 1 psi/ft = 22.6 kPa/m; 1 fps = 0.305 m/sec.

We determined the number of coatings damaged during pneumatic particle transfer. Essentially no breakage occurred with a Biso-coated thoria batch, which was collected after the transfer tangentially in a 0.23-m-diam (9-in.) stainless steel collection hopper. The batch was conveyed with an air speed of 15 m/sec (50 fps), resulting in an average particle velocity of about 9 m/sec (30 fps). Samples taken between runs were chlorine leached to determine the number of defective

coatings. Duplicate samples taken before transfer indicated failure fractions of 2×10^{-4} and 2×10^{-4}, while duplicate samples taken after 25 transfers exhibited failure fractions of 4×10^{-4} and 9×10^{-4}. A SiC-coated thoria batch was also transferred 25 times into the same collection hopper. Mercury intrusion analysis of samples taken during these runs indicated no increase in breakage with transfer.

Tests were also conducted with reference Triso-design uranium-loaded weak-acid-resin-derived particles coated through the SiC stage. These particles were transferred and collected tangentially in a 0.13-m-diam (5-in.) stainless steel collection hopper, as well as in a 0.13-m-diam dual-inlet collection hopper. Again, mercury intrusion analysis of the samples indicated no increase in breakage with transfer. The dual-inlet collection hopper was designed and tested with hope of eliminating a second collection hopper above a common piece of equipment. It has performed satisfactorily and has been permanently incorporated into the test loop.

Two-way transfer from a single-feed hopper was also successfully demonstrated. This requires pressurization of the collection hopper not receiving the particles to get air flow through this line back to the transfer hopper and into the second collection hopper.

Information obtained from operation of this test loop was used as a basis for design of the particle handling portion of the resin carbonization system. This system is described in Sect. 3.5.2.1.

3.5.3.3 Process Development: Laboratory-Scale SiC Coating — J. I. Federer

Process development work in 35- to 64-mm laboratory-scale furnaces consisted of determining the effects of various coating conditions on coating properties. Silicon carbide coatings were deposited by reacting methyltrichlorosilane (CH_3SiCl_3 or MTS) and hydrogen in a fluidized bed at elevated temperatures. This work will be published,[43] and the results are summarized below.

The principal variables of coating temperature and reactant gas composition (H_2/MTS ratio) have been correlated with coating rate, morphology, stoichiometry, microstructure, and density. The optimum temperature for highly dense coatings is in the range 1475 to 1675°C.

Lower temperatures result in silicon-rich deposits, while higher temperatures may cause unacceptable porosity. The optimum H_2/MTS ratio for highly dense coatings is 20 or more (∿5% MTS or less). The porosity increases as the H_2/MTS ratio decreases below 20. Evaluation of stoichiometry, morphology, and microstructure support the above mentioned optimum conditions of temperature and reactant gas composition.

3.5.3.4 Permability of Pyrocarbon Coatings — C. S. Morgan and G. L. Powell*

The permeability of pyrocarbon coatings for light inert gases has been investigated by annealing fuel particles at high temperature in an inert gas. The amount of gas diffusing through the coating into the buffer layer is then determined by breaking the LTI in a mass spectrograph and measuring the quantity of the gas released. Where necessary, particles were preannealed 1 hr in vacuum at 1800°C to remove gases entrapped during preparation. Fuel particles were broken one at a time, and the average emission from 14 particles was reported.

When the pyrocarbon coating of a fuel particle is broken nearly all the gas is released. Small additional amounts are evolved if the broken particles are ground. This indicates that the bulk of the void volume in the buffer layer is in the form of connected porosity. The additional gas released on grinding comes from small pores in the LTI and in the buffer layer structure.

A standard procedure to measure permeability has been developed. The specimens are annealed in 51 kPa Ne and 51 kPa He (0.5 atm each) at 1375°C for 1 hr. The ratio of moles of the two gases in the particles then represents a sensitive measure of the permeability. The use of two gases in the standard procedure for determining permability takes advantage of the sensitivity of a slower diffusing gas while the lighter, faster diffusing gas prevents mistaking the absence of gas release on breaking the pyrocarbon coating for very low permeability. It was necessary to base the neon determination on ^{22}Ne, as doubly ionized argon interferes with ^{20}Ne measurement. Table 3.9 gives the Ne/He ratio

*Development Division, Oak Ridge Y-12 Plant.

Table 3.9. Measurement of Permeability by Neon/Helium Ratio of Pyrocarbon Coatings

Specimen	Neon/Helium Ratio		Deposition Conditions		
	1375°C	1500°C	Temperature (°C)	MAPP Gas (%)	Coating Rate (μm/min)
OR-1978-HT	0.03	0.054			0.8
OR-2263-HT	0.13	0.32	1325	25	3.6
OR-2276-HT	0.13	0.30	1275	15	3.1
OR-2273-HT	0.14		1275	25	5.2
OR-2294-HT	0.15		1275	50	3.6
OR-2299-HT	0.19		1275	50	2.3
OR-2262-HT	0.20	0.45	1275	50	6.5
OR-2261-HT	0.23	0.49	1325	50	7.4
OR-2271-HT	0.23		1275	50	10.7
OR-2293-HT	0.23		1325	50	3.9
OR-2298-HT	0.24		1325	50	2.5
OR-2297-HT	0.27		1275	100	4.9
J-489	0.28	0.59	1350	50[a]	5.8
J-490	0.29	0.72	1350	100[a]	6.2
OR-2265-HT	0.32	0.66	1325	100	15.7
OR-2269-HT	0.40		1325	50	12.5
OR-2531-HT	0.40				
OR-2275-HT	0.41	0.82	1275	100	23.0
OR-2296-HT	0.44		1325	100	5.6
OR-2274-HT	0.50	0.89	1325	100	28.0
OR-2537-H	0.59				

[a]Coatings deposited from propylene.

for a selection of fuel particle batches. The Ne/He ratio at 1500°C is also included for some batches to show the sensitivity of the measurement to temperature. The deposition conditions are included and indicate that in general the permeability increases with increasing deposition rate. It has a less pronounced increase with increasing MAPP gas concentration and increasing temperature.

The argon permeability of pyrocarbon coatings was examined on several particle batches. After annealing under vacuum at 1800°C, the fuel particles still retained process argon. The argon content after a second 1800°C anneal, this time in an atmoshere of argon, was very similar to the initial anneal for most particle batches.

Since the pyrocarbon coatings of unirradiated fuel particles are impermeable to argon, it is assumed that the coatings are impermeable to krypton and xenon.

The effect of irradiation on the permeability of fuel particle coatings has been tested on particles with inert kernels. Data on permeability of inert particles from HT-30 and -31 are given in Table 3.10 along with design fluences and temperatures. The data show that at higher fluences and higher temperatures the permeability is substantially increased. However, these inert particles were irradiated under neon, and the permeability observed may represent gas diffusion during the lengthy reactor treatment. Low fluences result in pyrocarbon coatings with increased resistance to gas permeation.

Table 3.10. Neon/Helium Ratio of Fuel Particles Irradiated in HT 30 and HT 31

Batch	Fluence (n/cm^2)	Temperature (°C)	Content, moles/fuel particle		Ne/He
			Helium	Neon	
OR-2291-HT (Blank)	0×10^{21}		1.53×10^{-10}	0.41×10^{-10}	0.27
OR-2291-HT (ES1)	3.5	900	1.01	0.23	0.23
OR-2291-HT (EL1)	7.2	900	1.16	0.23	0.20
OR-2291-HT (MS1)	7.5	1250	1.01	0.90	0.89
OR-2291-HT (ML1)	8.6	1250	1.12	1.41	1.26
OR-2294-HT (inerts)	0		1.07	0.24	0.22
OR-2294-HT (inerts)	4.0	950	1.10	0.13	0.12
OR-2261-HT (included for comparison)	0		1.42	0.30	0.21

3.5.3.5 X-Ray Diffraction Determination of BAF — C. S. Morgan, C. J. Sparks, and O. B. Cavin

A fuel particle holder that will permit determination of x-ray diffraction from the (0002) planes of a small volume of the pyrocarbon coating has been designed and constructed. The device, the Spark's Anisotropy Device (SAD), can then be turned 90° and the diffraction from (0002) planes orthogonal to the first set is obtained from the same volume of coating. To obtain sufficient intensity, more than 100 fuel particles must be used. These are held in 0.89-mm (35-mil) holes in a 0.30-mm-thick (12-mil) niobium plate. Holes 0.1 mm (4 mils) in diameter are positioned in 0.1-mm-thick (4-mil) niobium sheets on each side of the center plate holding the fuel particles. The center holder can be moved in both directions so as to properly locate the fuel particles with respect to the 0.1 mm (4-mil) holes, allowing admission of the x-ray beam and exit of the diffracted beam. The ratio of the diffracted intensities from orthogonal planes is a measure of structural anisotropy in the pyrocarbon layer.

Testing of the SAD is continuing, and sufficient intensity of the diffracted beam is readily obtainable. Several modifications to improve performance are being made. If perfected, use of the SAD to determine anisotropy in the outer pyrocarbon coating will eliminate the need for mechanical polishing. It will give a measurement representing an average value within a 0.1-mm-diam (4-mil) volume within the thickness of the pyrocarbon layer.

3.5.4 Fuel Rod Fabrication (Subtask 350) — D. R. Johnson

The purpose of this work is to develop processes and equipment suitable for the remote refabrication of HTGR fuel rods. The fuel rods are 13 or 16 mm (1/2 or 5/8 in.) in diameter and 50 to 65 mm (2—2.5 in.) long and contain mixtures of fissile and fertile coated particles and graphite shim particles bonded by a matrix of pitch binder and graphite filler.

The principal activities in fuel rod fabrication are dispensing particles, blending them, and loading them into molds, injecting the matrix into the beds of particles to form fuel rods, and inspecting and assaying the rods.

3.5.4.1 Equipment Development: Fuel Rod Molding

3.5.4.1.1 Air Blender, D. R. Johnson. An experimental blender for mixing fuel particles before molding them into fuel rods has been evaluated for possible use on the cold prototype fuel rod molding machine.[46] The single-inlet conical air blender was designed by General Atomic Company for fabrication of fresh HTGR fuel. It consists of a conical chamber with an air inlet in the bottom. A pneumatically operated valve provides for discharge of the particles out the bottom of the cone. The particles are mixed by periodically levitating with pulses of air. The blender can be adjusted for best performance by varying the air flow rate, number of air pulses, and pulse time.

A range of fuel rod compositions considered to be all-inclusive for HTGR fuel refabrication was included in this investigation. Fort St. Vrain (FSV) type fuel rods [13 mm diam by 51 mm long (1/2 by 2 in.)] were blended, and the results were compared with the axial inhomogeneity specification for commercial large HTGR (LHTGR) fuel rods. The axial inhomogeneity coefficients of the rods were determined by mechanically separating the unbonded rods into five equal axial sections and counting the number of fissile and fertile particles in each section. A special fuel rod mold with a micrometer-controlled movable bottom was built for separating the particles into axial sections.[46] Once the shim particles were removed by shape separation, the two types of fuel particles could be distinguished by size and counted on the particle size analyzer.

The results of the investigation indicated that the homogeneity of the air-blended fuel rods depends on the particle ratio to be mixed as well as the air flow rate and the air pulse time. Shim behaved as a class, or qualitative, variable. An increase in the air flow rate

increased the inhomogeneity of shimmed rods but decreased the inhomogeneity of unshimmed rods. Longer pulse times apparently result in more homogeneous rods.

Low-fissile particle ratios are the most difficult to mix. The inhomogeneity index decreases with the square of the fissile content. More recent results indicate that small differences in the physical properties of the fissile particles may strongly influence the performance of the blender. The fuel rods fabricated for the Fort St. Vrain early validation reload test included two fuel loadings each for two very similar batches of fissile particles. In the case of the low-fissile loading, we had to radically change the blending conditions for one particle batch from the conditions used for the other. The average sizes and densities of the two batches were both within the fuel specifications and differed only slightly: density 2.130 vs 2.080 g/cm^3; size 653.9 vs 652.6 μm. Further tests are planned to investigate the effect of fissile batch on blending.

The tentative conlcusion drawn from the air blender evaluation is that FSV fuel rods can be blended to the axial LHTGR fuel specification with the air blender, but there is virtually no margin for error in some cases. We would prefer a more conservative design solution to the particle blending problem. In principal, a 20-way splitter-incremental blender can provide this conservatism (see Sect. 3.5.4.4.3). A 20-way splitter-blender has been designed and will be fabricated for testing on the engineering-scale fuel rod molding machine. A final decision on the blender design for the cold prototype fuel rod molding machine will be withheld until the latter device has been tested.

3.5.4.1.2 Twenty-Way-Splitter Incremental Blender, R. M. Delozier and D. R. Johnson. Theoretically, fuel rods made with a 20-way splitter-incremental blender will suffer only very slight temperature rises due to axial inhomogeneity, even if each 1/20 split completely segregates (Sect. 3.5.4.4.3). A practical demonstration of this blender concept will require a nonbiasing splitter and a mechanically reliable method for incrementally dispensing the 1/20 portions.

A conical 10-way splitter and a slide valve for incrementally dispensing the 1/10 parts into a fuel rod mold[47] were previously fabricated and tested on the engineering-scale fuel rod molding machine. The concial splitter appeared to be free of any systematic bias. However, relatively loose mechanical tolerances in the slide valve assembly occasionally allowed two splits to dispense simultaneously, resulting in inhomogeneous rods.

A 20-way splitter-blender has been designed for testing on the engineering-scale fuel rod molding machine. The design is such that the existing conical 10-way splitter will be used. Each 1/10 split will be subdivided into two parts. The 20 parts will be incrementally dispensed with 20 independent solenoid-actuated plug valves.

3.5.4.1.3 Volumetric Top-Off Dispenser, D. R. Johnson and R. M. Delozier. The monodisperse, highly spherical HTGR coated fuel particles can be reliably dispensed with pinch-valve-type volumetric dispensers. However, the graphite shim particles vary in size distribution, particle shape, and packing fraction from one batch to another. Thus, the precise quantity of shim required to fill out the rod length is difficult to predict in advance. Typically, we adjust the shim dispenser by cut-and-try methods. The irregular shim particles do not volumetrically dispense as reproducibly as fuel particles, either.

In an attempt to avoid the problems of shim variability, a volumetric top-off dispenser has been designed. A mockup will be fabricated for testing on the engineering-scale fuel rod molding machine. The top-off dispenser will be operated as follows: the fissile and fertile particles along with approximately three-fourths of the shim particles will be simultaneously dispensed via pinch-valve dispensers into a constant-volume chamber and vibrated for a fixed time. A second quatity of shim somewhat greater than required will be dispensed into the constant-volume chamber by the shim pinch valve dispenser. The chamber will be vibrated; the excess shim will overflow and be recirculated to the shim feed hopper. Presumably, the chamber will vibrate and overflow to a reproducible volume. The fixed volume of particles will then be unloaded into a blender.

3.5.4.1.4 PLC Controls for the Fuel Rod Molding Machine, D. R. Johnson, W. R. Hamel, and B. J. Bolfing. Programmable Logic Controllers (PLCs) are automatic control devices that control the timing and sequence of process steps. Such controls are envisioned for most HTGR fuel refabrication processes (see Sect. 3.5.7). As a test case, PLC controls (DEC 114/35) have been installed on the engineering-scale fuel rod molding machine.

The PLC offers several advantages over hard-wired control circuitry: the sequence and timing of the process steps can be changed by changing the PLC program, rather than physically changing wires and relays. The PLC has certain self-diagnostic capabilities. In the event of a failure in the control circuitry such as, for example, failure of a proximity sensor, the location of the failure can be determined with the PLC programming panel.

Proximity sensors were installed on each station of the fuel rod molding machine. As most of the mechanical operations on the fuel rod molding machine are accomplished with pneumatic cylinders, most of the proximity sensors are magnetic reed switches designed to be used in conjunction with the air cylinders. The PLC has been programmed such that verification of each sequential step (via a proximity sensor) is required before the next step is permited to begin. Thus, for example, the rotary index table is not permitted to index while the matrix injection ram is extended into a mold. If a sequential step cannot be verified, then an alarm condition is indicated on the control panel and operation of the machine is automatically halted until an operator makes the required repair or correction.

The PLC has been programmed for automatic start-up and shutdown of the engineering-scale fuel rod molding machine. These automatic programs have greatly simplified its operation. The built-in safeguards in the stepwise operate-and-verify logic of the PLC greatly reduce the potential for damage to the equipment by operator error. This feature will be very important in the remote operation of a fuel refabrication plant.

The PLC controller has been operated for approximately one year. It has functioned very reliably during this period. The fuel rod molding machine has been operated extensively, and the PLC controls have been

found convenient and efficient. However, the DEC VT14 programmer has failed twice in the past year. It would seem prudent to provide a redundant programmer for a remotely operated plant. The magnetic reed switches provided with BIMBA pneumatic cylinders have been less than satisfactory. These magnetic swithces occasionally fail to indicate, resulting in a false alarm condition in the PLC. More reliable proximity sensors for the pneumatic actuators are being sought.

3.5.4.2 Equipment Development: Fuel Rod Inspection

3.5.4.2.1 Homogeneity Inspection System, P. Angelini, D. Kiplinger, R. A. Gallman, and S. P. Baker. A nondestructive homogeneity inspection device has been conceptionally designed, and an engineering-scale device is being fabricated. The device will use multienergy gamma-ray attenuation for measurement of fuel rod homogeneity.

A brief description of the operating principle is as follows: a number of characteristic, discrete gamma-ray energies will be provided by a fission product gamma-ray source. The fission product sources are mechanically passive and thus advantageous for remote applications. The gamma rays will be collimated and directed at a spot on an HTGR fuel rod. A gamma-ray detector on the other side of the fuel rod will measure the intensity of the attentuated beam. The gamma rays will be attenuated differently by each species in the fuel rod, according to the following relationship:

$$I_i = {}_oI_i \exp\left(-\sum_{j=1}^{n} \mu_{ij} X_j\right) \qquad (1)$$

where

I_i = attenuated intensity of gamma ray having energy i,

${}_oI_i$ = incident intensity of gamma ray having energy i,

μ_{ij} = attenuation coeffecient of material j at energy i (these are known), and

X_j = concentration of material j.

To determine the values of X_j for each of n materials j, the values of I_i and ${}_oI_i$ will be measured at n or more discrete gamma-ray energies. The result will be n simultaneous equations in n unknowns for the values of X_j at one spot on a fuel rod.

By determining the concentrations of the constituent materials at many spots in a fuel rod, the homogeneity of the rod can be determined. The axial homogeneity can be determined by sampling a fuel rod at discrete positions down the central axis of the rod, or in the limiting cases by continuously scanning the rod length.

The radial homogeneity can be determined by a procedure illustrated in Fig. 3.35. A gamma-ray beam collimated on the central axis of the fuel rod yields information about the inner core of the rod, while a gamma-ray beam collimated well off the centerline yields information about the outer shell of the rod. Once the geometric factors are considered, the radial homogeneity can be determined.

ORNL-DWG 77-6838

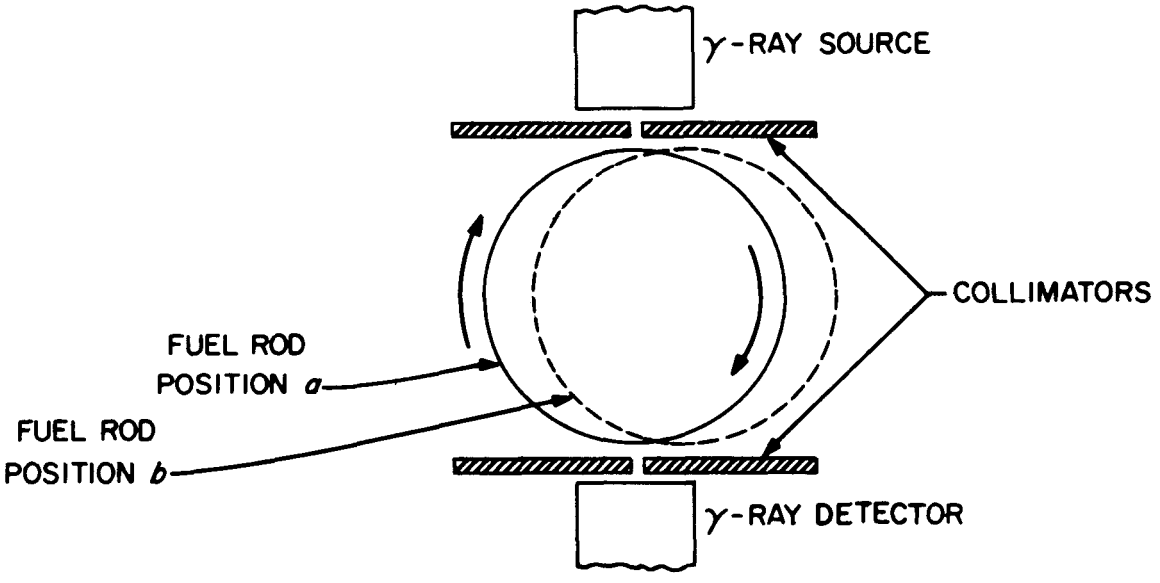

Fig. 3.35. Simplified Schematic Drawing of Radial Homogeneity Measurement Technique Showing (a) Inner Core Measurement and (b) Outer Radius Measurement.

The separation of uranium and thorium concentrations by gamma-ray attenuation is very difficult because the absorption coefficients of the two materials are nearly equal at most energies. The result is that normally insufficient information is available for a unique solution to Eq. (1). However, a method for uniquely determining the uranium and thorium concentrations by multienergy gamma-ray attenuation has been devised. In the energy region near the electron absorption edges the absorption coefficients of the two elements differ appreciably. Gamma rays of energy between the *K* edges of uranium and thorium will allow the unequivocal separation of uranium and thorium concentrations. Three fission product sources having long half-lives and gamma rays between the *K* edges of uranium and thorium have been identified: ^{169}Yb, ^{182}Ta, ^{177}Lu.

The homogeneity inspection device mockup is shown in Fig. 3.36. Fuel rods will be manually loaded into the device. The collimator and source shielding assembly is designed such that the collimator can be easily changed in order to empirically investigate collimator configuration.

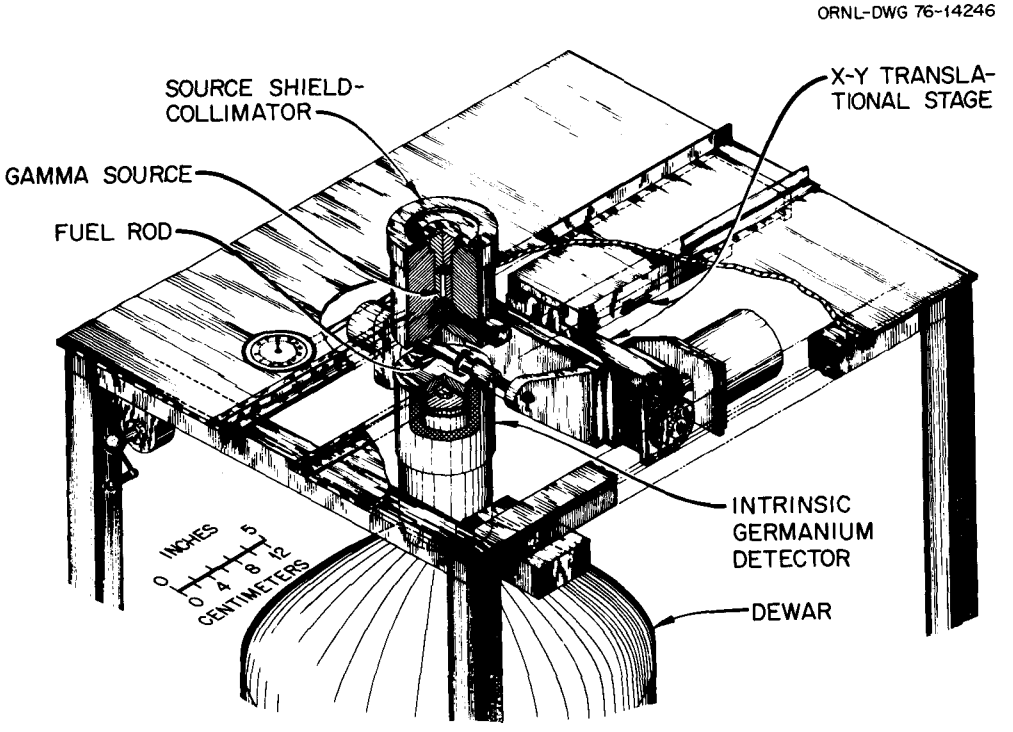

Fig. 3.36. Nondestructive Fuel Rod Homogeneity Inspection Device.

The fuel rod can be rotated about its axis at selectable, variable speeds ranging from 4 to 254 rpm. The rod can be translated at selectable, variable speeds ranging from 0.11 to 4.2 mm/sec (0.25 to 10 in./min). The position of the collimated beam with respect to the fuel rod radius can be selected manually. A programmable logic control system will be provided to allow complete versatility in the sequence and timing of the homogeneity inspection.

The homogeneity inpsection mockup will allow the feasibility testing of two separate methods. (1) Rapid on-line homogeneity inspection for process control — for this application, a Tl-doped NaI detector and single-channel analyzer will be employed. The rods will be inspected for the total mass homogeneity. (2) Precise inspection for uranium and thorium homogeneity — for this application a solid-state intrinsic Ge detector and multichannel analyzer will be used. Multienergy gamma-ray attenuation will be used to determine uranium, thorium, and light element concentrations as functions of position in the fuel rod.

3.5.4.2.2 Mechanical Inspection System, D. R. Johnson and M. E. Galyon. A device has been fabricated and tested for the rapid on-line inspection of fuel rods for mechanical defects such as chips, cracks, holes, etc. The device is a special air ring gage. Air ring gages are frequently used in industry for rapid measurement of the diameters of cylindrical parts. These devices employ a close-fitting ring [∿25-μm (0.001-in.) diametral clearance] with two diametrically opposite nozzles through which pressurized air flows. The diameter of the part is related to the back pressure in the air lines.

The pneumatic mechanical inspection device senses a pressure difference when a defect in a fuel rod passes under an air nozzle. The device tested contained four sets of three nozzles each. The pneumatic circuits are located in two planes — two circuits per plane. The three nozzles in a circuit are equally spaced — 120° apart — around the ring. The two circuits in a plane are rotated 60° apart. The two planes are rotated 30° out of phase with each other. The result is the location of an orifice every 30° around the inner periphery

of the ring. The back pressures in the two circuits in each plane are compared to inspect a rod. A small defect can pass between two nozzles undetected; however, this objection can be easily overcome by stacking up two or three of these devices and rotating them out of phase with each other.

In a prototypic system, the mechanical inspection system would interface with the rest of the fuel rod fabrication system via air levitation conveyor tracks. The rods would be conveyed up to the ring gage and then pushed through with a device very similar to that used for loading fuel rods into the fuel rod storage magazine (Sect. 3.5.5.1.1).

The back pressures in the four pneumatic lines are measured with pressure transducers. The output signals from the pressure transducers are fed to buffer amplifiers, which are used to null out the base-line voltages and match the gains of the four channels. The signals are then fed in pairs to difference amplifiers, and finally the two differences are added with a summer amplifier. Thus pneumatic disturbances that are not common mode for the pairs of channels appear at the output of the summer amplifier. This output is then compared with a predetermined "defect tolerance" voltage so as to trip an alarm when the defect is greater than the set point.

To test the mechanical inspection device, a set of aluminum rods with well defined defects was fabricated. The types of defects were edge bevel, edge notch, body hole, and body flat. In these initial tests, the rods were pushed through the device by hand. The test system was sensitive to the following defect sizes at an inspection rate of one rod per second:

Edge notch — ≤0.76 mm (0.030 in.) along end face and axis, 75° included angle.

Edge bevel — 0.76 mm (0.030 in.) measured on end face and axis.

Body hole — ≤1.52 mm (0.060 in.) diam, 1.59 mm (0.063 in.) deep.

Body Flat — 0.38 mm (0.015 in.) deep measured from rod circumferential surface.

The pneumatic mechanical inspection device has many advantages for a remote system: no moving parts, no sliding contacts or friction, self cleaning, low cost. This inspection system represents an appreciable improvement over visual inspection.

3.5.4.3 Nondestructive Fissile Assay — J. E. Rushton, R. W. Knoll, and S. R. McNeany

Quality assurance of the recycle fuel product is a significant cost factor in remote refabrication of HTGR fuel. Nondestructive measurements of Special Nuclear Material can provide automated analyses for inspection requirements and for material accountability. In addition, nondestructive assay (NDA) can provide rapid analysis for process decisions and perhaps for timely indication of material losses.

Three NDA systems are being demonstrated for use with recycle HTGR fuel that contains 100 to 1200 ppm of ^{232}U and hence has high gamma activity. The first system is a fuel rod scanner for measurement of the fissile loading in the uncarbonized fuel rods. A prototypic version of this scanner would be located in the process line and would measure 100% of the fuel rod output for process control, quality assurance, and material control.

The second NDA system, the Delayed Neutron Assay Device, is a small sample assay system designed to measure the total ^{233}U and ^{235}U mass in single fuel rods or multiparticle samples. The primary use of this instrument would be rapid analysis of samples from the process line for process control, e.g. rapid measurement of the uranium loading in resin kernels. Other applications are the cross-calibration of NDA standards for the in-line Fuel Rod Scanner and the verification of fissile uranium in bulk materials that can be weighed and sampled in the process line.

The third developmental device tests the potential of precision active calorimetry for measurements of fissile material in small samples. Because of the high sensitivity of the calorimeter (1 μW), this technique would be used for precise intercomparison of assay standards for the rod scanner and the small sample assay systems.

3.5.4.3.1 Fuel Rod Scanner, J. E. Rushton. A fuel rod scanner has been constructed to test and optimize a technique for the in-process measurement of the fissile content of carbonized HTGR recycle fuel rods. The development program has experimentally established parametric relations for signal-to-background ratios and absolute signal levels

as functions of the scanner configuration and has developed a preliminary calibration curve for static single fuel rod assays.

The fuel rod assay technique consists of an irradiator and moderator assembly and a sample-detector assembly. A ^{252}Cf neutron source is positioned at the center of the cylindrical moderator assembly composed of graphite, polyethylene, and heavy water. The fuel rod samples and detectors are positioned at the periphery of the moderator assembly. The rods are exposed to thermalized neutrons, which selectively fission only the ^{233}U or ^{235}U atoms within the rods. The neutron detectors, which are ^{4}He proportional counters, register the number of prompt fission neutrons emitted from the sample.

Figure 3.37 shows the fuel rod scanner with its single fuel rod channel. A prototypic scanner would have six to ten assay channels located symmetrically around the circumference of the moderator tank. The ^{252}Cf source is located in a source tube assembly, which is used to transfer the source from the scanner to a shielded storage facility. The prototypic assay device would be an in-line process instrument and hence would be contained in a shielded fabrication cell. Thus, integral radiation shielding is not a requisite component of the scanner and is not incorporated in the test assembly. The testing program has been conducted in a shielded cell with controlled access of personnel to facilitate equipment setup. The ^{252}Cf source is remotely installed in the irradiator with a bridge-mounted electromechanical manipulator and a master-slave (M-S) manipulator. Samples are also inserted, positioned, and removed remotely with a stepping-motor-driven transfer system and with M-S manipulators. All electronic instrumentation other than the detector preamplifier is located outside the cell.

The irradiator and moderator portion of the scanner is constructed to permit optimization studies on the moderator configuration. The cylindrical tank containing the D_2O is designed so that the D_2O thickness between the ^{252}Cf and the fuel rod position can be varied. Work at Los Alamos Scientific Laboratory on LWR fuel rod scanners demonstrated an advantage for including a hydrogenous moderator near the source.[48] This feature has been evaluated in the HTGR rod scanner by providing four interchangeable insert thimbles, which contain the source, a

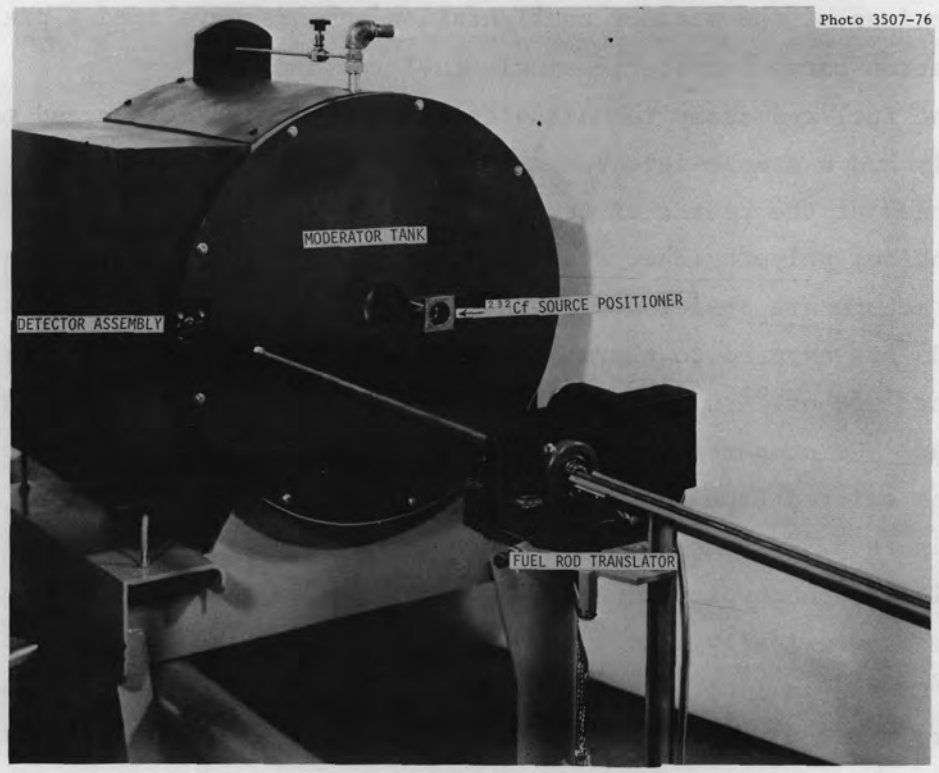

Fig. 3.37. Fuel Rod Scanner Test Assembly.

polyethylene moderator, and a tungsten shield. Each thimble has a different polythylene thickness so that various combinations of D_2O and polyethylene have been investigated. These studies will be used to specify the optimum moderator configuration for the prototypic device.

A preliminary calibration curve using ^{235}U-loaded Triso particles with weak-acid-resin-derived kernels has been measured and is shown in Fig. 3.38. The calibration curve relates the net detector signal to the ^{235}U mass. The curve is nonlinear because of the shadowing effect of the fissile particles. The nonlinearity is relatively small; the net detector signal per gram of ^{235}U is reduced only 10% between rod loadings of 0.15 and 0.45 g ^{235}U, a threefold increase in ^{235}U content. Measurements with the rod scanner are under way to verify the applicability of this system to ^{233}U fuel rods with surface gamma dose rates of 0.5 to 5 R/hr and to test the sensitivity of the scanner to variations in fuel rod and particle compositions.

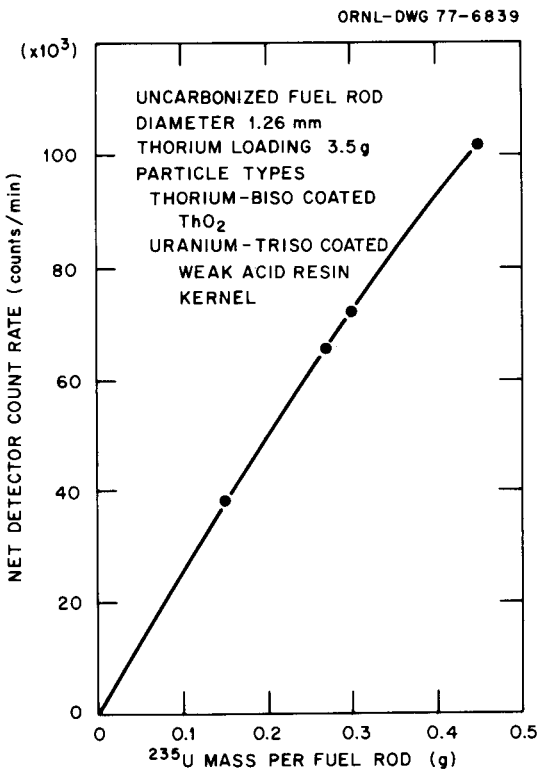

Fig. 3.38. Calibration Curve for HTGR Fuel Rod Scanner.

3.5.4.3.2 Delayed-Neutron Assay Device, R. W. Knoll. A nondestructive assay device that employs delayed-neutron counting to measure the fissile content of HTGR fuel rods has been designed, fabricated, and initially tested. It is a candidate for use in the sample inspection system of an HTGR fuel refabrication plant as envisioned in a recent conceptual design study.[49] As such, it would assay fuel samples in various stages of production and would serve as a calibration device for in-line fuel rod assay machines.

In the assay technique, the fuel sample is encapsulated in a polyethylene rabbit and irradiated in a thermal neutron flux for about 60 sec, which induces fissions in the sample's ^{233}U and ^{235}U. It is then transferred pneumatically to a detector assembly, where delayed neutrons emitted by the fission products are counted. The number of delayed neutrons emitted measures the sample's fissile content. The time-dependent behavior of the emission of the delayed neutrons depends on the fissile isotope; consequently, the method might be useful for determining the ^{233}U to ^{235}U isotopic ratio.

The schematic diagram in Fig. 3.39 identifies and indicates the layout of the system's main components. The device is located in the Thorium Uranium Recycle Facility (TURF), with the irradiator situated in Hot Cell B. The design and operation of the assay device are described in a report currently in preparation.

Several preliminary experiments have been conducted on the device using Fort St. Vrain type fuel rods. In one test of the precision of the device, a rod containing 0.300 g ^{235}U and 3.5 g ^{232}Th was irradiated and counted three times consecutively (60-sec irradiation, 80-sec count, 4.5-sec delay between end of irradiation and beginning of count). The rod yielded an average of 122,890 counts per cycle, with a standard deviation (1 σ) in the average of 0.25%. Another test showed the assay technique to be insensitive to the thorium content of the rod; that is, rod-to-rod variations in the thorium loading do not affect the fissile isotope assay.

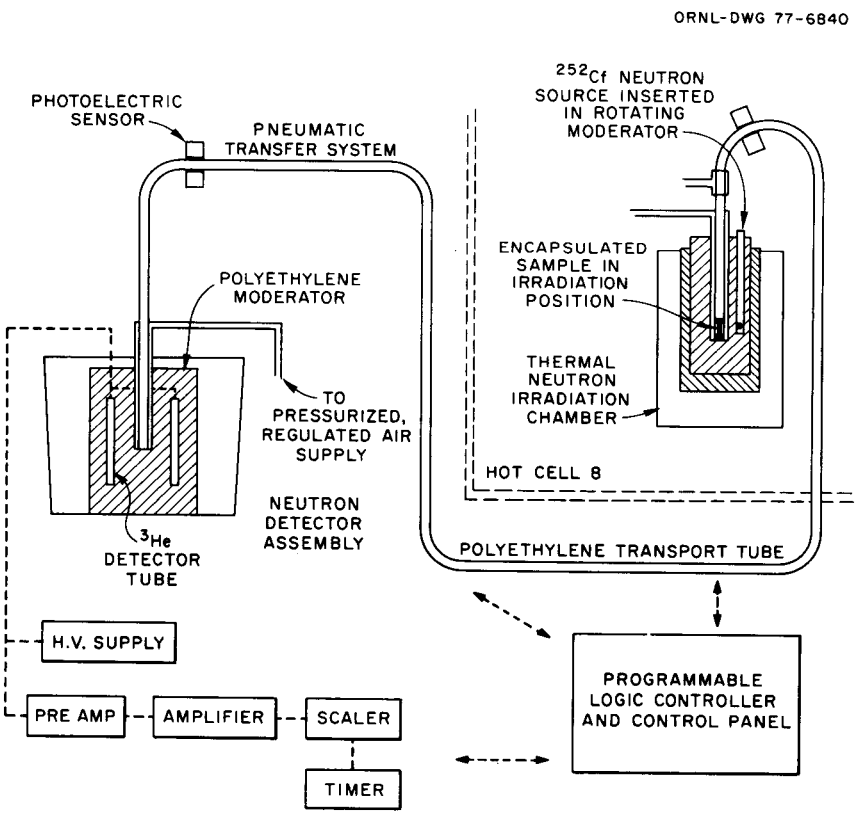

Fig. 3.39. Delayed-Neutron Nondestructive Assay Device.

3.5.4.3.3 Calorimetric Neutron Assay Device, S. R. McNeany. A calorimetric neutron assay device has been designed and fabricated for nondestructively assaying fissile content of HTGR fuel rods. The system consists of an isothermal twin-bridge calorimeter incorporated within a thermal neutron irradiator. The calorimeter was designed and built by personnel of Mound Laboratory under subcontract with the Thorium Utilization Program at ORNL. Figure 3.40 shows a schematic diagram of the calorimeter and irradiator.

The calorimeter consists of an active sample and a reference sample (non-heat-generating sample) enclosed in a single tube surrounded by an isothermal water jacket. Constant-temperature water is circulated through the system from an external isothermal reservoir. Heat generation in the active sample is measured by detecting the change in resistance of the nickel windings surrounding the active sample relative to that of the reference, the two sets of windings being connected as a Wheatstone bridge. Heater coils are provided around the sample holder for calibration.

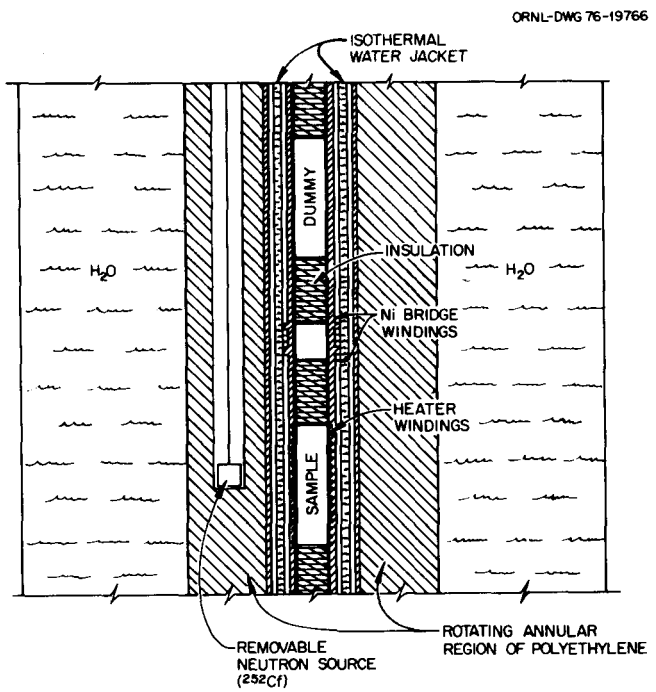

Fig. 3.40. Calorimetric Neutron Assay Device for HTGR Fuel Rods.

To make a measurement, a sample is inserted and the calorimeter is sealed. The calorimeter is allowed to equilibrate, and the neutron source is then inserted to induce fissions in the sample. After the calorimeter has again reached quilibrium, the incremental fission heating can be determined by removing the source and feeding a measured amount of power to the heater coils to reproduce the previously measured resistance change. The fissile content of the sample is then determined by comparison with fission heating rates measured in known calibration standards.

The device has been installed in an uncontaminated hot cell in the TURF at ORNL, and preliminary tests have begun using a 1-mg ^{252}Cf neutron source. Initial observations indicate that the calorimeter is sensitive to power variations of approximately 1 μW. Heat measurements have been made on rods of three different compositions. The results are summarized in Table 3.11. The heat generation observed in the non-uranium-bearing rods is believed to be attributable to gamma heating associated with the ^{252}Cf source and as such will constitute a required background correction. An additional experiment was performed to determine the axial neutron flux distribution in the sample chamber. The flux peaked 14 mm above the center of the sample chamber. The irradiator is being modified to lower the source. We believe that an axial flux variation of about 10% will be realized upon completion of this modification.

Table 3.11. Measured Heating Rates Observed in Three Different Rod Compositions During Irradiation by a 1-mg ^{252}Cf Source

Rod Composition	Heat Generation Rate (μW)
0.37 g ^{235}U 3.4 g ^{232}Th 2.4 g graphite 3.1 g "matrix"[a] 4.1 g Si, C, O	140
3.4 g ^{232}Th 4.2 g graphite 3.0 g "matrix" 2.6 g C, O	17.6
9.5 g optical glass 3.0 g "matrix"	5

[a]"Matrix" is used as a binder in the rods; the matrix consists primarily of graphite powder and petroleum pitch; the exact composition is proprietary to the General Atomic Company, San Diego, Calif.

3.5.4.4 Process Development

3.5.4.4.1 Fuel Rod Length Control, D. R. Johnson and C. K. Bayne. The requirement for the lengths of individual fuel rods is that a stack of 15 fuel rods must fit correctly within a fuel hole in an HTGR fuel element. That is, the column must not exceed the length of the fuel hole, which would result in the top rod protruding from the element, nor should the column be too short, which would result in a void space at the top of the fuel column. This requirement can be specified as follows: the length of a stack of 15 fuel rods of nominal length L shall be $15L \pm \delta$. We expect the value of δ for the 51-mm-long (2-in.) Fort St. Vrain fuel rods to be ±6.4 mm (0.25 in.).

To determine an operational process specification for our development program, a mathematical relationship between the length variation of individual fuel rods and the length tolerance of a stack of fuel rods was derived.[50] The variations in fuel rod lengths have been shown to be normally distributed. The mean and standard deviation of the fuel rod lengths will be known at all times on a prototypic fuel rod molding machine. If individual fuel rod lengths are within a length $L \pm \theta$, $(1 - \alpha)\%$ of the time and a stack of 15 rods is within $15L \pm \delta$, $(1 - \alpha)\%$ of the time, then the following relationship between θ and δ was determined for all values of α:

$$\theta = 0.258\delta$$

If δ for a 51-mm (2-in.) Fort St. Vrain fuel rod is 6.4 mm (0.25 in.), then the critical value of θ = 1.52 mm (0.060 in.). That is, if the fuel rods are manufactured to within ±1.52 mm (0.060 in.) of the nominal length, then a stack of 15 rods would be expected to be within ±6.4 mm (0.250 in.) of the nominal column height.

The length variation of our fuel rods depends upon the particulate behavior of the fuel particles. Over the last year, we have made rods to within ±0.25 to ±0.76 mm (0.010–0.030 in.) of the nominal 51-mm (2-in.) length, depending upon the particluar fuel particles used. These average

rod lengths correspond to predicted fuel rod stack length variations of only ±0.99 to ±2.97 mm (0.039–0.117 in.).

3.5.4.4.2 Residual Sulfur in Fuel Rods, P. Angelini, F. L. Layton, and D. A. Costanzo. The presence of sulfur in various portions of the HTGR fuel cycle can adversely affect both materials and processes. Excessive sulfur vapor in the nuclear reactor pressure vessel can lead to corrosion of stainless steel components. In fuel reprocessing, the adverse effects include corrosion of burner materials, corrosion of the off-gas system materials, and possible poisoning of various processes in the off-gas system necessary for the removal of radioactive effluents. Additional steps may be necessary in the reprocessing flowsheet to decrease the sulfur concentration of the off-gas to acceptable levels. Most of the sulfur in HTGR fuel rods comes from the petroleum pitch, which is a major constituent of the fuel rod matrix. The sulfur content of the pitch has more than doubled in recent years because of the increased sulfur content in the crude oil from which the pitch is made.

A specially developed pitch with sulfur content approximately one-tenth that of currently available petroleum is commercially available in limited quantities and is costly. The residual sulfur content of cured fuel rods and the effect of refabrication process variables on the residual sulfur were investigated to determine the impact of the sulfur impurity problem on the cost and/or quality of HTGR refabricated fuel. The sulfur concentrations of pitch materials and green and fired (cure-in-place) fuel rods were measured. The results are summarized in Table 3.12 and Fig. 3.41.

The results shown in Table 3.12 indicate that much of the sulfur initially present in the green unfired fuel rods is eliminated as a gaseous species during firing. These results suggest that the use of the special low-sulfur (0.4%) pitch has little effect on the residual sulfur concentration of fuel rods cured at 1800°C for 30 min. The test performed with the Ar–4% H_2 sweep gas yielded results very similar to those performed with nominally pure argon. These results indicate

Table 3.12. Residual Sulfur Concentration of HTGR Fuel Rods Cured in Graphite Tubes to Simulate Cure-in-Place

Pitch	Sulfur Concentration, % by Weight			Furnace Atmosphere
	Fuel Rods			
	Green	Carbonized at 1000°C	Heat-Treated 30 min at 1800°C	
3.4	0.326	0.135	0.016	Argon
1.5	0.145	0.034	0.012	Argon
0.4	0.031	0.026	0.026	Argon
3.4	0.326	0.116	0.024	Ar–4% H_2
1.5	0.145	0.071	0.022	Ar–4% H_2
0.4	0.031	0.029	0.020	Ar–4% H_2

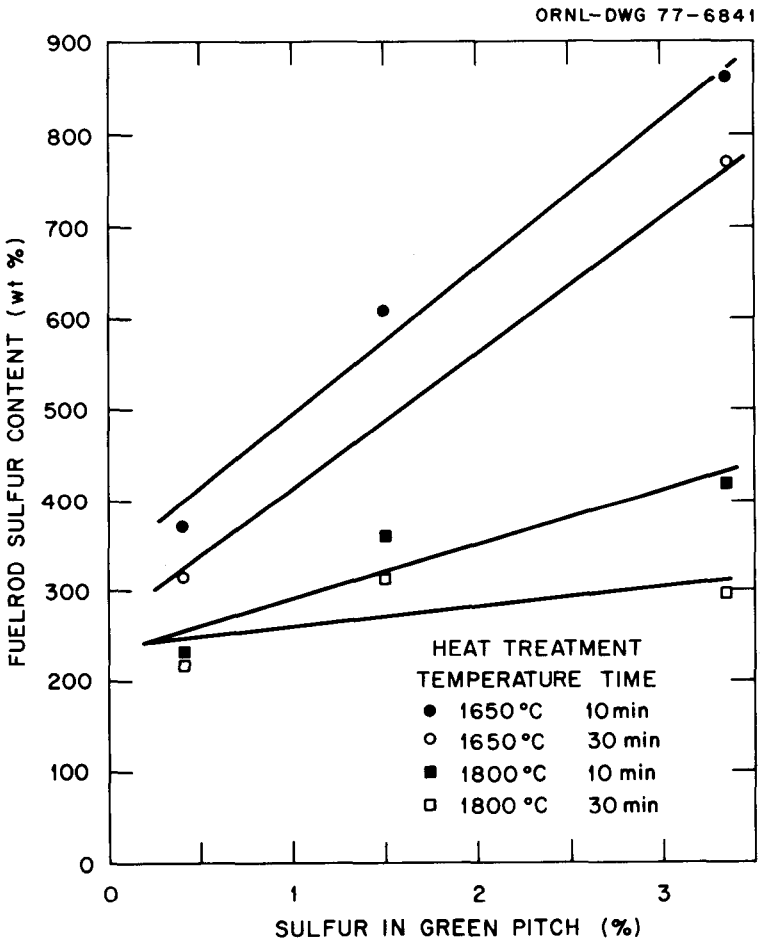

Fig. 3.41. Residual Sulfur Content in 51 by 13-mm (2 by 1/2-in.) Fuel Rods.

that the addition of hydrogen to the cure-in-place sweep gas would have little beneficial effect with regard to residual sulfur.

The data plotted in Fig. 3.41 illustrate the effects of cure-in-place temperature and time on the residual sulfur concentration. Curing for 30 min or longer at 1800°C resulted in a residual sulfur concentration of 200 to 300 ppm, regardless of which of the three pitch batches was used. On the other hand, the lower curing temperature, 1650°C, resulted in residual sulfur concentrations of 300 to 900 ppm, depending on the purity of the original pitch.

These initial results indicate that the residual sulfur concentration in cure-in-place fuel rods can be maintained at approximately 300 ppm by either of two methods, or a combination of the two: (1) specially prepared, low-sulfur pitch can be used in fuel rod fabrication or (2) high temperature (1800°C) and extended times (30 min) can be used for cure-in-place.

The analytical procedure used for sulfur determinations in this investigation makes use of a small 60-mg sample. Sampling problems arising from the necessity of the small sample resulted in a relative standard deviation for the sulfur determinations of 25%. To improve the precision of sulfur determinations in fuel rods, a technique is being developed whereby a complete fuel rod will be used as a sample. Initial tests have indicated a relative standard deviation of 10% with the new method. Samples from the above described experiment will be analyzed by the new technique to verify the conclusions with better data. Also, additional work is under way in which the fuel rods were cured in 1/6-segments of Fort St. Vrain fuel element blocks; these tests are more nearly prototypic than the initial tests, in which cure-in-place was simulated in graphite tubes.

The physical distribution of the sulfur in the matrix phase of fired fuel rods was investigated by scanning electron microscopy and electron-beam microprobe studies. These experiments indicated that, within the resolution of the instruments (<1 μm), the residual sulfur is uniformily distributed in the fired matrix. The chemical form of the residual sulfur could not be determined in these studies.

3.5.4.4.3 Effect of Blending on Fuel Rod Temperature Distributions, P. Angelini, J. L. Long, and D. E. Starnes. The consequence of poor blending of fuel particles before fuel rod molding is that localized regions within the fuel rods may have a higher density of fissionable material than the design value. The localized clusters of fissile material can result in hot spots, wherein the elevated temperatures cause premature failure of fuel particle coatings. The end result of this sequence of events beginning with poor mixing is that gaseous fission products are released into the primary coolant gas of the reactor.

One type of fuel particle blender under consideration for HTGR fuel refabrication is a splitter-incremental blender (see Sect. 3.5.4.1.2). Its operation is as follows: the charge of fissile, fertile, and shim particles for one fuel rod is split into N parts by a mechanically passive conical splitter. If the splitter has no biases, then each part will contain $1/N$ of the fissile particles, $1/N$ of the fertile particles, and $1/N$ of the shim particles. The N parts are then sequentially loaded into the fuel rod mold. This type blender absolutely precludes massive segregation of the fuel, such as all the fissile particles falling to one end of the mold. However, the particles commonly segregate into axial layers within each $1/N$ split. As the consequence of microsegregation was previously unknown, a theoretical study of the temperature profiles within fuel rods blended via 5, 10, and 20-way splitter-blenders was undertaken.

Temperature profiles were calculated for large HTGR (LHTGR) fuel rods that were considered to have been fabricated by use of the splitter-incremental blender. The calculations indicate that a 20-way-splitter incrementally blended fuel rod would meet the axial homogeneity requirements for LHTGR fuel rods. The heat generation rate within a fuel rod is determined by the fuel density and the thermal neutron flux at that location. It has been shown that the thermal neutron flux is nearly constant to within a few percent as a function of radius for a typically loaded fuel rod in a reactor. Thus the heat generation rate will vary in the same was as the fuel loading within a fuel rod. The heat generation profile in splitter-blended fuel rods was modeled as follows:

$$Q(Z) = a[1 + \cos(2\pi nz/L)] \ ,$$

where

a = constant related to total power density,

Z = axial distance along fuel rod,

L = length of the fuel rod, and

n = number of splits in an n-way splitter incremental blender.

The use of this type of heat generation function models an n-splitter incrementally blended fuel rod as having complete segregation between loaded increments as a function of axial position.

The Heating 3 heat transfer computer program was used to calculate the steady-state temperature profiles for fuel rods fabricated via 5-way, 10-way, and 20-way splitter-incremental blenders. The computer model used for the calculations is shown in Fig. 3.42.

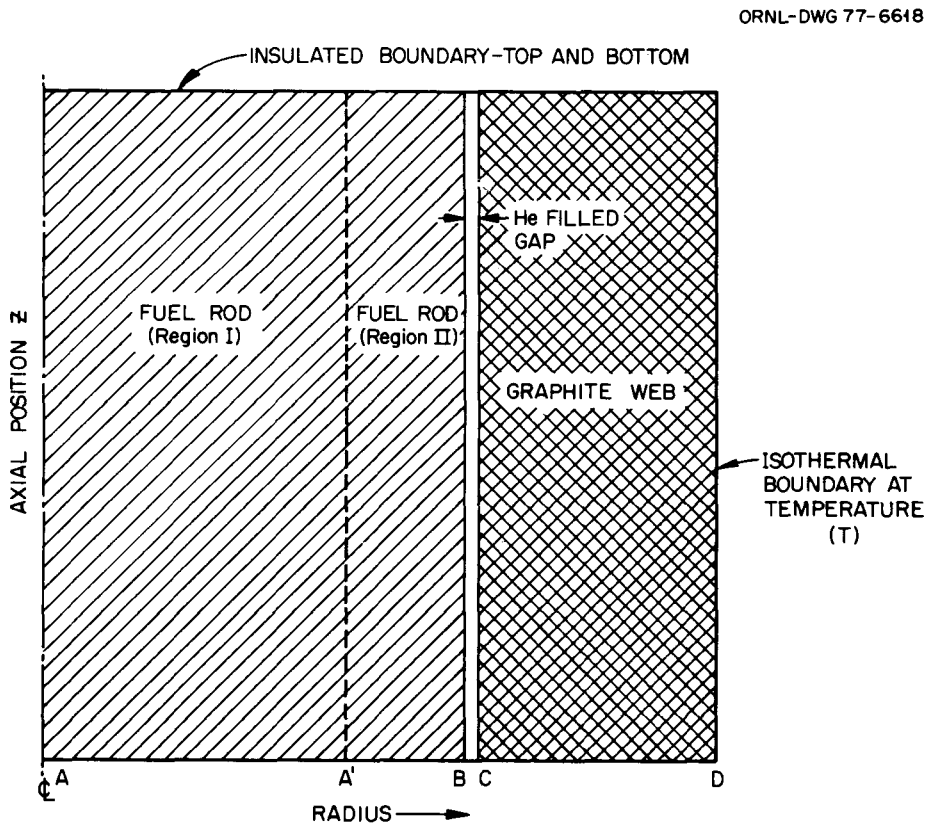

Fig. 3.42. Model for n-Way-Splitter Incrementally Blended Fuel Rods.

Given the symmetry only one increment (one cosine wavelength) was considered in the calculations. The parametric study assumed the following:

1. diameter of the fuel rod — 16 mm (5/8 in.)
2. thermal conductivity of the fuel rod — 5 and 10 W/m K
3. radial gap width — 0.10 and 0.25 mm (4, 10 mils)
4. thermal conductivity of the He-filled gap[51] 0.294 W/m K at 750°C
   0.380 W/m K at 1100°C
5. heat transfer across the gap was included —
   emittance of fuel rod — 0.9
   emittance of graphite web — 0.9
6. thickness of graphite web — 6.45 mm (0.254 in.)
7. thermal conductivity of unirradiated H-327 graphite web[52] —

temperature, °C	538	816	1093	1649
conductivity, W/m K	83.1	50.2	41.5	32.9

8. isothermal boundary on the graphite web — 750 and 1100°C
9. total power generation rate within the fuel rod — 6.6 and 13.1 kW/m (2000 and 4000 W/ft)

The heat generation rates per fuel rod of 6.6 and 13.1 kW/m (2000, 4000 W/ft are equivalent to those of an average fuel rod in a 1100-MW(e) reactor operating at 85 and 170% of the normal operating level. The thermal conductivity of the fuel rod depends upon the fissile, fertile, and shim loadings as well as irradiation history. The average thermal conductivity[53] for irradiated slug-injected fuel rods is approximately 10 W/m K. The effect of radiation on the thermal expansion and density of the components causes the gap size to vary as a function of irradiation history.

The typical radial gap size is approximately 0.1 mm (4 mils). Also, the thickness of the H-327 graphite annulus is approximately equal to the web thickness between a fuel rod and cooling hole in a fuel element. The outer boundary of the graphite was chosen to be 750°C or equal to the helium coolant gas temperature. The 1100°C boundary temperature and the 13.1 kW/m (4000 W/ft) power generation provide some indications of inhomogeneity effects in regions where there may be power excursions.

The results for the 6.6 kW/m (2000 W/ft), 750°C boundary temperature, 0.25-mm (10-mil) radial gap, and 5 W/m fuel rod thermal conductivity are presented in Figs. 3.43 and 3.44. Figure 3.43 shows the radial Temperature profiles for a plane at an axial position of maximum heat generation. Figure 3.44 shows the axial centerline temperature of the respective fuel rods. It can be seen that the 20-way-splitter incrementally blended fuel rod yields a temperature profile to within 2°C of the theoretical homogeneously blended case.

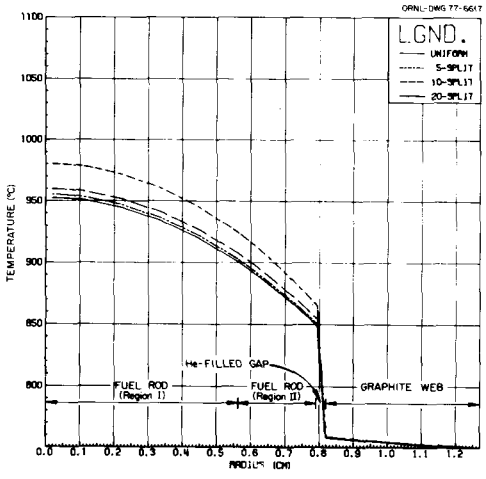

Fig. 3.43 Radial Temperature Profiles at Plane of Maximum Heat Generation.

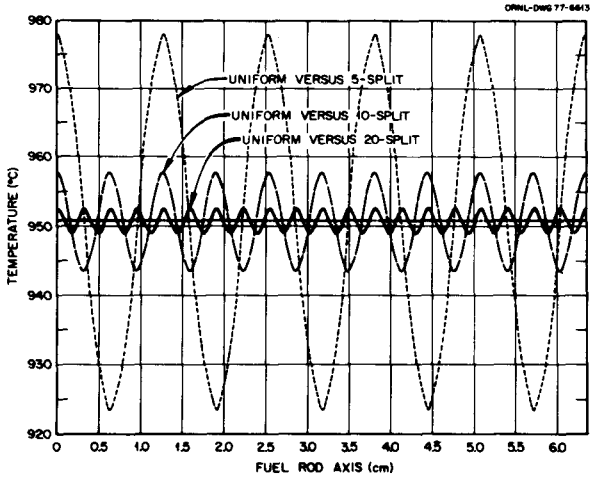

Fig. 3.44. Axial Centerline Temperature Profiles.

The maximum centerline temperature differences between the n-way and the uniformly loaded results for the $k_{\text{fuel rod}}$ = 5 W/m, radial gap = 0.25-mm (10-mil) case are listed in Table 3.13. These calculations reinforce the premise that 20-way-splitter incrementally loaded fuel rods will yield nearly uniform centerline axial temperature profiles in addition to meeting axial homogeneity requirements.

Table 3.13. Maximum Fuel Rod Centerline Temperature Variation for Splitter-Blended Fuel Rods

Power Generation Rate		Temperature Difference, °C, for Each Splitter Increment[a]			
(kW/m)	(W/ft)	5	10	20	Uniform
6.6	2000	27	7	2	0
13.1	4000	54	14	7	0

[a]Difference between maximum central temperatures n-way — uniform.

3.5.4.4.4 Fuel Homogeneity Inspection Technique, P. Angelini. An improved inspection technique for determining the uranium and thorium homogeneity indices in 13-mm-diam by 51-mm-long (1/2 by 2-in.) Fort St. Vrain (FSV) fresh fuel rods has been devised. The technique makes use of two independent methods for obtaining data related to the uranium and thorium contents per section of fuel rod. In one method, the number of fissile and the number of fertile particles are counted by means of an automated particle size analyzer (PSA). The second method is based on passive gamma counting of fuel particles from each fuel rod segment. The homogeneity indices from both methods agree well.

Fuel rods fabricated for the original Fort St. Vrain Reactor core were manufactured to a specification that compared fuel loading in the two axial halves of fuel rods. The Large HTGR (LHTGR) fuel homogeneity specification considers both axial and radial homogeneity on a one-tenth fuel rod scale. The LHTGR fuel rods are separated into five axial segments, with each segment cored into an outer annulus and inner core of equal volume. The uranium and thorium contents

in each one-tenth section are determined. Axial and radial homogeneity indices are calculated for both uranium and thorium. The numerical maxima are then reported for the rod.

In fabricating fuel rods for the Fort St. Vrain Early Validation Test (FSV-EVT), a homogeneity specification comparable to that for the LHTGR fuel rods was devised. Because of the relatively small diameter of the FSV fuel rods, it was agreed that only the axial homogeneity indices would be determined. The formula used for calculating the indices, by analogy with the LHTGR specification, is

$$H_{\text{axial},i} = \frac{0.5655C_i + 0.2173(C_{i\ \text{above}} + C_{i\ \text{below}})}{\overline{C}} - 1$$

where

$H_{\text{axial},i}$ = axial homogeneity index for segment i,

C_i = fuel loading for segment i,

$C_{i\ \text{above}}$ = fuel loading for the segment above the ith segment,

$C_{i\ \text{below}}$ = fuel loading for the segment below the ith segment, and

$\overline{C}$ = average fuel loading for the fuel rod of interest.

For an end segment $\overline{C}$ is used for $C_{i\ \text{above}}$ or $C_{i\ \text{below}}$. The maximum positive value for the index is reported for each rod. A general criterion (analogous to the LHTGR specification) is that at least 85% of the fuel rods have indices $\leqslant 0.20$. One would calculate separate uranium and thorium homogeneity indices for each fuel rod segment.

A special fuel rod sectioning device was designed and fabricated for this inspection technique. The device heats a fuel rod to 105°C and provides a means of measuring and advancing the fuel rod up to a cutting edge. Since the fuel rod matrix is soft at that temperature, the rod can be sectioned without cutting or breaking the fuel particles. The one-fifth segments were debonded with pyridine, and the graphite shim particles were eliminated by shape separation using a tilted

vibrating plate. At this point in the procedure, two independent methods were used to measure the relative uranium and thorium loading per axial segment. In one method, the numbers of fissile and fertile particles were counted with a particle size analyzer (PSA). The fissile and fertile particles are sufficiently different in size to allow their discrimination. The PSA method assumes that the total numbers of fissile and fertile particles per axial segment are proportional to the actual uranium and thorium contents, respectively. In order to test this hypothesis, the particle size distributions of fissile fertile particles from each rod segment were determined. A preliminary analysis of the particle size distributions indicates that there is no significant size segregation as a function of axial position. Typical data for one fuel rod are presented in Table 3.14.

Table 3.14. Mean Diameter and Standard Deviation of the Mean for Fuel Particles From Each Axial Segment of Fuel Rod 4-H-20

Fuel Rod Segment	Fissile Particle		Fertile Particle	
	Mean Diameter (μm)	Standard Deviation (μm)	Mean Diameter (μm)	Standard Deviation (μm)
Top	653.30	27.61	811.54	25.73
	655.18	27.79	813.24	26.02
	655.71	26.39	810.95	26.66
	655.38	27.06	810.06	25.85
Bottom	653.92	26.95	811.22	26.05

A second independent method using a gamma counting procedure was also developed for determining the relative fuel loadings per one-fifth axial rod segment. The method is based on passive gamma counting of fuel particles from each axial segment. In this case, the total counts from the 185-keV gamma peak are attributed to the uranium content, and the total counts from the 239-keV gamma peak are attributed to the thorium content.

The relative uranium and thorium distribution of a fuel rod as determined by the PSA and gamma-counting methods are compared in Fig. 3.45.

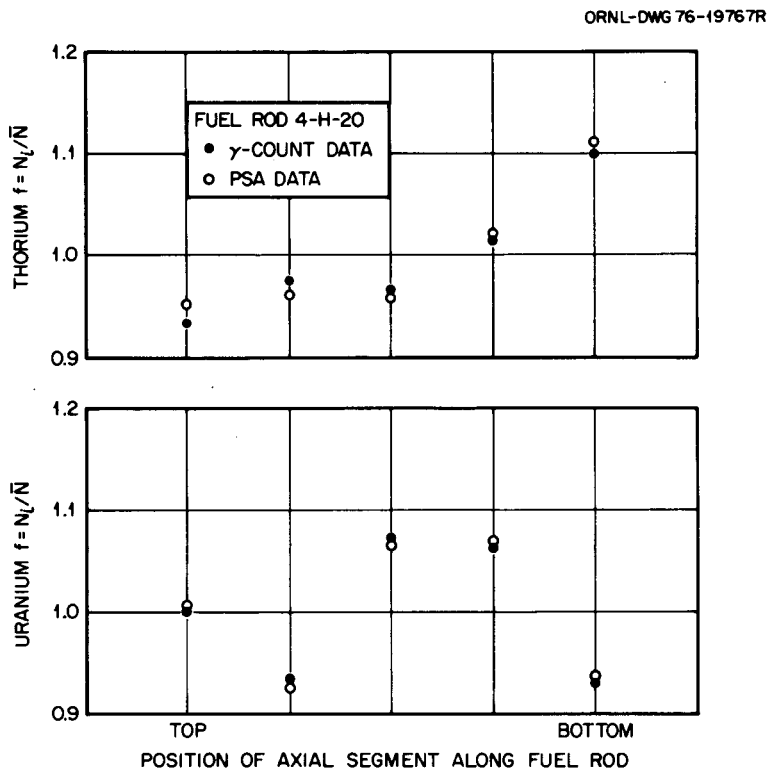

Fig. 3.45. Fuel Homogeneity Data Comparing Fuel Particle Counting and Gamma Counting.

This is a typical result for the fuel rods fabricated during the four FSV-EVT fuel rod production campaigns. In Fig. 3.45, the normalized relative fuel distributions are defined as follows:

$$f = N_i/\overline{N} \ ,$$

where

N_i = the PSA or gamma-count data per specific axial segment, and

$\overline{N} = (\sum_{i=1}^{5} N_i)/5$ for the fuel rod of interest.

The excellent correlation between the gamma-count and PSA data shown in this figure reinforces the conclusion that PSA data are directly related to the uranium and thorium contents. This is to say that

the number of fissile and number of fertile particles for each axial segment as determined by the PSA are directly proportional to the uranium and thorium contents.

The results of the fuel homogeneity calculations for samples from the FSV-EVT fuel rod production campaigns are presented in Table 3.15. The maximum positive index determined by each method is given for each fuel rod. The general agreement of the calculated indices indicates that each method yields data directly related to the uranium and thorium contents.

Table 3.15. Fuel Rod Homogeneity Indices Obtained by the PSA and Gamma Count Method for the FSV-EVT Fuel Rods Produced at ORNL

Campaign	Fuel Rod	PSA		Gamma Count	
		U Index	Th Index	U Index	Th Index
I	1-H-4	0.07	0.06	0.07	0.03
	1-H-46	0.07	0.09	0.04	0.04
	1-H-107	0.05	0.08	0.04	0.06
	1-H-128	0.03	0.06	0.05	0.08
	1-H-191	0.08	0.09	0.06	0.09
	1-H-210	0.07	0.09	0.09	0.07
	1-H-239	0.06	0.06	0.05	0.03
	1-H-246	0.06	0.08	0.04	0.05
II	2-H-21	0.07	0.07	0.08	0.06
	2-H-57	0.08	0.12	0.09	0.09
	2-H-100	0.07	0.07	0.09	0.07
	2-H-166	0.09	0.06	0.08	0.05
III	3-H-16	0.09	0.10	0.08	0.10
	3-H-55	0.08	0.07	0.05	0.07
	3-H-92	0.04	0.09	0.04	0.08
	3-H-133	0.07	0.07	0.06	0.06
	3-H-153	0.08	0.06	0.08	0.03
	3-H-197	0.03	0.08	0.04	0.05
	3-H-222	0.07	0.08	0.06	0.07
	3-H-259	0.11	0.10	0.09	0.11
IV	4-H-20	0.04	0.07	0.04	0.06
	4-H-79	0.04	0.08	0.03	0.11
	4-H-132	0.04	0.06	0.04	0.06
	4-H-172	0.10	0.03	0.10	0.02

3.5.4.5 Fabrication of Irradiation Test Specimens — D. R. Johnson, P. Angelini, and A. J. Caputo

Fuel rods were fabricated and characterized for use in three of eight test elements to be included with the first reload of the Fort St. Vrain (FSV) Reactor. The purpose of the fuel test elements is to demonstrate acceptable performance and safety of proposed future FSV fuel product specifications and processes.[54] In addition, the test elements are intended to demonstrate acceptable performance of the advanced fuel designs planned for the large commercial steam-cycle HTGR. These advanced fuel designs, including near-isotropic H-451 graphite fuel blocks, Triso-coated weak-acid-resin-derived fuel particles, Biso-coated throium oxide fertile particles, dense graphite shim particles, and cured-in-place fuel rods are also the designs planned for refabricated HTGR fuel and are the reference fuel designs in the Thorium Utilization Fuel Refabrication Program.

It is intended that some fuel particles and green fuel rods will be fabricated by ORNL, Commissariat a L'Énergie Atomique (CEA), and Hoch Temperatur Brennelement GMBH, Hanau (HOBEG) in addition to the General Atomic Company (GA). The fuel will be cured-in-place by GA in the pilot plant cure-in-place furnace, with the exception of a small amount of test fuel to be cured in alumina powder.

The fuel rods fabricated by ORNL are to go into three of the fuel test elements: FTE-4, -6, -8. The fuel rods were fabricated by the slug-injection process in the engineering-scale fuel rod molding machine. The Triso-coated weak-acid-resin-derived fissile particles were taken from batches coated by ORNL and irradiated in the OF-2 fuel irradiation experiment.[55,56]

The shim particles, matrix material, and Biso-coated thoria particles were supplied by GA from large lots from which CEA and HOBEG will also fabricate test fuel.

Fuel rods were fabricated with two fuel loadings for each of the two fissile particle batches. The fuel was fabricated in four separate campaigns of approximately 250 fuel rods each. Before each fabrication campaign sample fuel rods were molded and tested for several critical properties: heavy metal loading, fuel homogeneity, physical dimensions,

and mechanical integrity. Representative samples were taken by random selection from each fabrication campaign according to a Quality Assurance Plan for the experiment. Sample fuel rods were characterized via the following inspections; dimensional and weighing, radiography, fuel homogeneity, heavy metal assay, and filler distribution. The fuel rods were within the product specifications for the test elements. In addition to the characterizations performed by ORNL, sample fuel rods were identified by a random selection process for additional testing by GA according to the FTE test plan.

3.5.5 Fuel Element Assembly (Subtask 360) — D. R. Johnson

The fuel element fabrication development work is divided into four areas: (1) fuel element loading, in which green (unfired) fuel rods are loaded into the fuel element block; (2) carbonization and annealing, in which the loaded fuel element block is heated to about 1000°C to carbonize the pitch binder of the fuel rods and then annealed at 1800°C to remove residual volatiles and stabilize fuel rod dimensions; (3) end plug, dowel, and poison rod loading, in which poison rods are loaded into the element and graphite plugs and dowels are placed in the fuel holes and dowel holes and cemented into place; and (4) fuel element inspection, in which the assembled element is inspected and prepared for shipping to the reactor (or stored). Effort during the year has been confined to the carbonization and annealing area of this work.

3.5.5.1 Equipment Development

3.5.5.1.1 Fuel Rod Storage System, D. R. Johnson, S. P. Baker, and W. R. Hamel. The design of the fuel rod storage system has been reported previously.[57] The system consists of a fuel rod storage magazine, precision y-z indexing table, and the ancillary equipment for fuel rod loading, unloading, and stack height inspection. During the past year, the mechanical system has been installed and the instruments and controls have been designed, fabricated, and installed

(see Sect. 3.5.7). Testing and evaluation of the equipment are currently in progress; no serious design deficiencies have been uncovered. The system is shown in Fig. 3.46.

3.5.5.1.2 In-Block Carbonization Furnace, A. J. Caputo, D. Kiplinger, and B. J. Bolfing. The Lindburg vertical tube furnace previously used for firing graphite tubes to simulate cure-in-place was upgraded to allow the in-block carbonization of one-sixth segments of HTGR fuel elements. The high-temperature (1800°C) annealing operation is accomplished in a separate furnace. The upgrading consisted of installing new, higher power heating elements and designing, fabricating, and installing a new three-zone temperature program-and-control system, a packed-column perchloroethylene fume scrubber and cooler, and new Inconel furnace muffle and top. The performance of the furnace has been excellent. Axial temperature variations in the approximately 0.9-m-long (3-ft) hot zone are limited to about ±15°C. Heating profiles from ambient to 1000°C have been accurate to within ±1°C/min.

3.5.5.2 Process Development (Cure-in-Place)

3.5.5.2.1 Factors Affecting Failed Fuel Particle Coatings, A. J. Caputo, D. R. Johnson, and C. K. Bayne. The effect of various variables on the in-block carbonization process was investigated. Four laboratory in-block carbonization-annealing runs were made using full length [0.79-m (31-in.)] blocks but only about 1/6 segment of the block cross section. Each run contained about 300 fuel rods [13-mm-diam by 51-mm-long (1/2 by 2 in.)]. The runs investigated the effect of (1) fertile particle crushing strength, (2) heating rate, and (3) vertical position of the fuel rod in the block upon fuel failure fraction and coke yield at the nominal argon permeability value (17 liters/min at 28 kPa gage (4 psig)] determined for fuel elements made of H-327 graphite. Heating rates of 1, 5, 10, and 15°C/min provided a range of coke yields, and each run contained fuel rods made from three batches of fertile particles with crushing strengths of 22.9, 25.7, and 30.5 N

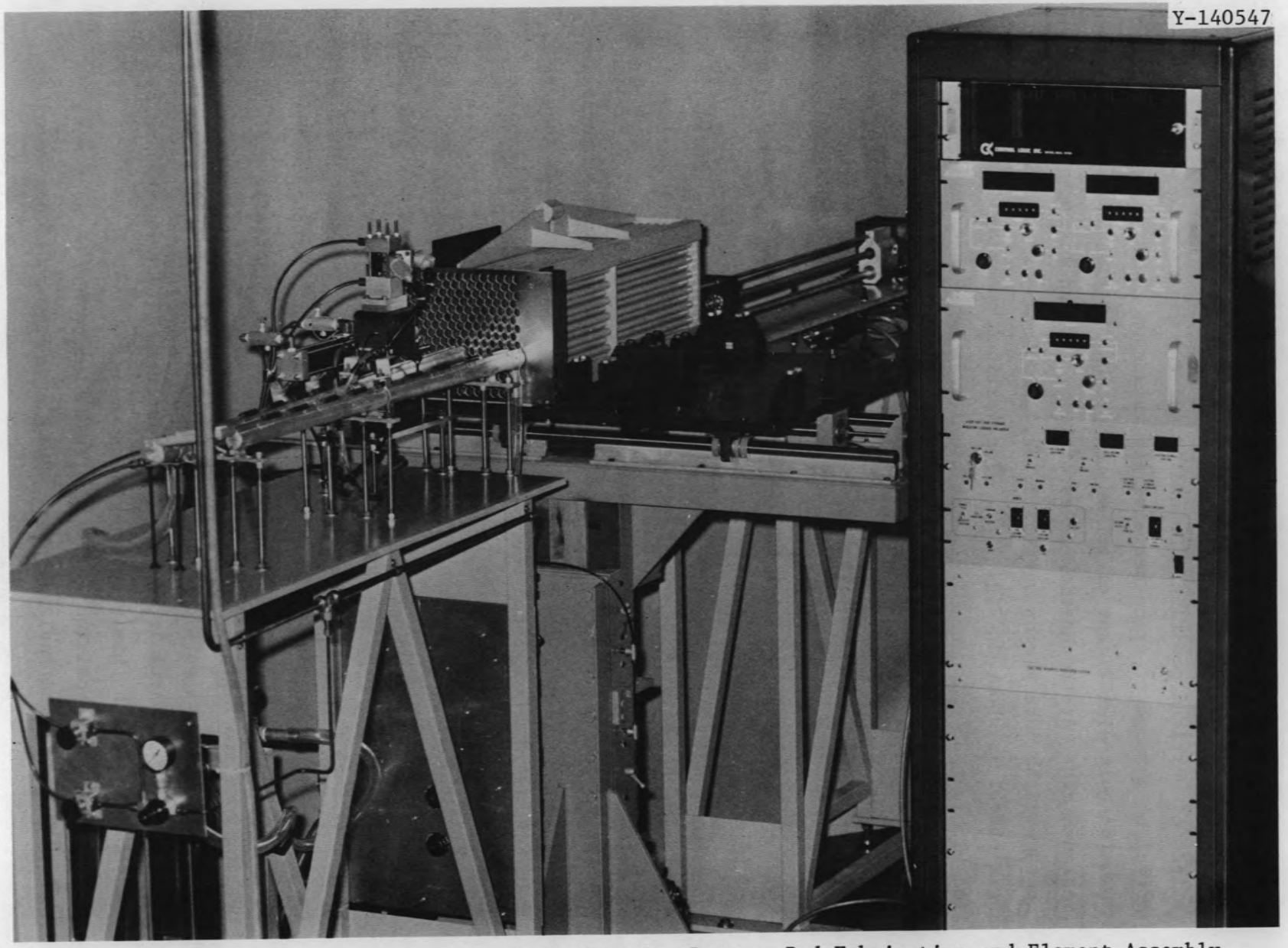

Fig. 3.46. Fuel Rod Storage System: Surge Capacity Between Rod Fabrication and Element Assembly.

(5.14, 5.78, and 6.85 lb). The rods were placed at the top, middle, and bottom of three fuel holes within each block to investigate the effect of vertical position. An additional run was made to see the effect of a range of argon permeability values on the same properties.

The only significant effect on the pitch coke yield was that of the heating rate. At the heating rates of 1, 5, 10, and 15°C/min the average pitch coke yields were 37.3, 32.4, 29.1, and 27.9%, respectively. This effect is shown in Fig. 3.47. The vertical position of the fuel rod within the fuel element did not significantly affect the coke yield.

The failed fuel data are summarized in Table 3.16. Fuel failure was dependent on both heating rate and particle crushing strength. The fuel cured under conditions of both low heating rate and low fertile particle crushing strength resulted in unacceptably high ($>1 \times 10^{-4}$) failed fuel fractions. The low-strength [22-N (5-lb)] particles can be cured at faster heating rates (10—15°C/min) and will yield acceptable results. Likewise, the fuel elements can be cured with very slow (1°C/min) heating rates if sufficiently strong fuel particles [30-N (7 lb)] are used. The reference cure-in-place process set points include a 10°C/min heating rate; at present particle crushing strength is not specified. Thus, the present results suggest that failure of Biso-coated thoria fuel particles during cure-in-place under the reference set point conditions would not be expected if the fertile particles have an average crushing strength exceeding 22 N (5 lb).

Failure of coated fuel particles during cure-in-place was previously attributed[56] to tearing of the particle coatings as a result of differential shrinkage between the fuel particles and matrix binder. In some cases, a tear is initiated during cure-in-place, then propagates during irradiation. The relativly dense matrix structure associated with low heating rate and high pitch coke yields offers more surface area for bonding to the fuel particles and is thus more likely to initiate a tear in the fuel particle as the matrix shrinks. The present results are consistent with this proposed mechanism.

The vertical position within the fuel element had no apparent effect on the failed fuel fraction. Such an effect could not be

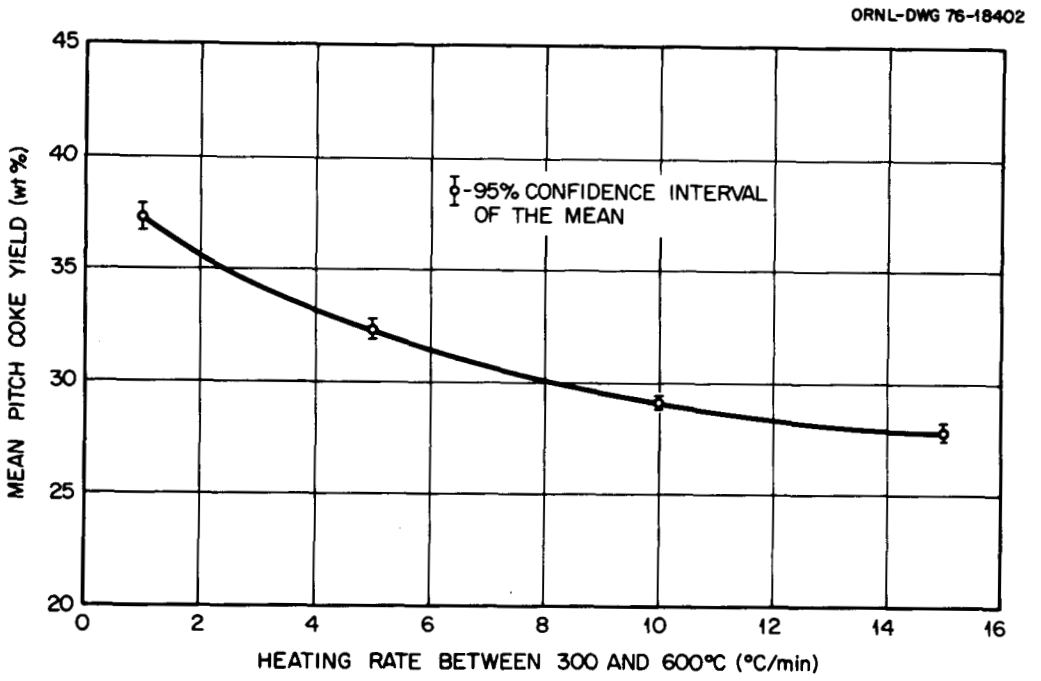

Fig. 3.47. Pitch Coke Yield of the In-Block Carbonization-Annealing Process (using additive-type matrix) as a Function of Heating Rate of the Carbonization Cycle.

Table 3.16. Failed Fraction of Biso-Coated Annealed Fertile Particles in In-Block Carbonization-Annealing Runs

Heating Rate[a] (°C/min)	Average Coke Yield (wt %)	Failures per 10,000 Particles[b] for Each Crushing Strength in N (lb)		
		22.9 (5.14)	25.7 (5.78)	30.5 (6.85)
1	37.3	1.55[c]	1.88[c]	0.05[d]
5	32.4	0.78[c]	0.23[d]	0.01[d]
10	29.1	0.02[d]	0.01[d]	0.01[d]
15	27.9	0.19[d]	0.16[d]	0.01[d]

[a]Between 300 and 600°C.

[b]Determined by chlorine leaching for 2 hr at 1500°C. Each value listed is an average of six samples.

[c]95% confidence that the failure fraction exceeds 1×10^{-4}.

[d]95% confidence that the failure fraction is less than 1×10^{-4}.

unequivocally determined because the particle strength variable confounded the comparison. However, as the vertical position in the fuel element had no statistically significant effect on coke yield, we inferred that the effect of position on failed fuel was insignificant.

Some preliminary work has been done on the effect of graphite permeability on failed fuel fraction. An additional run was made at a heating rate of 10°C/min using fuel holes that had argon permeabilities ranging from 4 to 17 liters/min. This range was chosen because it included the average permeability (17 liters/min) determined for blocks of H-327 graphite and the average (8 liters/min) estimated for blocks of H-451 graphite. The average coke yield of 29.8% was essentially the same as in the previous run at 10°C/min and did not vary significantly for rods that were in fuel holes of different permeabilities. The failed fuel fraction was within specification regardless of the permeability of the holes. The effect of graphite permeability at lower heating rates and higher coke yields, where fuel failure is more likely, has not yet been tested.

3.5.5.2.2 Gas Permeability of HTGR Graphite Fuel Elements, A. J. Caputo, D. R. Johnson, and C. K. Bayne. The HTGR fuel element is a large hexagonal graphite block 0.36 m (14 in.) across the flats and 0.79 m (31 in.) long. The block contains blind holes, which contain the fuel rods, and open holes for passage of a coolant gas. The graphite web separating the fuel holes from the coolant hole is nominally 4.52 mm (0.178 in.) thick.

During in-block carbonization about 70% of the weight of pitch binder and additives used in the fuel rod are volatilized. These gaseous products must diffuse through the graphite webs into the open coolant holes, where they are purged with an inert gas flow.

A significant variability in the gas permeability of the graphite webs might lead to corresponding variation in the properties of the cured-in-place fuel rods. Thus, the extent of the variations in gas permeability of graphite HTGR fuel element blocks was determined.[58] The specific gas permeability of the graphite was not determined, as the geometry of the fuel blocks was too complex. Rather, the flow rate of pressurized

argon escaping from individual fuel holes by diffusing through the graphite webs surrounding the fuel holes was measured. The argon pressure in the fuel holes was maintained at a constant value of 28 kPa gage (4 psig), a convenient value for measurement. In addition, the effect of argon pressure on the gas flow rates was also determined.

Figure 3.48 illustrates the device constructed for relative permeability measurements. The probe seals the top of the fuel hole while introducing argon at a regulated pressure. Provisions were made for measuring the resulting pressure at the top and bottom of the fuel hole; however, no appreciable differences were seen between the two pressures. The argon flows were measured with rotometers, and all measurements were corrected to standard conditions, 0.101 MPa (14.7 psia) and 21.1°C (70°F).

The fuel holes in three of the six triangular block segments were examined for permeability. The three segments examined were equally spaced 120°C apart. The holes on the borders between segments were also measured.

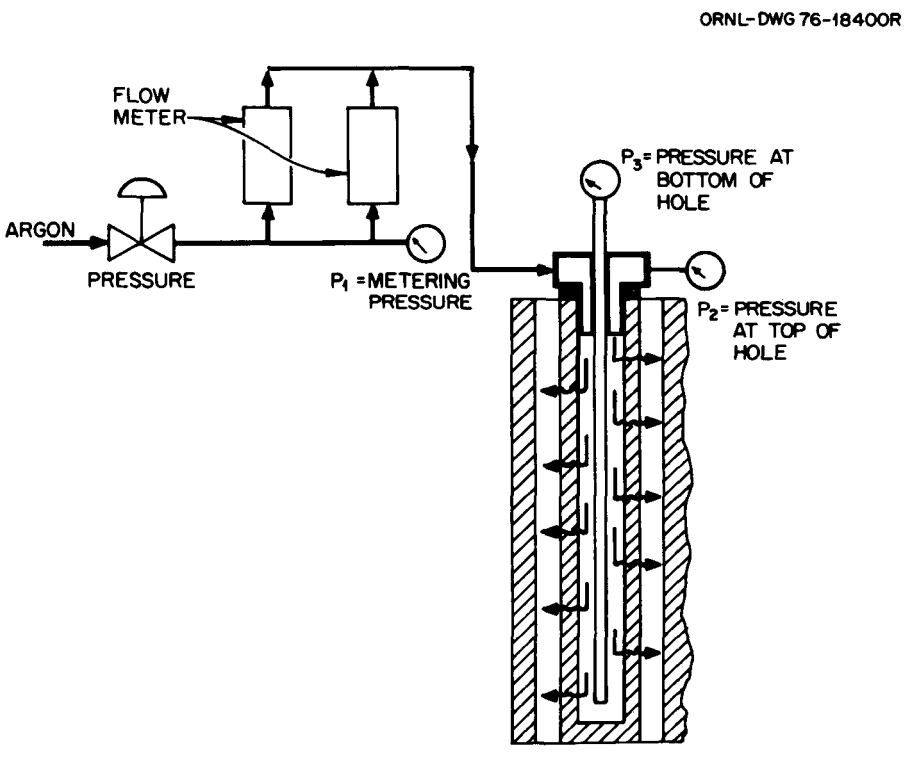

Fig. 3.48. Argon Permeability Measuring Device.

Some of the holes have atypical geometry. They were identified as follows:

I — Holes on the inner circle [radius = 37.6 mm (1.48 in.)]. These holes are closest to the center hole, and two of the three graphite webs between each fuel hole and coolant holes are thicker — 6.10 mm (0.240 in.) rather than 4.55 mm (0.178 in.) for normal webs — for these inner circle holes.

S — The second circle [radius = 49.8 mm (1.96 in.)] of fuel holes about the origin. These holes have one thick graphite web between fuel hole and coolant hole.

C — The holes on the corners of the hexagonal block. These are adjacent to only one coolant hole (instead of the regular three) but have access to the block surface through two 10.8-mm (0.427-in.) webs.

F — The holes along the flat sides of the block. These are adjacent to two coolant holes but have access to the block surface through a 10.8-mm (0.427-in.) web.

R — The remaining regular holes adjacent to three coolant holes separated by graphite webs of the nominal 4.55-mm (0.178-in.) thickness.

All the holes with atypical geometry (60) were measured in each block along with 86 at the 156 regular holes.

The results were analyzed by multiple linear regression and a summary of the results includes the following:

Pressure Effect

The effect of pressure on the permeability of porous materials, including graphite, has been reported elsewhere.[59—61] For the complex geometry involved in this investigation the overall pressure effect was determined by taking flow measurements at pressures ranging from 1.72 to 69 kPa gage (0.25—10 psig). The measurements were made in holes that represented the lowest, average, and highest relative permability values found in this investigation. This pressure effect is shown in Fig. 3.49. Thus, the results of this investigation can be extended to other pressures by estimating from Fig. 3.49.

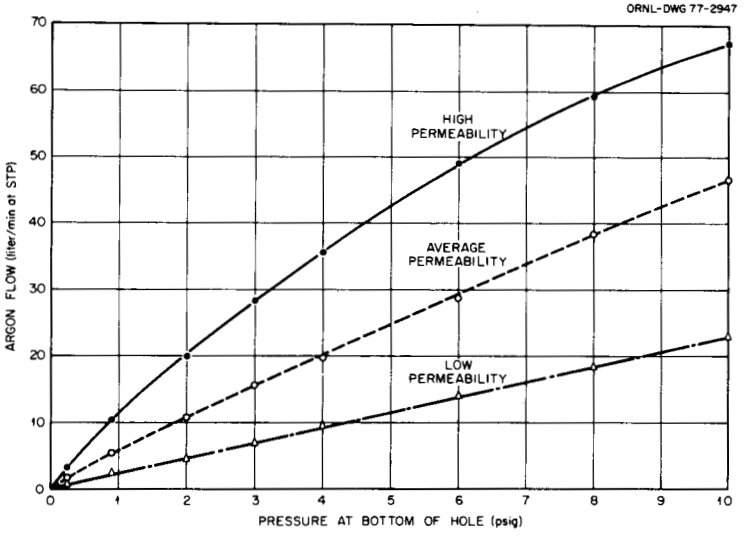

Fig. 3.49. Pressure Effect on the Argon Flow from HTGR Graphite Fuel Element Holes at Various Permeability Levels. 1 psig = 6.9 kPa (gage).

Permeability Among Blocks

Relative argon permeability varied appreciably among the fuel element blocks. The average permeability of each block is listed in Table 3.17. The overall average argon flow for all holes measured in the ten blocks was 14.9 liters/min. The average for an individual block ranged from a low of 6.2 to a high of 25.4 liters/min. This variation in the average permeabilities among blocks is no doubt primarily due to differences in the porosity of the graphite logs from which the fuel blocks were made. The surface condition of the fuel holes, which is determined by drilling speed, tool sharpness, etc., may also be a factor.

Permeability Within Blocks

Significant differences in argon permeability occurred within the individual blocks. The major source of the within-block variation was a systematic radial gradient in argon permeability. The permability was highest along the central axis of the block and decreased radially toward the outside surface. Figure 3.50 illustrates the radial variation for block 1-0637. Presumably the radial gradient in gas permeability

Table 3.17. Permeability of HTGR Fuel Element Blocks

Block	Relative Argon Flow, std liters/min	
	Block Mean	Range of Individual Holes
1-0372	6.2	1.5–12.9
1-0637	14.1	4.0–23.4
1-1046	6.7	0.8–16.4
1-1343	11.5	5.5–15.9
1-1622	11.4	2.3–25.6
1-2926	23.0	4.7–38.6
1-4748	21.4	2.0–37.1
1-4749	20.2	1.7–36.7
1-5285	9.1	1.5–22.3
1-5864	25.4	6.4–41.3
Overall Mean	14.9	
Overall Range	6.2–25.4	0.8–41.3

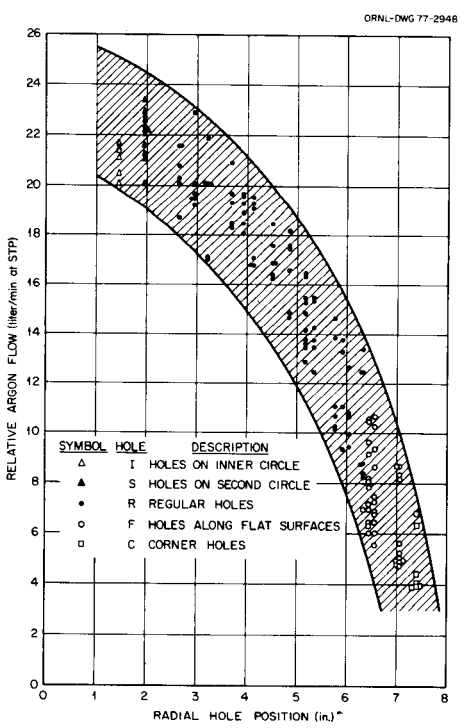

Fig. 3.50. Permeability of an HTGR Fuel Element (1-0637) at 28 kPa gage (4 psig) Versus Radial Hole Position. 1 in. = 25.4 mm

results from the impregnation step in the graphite fabrication. As the pitch is intruded into the shape from the outside, one might expect the porosity of the graphite to be highest in the center and lowest on the outer surfaces. The gas permeability would be expected to be higher in the porous center of the graphite log.

Permeability of Atypical Fuel Holes

The fuel holes near the center or the outside edges of the element have a different geometry for out-diffusion of gases. The argon permeabilities of the different geometry types were shown to be statistically different. The experimental data are summarized by hole type in Table 3.18. The large apparent difference in hole types is mostly due to the radial effect. In Table 3.18 the columns, from left to right, are in order of increasing radial position. However, in the statistical analysis of the data, the permeabilities of the different hole types were calculated as though the holes were all at the same radial position.

Table 3.18. Relative Argon Permeability of Different Fuel Hole Types in HTGR Fuel Element

Block	Average Argon Flow, std liters/min					
	Inner Circle I	Second Circle S	Regular R	Flat F	Corner C	All Holes
1-0372	9.1	10.7	6.9	3.0	2.2	6.2
1-0637	21.1	22.1	16.0	7.3	5.0	14.1
1-1046	11.7	12.2	7.7	2.6	1.3	6.7
1-1343	12.9	13.7	12.7	8.8	6.3	11.5
1-1622	17.1	18.4	12.9	5.7	3.5	11.4
1-2926	31.4	34.3	27.0	11.0	7.0	23.0
1-4748	31.5	33.6	24.6	10.5	5.0	21.4
1-4749	28.3	30.7	23.8	9.7	3.4	20.2
1-5285	18.8	20.3	10.2	2.4	1.6	9.1
1-5864	29.5	33.3	29.2	15.9	8.0	25.4
Average	21.1	22.9	17.1	7.7	4.3	14.9

The effect of the hole geometry is relatively small, when adjusted for the radius effect, even though it is statistically significant. Relative to the variation in argon permeability among blocks and along the radius within blocks, the effect of hole geometry appears to be of little practical importance.

Conclusion

The mean relative argon permeabilities of ten graphite HTGR fuel element blocks differed by approximately a factor of four. Within the blocks the argon permeability systematically varied along the radius of the elements. The permeability along the central axis of the elements is an order of magnitude higher than at the surface.

The effect of permeability on the resultant properties of carbonized fuel rods and the overall in-block carbonization process is uncertain. Property variations with permeability will be monitored during future development phases of in-block carbonization.

3.5.5.2.3 Characterization of Fuel Rod Carbonization Off-Gas, A. J. Caputo. After the green fuel rod has been molded it is heated to about 1000°C to carbonize the pitch binder. The in-block carbonization process produces an average pitch coke yield of about 30%, with the remaining pitch plus additives being volatilized during carbonization. The composition of this off-gas was determined by obtaining gas samples at various temperature intervals during a typical carbonization run and identifying the major constituents by mass spectrometry. A typical carbonization run uses 0.26 liter/sec (0.55 cfm) argon purge flow to carbonize about 300 fuel rods. The composition of the off-gas at various temperatures is shown in Table 3.19. Since the carbonization cycle is performed with an argon purge flow, argon is the main constituent. The other major constituents are hydrogen, which peaks at about 18 vol % at 700 to 800°C, and methane, which peaks at about 17 vol % at 500 to 550°C. Smaller amounts, up to 2 vol %, of ethane, propane, ethylene, and propylene are evolved between 400 and 600°C. The composition of these main constituents of the off-gas is shown graphically in Fig. 3.51.

Table 3.19. Composition of Fuel Rod Carbonization Off-Gas

Component	Content, vol %, at Each Carbonization Temperature, °C									
	200	300	400	450	500	550	600	735	800	850
Argon, Ar	99.77	99.68	99.04	94.71	78.74	73.21	84.54	76.56	78.05	89.79
Hydrogen, H_2	0	0.02	0.06	0.43	2.33	6.95	8.44	18.68	18.07	9.38
Methane, CH_4	<0.01	0	0.22	3.33	16.04	18.30	6.61	4.30	3.58	0.68
Ethane, C_2H_6	0	0	0.06	0.62	1.68	0.94	0.12	0.04	0.01	0
Propane, C_3H_8	0	0	0.14	0.59	0.76	0.22	0.03	0	0	0
Ethylene, C_2H_4	0	0	0	0	0.10	0.09	0.03	0.04	0.03	0.02
Propylene, C_3H_6	0	0	0.06	0.62	1.68	0.94	0.12	0.04	0.01	0
Nitrogen and/or Carbon Monoxide, N_2, CO	0.11	0.12	0.23	0.16	0.14	0.14	0.11	0.21	0.17	0.10
Carbon Dioxide, CO_2	0.07	0.14	0.16	<0.01	0	0.01	0.03	0.07	0.02	<0.01
Hydrogen Sulfide, H_2S	0	0	0	0	0.02	0.04	0.01	0.02	0.01	0
Oxygen, O_2	<0.01	0	0	<0.01	0	0.01	<0.01	0.01	<0.01	0
Water, H_2O	0.03	0.03	0.07	0.05	0	0.02	0.03	0.06	0.04	0.03

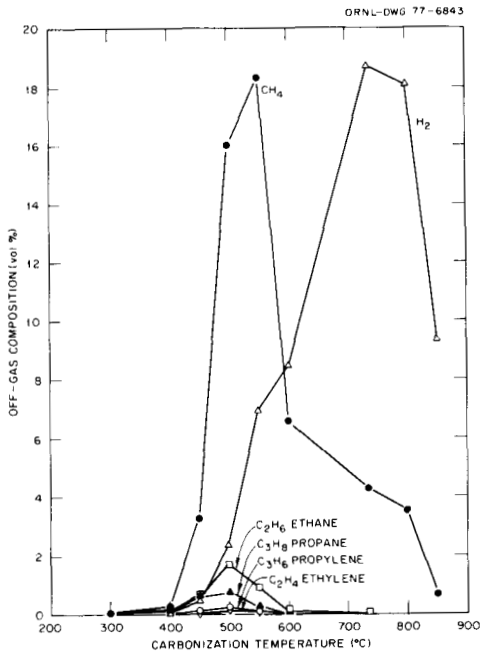

Fig. 3.51. Off-Gas from Fuel Rod Carbonization.

Only trace amounts of other constituents (N_2, CO, CO_2, H_2S, O_2, and H_2O) were found in the off-gas as shown in Table 3.19.

Trace amounts of higher mass components are also volatilized during the fuel rod carbonization cycle, and they are dissolved in a recirculating perchlorethylene scrubber. The materials removed by the perchloroethylene scrubber have been tentatively identified and reported elsewhere.[62]

3.5.5.2.4 Fuel Column Expansion and End Plug Joint Strength, A. J. Caputo. For the original loading of the Fort St. Vrain reactor the fuel rods were carbonized and annealed and then loaded by hand into the blind fuel holes of the fuel element block. The holes were sealed by cementing a tightly fitting graphite end plug flush with the top of the block. Because the graphite block shrinks relative to the fuel column during irradiation, an axial void space was provided between the top of the fuel column and the end plug. Otherwise, the differential contraction might mechanicaly damage the fuel rods and/or fuel block. However, the in-block carbonization and annealing process

requires the loading of green fuel rods and end plugs into the fuel element before carbonization and annealing.

Thus, a design change was proposed by General Atomic Company in which the void space would be distributed throughout the fuel column. This distributed void space could be obtained by placing plastic spacers between fuel rods when loading the fuel element. Volatilization of the plastic would leave the desired voids. Also a loosely fitting end plug [0.1—0.2 mm (0.004—0.008 in.) diametral clearance] would be placed on the top of the fuel column, below the top surface of the fuel element. It was proposed that the fuel column would expand during carbonization and annealing such that the resulting end plug position would be flush with the top of the fuel element. Restraint would be provided to prevent the end plug from rising above the element surface. The products of the pitch pyrolysis would cement the end plug in place, and vaporization of the plastic spacers would provide distributed void space between the fuel rods. End plug strengths of 0.22 to 0.44 kN (50—100 lb) were proposed for large HTGR elements.

Using the proposed design, numerous in-block carbonization and annealing runs were made during the year using the full length of fuel element but only about 1/6 segment of cross section. The fuel columns were loaded as required for the in-block carbonization planned for the fabrication of fuel elements for the FSV Early Vailidation Test. That is, the fuel columns were loaded to within about 10 mm (0.4 in.) of the top of the fuel element, contained seven 3.81-mm-thick (0.150-in.) plastic spacers distributed every second rod along the fuel column, and a loosely fitting end plug. Invariably the fuel column failed to rise to the top of the fuel block, and the end-plugs were not strongly cemented in place. In general, fewer than 10% of the fuel columns rose to the top surface of the element. The remaining columns expanded an average of approximately 2.5 mm (0.10 in.) but a range from 0 to about 5 mm (0.2 in.). If the fuel columns were loaded with the end plugs close to the top of the fuel element [about 2.5 mm (0.1 in.)], the number of columns flush with

the top of the fuel element after curing did increase somewhat, but the results were nevertheless erratic and undependable. The placement of fuel columns to such close tolerances is not desirable since it forces the fabrication of fuel rods to unreasonably close length tolerances.

The average strength of the end plugs was usually low, 22 to 44 N 4–10 lb), with individual values ranging from 0 to about 130 N (30 lb). In some runs 50 to 75% of the end plugs were loose. Although the bulk of our tests used the 13-mm-diam (1/2-in.) fuel rod of the FSV design, the loading plan was also used in limited tests using the 16-mm-diam (5/8-in.) fuel rods of the large HTGR design. Although the distance the column expanded [2.5–5 mm (0.1–0.2 in.)] was somewhat greater than that for 13-mm-diam fuel rods, the results were still unpredictable. The end plug strengths were also low, ranging from 0 to 67 N (15 lb).

The results of a typical run using both 13- and 16-mm-diam fuel rods are shown in Fig. 3.52. In this experiment six of the 16-mm-diam coolant holes of a FSV element segment were plugged to simulate the fuel holes of the large HTGR reactor, and surrounding 13-mm FSV fuel holes were bored through to simulate coolant holes. In this manner, the performance of both 13- and 16-mm-diam fuel rods could be compared in the same experiment. In this run the six 16-mm-diam holes and 11 of the 13-mm-diam holes were loaded to within about 10 mm (0.40 in.) of the top surface, and two holes were loaded to within about 2.5 mm (0.10 in.) of the top. The element section was cured-in-place via the pressure process. As can be seen in Fig. 3.52 the two holes loaded to within about 2.5 mm of the top remain considerably below the surface.

These results indicate that the proposed process for element assembly will not dependably produce fuel columns flush with the top surface of the fuel block nor strongly cemented end plugs. We recommend that the requirements of fuel column geometry and end plug strength with respect to fuel handling and performance be reevaluated. If precise end plug positioning and strongly cemented end plug joints are required for refabricated fuel, additional development work will be required.

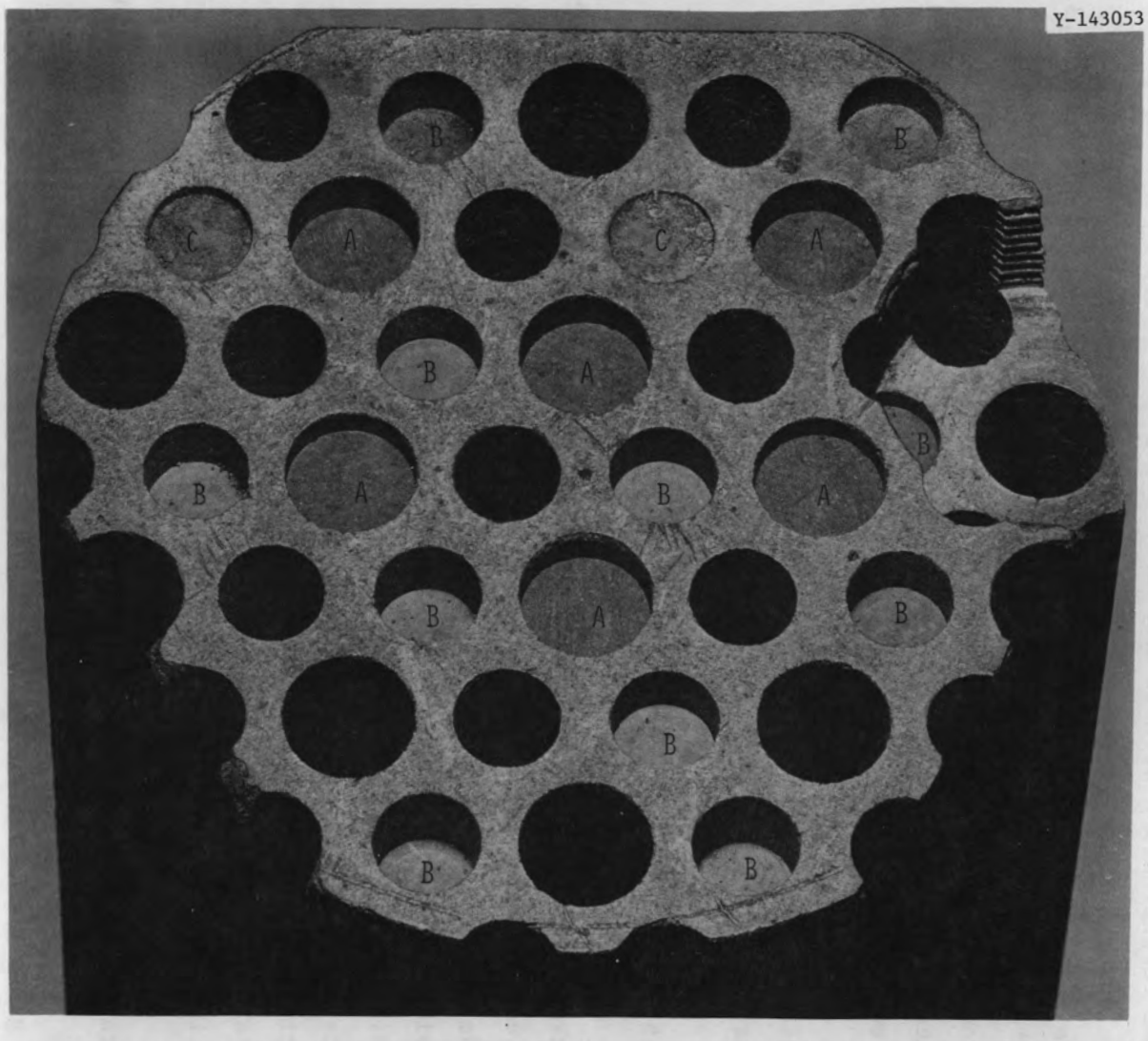

Fig. 3.52. Top Surface of 1/6 Segment of FSV-Type Fuel Element After In-Block Carbonization. Some 16-mm-diam (5/8 in.) coolant holes contain 16-mm-diam fuel rods to compare fuel column expansion. A: 16-mm-diam holes loaded to about 10 mm (0.40 in.) from the top surface. B: 13-mm holes loaded to about 10 mm. C: 13-mm-diam holes loaded to about 2.5 mm (0.10 in.)

3.5.6 Sample Inspection (Subtask 370): Equipment Development — J. E. Mack

The Sample Inspection System will function as a support system for the refabrication effort. It must provide the means for obtaining representative material samples inside the hot cell at various points in the refabrication process and transfering these samples to shielded glove boxes for analysis. Development of the analytical techniques to be employed are reported under Cold Laboratory Development, Sect. 3.3.2.

During this period, efforts were directed toward the development of remotely operable sample transfer systems and a particle sampling device. The feasibility of pneumatic transfer of loose particle samples and encapsulated fuel rod samples was demonstrated.

An automated particle size analyzer was modified for operation inside an inert-atmosphere glove box to permit analysis of pyrophoric material.

3.5.6.1 Particle Size Analysis — J. E. Mack

A device for sizing individual fuel particles based on a light blockage technique was developed during the previous reporting period.[63] The device, illustrated in Fig. 3.53, operated routinely in support of development activities throughout the current reporting period, providing data on particle size distribution and sample count for studies on rod homogeneity for the Fort St. Vrain Early Validation Tests as well as for characterization of the weak-acid resin and coated particles. The particle size analyzer was also utilized in the performance evaluation of particle sampling devices. Operating procedures for this device were formalized during this period.

A glove box was procured and a modified analyzer fabricated for operation in an inert atmosphere to permit sizing of pyrophoric material, such as the carbonized and converted loaded resin. Preparation of the glove box and installation of the analyzer are currently under way.

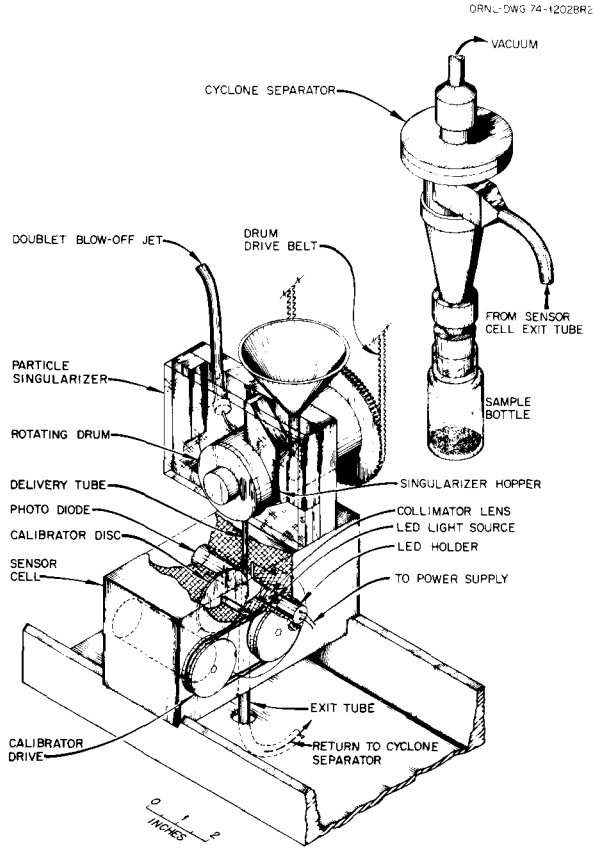

Fig. 3.53. Particle Size Analyzer: Configuration for Primary Calibration. Scale length is 51 mm.

3.5.6.2 Particle Sample Transfer — J. E. Mack

Particle samples will be obtained in cell from a sampling device and will have to be transported out of the hot cell for analysis. To evaluate the feasibility of vacuum transfer of loose particles, a 30-m (100-ft) test loop was constructed of 9.5-mm-OD by 1.65-mm-wall (3/8 by 0.065 in.) stainless steel tubing to determine transfer requirements for small particle samples (1–5 g). Particle holdup in the line was virtually eliminated by boring through the tubing unions and butting the tubing end to end. Individual particles have been transferred the length of the run and recieved in a nylon cylone

receiver. Visual inspections of transferred material have been indicated no particle breakage. A statistical analysis of sample size and analytical capabilities is currently under way to effectively determine particle breakage by chlorine leach, in view of the small sample size and the problems associated with obtaining identical samples.

3.5.6.3 Fuel Rod Sample Transfer — J. E. Mack

Fuel rod samples must also be obtained in cell and transferred out of the hot cell for analysis. Because of the brittleness of these rods, particularly after firing, they cannot be transferred without protection as are the particle samples. The method under development involves remote encapsulation of the fuel rod in a polyethylene "rabbit" and pneumatic transfer under vacuum to a Sample Inspection Station.

A fuel rod loader and an unloader were designed, fabricated, and tested at opposite ends of a 23-m (75-ft) test loop; they operated satisfactorily. Both use cushioned air cylinders to insert or eject resilient spherical plugs, which are held in place by collars internal to the polyethylene capsule. They essentially trap the fuel rod inside the capsule and prevent damage in transit. A compressive force of 4 to 9 N (1—2 lb) is all that is required to eject the rod. The simplicity of this technique makes it ideal for remote application.

3.5.6.4 Sampling — R. R. Suchomel

To assure on acceptable sampling device for inclusion in the cold engineering microsphere coating loop, two samplers were designed built, and tested. Qualification tests of these samples determined the range and consistency of both the batch-to-sample mass ratios and the mean particle diameter of the sample. Mean particle diameters were determined by use of the PSA. Figure 3.54 shows the mean particle diameters obtained from a batch of Biso-coated particles by use of each sampler and a random grab sampling technique. The two devices appear to give comparable results with respect to internal consistency, and they also show agreement among the samples. In contrast, the grab

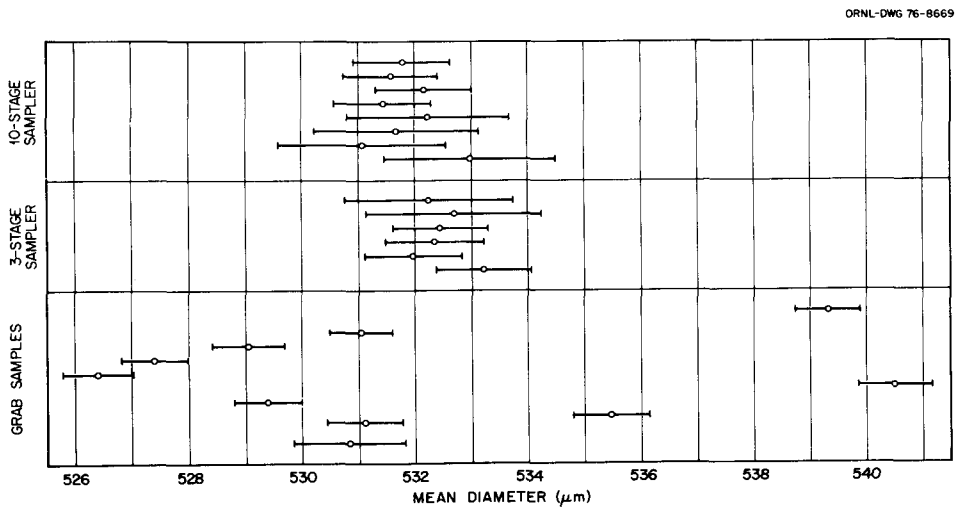

Fig. 3.54. Confidence Intervals (95%) for the Mean Particle Diameter of Biso-Coated Particles Sampled by Three Different Techniques.

sampling technique produced unacceptable data for sample inspection. A complete description of the two sampling units, experimental data, and test results are reported.[33]

3.5.7 Plant Management (Subtask 380) — W. R. Hamel

The objective of Subtask 380 is to develop and evaluate the instrumentation, control, and data handling technology required to support the demonstration of the remote refabrication of HTGR fuels.

The current and subsequent generations of instrumentation and control hardware appropriate for application to HTGR fuel refabrication processes involve the use of highly complex general-purpose devices such as minicomputer-based packages, microcomputers, and programmable logic controllers. These general-purpose devices will be the basic building blocks used in the design and construction of fuel recycle process control systems. Generally, recycle process control systems will comprise a network of these general-purpose devices and other types of hardware. The impact of factors such as synchronization and interfacing are obvious, creating a real-time environment with the operation of various engineering-scale process developmental equipment that is analogous to that expected in an actual recycle facility.

A development programmable logic controller and minicomputer are being used in the control and operation of four pieces of engineering-scale mockup equipment. Three additional programmable logic controller systems were procured for the dedicated support of other engineering-scale process developmental equipment.

3.5.7.1 Equipment Development — S. P. Baker, B. O. Barringer, B. J. Bolfing, and W. R. Hamel

The effort in this area has consisted primarily of the application and interfacing of the development computer system and the development programmable logic controller to refabrication processes.

3.5.7.1.1 Development Computer System. The PDP-11/40-based development computer system is currently being used to support position control system requirements for the fuel rod storage magazine loader-unloader (see Sect. 3.5.5.1.1) and to provide computational and data storage support for nondestructive inspection activities and for program development. A communications link will be established in the immediate future between the computer and the DEC 14/35 programmable logic controller. Future applications will be associated with fuel rod homogeneity inspection and future development of recycle process data handling techniques.

The development computer system has been expanded to include 64 K words of core memory and additional digital input points. The memory will soon by increased to 80 K words. This will allow the concurrent use of the computer by several people for program development and data acquisition. The real-time executive software package currently being used is RSX-11M version 2. It is expected that version 3 of this software will be installed soon.

The fuel rod storage magazine loader-unloader (FRSMLU) includes a two-coordinate position control system. The unloader portion of this system has been demonstrated in both automatic and semiautomatic modes with the development computer used as the controlling element. Plans have been made to replace the PDP-11/40 with and LSI-11 micro-computer as the controller, thus giving the FRSMLU a stand-alone capability.

The nondestructive radioassay development work is being done at TURF. Two modem-controlled communication links have been established between TURF and the development computer system. The computer is currently being used as a data storage medium for the various spectra generated.

Work is in progress on a communications link between the development computer system and the development programmable logic controller. When this work is completed, the computer will be able to store PLC program images and down-line load them at a speed much faster than is currently possible through a teletype. The computer will also be helpful in running PLC diagnostics both on-line and off-line.

3.5.7.1.2 Programmable Logic Controllers and Applications, B. J. Bolfing. HTGR fuel rods are currently being fabricated in an automated fashion on the engineering-scale fuel rod molding machine. The sequential action of this fuel rod machine was formerly controlled by conventional hard-wired relay circuitry. A DEC I14/35 programmable logic controller (PLC) has replaced hard-wired relay circuitry and is now controlling the fuel rod machine.

The PLCs are digital control devices designed to control sequential and conditional process operations. The PLC controls process actuators as a function of the conditional output control logic stored in memory. These conditional actuator control expressions interlock process sensor and actuator states with internal PLC timers, counters, and shift registers. This interlocking ensures safe operation and prevents out-of-sequence events from occurring. Before a given process actuator can be energized, certain sensor states must be present and certain previous process events must have occurred.

The conditional output control logic is loaded into the DEC I14/35 PLC core memory in ladder diagram format using a pushbutton program entry terminal with CRT display (DEC VT14). The VT14, shown in Fig. 3.55 adjacent to the fuel rod machine, allows an operator to monitor in real time the status of all process sensors and actuators and force each process actuator on or off independent of the normal

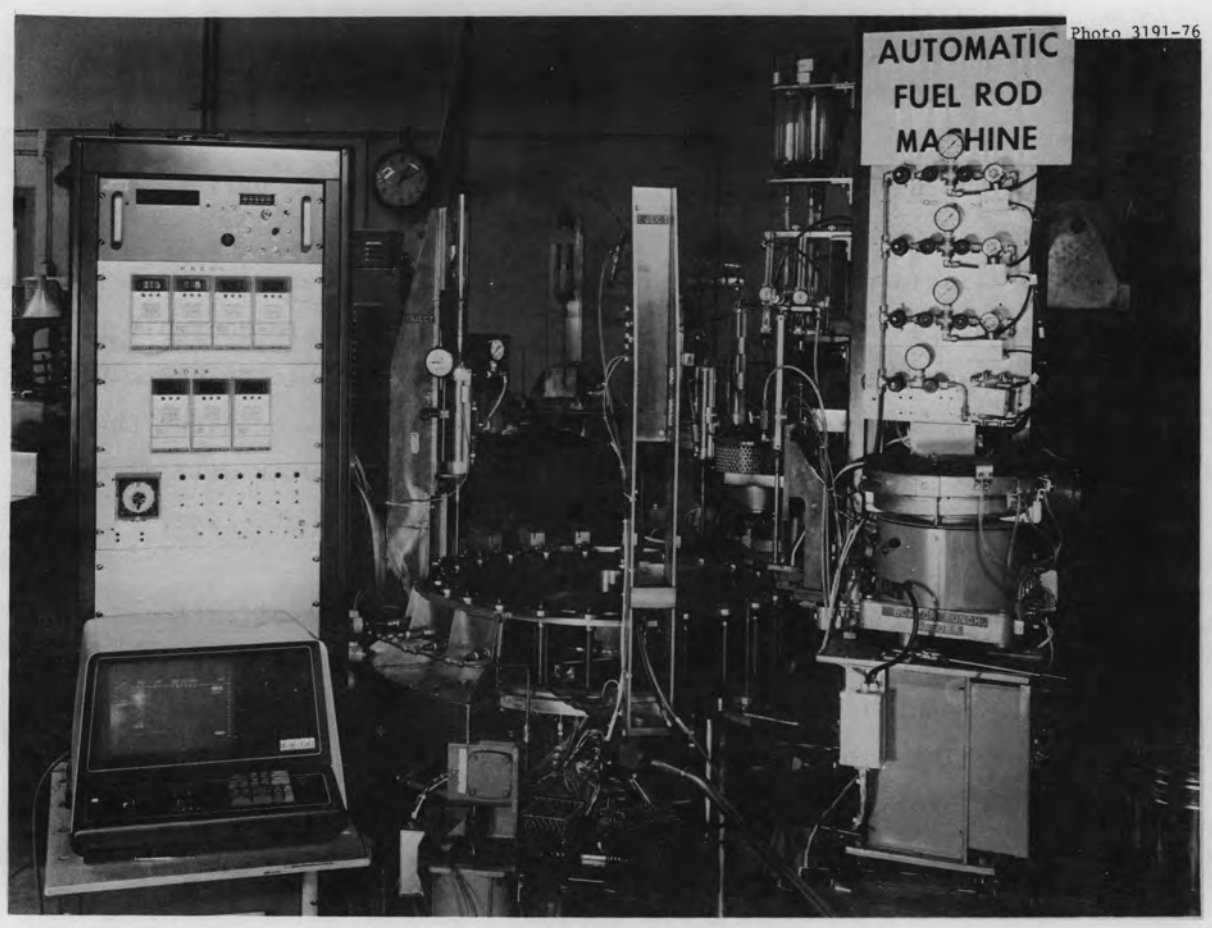

Fig. 3.55. Programmable Logic Controller Programming Terminal Monitoring Laboratory Fuel Rod Molding Machine.

control program. These features are important when considering the operation and maintenance of complex mechanical hardware in a remote hot cell environment.

Three operating modes have been developed for the engineering-scale fuel rod machine under PLC control. In the normal operating mode fuel rods are fabricated in a completely automated fashion. The fuel rod machine remains in this automatic mode unless an alarm event occurs or unless the operator initiates the automatic shutdown sequence. In the alarm mode, the PLC control system reacts to a fuel rod machine alarm event by notifying the operator that an alarm condition is present at a particular station and by halting all further process action. The operator reacts to the alarm notification by pressing the alarmed

station jog button on the local control panel, cycling the station to a safe position. The alarm mode provides an automatic diagnostic capability by indicating to the operator on the VT14 CRT display the cause of an alarm condition. The third operating mode occurs when the fuel rod machine is first started or when the shutdown sequence is initiated. During the period of start-up all stations are automatically phased into the fuel rod molding process in the proper order until all stations are operating simultaneously. In the automatic shutdown process, each station on the fuel rod machine is disabled from the process in the reverse order that it was enabled during start-up, resulting in the automatic unloading of all molds and automatic shutdown of all stations.

Thus, PLC control of fuel rod molding has provided a higher level of control than would be practical or possible with a hard-wired relay system. This higher level of control has been demonstrated by the automated start-up and shutdown routine, the alarm monitoring capability, the VT14's use as a remote troubleshooting aid, and the capability of the PLC to communicate with a computer in a real-time environment.

3.5.8 Waste and Scrap (Subtask 390) — J. E. Van Cleve, Jr., and S. M. Tiegs

Our goal is to develop overall waste and scrap handling capabilities for the HTGR refabrication system. Experimental work during the past year has primarily concentrated on the engineering-scale perchloroethylene reclamation system. Additionally, flowsheet planning of the overall refabrication scrap recovery system has progressed substantially.

Perchloroethylene is the solvent used in the off-gas scrubber systems attached to the coating and carbonization furnaces. During scrubber operation, the perchloroethylene traps soot, tars, and various hydrocarbon compounds from the furnace off-gas streams. To maintain scrubber efficiency, the dirty perchloroethylene must be replaced by fresh solvent. The dirty perchloroethylene can be reclaimed by distillation, and thereby the volume of waste from the scrubbing operation can be reduced.

The engineering-scale perchloroethylene still has been extensively operated this year, and approximately 0.26 m^3 (70 gal) of perchloroethylene has been recovered. This operating experience indicated the need for several piping modifications to improve the transfer capabilities of the system. Therefore, a liquid transfer line and an accumulation tank were installed to permit transfer of the perchloroethylene to and from the process scrubbers without removal from the system piping.

The composition of the still bottoms, the by-product of perchloroethylene distallation, is being intensively examined. These data are required to evaluate the operation of the scrubbers, to calculate material balances for the scrubber and the still, and to define the requirements for an incinerator to dispose of the still bottoms. The bottoms consist mainly of perchloroethylene, carbon soot, and both single-ring and condensed aromatic hydrocarbons. Since a large number of the condensed aromatic hydrocarbons are known to be biologically active, the handling procedures for the perchloroethylene bottoms are complicated and stringent release limitations must be met.

The overall refabrication scrap recovery system is being evaluated to determine both the character of each scrap stream and the treatment required for its re-entry into the reprocessing and refabrication systems. Figure 3.56 presents the various flowsheet options for overall scrap recovery. Experimental work is scheduled during the next year for development of the flowsheet details.

3.5.9 Material Handling (Subtask 395) — W. R. Hamel

The objective of Subtask 395 is to verify existing and to develop new remote material handling technologies necessary to support the remote fabrication of HTGR recycle fuels. Toward this goal, work activities were planned in the development of electromechanical manipulator position control and evaluation of advanced remote television viewing.

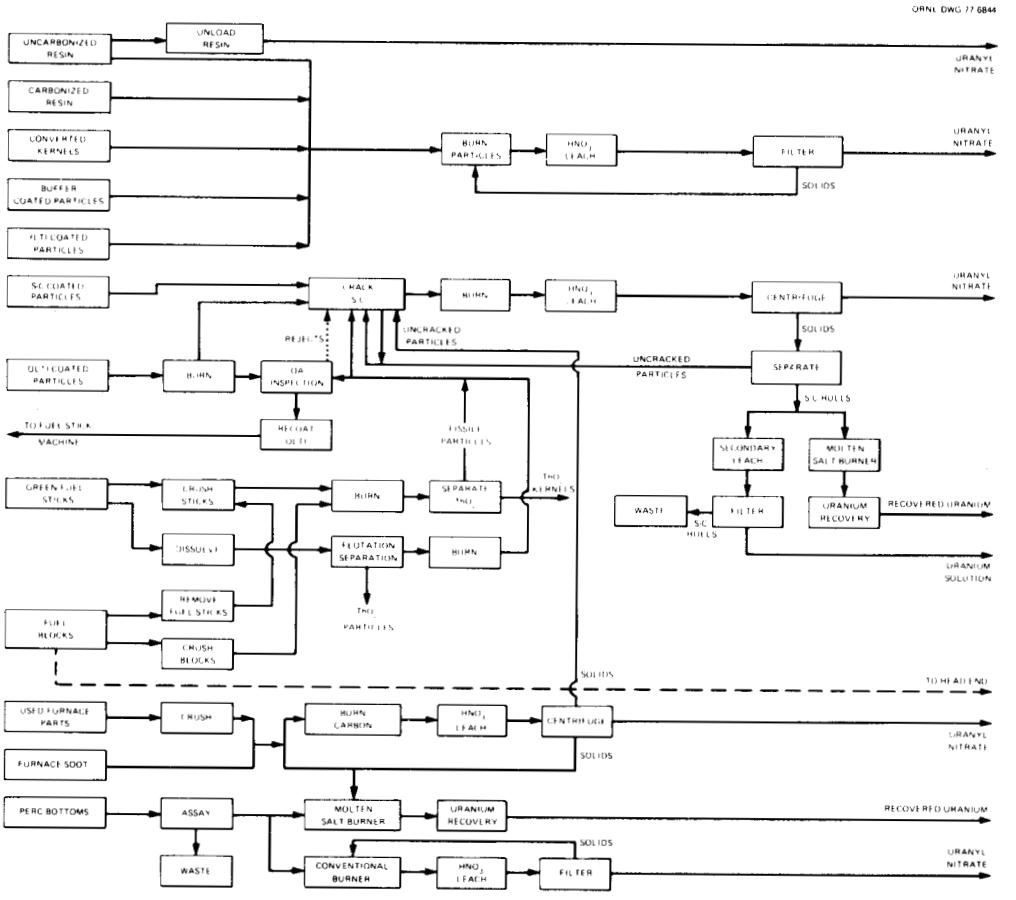

Fig. 3.56. Internal Recovery of Refabrication Scrap.

3.5.9.1 Equipment Development — J. G. Grundmann, R. C. Muller, and W. R. Hamel

During the previous reporting period[64] this subtask was initiated and activities during that period included several items worthy of reiterating. The existing TURF material handling system was studied in detail and was found to be of an adequate mechanical configuration but deficient in control functional capability and level of automation. Material handling technology was surveyed and 14 research and development facilities and 14 commercial vendors were contacted. Preliminary engineering design and testing was performed toward the implementation of master-slave control capability on the TURF cell E PaR manipulator. An advanced automated manipulator system with a level of robotic capability consistent with the operation and maintenance requirements of remote fuel refabrication equipment was conceived.

During this reporting period it was necessary to de-emphasize this subtask because of overriding project priorities. Work was principally directed toward remaining abreast of the technology.

An effort was made to coordinate these activities with other similar activities in the Laboratory. As a result, the experimental work plans in the LMFBR Fuel Reprocessing Program Remote Maintenance Task and the HTGR Fuel Refabrication Material Handling Subtask have been developed and modified to permit joint execution and attainment of objectives. Simplified boom electromechanical manipulators, heavy crane systems, and remote signal transmission techniques will be considered in addition to previously planned activities. Also, the existing TURF material handling intercell transfer system will be studied and upgraded. Cyclic performance of this key subsystem will be tested.

3.6 REFERENCES

1. R. A. Bradley and J. M. Chandler, "Recycle Fuel Specification," *Thorium Utilization Program Prog. Rep. Jan. 1, 1974—June 30, 1975,* ORNL-5128, p. 103.
2. M. S. Judd, R. A. Bradley, and A. R. Olsen, *Characterization of Effluents from a High-Temperature Gas-Cooled Reactor Fuel Refabrication Plant,* ORNL/TM-5059 (December 1975).
3. J. E. Till, *Assessment of the Radiological Impact of ^{232}U and Daughters in Recycled ^{233}U HTGR Fuel,* ORNL/TM-5049 (February 1976).
4. J. E. Till and D. C. Parzyck, "An Evaluation of Operational Exposures Which Could Result from Potential Environmental Releases of ^{232}U and Daughters," pp. 685—92 in *Operational Health Physics* (proc. Health Physics Society 9th Midyear Topical Symposium February 1976), Central Rocky Mountain Chapter, Health Physics Society, Boulder, Colo., 1976.
5. J. E. Till, "A Comparison of Environmentally Released Recycle Uranium-233 HTGR Fuel and LMFBR Plutonium Fuel," pp. 58—64 in *Radioecology and Energy Resources,* ed. by C. E. Cushines, Jr., Dowden, Hutchinson and Ross, New York, February 1976.

6. R. A. Bradley and J. E. Till, "Environmental and Safety Considerations," *Thorium Utilization Program Prog. Rep. Jan. 1, 1974–June 30, 1975*, ORNL-5128, pp. 101–03.

7. L. M. Petrie and N. F. Cross, *KENO IV — An Improved Monte Carlo Criticality Program*, ORNL-4938 (November 1975).

8. G. E. Hansen and W. H. Roach, *Six and Sixteen Group Cross Sections for Fast and Intermediate Critical Assemblies*, LAMS-2543 (1961).

9. D. Graber et al., *Data Formats and Procedures for the Evaluated Nuclear Data File, ENDF*, BNL-NCS-50496 (ENDF 102) (October 1975).

10. S. R. McNeany, "Material Accountability and Safeguards," *Thorium Utilization Program Prog. Rep. Jan. 1, 1974–June 30, 1975*, ORNL-5128, pp. 103–04.

11. J. N. Strode and H. H. Van Tuyl, *PUSHLD — A Code for Calculation of Gamma Dose Rates for Plutonium in Various Geometries*, HEDL-TME 73–89 (1974).

12. P. A. Haas, *HTGR Fuel Development: Loading of Uranium on Carboxylic Acid Cation Exchange Resins Using Solvent Extraction of Nitrate*, ORNL/TM-4955 (September 1976).

13. C. F. Baes, Jr., and R. E. Mesmer, *The Hydrolysis of Cations*, Wiley, New York, 1976, p. 174.

14. Ibid, p. 158.

15. K. J. Notz and C. W. Greene, *Loading Ion Exchange Resins with Uranium for HTGR Fuel Kernels*, ORNL/TM-5647 (in preparation).

16. P. A. Haas, *HTGR Fuel Development: Use of UO_3 to Load Cation Exchange Resin for Microsphere Preparation*, ORNL/TM-3817 (September 1972).

17. J. L. Botts, R. J. Raridon, and D. A. Costanzo, *Density, Acidity and Conductivity Measurements of Uranyl Nitrate-Nitric Acid Solutions*, ORNL-5260 (in preparation).

18. D. E. LaValle, D. A. Costanzo, W. J. Lackey, and A. J. Caputo, *The Determination of Defective Particle Fraction in HTGR Fuels*, ORNL/TM-5483 (November 1976).

19. S. D. Ruder, J. R. Delmastro, and P. C. Murillo, "Analysis of HTGR Coated Fuel Particles for Uranium and Thorium," *Anal. Chem. Branch Annual Report, October 1974*, ICP-1056, p. 78.

20. J. W. Snider, *The Design of Engineering-Scale Solex Equipment*, ORNL-4256 (April 1969).

21. P. A. Haas, *Loading a Cation Exchange Resin with Uranyl Ions*, (to U.S. Energy Research and Development Administration) U.S. Patent 3,800,023. March 26, 1974.

22. J. N. Nora et al., *Development of Optimum Conditions for Drying Ion Exchange Resin in a Fluidized Bed Dryer*, ORNL/MIT-224 (Feb. 25, 1976).

23. W. J. Lackey, W. H. Pechin, C. F. Sanders, F. C. Davis, and F. J. Furman, "Microsphere Coating," *Gas-Cooled Reactor and Thorium Utilization Programs Annu. Prog. Rep. Sept. 30, 1971*, ORNL-4760, pp. 45–52.

24. J. P. Drago and P. A. Haas, *Design and Test of a Thermosyphon Evaporator for Acid-Deficient Uranyl Nitrate*, ORNL/TM-5518 (November 1976).

25. J. H. Shaffer and G. W. Greene, unpublished results.

26. J. P. Drago and P. A. Haas, *Drying of Uranium-Loaded Cation-Exchange Resin with Microwave Heating*, ORNL/TM-5508 (November 1976).

27. J. P. Drago, P. A. Haas, and D. L. Million, "Drying of Ion-Exchange Resins for Resin-Based Preparation of Nuclear Reactor Fuels," paper presented at the 82nd National Meeting of American Institute of Chemical Engineers in Atlantic City, New Jersey, Aug. 29–Sept. 1, 1976.

28. D. R. Johnson, W. J. Lackey, and J. D. Sease, *The Effects of Processing Variables on HTGR Fuel Kernels Fabricated from Uranium-Loaded Cation-Exchange Resin*, ORNL/TM-4989 (August 1975).

29. G. W. Weber, R. L. Beatty, and V. J. Tennery, *Properties of Carbonized and Converted Uranium-Loaded Weak-Acid Resin*, ORNL-5201 (February 1977).

30. D. A. Lee, D. A. Costanzo, D. P. Stinton, J. A. Carpenter, Jr., W. T. Rainey, Jr., C. D. Canada, and J. A. Carter, *In-Line Monitoring of Effluents from HTGR Fuel Particle Preparation Processes Using a Time-of-Flight Mass Spectrometer*, ORNL/TM-5579 (August 1976).

31. W. J. Lackey, D. P. Stinton, L. E. Davis, and R. L. Beatty, "Crushing Strength of High-Temperature Gas-Cooled Reactor Fuel Particles," *Nucl. Technol.* 31: 191–201 (November 1976).

32. R. B. Pratt, J. D. Sease, W. H. Pechin, and A. L. Lotts, "Pyrolytic Carbon Coating in an Engineering-Scale System," *Nucl. Appl.* 6(3): 241–55 (March 1969).

33. R. R. Suchomel and W. J. Lackey, *Devices for Sampling HTGR Recycle Fuel Particles*, ORNL/TM-5739 (March 1977).

34. W. J. Lackey, J. D. Jenkins, and F. J. Homan, *Assessment of Coater Size for the Fuel Refabrication Prototype Plant*, ORNL/TM-4567 (July 1974).

35. W. J. Lackey, W. H. Pechin, C. F. Sanders, F. C. Davis, and D. D. Cannon, "Microsphere Coating," *Gas-Cooled Reactor Programs Annu. Prog. Rep. Dec. 31, 1972*, ORNL-4911, pp. 33–45.

36. W. J. Lackey, W. H. Pechin, F. C. Davis, M. K. Preston, and R. S. Lowrie, "Microsphere Coating," *Gas-Cooled Reactor Programs Annu. Prog. Rep. Dec. 31, 1973*, ORNL-4975, pp. 36–37.

37. W. J. Lackey and J. D. Sease, *Means for Effecting Fluidization in Pyrolytic Carbon Coating Processes* (to U.S. Energy Research and Development Administration), U.S. Patent 3,889,631. June 17, 1975.

38. W. J. Lackey, "Microsphere Coating," *Thorium Utilization Program Prog. Rep. Jan. 1, 1974–June 30, 1975*, ORNL-5128, pp. 153–58.

39. W. J. Lackey, D. P. Stinton, and J. D. Sease, *Improved Gas Distributor for Coating HTGR Fuel Particles*, ORNL/TM-5731 (January 1977).

40. D. W. Stevens, "Optical Anisotropy in Nearly Isotropic Pyrolytic Carbons," *Eleventh Biennial Conference on Carbon, Gatlinburg, Tennessee, 1973*, Paper SS-3, pp. 167–68, CONF-730601.

41. G. W. Weber, R. L. Beatty, V. J. Tennery, and W. J. Lackey, Jr., *Uranium Dispersion in Coated Weak-Acid-Resin-Derived HTGR Fuel Particles*, ORNL/TM-5133 (February 1976).

42. W. J. Lackey, J. D. Sease, D. A. Costanzo, and D. E. LaValle, "Improved Coating Process for High-Temperature Gas-Cooled Reactor Fuel," *Trans. Am. Nucl. Soc.* 22: 194–95 (November 1975).

43. J. I. Federer, *Fluidized Bed Deposition and Evaluation of Silicon Carbide Coatings on Microspheres,* ORNL/TM-5152 (January 1977).

44. D. P. Stinton and W. J. Lackey, *Effect of Deposition Conditions on the Properties of Pyrolytic SiC Coatings for High-Temperature Gas-Cooled Reactor Fuel Particles,* ORNL/TM-5743 (in press).

45. J. Holder, C.E.N., Grenoble, France, personal communication, April 1975.

46. D. R. Johnson, *Evaluation of a Blender for HTGR Fuel Particles,* ORNL/TM-5673 (to be published).

47. R. A. Bradley, J. D. Jenkins, J. E. Rushton, and M. G. Willey, "Fuel Rod Fabrication," *Gas-Cooled Reactor Programs Annu. Prog. Rep. Dec. 31, 1973,* ORNL-4975, pp. 37–45.

48. R. A. Farster, D. B. Smith, and H. O. Menlove, *Error Analysis of a ^{252}Cf Fuel-Rod-Assay System,* LA-5317 (1974).

49. J. D. Jenkins, S. R. McNeany, and J. E. Rushton, *Conceptual Design of the Special Nuclear Material Nondestructive Assay and Accountability System for the HTGR Fuel Refabrication Pilot Plant,* ORNL/TM-4917 (July 1975).

50. C. K. Bayne and D. R. Johnson, *Relationship Between Length Variations of HTGR Fuel Rod Stack Lengths and Individual Rod Lengths,* ORNL/TM-5544 (October 1976).

51. R. W. Powell, *Thermal Conductivity of Selected Materials, Nat: Bur. Stand.* 8:149 (November 1966). (Category 5 - Thermodynamic and Transport Properties.)

52. *Preliminary Safety Analysis Report for the Fort St. Vrain Reactor,* Public Service Commission of Colorado, DOCKET 50-267.

53. J. P. Moore, ORNL, unpublished data.

54. G. B. Bradshaw, N. I. Marsh, and C. F. Wallroth, *Safety Analysis Report for Fort St. Vrain Test Elements FTE-1 Through FTE-8,* GA-A13903 (Aug. 31, 1976).

55. M. J. Kania, K. R. Thoms, and T. N. Tiegs, "Irradiation Tests in the ORR," *HTGR Base-Technology Program Annu. Prog. Rep. Jan. 1, 1974–June 30, 1975,* ORNL-5108, pp. 360–95.

56. D. R. Johnson, A. J. Caputo, and W. G. Cobb, "Fuel Element Assembly," *Thorium Utilization Program Annu. Prog. Rep. Jan. 1, 1974–June 30, 1975,* ORNL-5128, pp. 191–201.

57. D. R. Johnson, P. Angelini, J. E. Rushton, S. R. McNeany, R. W. Knoll, R. A. Bradley, and R. M. DeLozier, "Fuel Rod Fabrication," *Thorium Utilization Program Prog. Rep. Jan. 1, 1974–June 30, 1975,* ORNL-5128, pp. 176–90.

58. A. J. Caputo, D. R. Johnson, and C. K. Bayne, *Argon Permeability of Graphite Fuel Elements for the High-Temperature Gas-Cooled Reactor* (in preparation).

59. H.P.G. Darcy, *Les Fontaines Publique de la Ville de Dijon,* Victor Dalment, Paris, 1856.

60. P. C. Carman, *Flow of Gases Through Porous Media,* Academic Press, London, 1956.

61. W. P. Eatherly et al., "Physical Properties of Graphite Materials for Special Nuclear Applications," Vol. 7, pp. 389–401 in *U.N. Intern. Conf. Peaceful Uses At. Energy, 2nd Geneva, 1958.* United Nations, New York, 1958.

62. M. S. Judd, J. E. Van Cleve, Jr., and W. T. Rainey, Jr. *Recovery of Perchloroethylene Scrubbing Medium Generated in the Refabrication of High-Temperature Gas-Cooled Reactor Fuel,* ORNL/TM-5620 (November 1976).

63. J. E. Mack, "Particle Size Analyzer," *Thorium Utilization Program Prog. Rep. Jan. 1, 1974–June 30, 1975,* ORNL-5128, pp. 202–3.

64. W. R. Hamel, J. G. Grundmann, and R. C. Muller, "Material Handling," *Thorium Utilization Program Prog. Rep. Jan. 1, 1974–June 30, 1975,* ORNL-5128, pp. 216–20.

4. WASTE TREATMENT DEVELOPMENT (TASK 400)

K. J. Notz

4.1 INTRODUCTION

The objective of this task is to develop the necessary technology to convert HTGR source wastes into a form suitable for terminal storage and/or disposal. Wherever possible, processes and techniques developed (or being developed) for LWR source wastes will be utilized, either directly or with the necessary modifications. There will, however, be some wastes unique to HTGR for which specific methods will need to be developed. This task is presently funded at a low level, in accordance with schedular requirements. The major effort at this time is in identifying needs and establishing a working liaison with LWR development projects. In addition, some process and hardware research and development have been done on $^{14}CO_2$ fixation.

The lead contractor for this task is INEL, and we anticipate that it will do some of the specific required research and development with portions assigned to ORNL and to GA. Because of ORNL's overall technical responsibility for the thorium utilization program, we have made a significant effort at characterization of HTGR source wastes and will continue this type activity in the future, but at a reduced level. The present organization of this task is in terms of these subtasks:

Subtask 401 — Task Management and Coordination
Subtask 405 — Reprocessing: Gaseous Source Wastes
Subtask 410 — Reprocessing: Miscellaneous High-Level Solid Wastes
Subtask 415 — Reprocessing: Miscellaneous Low- to Intermediate Level Solid Wastes
Subtask 420 — Reprocessing: High-Level Liquid Wastes
Subtask 425 — Reprocessing: Low- and Intermediate-Level Liquid Wastes
Subtask 430 — Refabrication: Solid Wastes
Subtask 435 — Refabrication: Liquid Wastes
Subtask 440 — Waste Packaging

Subtask 445 — On-Site Storage Facilities
Subtask 450 — Transportation Equipment
Subtask 455 — HETF Wastes

Formerly, this task was more simply organized into two subtasks, one each on reprocessing wastes and refabrication wastes, which is the format for the following sections.

4.2 REPROCESSING WASTES (Formerly Subtask 410) — K. H. Lin

4.2.1 Characterization Study of Reprocessing Wastes — K. H. Lin

A topical report[1] presents the results of the paper study to identify and characterize major waste streams. In continuation of the characterization study, properties of four selected waste streams [retired 25W fissile particles, SiC hulls, high-level liquid wastes (HLLW), and thorium nitrate solution] were estimated as a function of cooling time. The data thus obtained were utilized in the evaluation of various waste processing alternatives described in the next section. The highlights of the calculated results listed in Table 4.1 indicate that fission products initially (i.e., 180 days after discharge from the reactor) account for most (>80%) of the radioactivity and the decay heat in all four streams. This trend persists for SiC hulls and HLLW even after a prolonged cooling time (i.e., eight years). However, for retired fissile particles and thorium nitrate solution the differences in the radioactivity and the rate of heat generation between the fission products and the actinides become less pronounced as the cooling time is extended. Thus, after five to eight years of cooling, the values of these properties are of the same orders of magnitudes for both types of nuclides. In all cases (four waste streams), the initial (180-day) values of total radioactivity and total heat generation rate are reduced by factors of about 4 to 10 by the end of the eight-year cooling period.

Table 4.1. Variation in Characteristics of Selected Waste Streams with Cooling Time (Summary)[a]

Waste Stream	Approx. Quantity	Nuclide Types	Specific Radioactivity (Ci/Unit Quantity) for Each Time after Discharge from Reactor			Rate of Heat Generation (W/Unit Quantity) for Each Time after Discharge from Reactor		
			180 days	5 years	8 years	180 days	5 years	8 years
Retired Fissile Particles (25W)	4 Metric Tons (100 ft^3)	Fission Products	6.23(5)/ft^3	1.25(5)/ft^3	9.84(4)/ft^3	304(3)/ft^3	520/ft^3	350/ft^3
		Actinides	2.92(4)/ft^3	2.49(4)/ft^3	2.34(4)/ft^3	660/ft^3	570/ft^3	555/ft^3
		Total	6.52(5)/ft^3	1.50(5)/ft^3	1.22(5)/ft^3	3.70(3)/ft^3	1.90(3)/ft^3	905/ft^3
SiC Hulls	20 Metric Tons (235 ft^3)	Fission Products	2.97(5)/ft^3	7.00(4)/ft^3	5.59(4)/ft^3	1.45(3)/ft^3	290/ft^3	205/ft^3
		Actinides	18/ft^3	16/ft^3	15/ft^3	∿0	∿0	∿0
		Total	2.97(5)/ft^3	7.00(4)/ft^3	5.59(4)/ft^3	1.45(3)ft^3	290/ft^3	205/ft^3
High-Level Liquid Wastes (HLLW)	2×10^5 gal	Fission Products	7.12(3)/gal	1.00(3)/gal	990/gal	33/gal	4.9/gal	3.5/gal
		Actinides	470/gal	17/gal	16/gal	1/gal	0.4/gal	0.4/gal
		Total	7.59(3)/gal	1.02(3)/gal	1.01(3)/gal	34/gal	5.3/gal	3.9/gal
Thorium Nitrate Solution	5×10^4 gal	Fission Products	44/gal	4/gal	3.2/gal	0.2/gal	0.0/gal	0.0/gal
		Actinides	1/gal	2.2/gal	2.4/gal	0.0/gal	0.1/gal	0.1/gal
		Total	45/gal	6.2/gal	5.6/gal	0.2/gal	0.1/gal	0.1/gal

[a] 1 ft^3 = 0.0283 m^3, 1 gal = 0.003785 m^3, 1 Ci = 3.7×10^{10} Bq. Numbers in parentheses indicate multiplication by 10 to the indicated power.

4.2.2 Evaluation of Waste Processing Alternatives — K. H. Lin

The major objectives of this phase of the study are: (1) to critically review and evaluate available information related to treatment and processing of waste streams from HTGR fuel reprocessing, (2) to identify the existing data and development work that are applicable to the HTGR wastes with little or no modification, and (3) to define the development needs for wastes that are unique to HTGR.

To achieve successful closure of the HTGR fuel cycle, technologies must be developed for processing of individual waste streams that have already been identified.[1] The overall schematic flow diagram depicted in Fig. 4.1 illustrates the sources and types of waste streams as well as potential waste processing schemes. Some of the primary wastes (e.g., off-gas from the head-end system and from combustible wastes) may be released to the environment after treatment to reduce the radionuclide contents to below the levels required by applicable regulations and standards. The secondary wastes from such treatments and other types of primary wastes must then be converted to forms acceptable for handling, transportation, and ultimate isolation from the biosphere. Many of the alternatives being developed for processing of the LWR wastes are adaptable to the HTGR case. This is especially true of the wastes from the solvent extraction system. However, wastes from the HTGR head-end system are unique, and special methods must be developed for processing them.

4.2.2.1 Factors Affecting Selection of Processing Alternatives

Selection of suitable methods for treatment and/or conversion of different wastes is governed by a number of factors. Among these are: (1) waste type, (2) technical and economic feasibility of the process, (3) Federal and local regulations and standards pertaining to the effluents discharged to the environment, and (4) Federal regulations that specify the final waste form for shipment to the isolation repository. Factors (3) and (4) for wastes from the back end of the nuclear fuel cycle have not yet been fully defined.

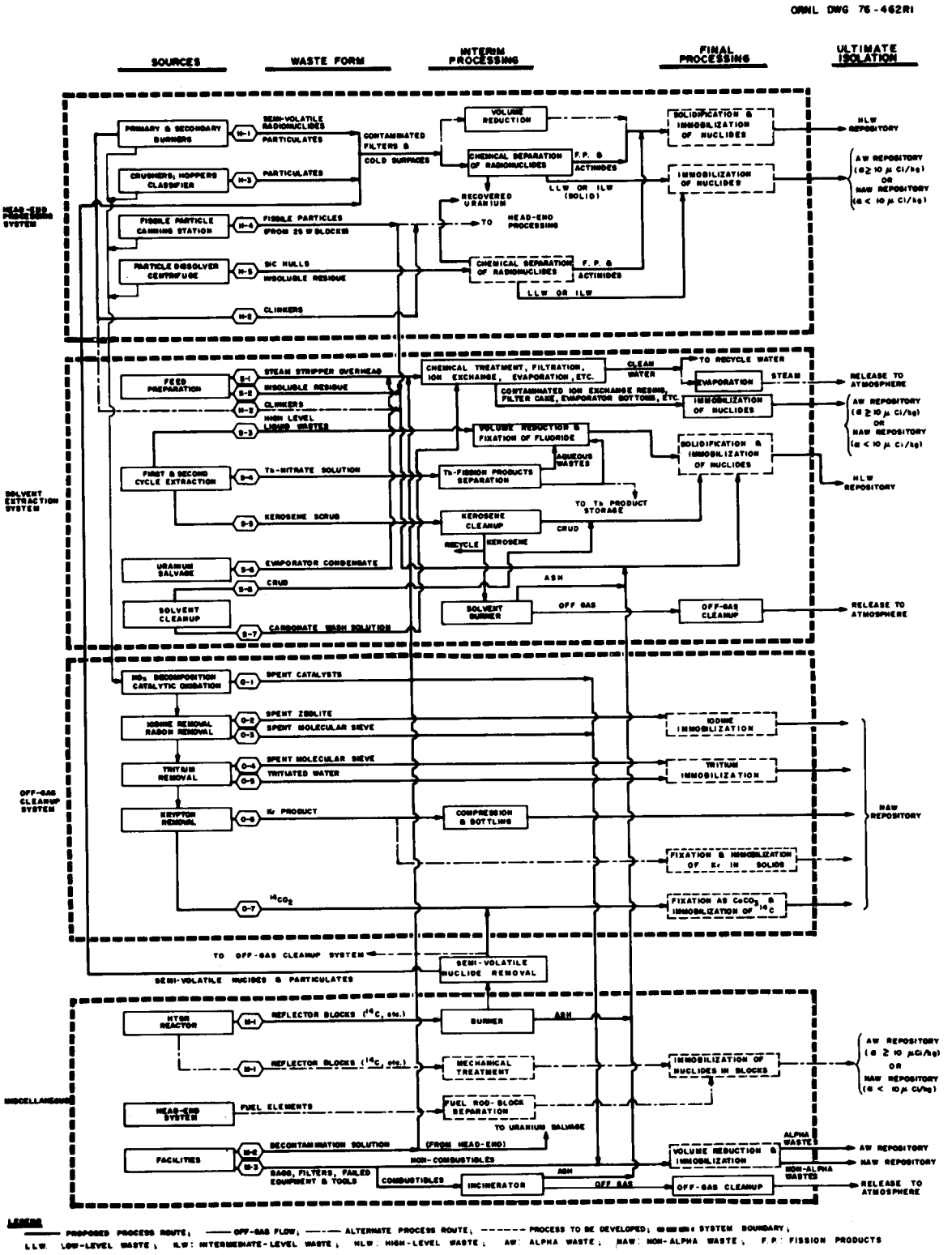

Fig. 4.1. Overall Schematic Flow Diagram for Processing and Isolation of HTGR Fuel Reprocessing Wastes.

4.2.2.2 General Criteria for Evaluation of Processing Alternatives

Published technical data and existing technologies, including those being developed for the LWR fuel cycle, were critically reviewed to identify information that may be utilized in the development of processing alternatives for HTGR wastes. The criteria listed below were used as the basis in the evaluation of potential alternatives. They also served as the guideline in defining the development needs for processing wastes that are unique to the HTGR fuel cycle:

1. the process must be able to convert the waste into a form that can assure long-term safety in the isolation repository;
2. process and equipment should be simple;
3. the process should be relatively insensitive to the waste composition;
4. the process should generate little or no secondary waste streams;
5. the number of interim waste treatment steps should be minimized and different waste streams combined whenever possible;
6. the process should use easily maintained equipment.

This evaluation will be published as a topical report.[2]

4.2.3 Evaluation of Options for the Disposal of ^{14}C-Contaminated CO_2 as $CaCO_3$ — A. G. Croff

A completion report on this study was issued.[3] The abstract follows:

> A paper study was conducted to determine the best method for fixing the ^{14}C-contaminated CO_2 resulting from an HTGR fuel block burner as $CaCO_3$, and to determine the best methods for disposing of the $CaCO_3$ thus produced. The fixation method selected was the direct reaction of a $Ca(OH)_2$ slurry with the CO_2. The least expensive disposal options which are likely to be acceptable appear to be the shallow-land burial of either drummed $CaCO_3$ solid (total cost = \$18.47/kg heavy metal) or drummed $CaCO_3$ concreted with cement (total cost = \$43.33/kg heavy metal). Neither placing the CO_2 fixation process before the Kr removal process nor separating the bulk of the graphite fuel block from the fuel particles is attractive on both technical and economic grounds. However, reduction of the HTGR fuel nitrogen content appears to be a more attractive method of reducing the ^{14}C release rate.

4.2.4 Fixation of $^{14}CO_2$ as $CaCO_3$ — D. W. Holladay

Based on the paper evaluation[3] described in the Sect. 4.2.3, the process of choice for converting ^{14}C-contaminated CO_2 to $CaCO_3$ is direct reaction with $Ca(OH)_2$ in aqueous suspension. Although this process is well-known, existing industry experience is keyed to the production of pigment-grade $CaCO_3$, and complete CO_2 utilization is not a requirement. For our needs, the precipitate needs to be amenable to handling as a waste, and CO_2 conversion should be essentially complete. Therefore, this bench-scale study was done.

The reaction of CO_2 with slaked lime in a stirred tank reactor was studied to determine the decontamination factor (DF) and the mass transfer coefficient as functions of agitator speed, gas composition, gas flow rate, temperature, and $Ca(OH)_2$ concentration. The rate of the reaction was found to be liquid phase controlled; the pH of the slurry remained high and constant even at very high gas feed rates, indicating that the slaked lime dissolved very rapidly. The utilization of the $Ca(OH)_2$ is nearly complete, as indicated by a sharp drop in pH when the conversion to $CaCO_3$ is complete. Virtually complete reaction of 100% CO_2 feed gas occurred at flow rates up to 10 liters/min at 20°C, 1 atm into a stirred reactor (at an agitator speed of 800 rpm) containing 6.7 liters of 1 *M* $Ca(OH)_2$. For feed gas containing 90% CO_2 and 10% O_2 the DF was 3600 at a gas flow rate of 3 liters/min. The mass transfer coefficient increased in proportion to agitator speed from 12.3×10^{-5} gmole/cm^3·sec·atm at 800 rpm to 23.9×10^{-5} gmole/cm^3·sec·atm at 1700 rpm. The impurities in slaked lime from commercial sources [~85% $Ca(OH)_2$] had negligible effects on the rate of the CO_2-$Ca(OH)_2$ reaction.

The settling rate of the $CaCO_3$ product was measured to provide a qualitative indication of particle size for estimating separation of it from the reacting mixture. The settling time, as measured by the time required for the $CaCO_3$ product to settle to about 40% of the initial height of the reacting mixture, ranged from 14 to 200 min. The settling rate increased as gas flow was decreased, as agitator speed was increased, and as temperature was increased.

4.3 REFABRICATION WASTES (Formerly Subtask 420)

4.3.1 Characterization Study of Refabrication Wastes — J. E. Van Cleve, Jr.

The waste characterization work has continued with the emphasis on further refinement of the data previously obtained. The characteristics of the waste streams have not materially changed. However, the treatment schemes have been further defined. Two areas requiring further development work will be described, and additional areas will undoubtedly be recognized in the ensuing work.

The uranium-loaded fuel particles release ^{220}Rn during resin carbonization and through the application of the buffer and inner low-temperature isotropic carbon coatings. This radon may be trapped out of the off-gas stream by use of molecular sieves; however, the trapping efficiency of the molecular sieves is lowered by the presence of other contaminants in the stream. In both cases just mentioned the off-gas stream will contain perchloroethylene vapors originating from the scrubbers used to remove carbon, soot, and pyrolsis products. We are presently using a demister and a heat exchanger to minimize perchloroethylene vapors but do not know how efficiently these units are working. An experiment should be performed to determine the maximum concentration of perchloroethylene vapors that can be in the off-gas stream without deleterious effects on the radon trapping medium. This experiment was originally scheduled to be performed by Allied Chemical Co.; however, funding restrictions preclude doing the work.

The operation of carbonization, coating, and whole-block annealing furnaces produces noxious off-gases, which are presently being cleaned by a perchloroethylene scrubber. We have developed a distillation procedure to clean and recycle approximately 80% of the perchloroethylene to the scrubbers; however, the remaining 20%, as still bottoms, presents a unique waste stream. This material contains large amounts of carbon, soot, and the pyrolysis products produced by the coating gases. The bottoms have been burned in a crude burner to demonstrate their

combustibility. Several types of incinerators are being evaluated, in a paper study, to determine a type that might burn the bottoms with little or no attendant clean-up before atmosphere release.

4.4 REFERENCES

1. K. H. Lin, *Characteristics of Radioactive Waste Streams Generated in HTGR Fuel Reprocessing*, ORNL/TM-5096 (January 1976).
2. K. H. Lin, *Process Alternatives for HTGR Fuel Reprocessing Wastes — An Engineering Evaluation*, ORNL/TM-5823 (in preparation).
3. A. G. Croff, *An Evaluation of Options Relative to the Fixation and Disposal of* ^{14}C*-Contaminated* CO_2 *as* $CaCO_3$, ORNL/TM-5171 (April 1976).

5. FUELS IRRADIATION AND EXAMINATION

T. N. Tiegs

5.1 INTRODUCTION

The objective of the fuels irradiation and examination task is to verify the performance reliability of recycle fuel produced in the various development stages of the refabrication development (Task 300). This includes testing of fuel under accelerated and real-time conditions. The HTGR fuel irradiation experiments have traditionally been accomplished in two phases. The HFIR Target (HT) series of experiments is used to screen potential fuel and fuel rod matrix designs and identify poor performers. Successful designs are translated into prototype fuels and matrices and irradiated in the instrumented facilities in the HFIR Removable Beryllium (HRB) facilities and in the ORR. Because of the accelerated irradiation conditions, full HTGR burnups and fast fluences are achieved in relatively short periods of time: about 4 months in the HT facility, about a year in the HRB facility, and about 1.5 years in the ORR facility. State-of-the-art materials and processes derived from the above accelerated tests are then tested under real-time HTGR conditions in the Peach Bottom Reactor (now out of operation) and the Fort St. Vrain Reactor (just beginning operation).

It has always been recognized that many parallel activities are involved in the development of fresh and recycle fuel, and in fact the same personnel and irradiation facilities at ORNL are used in both the Thorium Utilization (ThU) and HTGR Base Programs. Therefore some of the irradiation tests are jointly funded. All work supported solely by the ThU program will be reported in this annual report, while work funded by both the Base Program and the ThU Program will be reported elsewhere.[1]

Task 500 is divided into the following subtasks, which are in logical sequence for conducting irradiation tests.

1. Subtask 510 — Planning and Experimental Design
2. Subtask 520 — Test Element Assembly

3. Subtask 530 — Irradiation
4. Subtask 540 — Postirradiation Examination
5. Subtask 550 — Data Analysis and Reporting

Under each subtask are work units, which correspond to the various development stages of the refabrication task (Task 300), which are explained in Chap. 3.

Three series of irradiation tests are funded under the ThU Program (in part or in whole): Peach Bottom irradiations, ORR irradiations, and FSVR Early Validation Tests. Each tests a fuel product from a different fuel refabrication development stage and all are presently at different levels of the irradiation testing sequence.

5.2 PEACH BOTTOM IRRADIATIONS

Seven Recycle Test Elements (RTE) have been irradiated in the Peach Bottom Reactor. Four elements were examined and reported previously.[2—4] Progress on the postirradiation examination of the remaining RTEs is reported below. This work was completed during this reporting period. The RTE series tested the fuel product from the cold laboratory development of Task 300.

While postirradiation examination of the Peach Bottom elements is complete, data analysis will continue through FY 1977. Many of the performance characteristics noted depend highly on temperature and temperature gradient. The thermal analysis for all seven elements is being performed under contract with General Atomic Company (GA) and is scheduled for completion by mid-1977. A final report for the Recycle Test Element series is scheduled for completion in September 1977.

5.2.1 Postirradiation Examination of RTE-6 — T. N. Tiegs, E. L. Long, Jr., and E. L. Ryan

The fifth in a series of seven recycle elements, RTE-6, was shipped from the Peach Bottom Reactor site to ORNL in June 1975. This element resided in the reactor until operations ceased on October 31, 1974, and accumulated 897.4 equivalent full-power days. The fuel rods used in this element are shown in Table 5.1. The overall appearance of the

element was normal, with no unusual or unexpected features. The fission-product trap and end fittings were cut off and the six fuel bodies removed from the graphite sleeve. Dimensional measurements taken on graphite components of the fuel element include the sleeve, fuel bodies, and fuel rods. The results were compiled and forwarded to GA for incorporation in the detailed thermal analysis for the RTE series.

Table 5.1. Fuel Loading Scheme for RTE-6

Body	Fuel Type[a]	Medium Carbonized in	Fuel Particle Type	
			Fissile	Fertile
6	g	Packed Al_2O_3	UO_2 Biso	ThO_2 Biso
5	f	Fuel body	UC_2 Triso	ThC_2 Biso
4	f	Fuel body	UC_2 Triso	ThC_2 Biso
3	d	Packed Al_2O_3	$(2Th,U)O_2$ Biso	ThC_2 Biso
2	f	Fuel body	UC_2 Triso	ThC_2 Biso
1	e	Fuel body	UC_2 Biso	ThC_2 Biso

[a]The fuel types for all seven Recycle Test Elements are identified in a report by E. L. Long, Jr., R. B. Fitts, and F. J. Homan, *Fabrication of ORNL Fuel Irradiated in the Peach Bottom Reactor and Postirradiation Examination of Recycle Test Elements 7 and 4*, ORNL/TM-4477 (September 1974).

Fuel rods were removed from holes 1, 5, and 7 in bodies 1, 2, 4, 5, and 6 and holes 1, 3, 5, and 7 in body 3. As has been the experience with the previous recycle test elements, the fuel rods that had been carbonized in the graphite bodies (bodies 1, 2, 4, and 5) were more difficult to remove than those carbonized before being loaded in the graphite bodies (bodies 3 and 6). The rods appeared to be in good condition except some particles on the surface incurred abrasion damage during removal from the fuel bodies.

Fuel was selected from the highest temperature region of each of the fuel bodies and submitted for metallographic examination. The results of these examinations are summarized below.

Body 1 — The Biso-coated UC_2 particles appeared in good condition (Fig. 5.1), with no broken coatings observed. The Biso-coated ThC_2 particles were in good condition, with no amoeba effect observed.

Body 2 — The Triso-coated UC_2 particles appeared in fair condition with some graphitization of the inner LTI (low-temperature-deposited isotropic carbon coating). Approximately 10% of the particles observed had broken outer LTIs caused by fast-neutron-induced shrinkage (Fig. 5.2). This type of observation has been made previously.[4] The Biso-coated ThC_2 particles were in good condition, with no amoeba affect observed.

Body 3 — The Biso-coated $(2Th,U)O_2$ particles and ThC_2 particles looked in good condition, with no amoeba effect observed (Fig. 5.3). No failed particles were noted, although many had faceted coatings.

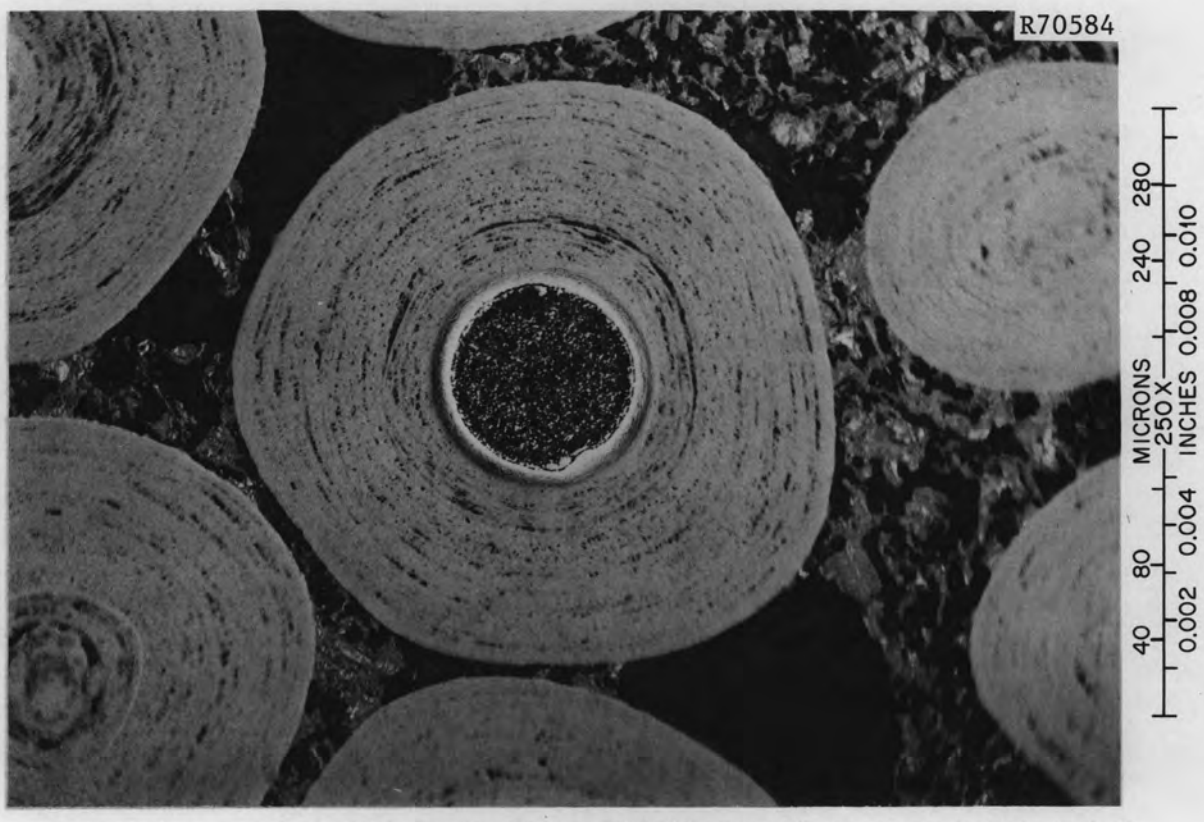

Fig. 5.1. Typical Biso-Coated UC_2 Fissile Particle from RTE-6-1-1-5.

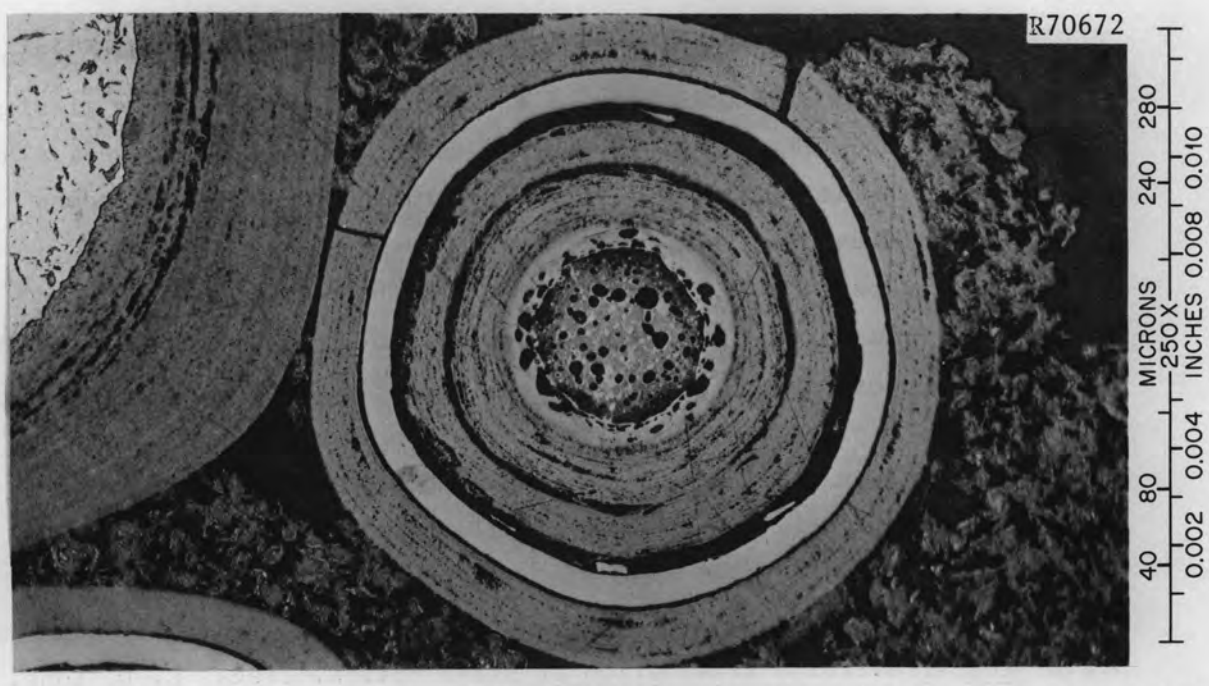

Fig. 5.2. Typical Triso-Coated UC_2 Fissile Particle from RTE-6-2-7-6. The failed outer LTI is a result of fast-neutron damage.

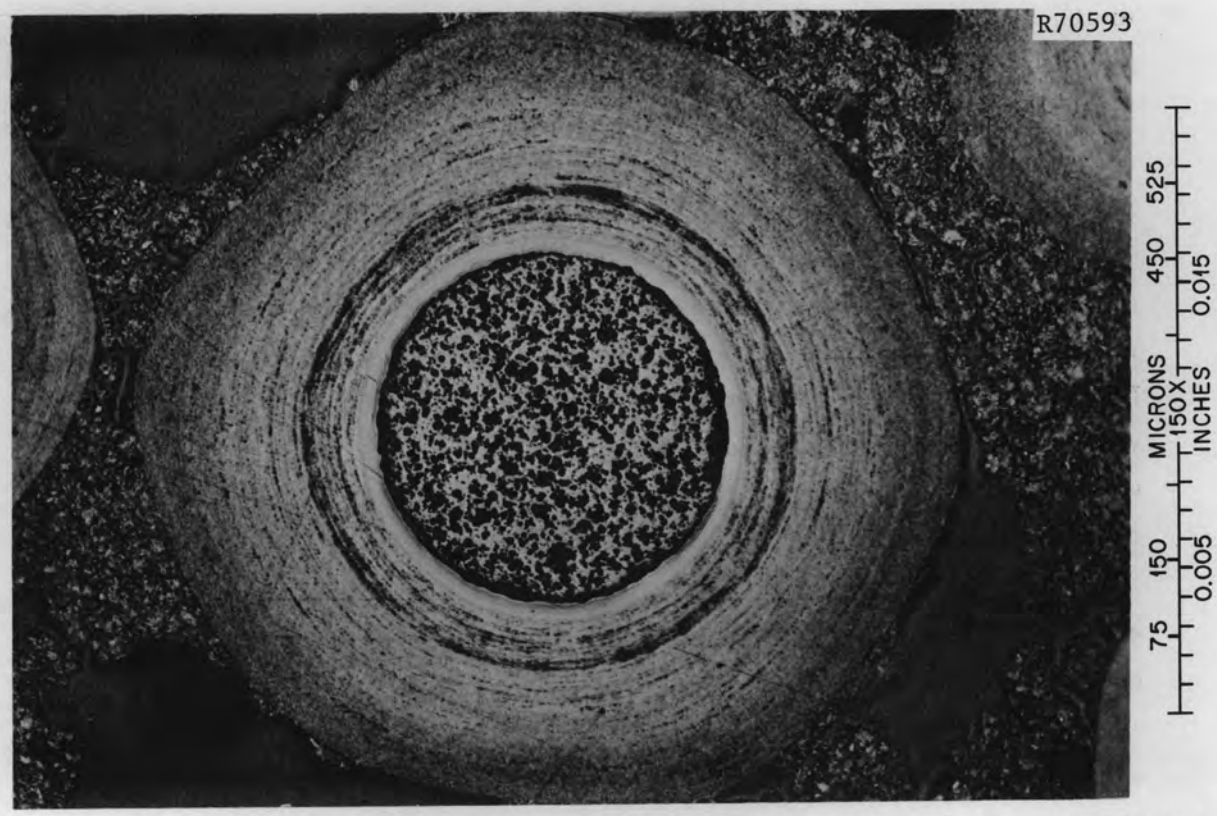

Fig. 5.3. Typical Biso-Coated $(2Th,U)O_2$ Fissile Particle from RTE-6-3-1-6.

Body 4 — Most Triso-coated UC_2 particles (>90%) showed graphitization of the inner LTI on the cold side of the particle with evidence of slight attack of the SiC (Fig. 5.4). No broken outer LTIs were observed. The Biso-coated fissile particles were in good condition, with no amoeba effect or failures observed.

Body 5 — Observations were identical to those from body 4.

Body 6 — Amoeba effect was observed in many Biso-coated UO_2 particles (<25 μm). Approximately 4% of the fissile particles had failed coatings. Two minor cases of matrix-particle interaction were observed. The Biso-coated ThO_2 particles were in good condition, with no failures or amoeba effect noted. A typical fissile particle from body 6 is shown in Fig. 5.5.

5.2.2 Postirradiation Examination of RTE-5 — T. N. Tiegs, E. L. Long, Jr., and E. L. Ryan

This was the sixth recycle test element to be examined in the series of seven. The element resided in the Peach Bottom Reactor until operations ceased on October 31, 1974 and accumulated 897.4 equivalent full-power days. Table 5.2 identifies the types of fuel in RTE-5. In addition, 12 fuel samples made from six types of graphite filler were located in the spine positions in bodies 2 and 4. Table 5.3 shows the types of graphite fillers and fuel used in the spine samples.

The overall appearance of the element was normal, with no unusual or unexpected features. The fission product trap and end fittings were cut off and the six fuel bodies removed from the graphite sleeve. Dimensional measurements taken on graphite components of the fuel element include the sleeve, fuel bodies, and fuel rods. The results were compiled and forwarded to GA for incorporation in the detailed thermal analysis for the RTE series.

Fuel rods were removed from all holes in body 3 and holes 1, 3, 5, and 7 in bodies 1, 2, 4, 5, and 6. The rods were in generally good condition with some debonding.

Fuel was selected from the fuel bodies for metallographic examination to cover all fuel types. Bodies 1, 2, 3, and 4 contained the same fuel types, so of these only fuel from body 3 was examined

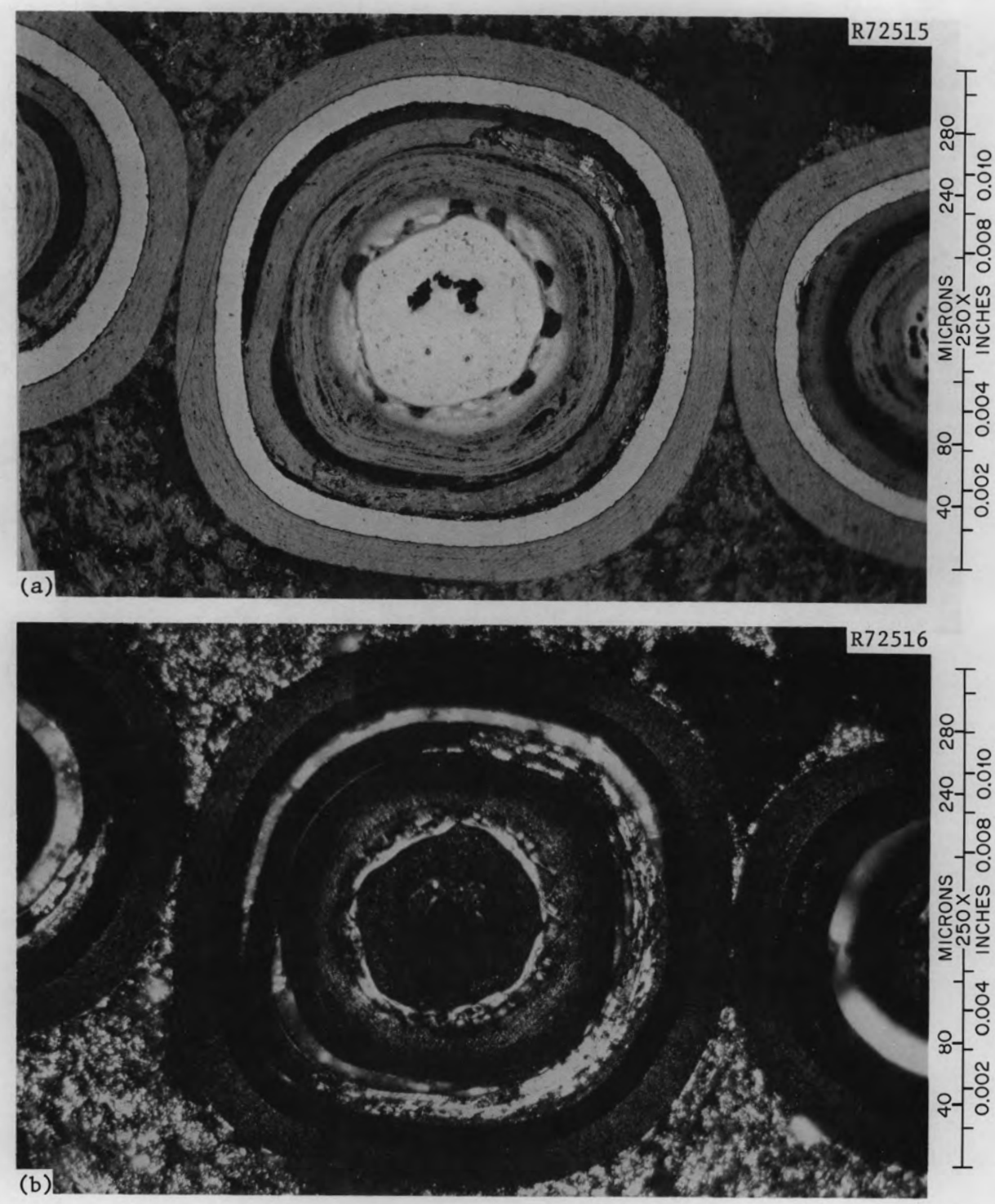

Fig. 5.4. Typical Triso-Coated UC_2 Fissile Particle from RTE-6-4-1-1. (a) Bright field. (b) Polarized light. The cold side of the particle is on the right. Optical anisotropy apparent under polarized light is a result of graphitization of the inner LTI.

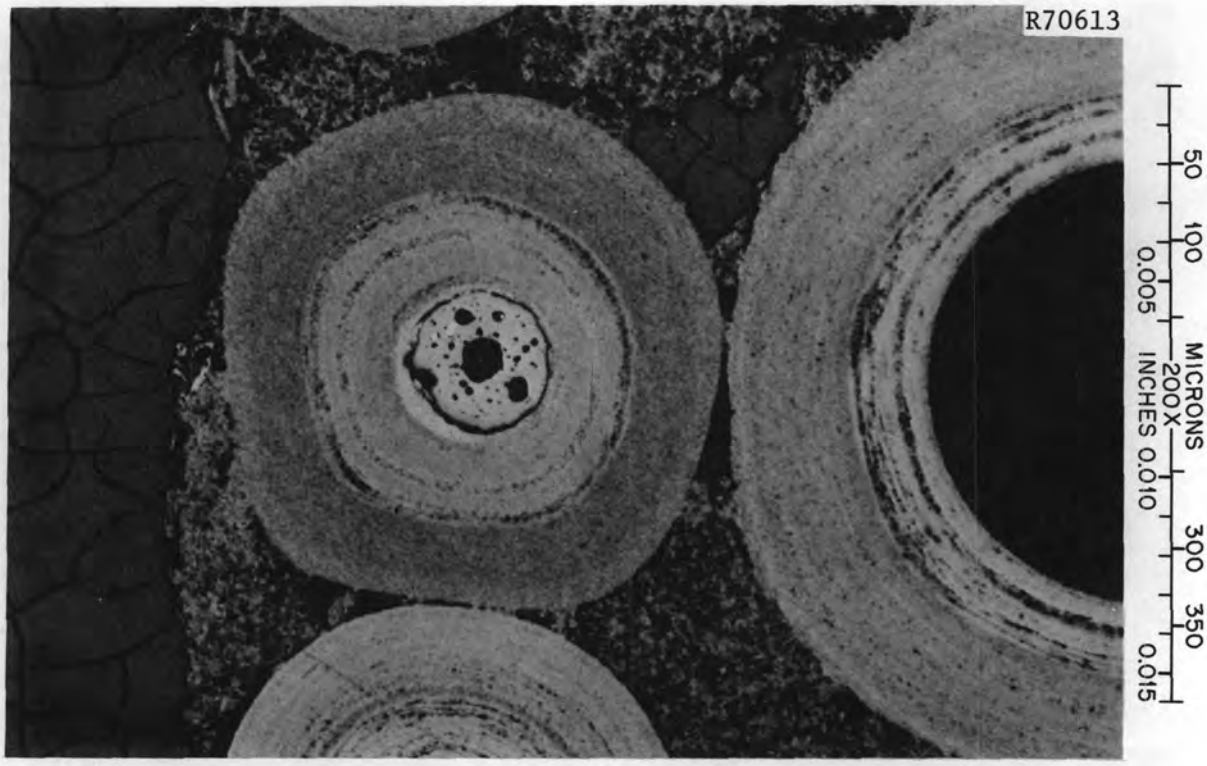

Fig. 5.5. Typical Biso-Coated UO_2 Fissile Particle from the Outer Edge of RTE-6-6-1-1. Note migration (∿10 μm) of kernel towards rod center.

Table 5.2. Fuel Loading Scheme for RTE-5

			Fuel Particle Type	
Body	Holes	Type[a]	Fuel Particle Type	
			Fissile	Fertile
6	1, 2	b	UO_2 Biso	ThC_2 Biso
	3, 4	d	$(2Th,U)O_2$ Biso	ThC_2 Biso
	5, 6	e	UC_2 Biso	ThC_2 Biso
	7, 8	i	UC_2 Triso	ThC_2 Triso
5	1, 2	b	UO_2 Biso	ThC_2 Biso
	3, 4	e	UC_2 Biso	ThC_2 Biso
	5, 6	h	UC_2 Biso	ThO_2 Biso
	7, 8	d	$(2Th,U)O_2$ Biso	ThC_2 Biso
4, 3	1, 2	a	$(4Th,U)O_2$ Biso	ThC_2 Biso
2, and 1	3, 4	c	$(2Th,U)O_2$ Biso	ThO_2 Biso
	5, 6	f	UC_2 Triso	ThC_2 Biso
	7, 8	g	UO_2 Biso	ThO_2 Biso

[a]The fuel types for all seven Recycle Test Elements are identified in a report by E. L. Long, Jr., R. B. Fitts, and F. J. Homan, *Fabrication of ORNL Fuel Irradiated in the Peach Bottom Reactor and Postirradiation Examination of Recycle Test Elements 7 and 4*, ORNL/TM-4477 (September 1974).

Table 5.3. Bonding Materials Selected for Irradiation Testing in RTE-5[a]

Sample	Matrix Filler	
	Content (%)	Material
1A, 1B	35	<40 μm JOZ Graphite
2A, 2B	50	Thermax Carbon Black
3A, 3B	40	<27 μm Robinson Graphite
4A, 4C	35	<27 μm Poco Graphite
5A, 5C	40	<40 μm Santa Maria Graphite
6A, 6B	35	<40 μm Asbury Graphite

[a]All kernels are Biso-coated fissile UO_2 or fertile ThO_2.

metallographically. The graphite filler samples were also examined metallographically. The results of these examinations are summarized below.

Body 3 — The Biso-coated $(4Th,U)O_2$ particles appeared in good condition with no failures or observable amoeba effect (Fig. 5.6). The Biso-coated $(2Th,U)O_2$ particles were observed to be in good condition, with no failures. Slight amoeba effect (<5 μm) was seen in some particles. Typical fissile particles were very similar to those shown in Fig. 5.3 from RTE-6. The Biso-coated ThO_2 particles were in good condition, with no failures or amoeba effect. One case of matrix-particle interaction was observed.

The Triso-coated UC_2 particles appeared in fair condition, with graphitization of the inner LTI on virtually every particle. Approximately 5% of the particles observed had broken outer LTIs caused by fast-neutron-induced shrinkage.[4] Typical fissile particles were very similar to those shown in Fig. 5.4. The Biso-coated ThC_2 fertile particles appeared in good condition with no failures or amoeba effect.

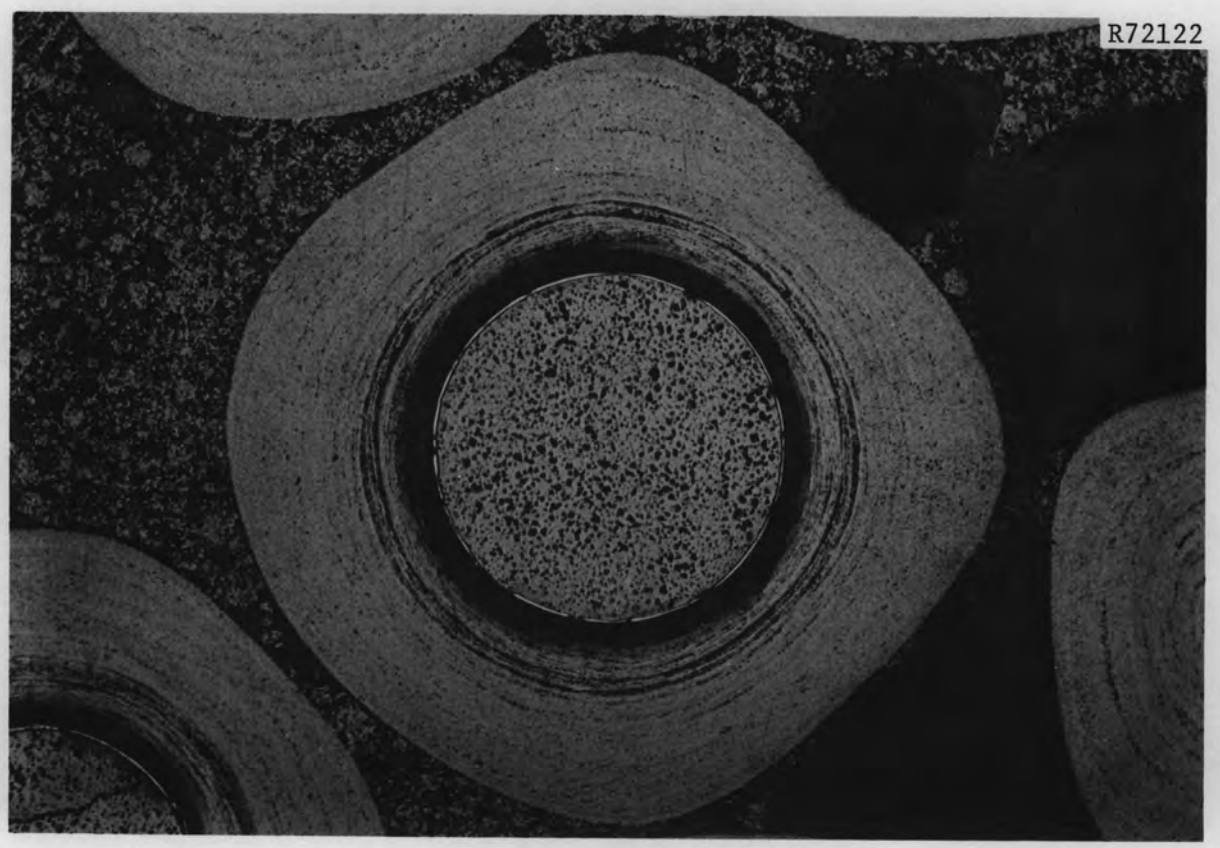

Fig. 5.6. Typical Biso-Coated $(4Th,U)O_2$ Fissile Particle from RTE-5-3-1-6. 125×.

The Biso-coated UO_2 particles were in poor condition. Amoeba type migration through the buffer coatings was very apparent on more than 50% of the particles observed. Typical fissile particles were very similar to those shown in Fig. 5.5. The ThO_2 fertile particles appeared in good condition with no failures or amoeba effect.

Body 5 — The Biso-coated UO_2 particles were in poor condition, with amoeba migration through the buffer in virtually every particle (Fig. 5.7). The kernels appeared to be broken up into separate parts and amoeba effect was observed in all directions. The Biso-coated ThC_2 particles looked to be in good condition, with no failures or amoeba effect.

The Biso-coated UC_2 particles appeared in good condition with no broken outer LTIs. Typical fissile particles were very similar to those shown in Fig. 5.1. Slight amoeba (<5 μm) was observed in the

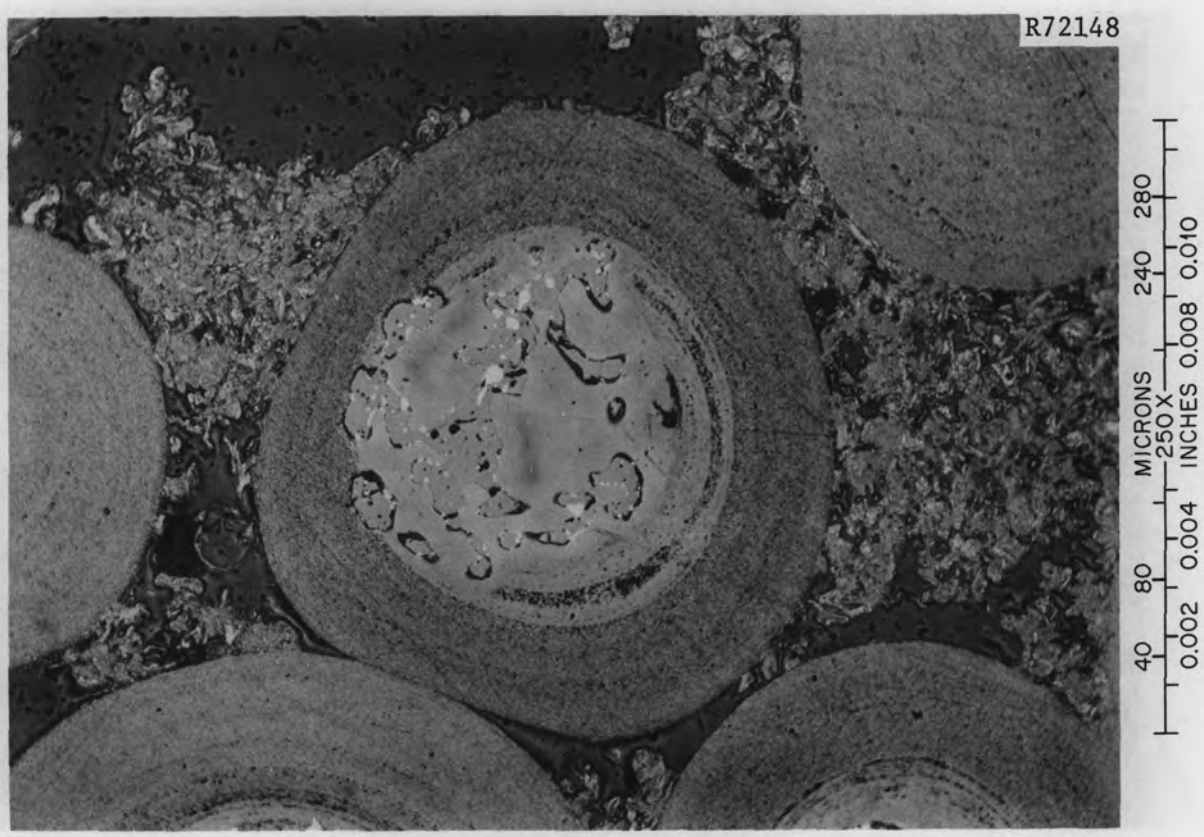

Fig. 5.7. Typical Biso-Coated UO_2 Fissile Particle from RTE-5-5-1-1.

Biso-coated ThC_2 fertile particles. The observations on the Biso-coated $(2Th,U)O_2$ particles were the same as on those from body 3.

Body 6 — The Triso-coated UC_2 particles appeared in fair condition, with some graphitization of the inner LTI. Approximately 20% of the particles observed had broken outer LTIs similar to those from body 3. The buffers separated from the inner LTI and densified around the kernel of nearly all the Triso-coated ThC_2 particles. The outer LTIs on approximately 25% of the fertile particles had failed from fast neutron damage. A typical fertile particle is shown in Fig. 5.8. Typical fissile particles were very similar to those shown in Fig. 5.2. Other fuel types in body 6 were included in body 5 and were examined there.

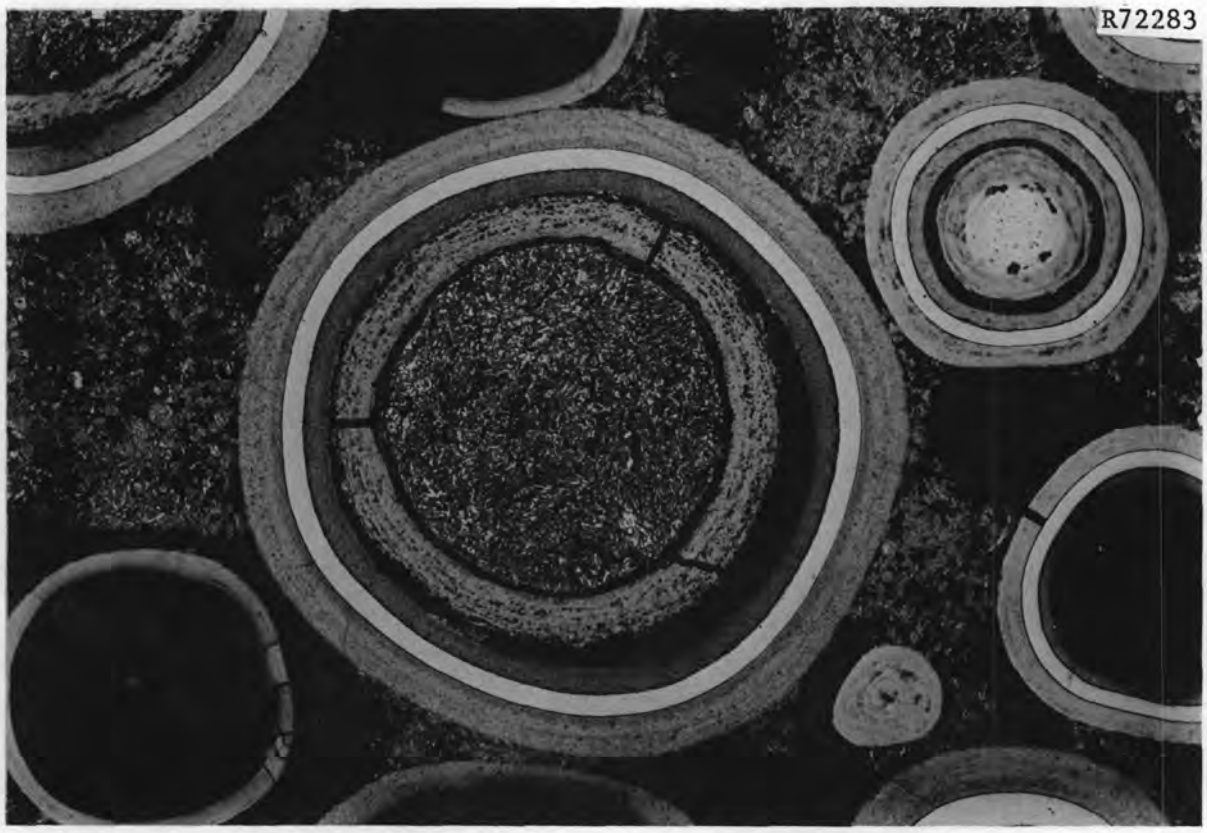

Fig. 5.8. Typical Triso-Coated ThC_2 Fertile Particle from RTE-5-6-7-1. 125×.

Matrix-Filler Samples — In the metallographic sections examined, no matrix-particle interactions were observed with any of the matrices. Though each matrix was different, they were similar in that all formed dense microstructures. In each case the filler particles seemed to clump together, and individual filler particles were not readily discernable.

5.2.3 Postirradiation Examination of FTE-11 (RTE-1) — T. N. Tiegs, E. L. Long, Jr., and E. L. Ryan

The last in the recycle test element series, FTE-11, was discharged from the Peach Bottom Reactor on October 31, 1974, after 645 effective full-power days. The element had been originally designated RTE-1. The fuel loading scheme for FTE-11 is shown in Table 5.4. The overall appearance of the element was normal. The fission product trap

Table 5.4. Fuel Loading Scheme for FTE-11

Body	Holes	Type[a]	Full Particle Type	
			Fissile	Fertile
1,2,3,4	1, 5	a	$(4Th,U)O_2$ Biso	ThC_2 Biso
	2, 6	f	UC_2 Triso	ThC_2 Biso
	3, 7	c	$(2Th,U)O_2$ Biso	ThO_2 Biso
	4, 8	g	UO_2 Biso	ThO_2 Biso
5	1, 5	d	$(2Th,U)O_2$ Biso	ThC_2 Biso
	2, 6	e	UC_2 Biso	ThC_2 Biso
	3, 7	h	UC_2 Biso	ThO_2 Biso
	4, 8	o	UO_2 Triso	ThO_2 Biso
6	1, 5	d	$(2Th,U)O_2$ Biso	ThC_2 Biso
	2, 6	e	UC_2 Biso	ThC_2 Biso
	3, 7	i	UC_2 Triso	ThC_2 Triso
	4, 8	o	UO_2 Triso	ThO_2 Biso

[a]The fuel Types for all seven Recycle Test Elements are identified in a report by E. L. Long, Jr., R. B. Fitts, and F. J. Homan, *Fabrication of ORNL Fuel Irradiated in the Peach Bottom Reactor and Postirradiated Examination of Recycle Test Elements 7 and 4*, ORNL/TM-4477 (September 1974).

and end fittings were cut off and the six fuel bodies removed from the graphite sleeve. Dimensional measurements taken on graphite components of the fuel element include the sleeve, fuel bodies, and fuel rods. The results were compiled and forwarded to GA for incorporation in the detailed thermal analysis for the RTE series.

Fuel rods were removed from holes 1, 3, 6, and 8 in bodies 1, 2, and 3 and all holes in bodies 4, 5, and 6. The rods appeared in generally fair condition with some debonding. Some fuel rods had extensive particle discoloration from some reaction. Because the affected area had a brownish appearance, the reaction was believed to be caused by iron contamination, which had been observed before in RTE fuel rods. Fuel was selected from the fuel bodies for metallographic examination to

cover all fuel types. There was a great deal of fuel type duplication, so only one of each fuel type was examined metallographically. The samples were chosen from the bodies with the highest temperatures. The results of these examinations are summarized below.

Body 3 — The Biso-coated $(2Th,U)O_2$ particles were in good condition, with no failures or amoeba effect observed. Typical fissile particles were very similar to those shown in Fig. 5.3. The Biso-coated ThO_2 fertile particles appeared in good condition with no failures or amoeba effect.

The Triso-coated UC_2 particles were in fair condition, with graphitization of the inner LTI on the cold side in most (>50%) of the particles. A few particles had the outer LTIs broken from fast-neutron-induced shrinkage.[4] Typical fissile particles were very similar to those shown in Fig. 5.4. The Biso-coated ThC_2 fertile particles appeared in good condition with no failures or amoeba.

Body 4 — The Biso-coated $(4Th,U)O_2$ particles appeared in good condition with no failures or observable amoeba effect. The appearance of these particles was very similar to those shown in Fig. 5.6, which are the same particles irradiated in RTE-5.

The Biso-coated UO_2 particles were in poor condition. The kernels appeared to be broken up into separate parts, and amoeba effect was observed in all directions. Typical fissile particles were very similar to those shown in Fig. 5.7. The Biso-coated ThC_2 particles looked in good condition with no failures or amoeba effect.

Body 5 — The Biso-coated $(2Th,U)O_2$ particles were in good condition and appeared very similar to those in body 3. The Biso-coated ThC_2 particles looked in good condition with no amoeba effect.

The Biso-coated UC_2 particles looked in good condition with no failures. Typical fissile particles were very similar to those shown in Fig. 5.1. The Triso-coated UO_2 particles looked in fair condition with amoeba effect prevalent in most particles (Fig. 5.9).

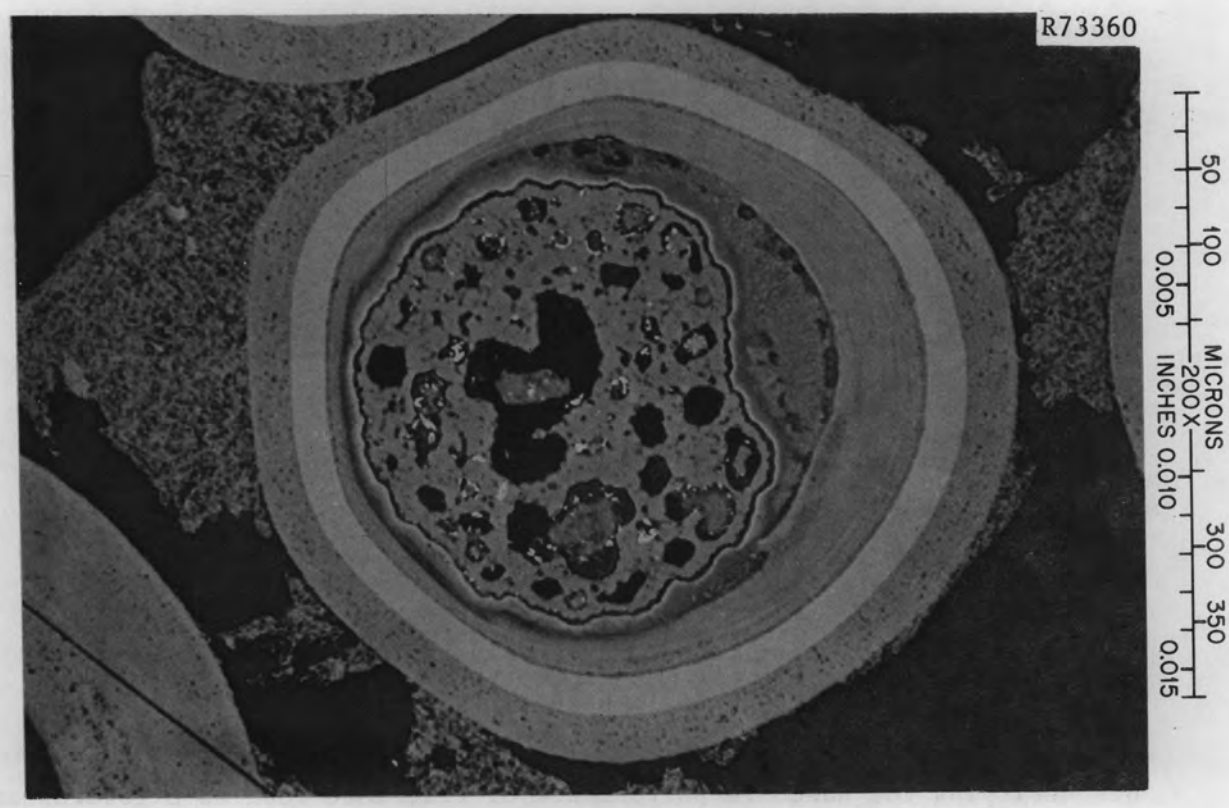

Fig. 5.9. Typical Triso-Coated UO_2 Fissile Particle from RTE-1-5-8-1. Note amoeba migration of kernel towards hot side of particle (on left).

5.3 ORR IRRADIATIONS

The ORR series of irradiations include two capsules designated OF-1 and OF-2. The results from OF-1 have been reported previously[5] and a final report was written during this reporting period.[6]

The OF-2 capsule was jointly funded from the HTGR Base Program and the ThU Program so the results will be reported elsewhere.[1] It tested the fuel product from the cold engineering development of task 300. During this reporting period the irradiation was completed and postirradiation examination initiated.

5.4 FSVR EARLY VALIDATION TESTS

The Fort St. Vrain Reactor (FSVR), operated by Public Service Company of Colorado, offers an opportunity to test candidate recycle fuels in a true large HTGR neutron spectrum and helium coolant

environment. The Early Validation Tests (EVT) will test the fuel product from the cold prototype development of Task 300. Fabrication of this fuel is described in Chap. 3. The objectives of this experiment are:

1. real-time testing of pre-production batches of Triso-coated fissile and Biso-coated fertile particles prepared in large-scale coating furnaces and comparing results with accelerated tests conducted in the ORR and HFIR test reactors;
2. testing of fresh and recycle products and fabrication processes;
3. testing of statistically representative numbers of samples from production-size batches;
4. determining if design and performance model specifications are adequate;
5. surveillance testing of production-size batches of fissile and fertile particles and fuel rods at 1/3, 2/3, and full-term exposure levels;
6. verifying the adequate performance of reference fuel as a forerunner for proof-testing large-scale recycle elements (LSREs) at a later date in Fort St. Vrain;
7. providing reference fuel for reprocessing verification.

The fuel will be incorporated in three reference-design FSVR fuel blocks. A test array of six fuel rod holes that surround a coolant hole will be reserved for ORNL fuel in each of the fuel blocks. Each fuel block will contain 88 rods of ORNL fuel (15 rods in each of 4 holes and 14 rods in each of 2 holes), which represents less than 3% of the fuel in a block. In addition to the ORNL fuel, 5 identical test arrays are scheduled to contain GA, KFA, and CEA fuel; the remainder of the block will contain reference FSVR fuel rods.

General Atomic Company supplied the matrix, shim, and fertile particles used with ORNL fissile particles in fabricating green fuel rods. The green fuel rods will be shipped to GA, loaded into the test arrays reserved for ORNL fuel in three FSVR fuel blocks, and carbonized. The quality of the fuel after carbonizing will be certified by GA employing its QA procedures. The fuel blocks will then be shipped to the FSVR site for incorporation into the core during reload.[1]

5.5 REFERENCES

1. F. J. Homan et al., "HTGR Fuel Qualification," *HTGR Base-Technology Program Prog. Rep. July 1, 1975–Sept. 30, 1976*, ORNL-5274, Chap. 6.
2. E. L. Long, Jr., "Recycle Test Elements," *Gas-Cooled Reactor Programs Annu. Prog. Rep. Dec. 31, 1973*, ORNL-4975, p. 153.
3. E. L. Long, Jr., R. B. Fitts, and F. J. Homan, *Fabrication of ORNL Fuel Irradiated in the Peach Bottom Reactor and Postirradiation Examination of Recycle Test Elements 7 and 4*, ORNL/TM-4477 (September 1974).
4. E. L. Long, Jr., and T. N. Tiegs, "Peach Bottom Irradiations," *Thorium Utilization Program Prog. Rep. Jan. 1, 1974–June 30, 1975*, ORNL-5128, pp. 278–304.
5. M. J. Kania, K. R. Thoms, and T. N. Tiegs, "Irradiation Tests in the ORR," *HTGR Base-Technology Program Prog. Rep. Jan 1, 1974–June 30, 1975*, ORNL-5108, pp. 360–95.
6. T. N. Tiegs, E. J. Allen, M. J. Kania, E. L. Long, Jr., and K. R. Thoms, *ORR Irradiation Test OF-1: Accelerated Testing of HTGR Fuel*, ORNL-5234 (in press).

6. HTGR FUEL RECYCLE DEMONSTRATION FACILITY (TASK 600)

6.1 INTRODUCTION — R. K. KIBBE*

During the period of this report, as a part of the program redirection[1] the National Thorium Utilization Program adopted a specific objective of providing a demonstration plant for the recycle of HTGR fuels. Achieving this objective involves two major efforts: the development of the necessary technological base for such a facility and the actual design and construction of the facility. The latter effort — the design, construction, proof testing, and demonstration operation of the facility — is the specific objective of Task 600. There are several supporting objectives for Task 600:

1. to provide a comprehensive demonstration that addresses all aspects of HTGR fuel recycle operations;
2. to provide a significant production recycle capacity to support early large HTGR commitments;
3. to demonstrate a commercially desirable facility to permit eventual sale or lease to industry — specific attributes of the HTGR Fuel Recycle Demonstration Facility (HRDF) that will help achieve this subobjective include (a) full-scale equipment, (b) a comprehensive maintenance plan including remote maintenance, where required, (c) meeting all licensing requirements, and (d) integrated and economic operations;
4. to establish and maintain a current, precise, and fully traceable hierarchy of HRDF requirements documents to help guide development and design activities within the program.

During the program redirection, effort on Task 600 and the HRDF was reduced substantially. Work accomplishments include finalizing of HRDF preconceptual layout studies by UCC-ND Engineering and completing the first draft of the top two levels of HRDF requirements documents.

---

*On assignment from General Atomic Co. Present address, Office of Waste Isolation, Union Carbide Nuclear Co., Oak Ridge.

6.2 HRDF PRECONCEPTUAL LAYOUT STUDIES — T. F. Scanlan

These efforts are reported in detail in the previous report.[2] Although work was initiated in the above time period, a major portion of the effort occurred after June 30, 1975, including preparation of a final draft report. Revisions to this report, incorporating internal review comments, have been delayed by higher priority work.

6.3 HRDF REQUIREMENTS DOCUMENTS — R. K. Kibbe*

Draft versions of the Level 0 and two of the Level 1 HRDF requirements were issued in September 1975 for review and comment by program contractors and ERDA. The level 0 document is the highest level in the tree structured hierarchy of requirements documents for the HRDF, addressing itself to the HRDF complex as a whole and identifying the overall requirements that the various operational entities (or facilities) within the complex must satisfy. There will be one Level 1 document for each HRDF facility as shown below.

Facility	Functional Operation
1000	Reprocessing
2000	Fefabrication
3000	Waste Treatment
4000	Operational Support
5000	General Support
6000	Receiving, Storage, and Shipping

During the reporting period, two Level 1 documents were completed in draft form. They are currently in the ERDA contractor review cycle.

6.4 REFERENCES

1. National HTGR Fuel Recycle Development Program, *National Program Plan for HTGR Fuel Recycle Development*, ORNL internal document (Oct. 1, 1976).

---

*On assignment from General Atomic Co. Present address, Office of Waste Isolation, Union Carbide Nuclear Co., Oak Ridge.

2. C. C. Haws, L. C. Hensley, W. H. Pechin, F. E. Harrington, A. R. Olsen, J. E. Van Cleve, T. F. Scanlan, K. H. Lin, and M. S. Judd, "20/10 HRDF Preconceptual Design Study," *Thorium Utilization Program Prog. Rep. Jan. 1, 1974—June 30, 1975*, ORNL-5128, pp. 327—30.

7. HOT ENGINEERING TEST PROJECT

B. J. Baxter* and D. P. Reid

7.1 INTRODUCTION

The Hot Engineering Test Project (HETP) is administered by the National Thorium Utilization Program and is intended to provide technology relevant to the recycle of High-Temperature Gas-Cooled Reactor (HTGR) nuclear fuels. Conceptual design of the necessary fuel reprocessing and refabrication systems and associated support facilities was begun and is scheduled to be issued in report form on April 15, 1977. During the period July 1, 1976 to September 30, 1976 substantially all the refabrication systems were conceptually designed, reprocessing systems were designed to 30% completion, and associated facility requirements were conceptually defined.

7.1.1 Purpose

The purpose of the HETP is to provide experience and engineering data for the design of an HTGR Fuel Recycle Demonstration Facility (HRDF) by demonstrating selected reprocessing and refabrication processes in the radiation environment expected of HRDF operations.

7.1.2 Project Objectives

The overall objective of the Hot Engineering Test (HET) program is to demonstrate in engineering-scale equipment those aspects of spent HTGR fuel recycle processes that cannot be done without the presence of high levels of fission products or the radioactivity associated with ^{233}U containing significant amounts of ^{232}U. Test data resulting from hot operations will be emphasized, and not the fundamental operability of base-line processes. Accordingly, essential equipment design characteristics are to adequately simulate production operating

---

*On assignment from General Atomic Co.

conditions related to the effects of high levels of fission products, thereby providing representative data for HRDF process selection and equipment design.

The issues relevant to process selection and equipment design are as follows:

1. demonstration of effluent treatment capability,
2. identification of radioactive species distribution,
3. production of samples for assay technique development,
4. demonstration of practical methods for assay and quality control of process streams,
5. control of radiation hazards associated with the ^{232}U content of recycled ^{233}U fuel to permit the activities of sampling and analytical procedures to be conducted safely,
6. confirmation of established flowsheets for both the reprocessing and refabrication aspects of fuel recycle.

7.1.3 Specific Technical Issues

A number of specific technical issues relative to a final HRDF design are to be answered by the HET Project. These issues derive primarily from lack of detailed information and data on the effects of ^{232}U decay products on processes, equipment performance, radioactivity emissions, maintenance methods, and personnel exposure. The HET Project is designed to eliminate these deficiencies.

The reprocessing test will use 96 fuel elements discharged from the Fort St. Vrain High-Temperature Gas-Cooled Reactor after one equivalent full-power year, cooled 180 days. Each element will contain 66,000 Ci of activity.

The influence of such high levels of irradiation and fission products in reprocessing is primarily associated with the distribution of fission products within the process. The extent to which oxidation and/or volatilization occur during crushing and burning significantly affects the equipment design. In addition, the physical nature of the fission products in the burner ash affects the chemistry of dissolution, the methodology, and the final fissile material recovery. In the

solvent extraction stage of processing, radiation damage to the solvent or emulsion formation is affected by the heat generation of suspended particulate fission products and the degree to which these products have been dissolved. Consequently, the HET reprocessing must encompass the operations from initial fuel element size reduction through the first stage of solvent extraction to adequately address HRDF requirements.

The effects of radioactivity on refabrication processes are pronounced in the chemical and thermal processes associated with the preparation of coated fissile fuel particles. The refabrication process uses weak acid carboxylate resin in contact with uranyl nitrate solution to produce a uranium-loaded weak-acid resin microsphere. Uranium loading is controlled by the degree to which the uranyl nitrate is acid deficient. Control of acid deficiency is strongly influenced by chemical disturbances initiated by the presence of radioactivity, such as radiolysis of the water or organic solutions, foaming of solutions owing to radiolytic gas release or energy absorption, and possible changes in the resin ion-exchange characteristics with radiation exposure. HET will include the resin loading process carried through carbonization and conversion steps because experience has shown that some resin loading problems become apparent only after the carbonization and conversion steps. In addition, the carbonization and coating systems will include engineering-scale perchloroethylene and sodium hydroxide off-gas scrubbers to characterize the performance of these systems in a radiation environment and to generate typical HRDF waste streams.

In the area of waste handling, HET will demonstrate radon trapping and perchloroethylene recycle. Radon will be released during each heating operation in refabrication, and an adequate radon-trapping device on the resin drier and carbonization and coating furnaces must be demonstrated before HRDF design. The influence of radiation on the recycle of perchloroethylene must be determined before HRDF design. The principal concern is the generation and/or concentration of irradiation-caused degradation products in recycle perchloroethylene.

In addition, engineering data on partitioning factors and content of distillate bottoms (principally, radioactivity levels) must be obtained before design of an HRDF waste and scrap handling system.

In summary, the following specific technical issues will be addressed by the reprocessing and refabrication tests to be conducted in the HET Project:

1. confirmation of the process operability in the presence of the radioactivity;
2. confirmation of the capability of the tested portions of the process to produce a radioactive product meeting the HTGR fuel specifications;
3. confirmation of the gaseous effluent treatment processes;
4. information on the distribution of radioactivity in the process equipment, products, and waste effluents;
5. information on the remote operational and maintenance procedures for those equipment components used in the tests; and
6. information on various nondestructive assay techniques to be used.

7.1.4 Project Schedule

The HET Project schedule is shown in Fig. 7.1 to be organized according to five principal time phases and four Thorium Utilization Program Tasks. The principal time phases are as follows:

1. preliminary design,
2. detailed design,
3. procurement and installation,
4. cold testing,
5. hot testing.

The Thorium Utilization Program tasks are as follows:

Task 100 — Facilities and Management Planning,

Task 200 — Reprocessing,

Task 300 — Refabrication,

Task 400 — Waste Treatment.

The preliminary design phase was initiated during FY 1976 and will be concluded by April 29, 1977. Preliminary design includes the preparation of requirements and criteria documents, a conceptual design

ORNL-DWG 77-6845

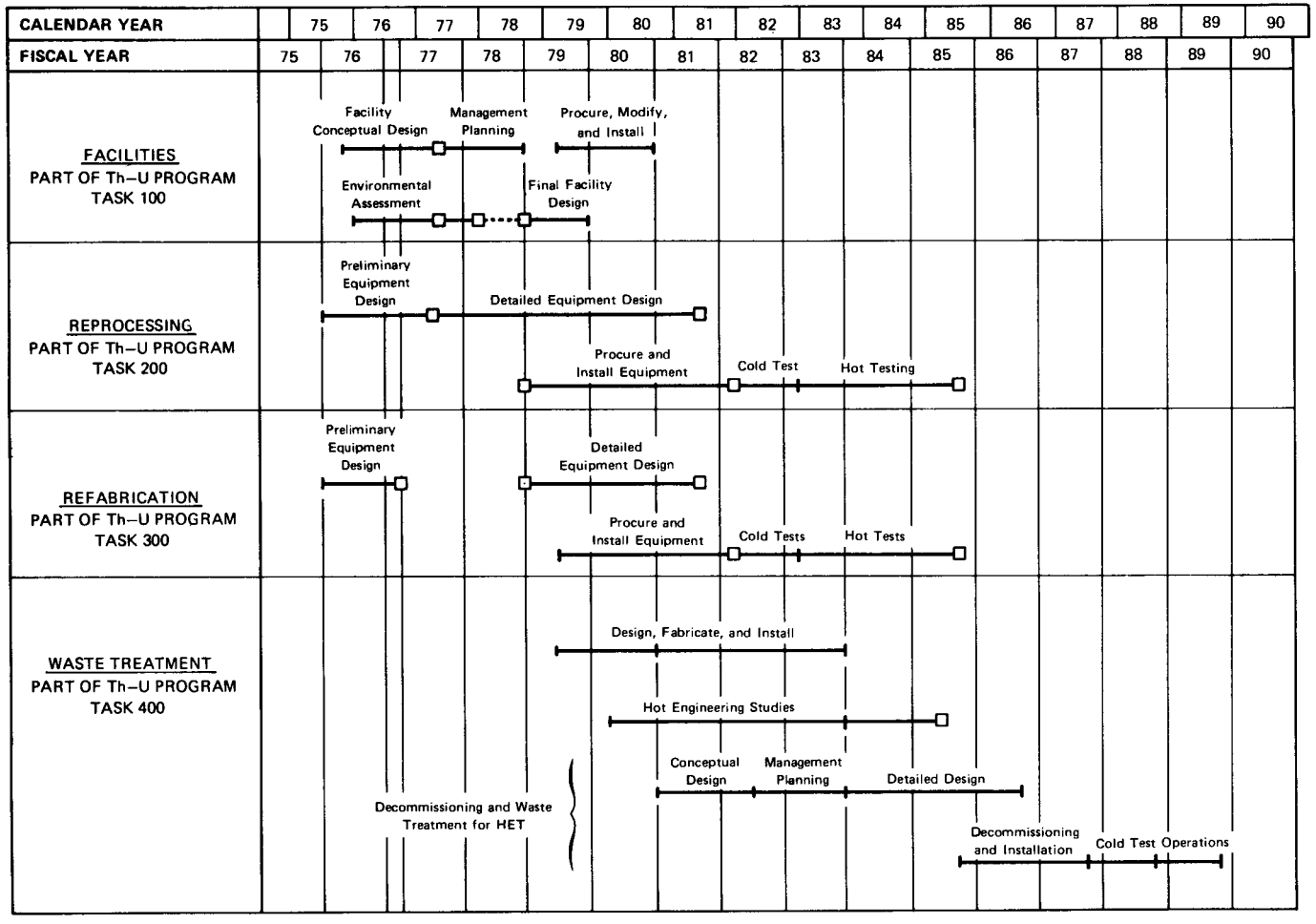

Fig. 7.1. HTGR Hot Engineering Test Project Schedule.

report, and an estimate of the project cost. In addition, an environmental impact assessment is to be prepared during this phase.

Final design of reprocessing and refabrication equipment, its procurement, and installation are scheduled for completion by the end of 1981.

Cold testing will be performed during FY 1982 and continue into the early part of FY 1983.

The cold testing phase for reprocessing will include initial equipment checkout using unloaded graphite blocks, inert SiC particles, and unirradiated Triso fissile and fertile particles. Final cold tests will use unirradiated Fort St. Vrain (FSV) fuel to obtain data for comparison with hot test results, and provide a basis for normalization with cold pilot plant data and extrapolation to the HRDF process equipment.

The cold testing phase for refabrication includes initial equipment checkout using normal or depleted uranyl nitrate.

Hot testing is scheduled for a 2.5-year period and terminates in FY 1985.

The hot testing plan for refabrication is based on processing 96 FSV spent fuel elements through the primary head-end systems: fuel element crushing, primary burning, and classification. The separate fissile and fertile particle fractions from 36 fuel elements will be processed through the secondary head-end systems: particle crushing and secondary burning, to provide feed for the aqueous separations systems. The hot testing plan is expected to consist of eight campaigns of 12 fuel elements per campaign — each campaign to be approximately three months in duration.

The hot testing for refabrication will involve a maximum of eight campaigns, each of approximately three months duration. The processing time is controlled by the conversion and coating of a nominal batch size containing 0.5 kg U. The length of the refabrication campaign has been limited to three months by an allowable build-up of radioactivity in the product samples to be handled by sample inspection equipment.

The schedule for HET waste treatment is multifaceted and principally accounts for disposal of process waste streams generated by reprocessing and refabrication operations. The waste treatment schedule further accounts for the decontamination of facilities and equipment as a major activity during FY 1985 and 1986.

7.1.5 Project Status

During the reporting period preliminary criteria documents were generated by ORNL for the three divisions of this project; support facilities, reprocessing equipment, and refabrication equipment. These internal documents were reviewed by General Atomic Company (GA) and an Architect-Engineer (Ralph M. Parsons Co.), revised, and distributed. Conceptual design for the support facility was initiated by the Architect Engineer September 3, 1976, and is progressing on schedule. The conceptual design of the reprocessing equipment was initiated by GA, with support from the Architect Engineer, in early September and is proceeding on schedule. The conceptual design of the refabrication equipment was performed by ORNL and is essentially complete.

Final issue of the conceptual design report and estimated cost of this Project is scheduled for April 15, 1977.

7.2 DESCRIPTION OF HET PROJECT — B. J. Baxter and D. P. Reid

The HET Project will utilize a number of existing facilities and services both at ORNL and at the Idaho National Engineering Laboratory Chemical Processing Plant to demonstrate the reprocessing and refabrication processes necessary to the recycle of spent HTGR fuel. The flowsheets for these processes are shown in Figs. 7.2 and 7.3.

The modifications and/or additions to the existing ORNL buildings and the activities being proposed for each are described below.

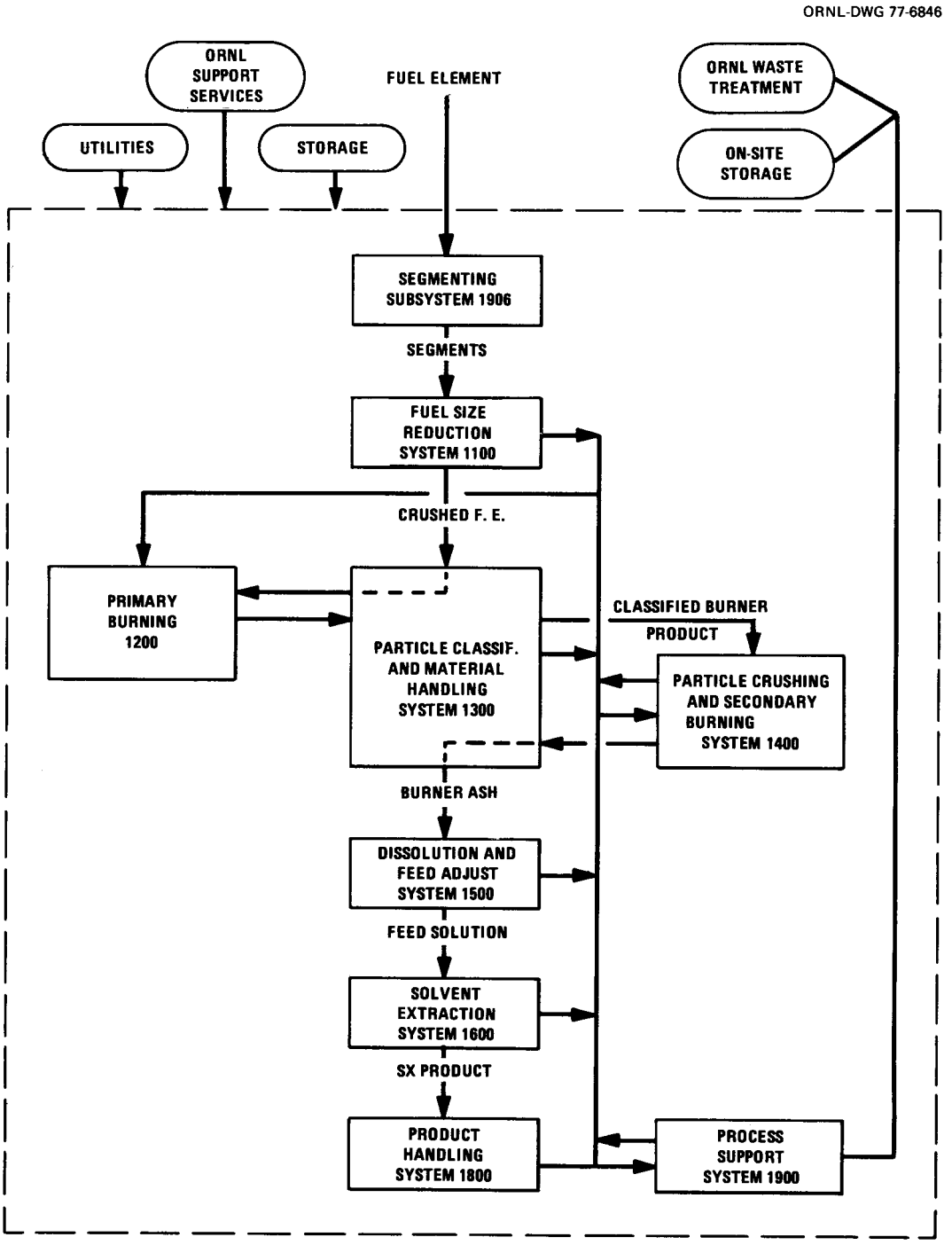

Fig. 7.2. Generalized HET Fuel Reprocessing.

ORNL-DWG 76-20772A

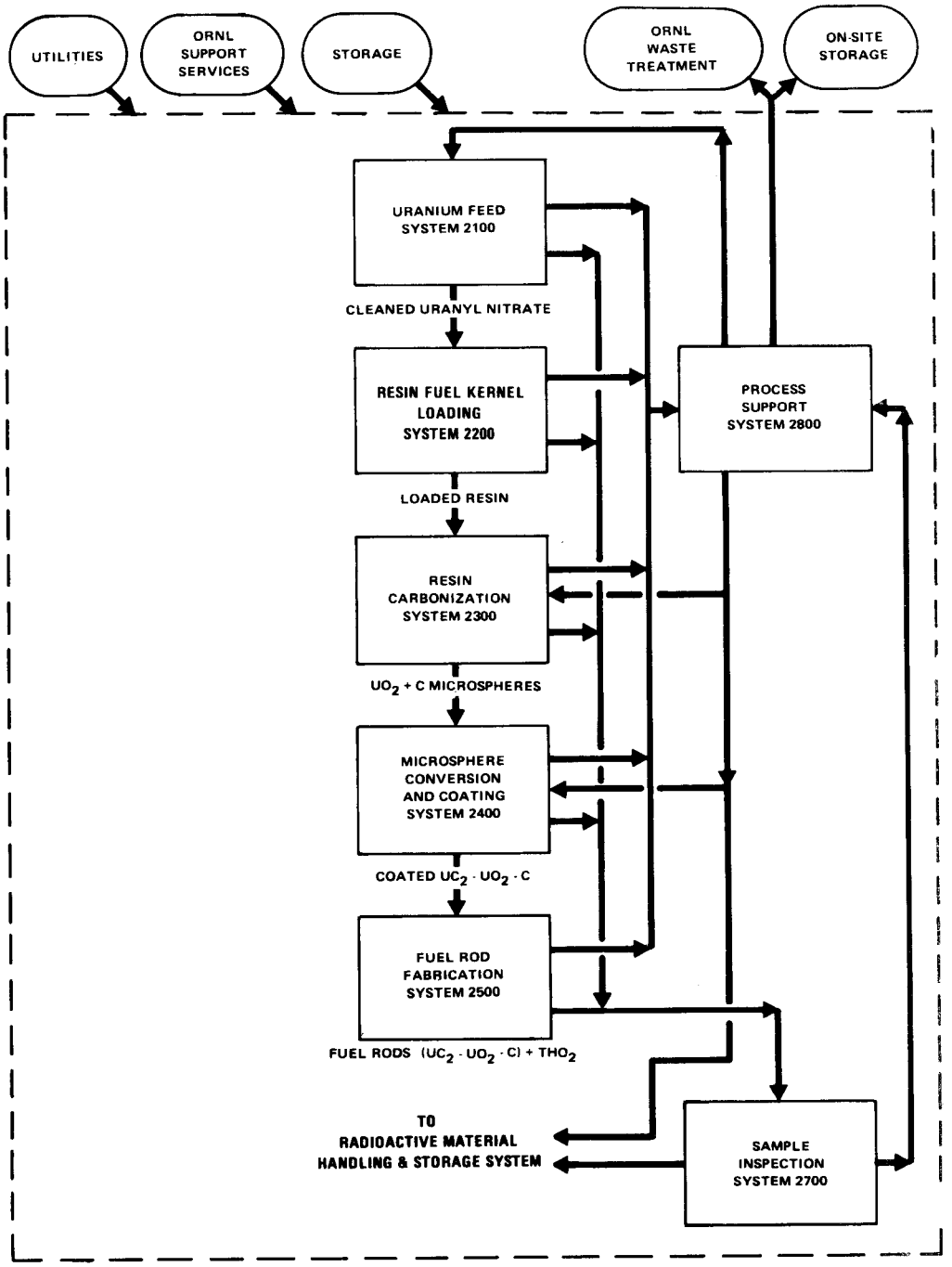

Fig. 7.3. Generalized HET Fuel Refabrication.

7.2.1 HET-Facilities — D. P. Reid and P. Stein

Building 7930 — Thorium Uranium Recycle Facility (TURF) — will contain the major efforts of the HET Project. TURF will provide the necessary facilities and services to demonstrate the fuel recycle areas of reprocessing and refabrication.

The TURF is a three-story structure with a partial basement, which was designed in accordance with the Southern Building Code for group-G industrial occupancy. It is constructed of structural steel, reinforced concrete, and masonry.

The first floor provides space for technical personnel offices, cell operation and maintenance, a receiving area, a fuel storage room, hot and cold change rooms, a compressor room, and an elevator room, as shown in Fig. 7.4.

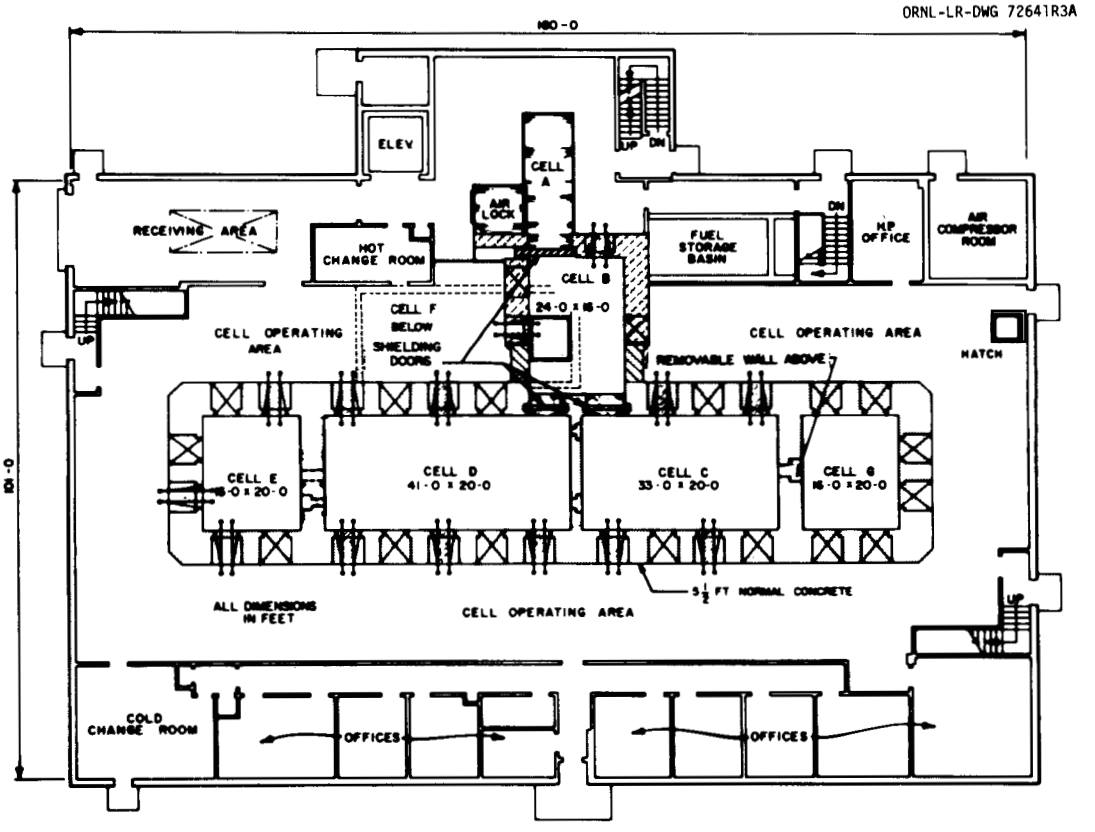

Fig. 7.4. First-Floor Plan of Building 7930 (TURF). To convert dimensions to meters, multiply by 0.305.

The second floor provides space for chemical makeup, sampling of radioactive materials, a development laboratory, a shop, a maintenance area, mechanical and electrical equipment rooms, a cask decontamination station, a checking and holding area, and working space around Cell A.

The third floor, a high bay, includes the cell roof area and provides facilities for cell access and entry of cell services. It is equipped with a 0.44-MN (50-ton) overhead traveling bridge crane with a 44-kN (5-ton) auxiliary hoist. Some of the third-floor space is used for cell and building ventilation equipment, and other portions will be used as necessary for mockup of cell process equipment.

The facilities for receiving, handling, and storing radioactive materials consist of six heavily shielded cells served by an overhead crane and electromechanical manipulator system along with master-slave manipulators. In addition, there is an unshielded gloved maintenance cell, a fuel storage room, and a cask support and decontamination area.

Figure 7.5 shows the four operating cells (Cells C, D, E, and G). These are described elsewhere.[1] A partial basement provides space for access to Cell F and for installation and maintenance of equipment in a pump room adjacent to Cell G.

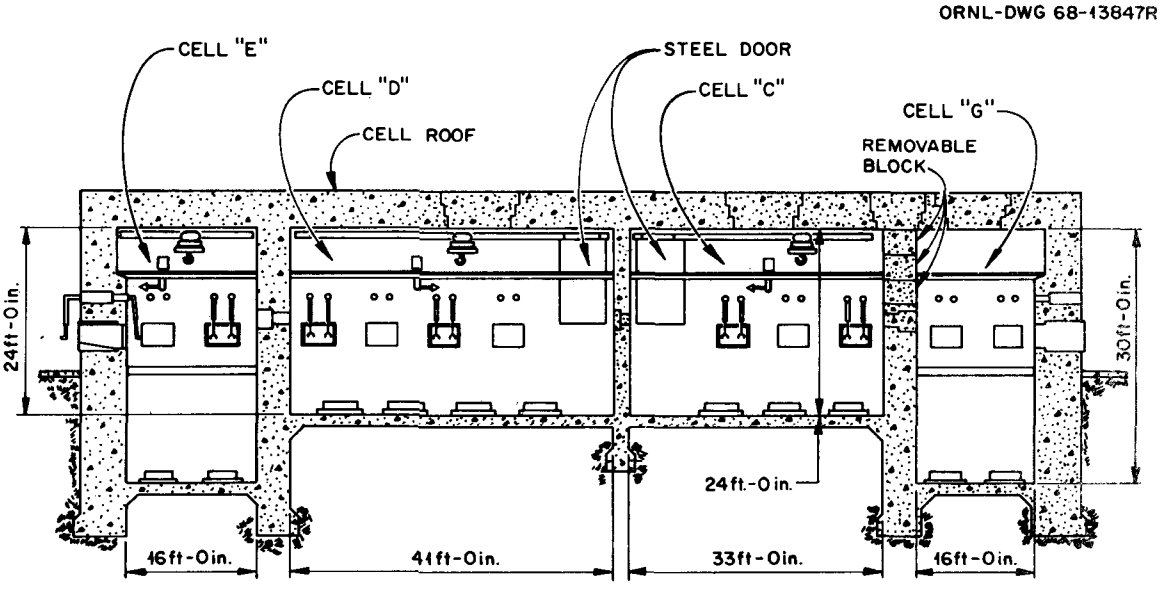

Fig. 7.5. Elevation View of TURF Operating Cells. To convert dimensions to meters multiply by 0.305.

The existing cells will accommodate the process systems involved, but modifications to the existing building will be required to provide the necessary services. The existing building will be modified to provide adequate mechanical equipment space and to provide a shielded glovebox area for sample handling. The building will be upgraded to withstand natural phenomena by criteria specified by ERDA. The existing cell bank will have minor modifications to admit material handling systems.

Specific modifications to Building 7930 are expected to include:

1. adding the third level on the east side of TURF,
2. increasing the plant air system,
3. providing for waste treatment,
4. adding a process gas storage and distribution system,
5. providing shielded transfer ports,
6. modifying the fuel storage basin,
7. adding a nonmoderating process cooling system,
8. adding an electrical substation,
9. adding the remaining viewing windows and master-slave manipulators,
10. adding a computer systems area.

Building 3026D contains dismantling and examination hot cells. Cell A of this building will be used for the segmenting of irradiated HTGR reactor fuel elements. The segmented fuel elements are subsequently transferred to TURF and consumed in the reprocessing equipment to be located there.

Building 7503 is the Molten Salt Reactor Building. It will provide storage for some of the product from reprocessing operations in TURF. In addition, a number of irradiated fuel elements are expected to be stored here before segmenting in Cell A of Building 3026D.

Building 3019, the National Repository for ^{233}U, will supply uranyl nitrate feed solution to the refabrication portion of the HET Project. Building 3019 will be further utilized in the "conversion" of liquid uranyl nitrate received from the reprocessing portion of the HET Project. The conversion will involve the transformation of uranyl nitrate solution received as a liquid from TURF into a solid compound more suitable for storage.

7.2.2 HET Reprocessing — F. E. Harrington and C. C. Haws

The reprocessing processes consist of the following systems, as shown in the overall reprocessing block flow diagram, Fig. 7.2:

System 1100 — Fuel Size Reduction

System 1200 — Primary Burning

System 1300 — Particle Classification and Material Handling

System 1400 — Particle Crushing and Secondary Burning

System 1500 — Dissolution and Feed Adjustment

System 1600 — Solvent Extraction

System 1800 — Product Handling

System 1900 — Process Support.

The specific space assignments made to System 1300 is Cell D, Systems 1200 and 1400 were assigned to Cell E, and the aqueous Systems 1500, 1600, and 1800 were assigned to Cell G.

7.2.2.1 System 1100 — Fuel Size Reduction

The purpose of this system is to crush segmented spent fuel elements to a granular form that can be fed to the primary burner. This task is carried out in the following functions:

1. charge segmented fuel elements to the system via the jaw crusher air lock;
2. crush, scalp oversized fragments, recycle, and roll crush to a product with 4.8 mm (3/16 in.) maximum particle size and of a distribution suitable for fluidized bed combustion; and
3. maintain an inert atmosphere during crushing.

These functions of the Spent Fuel Size Reduction System are executed through subsystems 1111, Jaw Crushing; 1121, Scalping and Recycle; and 1131, Roll Crushing.

Subsystem 1111 includes (1) a charging airlock to receive up to a single fuel element segment from the transfer container while maintaining an inert atmosphere; (2) the primary crusher, which reduces the fuel element segment to nominally below 19-mm (3/4-in.) ring size; and (3) provisions to weigh, open, and empty fuel canisters before transfer to the crusher.

Subsystem 1121 includes the scalper and a recycle apparatus. The scalper separates the over 19-mm ring size primary crusher product, diverting it to the recycle apparatus and letting the product not exceeding 19 mm pass to the secondary crusher. The recycle apparatus returns oversize primary crusher product to the primary crusher feed.

Subsystem 1131 is a double roll crusher that reduces the primary crusher product to below 4.8-mm (3/16-in.) ring size material. Product removal is compatible with the pneumatic transfer system (part of System 1300).

The system is sized to provide a throughput of at least one FSV fuel element per hour and to start fully loaded. It should be either self-enclosed or shrouded to prevent escape of particulates and to allow for blanketing. Sampling exit purge gases must be possible.

7.2.2.2 System 1200 — Primary Burning

This system burns away graphite and exposed outer carbon coatings from irradiated HTGR fuel particles to produce uniform batches of burned-back fissile-fertile particles and ash with a minimum of particle breakage. This task involves the following system functions:

1. receive batches of crushed spent fuel elements from System 1300 and feed this material to the primary fluidized bed burner;
2. burn away graphite and exposed carbon from the fuel particles in a fluidized bed at a rate of 3 fuel elements per day;
3. remove and collect fines and particulates from the burner off-gas and return them to the burner for further oxidation of carbon;
4. transfer burner ash from the burner to System 1300;
5. provide adequate sampling and process control to achieve the development objectives of the program.

These function of the primary burner system shall be executed through operation of the subsystems 1201, Primary Burner Feeding; 1211, Primary Burning; 1221, Fines Collection, Recycle, and Sampling; and 1231, Product Removal.

Subsystem 1201 includes a primary burner feed hopper and a feeder. These handle all possible mixes of materials in the primary burner feed and feed this material to the burner within 5% of 240 g/min.

Subsystem 1211 includes the primary burner and its direct accessories. It is a fluidized-bed combustion reactor with heating and cooling adequate for initial start-up, final burnout of graphite to less than 2 wt % C in the product, and operation in both exothermic and endothermic modes. The primary fluidizing gas is CO_2 plus O_2. The bottom of the burner is remotely removable for cleanout of clinkers.

Subsystem 1221 includes a cyclone followed by a set of metallic filters for particulate removal and hoppers for collecting and transferring the fines to the primary burner. Means are provided to sample the fines and determine the path of "semivolatile" fission products in the off-gas train.

Subsystem 1231 permits controlled removal of primary burner product for delivery to System 1300.

7.2.2.3 System 1300 — Particle Classification and Material Handling System

The particle classification system separates the batches of mixed fissile and fertile particles and graphite from the primary burner into a fissile fraction and a fertile fraction with minimum crossover. The material handling system provides inter-system handling of solid material for the head-end processes. These function are performed by process subsystems whose interactions with each other and with other systems are diagrammed in Fig. 7.6. A brief description of each subsystem follows.

<u>Subsystem 1301 — Receiving and Weighing</u>

Material is received from Systems 1100, 1200, 1300 (recycle), and 1400. Material from Systems 1100 and 1400 are dispensed for transport to System 1200, and material from Systems 1200, and 1300 (recycle) are dispensed by gravity flow through the classifier.

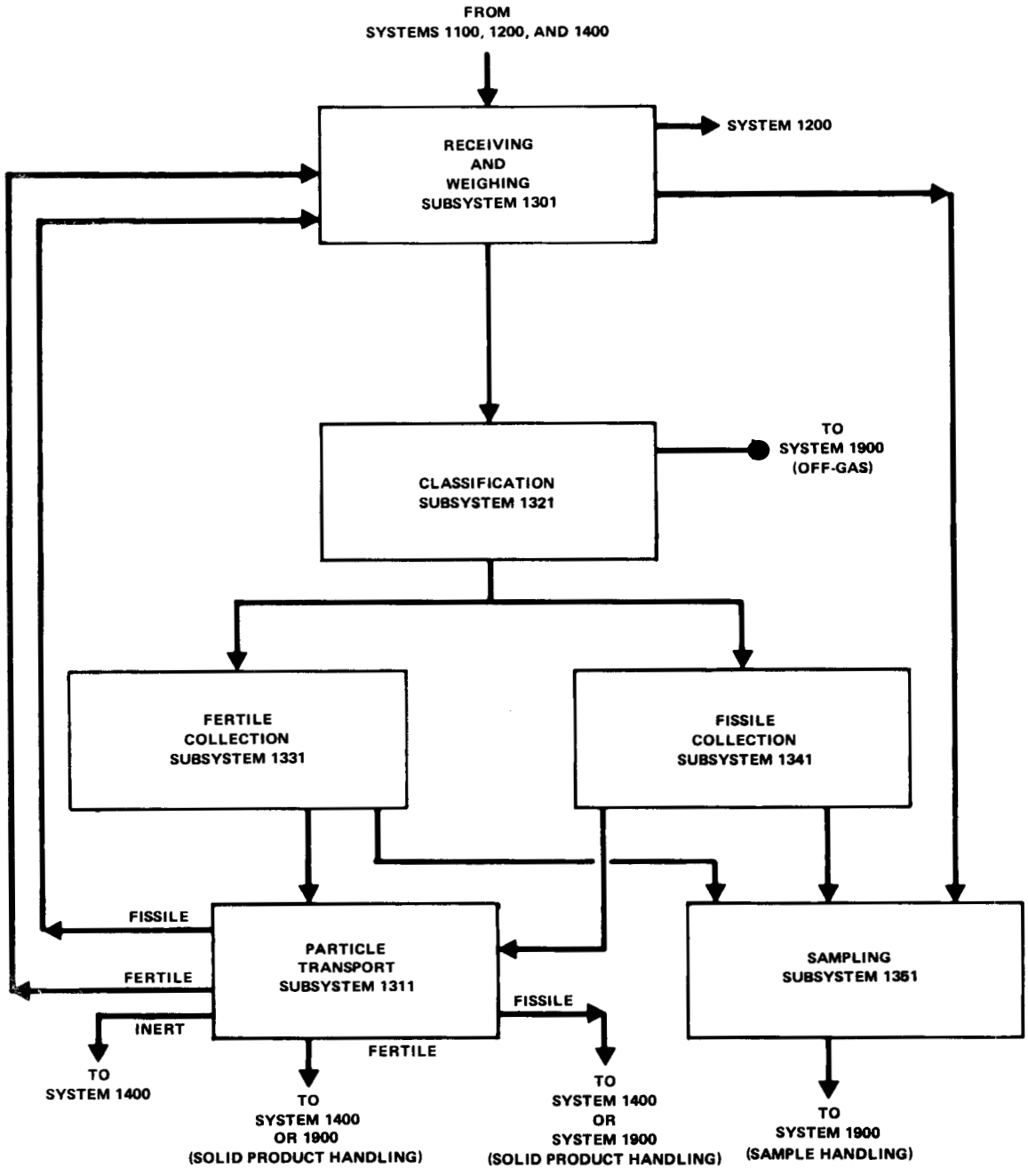

Fig. 7.6. Process Block Diagram for System 1300, Particle Classification and Material Handling System. Ralph M. Parsons Company drawing.

Subsystem 1311 — Particle Transport

The heavy fertile and fissile products are transferred pneumatically to Subsystem 1301 and remotely and manually to Subsystem 1401 and to System 1900.

Subsystem 1321 — Classification

The classifier separates the fissile and fertile particles and reclassifies them if necessary. It also separates inert particles from the primary burner product. The fissile stream is discharged to the fissile stream collection subsystem from classifier off-gas stream, and the fertile stream and inert material are discharged by gravity into the fertile collection system.

Subsystem 1331 — Fertile Collection

This subsystem collects and weighs the fertile bottom stream and the inert stream from the classifier and dispenses the streams for transfer to the other systems.

Subsystem 1341 — Fissile Collection

This system collects and weighs particles from the classifier fissile stream and dispenses the material for transfer to other systems downstream in the process.

Subsystem 1351 — Sampling

Samplers are located (1) in the discharge line from the central receiving weigh hopper to the crushed fuel element storage hoppers, (2) in the fines discharge line to the fissile particle weigh hopper, and (3) in the coarse discharge line to the fertile particle weigh hopper.

7.2.2.4 System 1400 — Particle Crushing and Secondary Burning System

System 1400 receives classified batches of Triso particles, crushes them, burns away the exposed carbon coating, and oxidizes thorium and/or uranium carbides. These processes are carried out through the following subsystems.

Subsystem 1401 — Fertile Crushing

Batches of fertile Triso particles and unburned graphite from System 1300 are fed through a roll crusher and into the secondary burner. Gas sampling and carbon dioxide gas blanketing of the crushed materials are provided. The crushed fertile material is recycled to the Primary Burner via System 1300.

Subsystem 1411 — Fissile Crushing

Batches of fissile Triso particles from System 1300 are fed through a roll crusher and collected in a hopper above the secondary burner feed system.

Subsystem 1421 — Burner Feed

Crushed particles are received from the fertile or fissile crushing subsystem. Components are mounted sufficiently close to the secondary burner. They are separable from the burner for maintenance.

Subsystem 1431 — Secondary Burning

The secondary burner burns away exposed carbon from silicon carbide shells and exposed uranium or thorium particles and oxidizes the carbides to oxides. The fluidized-bed combustion vessel is equipped with heating and cooling, insulation, a distributor plate for bed support and gas distribution, and means for product and clinker removal. The fluidizing gas shall be CO_2 and O_2.

Subsystem 1441 — Product Removal

This subsystem permits controlled removal of secondary burner product for delivery to System 1300. Discharge shall be by gas transport from the burner while the burner product is fluidized.

Subsystem 1451 — Solid Sampling

Samples are required for roll crusher performance and burner feed characterization.

All systems provide containment for dust and other particles.

7.2.2.5 System 1500 — Dissolution and Feed Adjustment System

System 1500 receives secondary burner ash, converts the heavy-metal-bearing solids to an aqueous solution, separates and dries insolubles, and adjusts the solution for solvent extraction feed. The following is a list of the subsystems.

Subsystem 1501 — Dissolution

Secondary burner ash is dissolved. Solution is removed by submerged open-suction steam jet. The off-gas is cooled in a down-draft condenser, with the condensate returned to the dissolver and the off-gas exhausted to Subsystem 1931, Off-Gas Treatment.

Subsystem 1511 — Solid-Liquid Separation

The dissolver product solution is separated from contained solids. The insolubles from the dissolution are washed, and the liquors are combined with clarified dissolver product solution. The washed and rinsed solids are transferred to Subsystem 1521.

Subsystem 1521 — Insolubles Drying and Storage

The washed and rinsed insolubles from Subsystem 1511 are dried and recycled to System 1900 for sampling and canning.

Subsystem 1531 — Feed Adjustment

Clarified dissolver product solution from Subsystem 1511 (plus wash and rinse liquors) is collected in the dissolver solution sample tank. Shell-and-tube condensers are provided for the feed adjustment tanks off-gas.

Subsystem 1541 — Storage

A feed surge tank provides capacity for seven days solvent extraction requirements. A metering pump meters feed solution to solvent extraction.

Subsystem 1551 — Sampling

Samplers are provided at appropriate locations. Tank samples are taken at completion of each batch operation.

7.2.2.6 System 1600 — Solvent Extraction System

System 1600 receives adjusted aqueous feed and uses the Acid Thorex Process for recovering and partially purifying the thorium and uranium and separating them from contained fission products, chemical impurities, and each other. This system also recovers and purifies the uranium from the dissolution of fissile particles via the Purex Process.

The functions of the Solvent Extraction System (Fig. 7.7) are executed through the following subsystems.

Subsystem 1601 — Extraction

This subsystem consists of a pulse column and the necessary feed and surge tanks, metering pumps, and high-level waste interim storage tank. The lower portion of the column is the extraction section, the upper the scrubbing section.

Subsystem 1606 — Partition

This subsystem consists of a pulse column, surge tanks, and metering pumps.

Subsystem 1611 — Partition Scrub

This subsystem consists of a single pulse column, a surge tank, and metering pumps.

Subsystem 1616 — Stripping

This subsystem consists of surge tanks, a metering pump, and a pulse column.

Subsystem 1621 — Solvent Regeneration

This subsystem consists of a solvent cleanup column, solvent surge tanks, and an organic waste interim storage tank. The solvent surge tanks need sufficient capacity to store the solvents for the Acid Thorex Process.

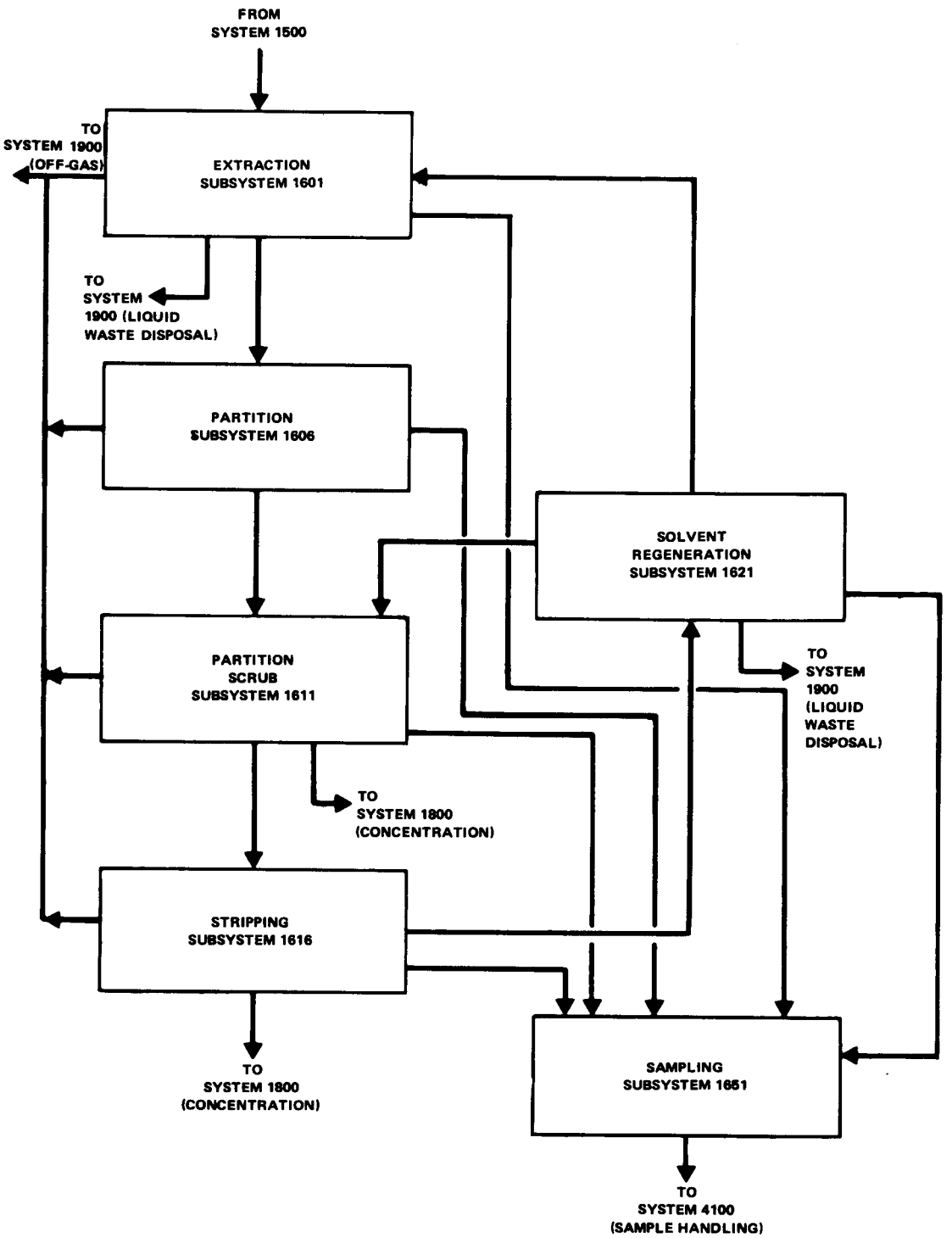

Fig. 7.7. Process Block Diagram for System 1600, Solvent Extraction. Ralph M. Parsons Company drawing.

Subsystem 1651 — Sampling

Samplers are located at appropriate places in the system (Fig. 7.7).

7.2.2.7 System 1800 — Product Handling System

The Product Handling System receives, concentrates, and stores thorium and uranium product solutions from the Acid Thorex Process and stores uranium product from the Purex process. Its functions involve operation of the following subsystems.

Subsystem 1811 — Concentration

This subsystem concentrates dissolver product solutions by evaporation. Product solution is removed by gravity outflow.

Subsystem 1851 — Sampling

Samplers are located as appropriate.

Subsystem 1881 — Storage

This subsystem provides storage for thorium nitrate, uranium nitrate, and intermediate level waste from Acid Thorex and Purex operation.

7.2.2.8 System 1900 — Process Support System

The Process Support System incorporates operations or processes needed to support previously described processes or operating equipment. The system is made up of a series of discrete and somewhat unrelated subsystems listed as follows.

Subsystem 1901 — Unirradiated Feed Material Handling

This subsystem is not a part of the ORNL HET facility.

Subsystem 1906 — Segmenting

This subsystem provides for the segmenting of fuel elements to a size suitable for introduction into System 1100 at the rate of two FSV fuel elements per week. Provision are included in the following:

1. weighing, identifying, and leak checking all canisters before segmenting the fuel elements;
2. opening the canister and removal, inspection, and identification of the fuel element;
3. segmenting;
4. reloading the segmented element into the canister (including all necessary equipment to handle broken fuel elements); and
5. sealing the canister, inspecting it, and preparing it (including decontamination) for transfer by System 4100, the Radioactive Materials Handling and Storage System.

Subsystem 1921 — Burner Off-Gas (BOG)

This subsystem consists of the following:

1. a water-cooled condenser to reduce off-gas temperature to provide cold surfaces for semivolatile plate-out and downstream treatment;
2. a particulate filter located after the condenser;
3. a silver zeolite absorber to remove iodine and having the capacity to contain all the iodine generated in the program;
4. a combination catalytic converter to convert carbon monoxide to CO_2 and oxidize any tritium, a gas heater in front of the converter, and a cooler after;
5. a molecular sieve adsorber preceded by steam injection to adsorb tritium from the off-gas and remove it as tritiated water;
6. a molecular sieve bed to contain radon for an adequate decay time before discharge to the TURF hot off-gas (HOG) system;
7. an HEPA filter to retain any particulates from adsorbent breakdown or dislodged solid radon decay products before release to the TURF hot off-gas system;
8. a charcoal bed to retain any gaseous matter absorbent breakdown.

Off-gas stream sampling is provided at the BOG feed point, between successive system units, and at the system discharge. The samples are taken remotely by use of a gas bomb.

Subsystem 1931 — Dissolver Off-Gas

This subsystem is to receive and heat vented gases for removal of radioactive contaminants and NO_x. It consists of the following:

1. A catalytic zeolite bed converter converts NO_x to innocuous gaseous by-products. A gas heater precedes the converter and a cooler follows. Ammonia gas is supplied for the reduction.

2. A silver zeolite adsorber (same design as for BOG) removes iodine.

3. Dual gas dryers in parallel remove water vapor from the dissolver off-gas and vessel off-gas as well as the off-gas from the NO_x converter. Regeneration is by hot gas (CO_2) back purging with moisture condensed, sampled, and released to the cell radioactive waste drain.

4. A molecular sieve (same design as for BOG) removes and retains radon for an adequate decay time before discharge to the TURF HOG system.

5. A HEPA filter retains any particulates from adsorbent breakdown or dislodged radon solid decay products before release to the TURF HOG.

6. A charcoal bed retains any gaseous matter from absorbent breakdown.

Off-gas stream sampling is provided at the dissolver off-gas feed point, between consecutive system units, and at the system discharge. The samples are taken remotely by use of a gas bomb.

Subsystem 1941 — Burner Cooling

During combustion with CO_2, this subsystem provides for burner cooling through the annular gap between the burner wall and the induction heater susceptor. The upper section is separately cooled with CO_2 inside an annular gap. This subsystem is a closed loop system with a recirculation blower and heat removal via a secondary recirculating liquid loop penetrating the alpha shielding barrier. A redundant or alternate source of cooling allows safe shutdown cooling of the burner if either cooling gas or fluidizing gas is reduced or lost. The burner cooling subsystem is shared by the primary and secondary burner and thus must be sized for the maximum heat load.

Subsystem 1951 — Liquid Waste Disposal

This subsystem provides for interim storage of all process liquid wastes generated during HET reprocessing operations. Waste treatment withing TURF is limited to the minimum necessary to permit transfer to building and laboratory waste handling facilities. Collecting, sampling, flow monitoring, storing, and dispatching the liquid waste products generated directly to System 4900, the Waste and Scrap Disposal System, are provided for (as required). Systems are likely to be located in the same cell in TURF. The liquid organic wastes are mixed with vermiculite, packaged in 0.11-m^3 containers, and delivered to System 4900 for further handling.

Subsystem 1956 — Solid Waste and Scrap Removal

This subsystem receives solid scrap and waste from the process system, sorts, compacts (if feasible), packages, and transfers solid waste via System 4100 to System 4900; disposes of failed equipment; and collects insolubles from the dryer in special cans compatible with residual acids.

Subsystem 1961 — Solid Product Handling

This subsystem receives and dispenses burner product from hot and cold tests.

Subsystem 1971 — Sample Handling

This subsystem prepares samples from Cells D and E and transfers them to the sample transport system.

Subsystem 1981 — Liquid Product Handling

Aqueous product from System 1800 is transferred via a cask provided by System 4100. A transfer station is provided to safely handle solution transfer from the in-cell accountability vessel to the transfer cask out of cell.

7.2.3 HET Refabrication — L. C. Hensley and C. C. Haws

The refabrication processes consist of the following systems, as shown in the overall refabrication block flow diagram, Fig. 7.3.

System 2100 — Uranium Feed Preparation

System 2200 — Resin Fuel Kernel Preparation

System 2300 — Resin Carbonization

System 2400 — Conversion and Coating

System 2500 — Fuel Rod Fabrication

System 2700 — Sample Inspection

System 2800 — Process Support

The related equipment will be operated in ORNL Building 7930 (TURF), except System 2100, which will be located in Building 3019. Cell C of TURF is assigned specifically to Systems 2000 through 2500. Equipment associated with other refabrication systems will be located in other shielded areas of TURF (see Fig. 7.4).

7.2.3.1 System 2100 — Uranium Feed Preparation

The Uranium Feed System (UFS) is a radiochemical processing system designed to provide purified ^{233}U uranyl nitrate feed solution for refabrication tests in the HETF. The UFS can receive and purify scrap uranyl nitrate solution from the HET-Refabrication for reintroduction into the feed stream or interim storage. Source material for the UFS is the National ^{233}U Repository (NUR) located in Building 3019, in which the material is stored in solid form as UO_3 and in solution form as aqueous uranyl nitrate. The stored solids contain greater than 10 ppm ^{232}U; the stored solution contains less than 10 ppm ^{232}U.

The functions of the UFS are to:

1. transfer ^{233}U in solid or solution form from the NUR,
2. dissolve if in solid form,
3. purify to specifications,
4. load purified solution into the transfer cask,
5. receive scrap solution from the HET and reprocess,
6. return ^{233}U to storage,
7. transfer waste materials generated within the system.

In general, the existing facilities can perform most of the required functions of the UFS. However, specific design requirements will require some new equipment and upgrading and modification of some existing plant components.

The subsystems that make up and support the UFS are designed to perform one or more of the system functional requirements. These subsystems are listed and briefly described.

Subsystem 2101 — ^{233}U Solids Transfer

This subsystem removes the $^{233}UO_3$ powder from the NUR and charges it to the dissolver of Subsystem 2121. The operation is semiremote and carried out in heavily shielded and contained equipment.

Subsystem 2111 — ^{233}U Liquid Scrap Receiving

This subsystem receives the scrap uranium from the HET as a uranyl nitrate solution in a transfer cask and transfers it to the accountability tank. The transfer cask itself is shielded, and the operation is performed semiremotely in contained equipment requiring some shielding.

Subsystem 2121 — Purification

This subsystem receives uranium oxide powder from Subsystem 2101 and dissolves it to a uranyl nitrate solution. The solution is purified by liquid-liquid extraction and ion exchange and held for a short time in product tanks before transfer to Subsystem 2131. This subsystem can also receive uranyl nitrate solution directly from the NUR and treat it as above. All operations are entirely remote and carried out in heavily shielded cells.

Subsystem 2131 — ^{233}U Product Dispensing

This subsystem transfers the purified uranyl nitrate product solution from Subsystem 2121 to a transfer cask for transporting to the HETF. The transfer cask (different from the one used in Subsystem 2111) is also shielded. The operation is performed semi-remotely in contained equipment requiring some shielding.

Subsystems 2811, 2821, and 2831

These subsystems provide support for the UFS and are summarized in the Process Support System, System 2800, Sect. 7.2.3.7.

7.2.3.2 System 2200 — Resin Fuel Kernel Preparation

The purpose of the Resin Fuel Kernel Preparation System (RFKPS) is to produce batches of uranium-loaded resin kernels to established specifications. The functions of the RFKPS will be executed through the operation of the following process subsystems.

Subsystem 2801 — Uranyl Nitrate Receiving and Dispensing

Purified solution from System 2100 is received in a shipping cask and delivered through the receiving station and washdown vessel located above the cell on the roof.

Subsystem 2201 — Uranyl Nitrate Solution Storage and Feeding

The solution is transported from the receiving station to the storage tank via air pressure and gravity. The RFKPS is a batch process (4 kg U basis and 11 liters resin per batch), with the 4 kg batch pumped by a metering pump to the process surge tank.

Subsystem 2221 — Resin Loading

Resin beads prepared to specification are received on the roof in the Resin Charging Tank, where 11 liters per batch is transported to the Resin Loading Contactor in the cell. Uranium is loaded on the resin beads at an eventual flow rate of 4 liters/min at approximately 50°C. Full loading requires approximately 4 hr.

The uranium loading on resin beads is an ion exchange reaction where free hydrogen ions are released as loading occurs. As the free hydrogen ions build up, reaction favoring uranium is reduced; therefore, nitric acid must be removed from the solution by the Nitrate Extraction Subsystem to maintain acid-deficient uranyl nitrate (ADUN) solution, a requirement for optimum loading.

Subsystem 2231 — Evaporator

The ADUN uranium concentration is controllable during the loading reaction by evaporating water from the ADUN semicontinuously in a thermosyphon. Steam supplies enough heat for an approximate evaporation rate

of 30 liters/hr. Shell-and-tube condensers (water cooled) will condense the evaporation overhead and cool the evaporator concentrate.

Subsystem 2211 — Nitrate Extraction

ADUN will be derived from the uranyl nitrate solution in the nitrate contactor by a solvent extraction process using Amberlite LA-2 diluted by diethylbenzene as the organic extractant. The nitric acid is extracted into the organic phase and the ADUN sent to the process surge tank.

The NO_3^--saturated organic goes through four solvent extraction contactors for washing, regeneration, and rinsing, using H_2O and NaOH. After regeneration, it is recirculated to the nitrate extraction contactor for further ADUN production.

Subsystem 2241 — Resin Drying and Transferring

The uranium-loaded resin beads are pumped via process solution to a glass column for microwave drying and water vaporization. Instrument air flows through the resin and takes off the water vapor until the resin contains 13 ± 4% water. The water is condensed from the purge gas in a shell-and-tube condenser, with the condensate evantually going to waste. The dried resin is pneumatically transferred to System 2300.

Subsystem 2816 — TURF Liquid Waste Disposal

Liquid wastes produced at various process points are initially sent to waste surge tanks. From these tanks, the wastes are jetted to building waste tanks, then to the ORNL intermediate-level waste system. All tanks are vented to an in-cell vessel off-gas system. The vessel off-gas is treated to hold up any radon released, then sent to the ORNL off-gas system.

7.2.3.3 System 2300 — Resin Carbonization System

The Resin Carbonization System receives solid fissile material in the form of uranium-loaded resin beads from the Resin Fuel Kernel

Preparation System. The resin particles are heated to volatilize all the hydrogenous material to yield a product consisting of UO_2 dispersed in elemental carbon. The particles are then called carbonized fuel kernels.

This system comprises four process subsystems:

1. Loaded Resin Handling Subsystem,
2. Carbonization Furnace Subsystem,
3. Carbonized Kernel Handling Subsystem,
4. Off-Gas Pretreatment Subsystem.

The Loaded Resin Handling Subsystem receives loaded resin in approximately 8-kg (50 wt % U) lot quantities. After an accurate weight of the lot is obtained, a small statistically representative sample is dispensed to the Sample Inspection Subsystem. The lot is then subdivided into eight approximately equal batches (0.5 kg nominal uranium content) and transferred, a batch at a time, to the Carbonization Furnace Subsystem.

The batches of resin are heated in the carbonization furnace according to a specific time-temperature schedule to form the desired carbonized fuel kernel product. Batches of carbonized fuel kernels are then transferred to the Carbonized Kernel Handling Subsystem.

After the batch of particles is collected, it is accurately weighed. Another small representative sample is dispensed to the Sample Inspection System, and the batch is transferred to the Microsphere Coating System.

The Off-Gas Pretreatment Subsystem will consist of a scrubber and its related equipment. The scrubbing medium will be a nonmoderating organic solvent that will rapidly cool and remove condensible hydrocarbons and other particulates from the furnace effluent. After this pretreatment the gaseous effluent is routed to the Combustible Off-Gas Subsystem of the Process Support System.

7.2.3.4 System 2400 — Microsphere Coating System

The purpose of the Microsphere Coating System is to convert approximately 50% of the UO_2 in the received carbonized fuel kernels

to uranium carbide (UC_2) and then apply four coatings to the fissile fuel particles. The first two coatings are pyrolytic carbon, one of low density and the other of high density. The third is pyrolytic silicon carbide, and the fourth is another high-density pyrolytic carbon coating. This system processes batches with a nominal uranium content of 0.5 kg. It comprises four process subsystems:

1. Coating Furnace Subsystem,
2. Furnace Loop Particle Handling Subsystem,
3. Coated Particle Handling Subsystem, and
4. Off-Gas Pretreatment Subsystem.

The Coating Furnace Subsystem first receives batches of carbonized fuel kernels from the Resin Carbonization System. The particles are heated in the coating furnace to about 1700°C and held at this temperature for about 30 min to obtain the desired uranium oxide-to-carbide conversion. After the furnace is unloaded, the particles are screened to remove pieces of soot and transferred to the Furnace Loop Particle Handling Subsystem.

After the batch is accurately weighed and a small statistically representative sample is dispensed to the Sample Inspection System, it is transferred back to the Coating Furnace Subsystem. By controlling the temperature of the particles in the furnace and the flows of the coating gases, the particles are given the appropriate coatings. Each time a coating is applied, the furnace is unloaded, and the batch is weighed and sampled in the Furnace Loop Particle Handling Subsystem. After the last pass through this subsystem, the batch is transferred to the Coated Particle Handling Subsystem.

The batch is collected and dispensed into a suitable storage container to be transported to the Fuel Rod Fabrication System. If the sample analysis shows that the batch is not specification grade fuel, it will be transported to the Solid Waste Handling Subsystem of the Process Support System. The storage container must therefore be compatible with both systems.

The Off-Gas Pretreatment Subsystem rapidly cools the furnace effluent and scrubs it of condensible hydrocarbons and other particulate

material. This carbon scrubber uses perchloroethylene, a nonmoderating organic solvent, as a scrubbing medium. Since the scrubber does not remove the hydrogen chloride gas generated during the silicon carbide coating, a second scrubber is used during this operation. An aqueous caustic solution (20 wt % NaOH) scrubs and neutralizes the HCl from the effluent. This second scrubber is bypassed during conversion and pyrolytic carbon coating. After this pretreatment the gaseous effluent is routed to the Combustible Off-Gas Subsystem of the Process Support System.

7.2.3.5 System 2500 — Fuel Rod Fabrication

The purpose of the Fuel Rod Fabrication System is to form a limited number of "green" (uncarbonized) fuel rods as needed to test the suitability of System 2400 product for continued processing and to prepare fuel rods to supply the needs of the nondestructive assay development program. The process for the Fuel Rod Fabrication System is basically a manually controlled sequential operation with a single line of equipment in series. The process takes basic material — particles and matrix slugs — and fabricates fuel rods one at a time. The Fuel Rod Fabrication System process receives coated fissile particles from the Microsphere Coating System, coated fertile particles from outside the cell, and carbon shim particles from outside the cell.

The process involves basically the precise blending of these particles and loading the blended mix into a cylindrical mold, then injecting into the particle bed, under controlled high temperature and pressure, a "matrix slug" consisting of a precisely blended compound similar to coal tar or pitch (Fig. 7.8).

After the matrix has been injected into the particle bed the mold is cooled to ambient temperature and the formed fuel rod is then ejected from the mold to complete the process. This process is repeated for each fuel rod to be fabricated in the HET. The accepted name for this process is the "slug injection method" of fuel rod forming. Figure 7.3 shows how the Fuel Rod Fabrication System interfaces with other systems.

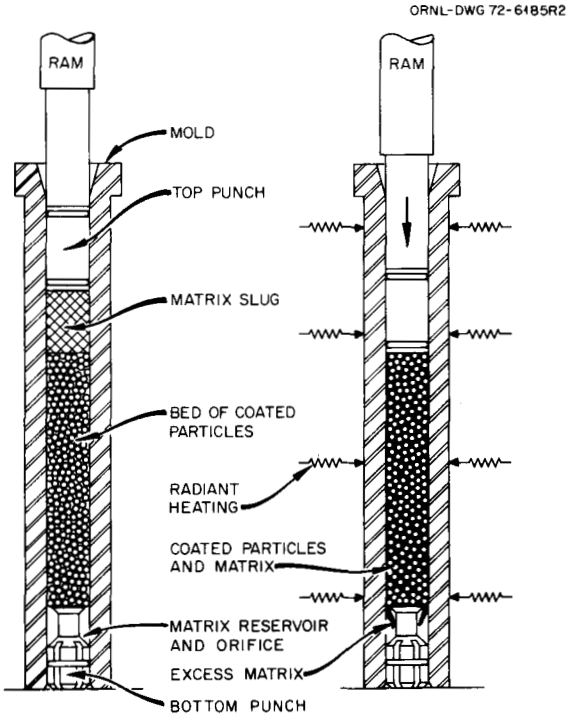

Fig. 7.8. Slug Injection Technique for Making Fuel Rods.

7.2.3.6 System 2700 — Sample Inspection System

The Sample Inspection System will receive samples from all stages of processing in the systems of the refabrication portion of the HET, perform the necessary sample preparation operations, and package these samples for forwarding to various ORNL facilities for analysis.

Most sample transfers will be in vacuum pneumatic lines. The three basic types of samples will be transferred as follows:

1. Fuel rods will be transferred in capsule containers between special loading and unloading valves.

2. Particle samples will be moved without such containers to facilitate handling by gravity transfer from receiving hoppers to glove box operations.

3. Liquid samples will be transferred in sample vials inside capsule containers.

The Sample Inspection System will perform the following functions:

1. transfer of samples from the process system;
2. subdivision of particulate samples, as required;
3. weighing, packaging, and dispatching of samples to other ORNL laboratories;
4. performing particle size analysis;
5. weighing, packaging, and dispatching of archive samples to storage; and
6. weighing and transferring excess sample material to waste and scrap handling.

7.2.3.7 System 2800 — Process Support

System 2800 handles feed materials between Systems 2100, UNH Feed Preparation, and 2200, Resin Kernel Preparation, and it handles a wide variety of wastes. The wastes and scraps from the TURF operation are as follows:

<u>Type of Waste</u>

Failed equipment

Resin contactor filter elements

Noncombustible organic gases

Vents from waste tank — aqueous and organic noncombustible gases

Aqueous liquid ($NaNO_3$)

Organic liquid (Amberlite + diethylbenzene)

Traps and filters

Carbon clinkers from coating furnace

Effluent from coating furnace scrubber

Mold parts and general waste

<u>Type of Scrap</u>

Uranyl nitrate scrap solution

Coated reject particles

Miscellaneous feed materials, out of specification fuel rods

The system performs the following functions:

1. dispense UNH feed solution into the transfer cask from System 2100 in Building 3019;

2. transfer the feed solution from System 2100 to a receiving station at TURF, at which point it is dispensed into a storage tank of System 2200;
3. receive scrap feed solution from System 2200 for transfer back to System 2100 for reprocessing;
4. collect, sample, and recycle or dispose of liquid wastes generated during operations of System 2100;
5. collect, sample and monitor, package, and dispose of solid wastes generated during operations of System 2100;
6. remove biologically and environmentally harmful gases and particulates from process vessel off-gas streams at Building 3019 before their discharge to the ORNL Off-Gas System;
7. connect the liquid waste collection tank to the TURF waste collection tank and to the TURF waste system.
8. transfer combustible and noncombustible gaseous waste streams to the facility waste treatment, System 4100;
9. sort, weigh, and package for storage or disposal solid waste, organic liquid waste, and scrap material;
10. transfer the above materials to System 4900 for storage or disposal;
11. reclaim used percholorethylene and return it to be reused in System 2300.

7.3 REFERENCE

1. J. W. Anderson, S. E. Bolt, and J. M. Chandler, *Safety Analysis for the Thorium-Uranium Recycle Facility*, ORNL-4278 (May 1969).

8. COLD PROTOTYPE REFABRICATION DEVELOPMENT

R. A. Bradley and W. J. Lackey

8.1 INTRODUCTION

The objective of the cold prototype development stage is to establish the configuration and operating characteristics of equipment designed for use in HRDF. Although this development stage is cold in the sense that highly radioactive material will not be used, the cold prototype equipment will: (1) be full scale, (2) incorporate remote features that may affect the performance of equipment or the quality of the product, and (3) incorporate essential features that are required to demonstrate that equipment can be disassembled, reassembled, or otherwise maintained remotely.

During this report period, effort was concentrated on the design of a microsphere coating furnace, a fuel rod fabrication machine, and a cure-in-place furnace.

8.2 MICROSPHERE COATING — R. R. Suchomel, J. L. Heck, M. K. Preston, and D. P. Stinton

The object of cold prototype development is to design, construct, and operate a prototypic microsphere coating system. The coater will be a 0.24-m-diam furnace capable of coating a 3.2-kg uranium batch. This is the size and capacity anticipated for a commercial facility. As with other cold prototype systems, the coater will demonstrate remote operability and maintainability.

During this reporting period, a criteria statement (Thorium Utilization Program Management Document D-11387-TB-C05-U-1) for the conceptual design work was written. A conceptual design study is now being undertaken with this criteria statement as a guide. The conceptual design phase, to be completed in March 1977, will include a critical path study and a cost estimate for the design and construction of the coater system.

8.3 FUEL ROD FABRICATION — D. R. Johnson, R. M. DeLozier, and S. P. Baker

The conceptual design of a 40,000 rod per day cold prototype fuel rod molding machine has been previously described.[1] The design criteria for fuel rod molding are currently being modified to take advantage of recent developmental experience (see Sect. 3.5.4). A study and estimate for the cold prototype will be performed in the near future. It is intended that the detailed mechanical design will be executed by a time-and-materials contractor once the study and estimate has been completed.

8.4 FUEL ELEMENT ASSEMBLY — CURE-IN-PLACE FURNACE — D. R. Johnson, A. J. Caputo, W. G. Cobb, J. R. Horton, and D. P. Reid

A general description of the cure-in-place furnace, including a cut-away drawing, was published previously.[2] A study and estimate of the cost and effort required to design and install the cold prototype furnace and necessary auxiliary systems has been performed. The furnace will be installed at ORNL. The basic criteria for the conceptual design came from the system description for the HTGR Fuel Refabrication Pilot Plant (FRPP). The cold prototype installation meets the same criteria outlined for the System 6 equipment development portion of the project. The remote installation and removal capabilities outlined for the FRPP were maintained in the basic furnace design. A directive will be requested from ERDA in early calendar 1977 for authority to begin construction and procurement.

A description of the cold prototype cure-in-place furnace system follows:

8.4.1 General Layout

The proposed furnace and related equipment will be located in the northwest corner of Building 4508. The furnace will be installed in an existing pit approximately 3 m (10 ft) below floor level. The top will extend approximately 6 m (20 ft) above floor level. The off-gas scrubber will be located adjacent to the furnace.

A process room for instruments and controls approximately 2.1 × 5.5 m (7 by 18 ft) will be constructed 2.7 m (9 ft) above the high-bay area floor along the northwest wall of Building 4508. Valves and sensing elements for the process piping will be located along the main entrance platform to the control room and to critical points on the furnace. A high-bay building crane will be available for use in loading and unloading fuel elements. Utility services for the furnace will be extended from various locations in Building 4508. Auxiliary equipment will be installed to be readily accessible to the furnace. Platforms will provide access to the furnace and the control room. Structural shapes will be installed to provide lateral support to the furnace structure.

The carbonization-annealing furnace will consist of a vertically standing, atmosphere controlled, electrical resistance heated tube furnace with associated controls and materials handling equipment for continuous processing of HTGR fuel elements and sample-holding dummy blocks.

8.4.2 Processing Chamber

The processing chamber will include the furnace heating zone and the water-cooled jacket. The length of approximately 5.2 m (203 in.) contains five graphite-lined heating zones starting from the top and an unlined extraction zone at the bottom. Gate valves at the top and bottom will provide selective isolation for inert-atmosphere containment and openings for passage of blocks as they are moved progressively downward during processing. Retractable plunger forks to be mounted immediately above the lower valve will provide an interim support for the column of blocks in the chamber by engaging the spacer pallet for the bottom block in the chamber so that the block below may be passed beyond the lower valve and allow valve closure.

A double-wall, water-cooled metal shell structure will enclose the chamber between the lower valve and the upper valve, including the heaters and their thermal insulation, and providing containment for an inert atmosphere.

The heaters for the two highest temperature zones will be machined graphite resistance heaters surrounded with carbon insulation. Heaters in the preheat zones will be metal ribbon located outside an atmosphere-containing metal liner tube. Formed thermal insulation will surround the cylindrical heater support. Electrical terminals for the graphite heaters will be water-cooled and sealed through the containment shell with machined graphite conductors connecting into heater elements.

The furnace effluent discharge line will pass radially from the preheat zones, and it will be provided with heaters for maintaining its temperature.

Sealed penetration ports and protective wells will be distributed over the various heating zones for pyrometric viewing and controlling instruments and for thermocouples to provide the required thermal control of the furnace.

8.4.3 Discharge Chamber

A discharge chamber extending almost to the bottom of the furnace structure will be attached to the lower flange of the bottom valve. This chamber will be a double-ported atmosphere lock required for maintaining the inert atmosphere in the process chamber while processed fuel elements are unloaded.

The chamber will contain a motor-driven elevator platform, which will support the entire column of fuel elements, with pallets, as they progress downward through the various heating and cooling zones of the process chamber. The platform will be supported by four synchronously driven screws penetrating the top of the chamber.

The elevator position will be indicated by limit switches and a position indicating transducer. A remotely controlled door will be installed in one wall of the discharge chamber. This door will provide atmospheric containment during fuel element processing and access for fuel element unloading after the processing chamber is sealed by the lower valve.

8.4.4 Fuel Element Unloading Equipment

A fuel element unloading fixture will be located in front of the opening in the discharge chamber. It will consist principally of a way-mounted horizontally cantilevered fork, which will be motor-driven through the opening. The upper surface of the fork will be positioned under the pallet rim. The fork will support the fuel element via the pallet for removal from the discharge chamber. A frame will be installed on top of the fork to confine the element if the pallet is broken. The unloading equipment will withdraw the fuel element and pallet from the furnace to a position accessible to the overhead handling equipment in the high bay.

8.4.5 Charging Chamber

A furnace charging chamber will be seated on the upper face of the top valve of the processing chamber for charging elements into the furnace. This chamber will be an open-ended flanged cap enclosing a screw-driven elevator with a remotely controlled fuel element handling grapple located in its center. The elevator screws will penetrate the chamber top, where they will be synchronously driven by an electric motor. Electrically operated safety latches will prevent dropping a fuel element through the open-ended bottom in the event of a handling failure.

The top of the charging chamber will be designed to be remotely engaged and lifted by the hook of the existing building crane. An electrical and gas connector will be located at the chamber flanged face to mate with a connector on top of the furnace. These will provide makeup of all control and power circuits for chamber operation and connection of sparging gas. An O-ring gasket will be held in a groove in the lower face.

The elevator will be equipped with position limiting switches and a position indicating transducer. The grapple will be equipped with position and condition indicating switches. Safety latch position indication switches will be installed for their control.

8.4.6 Charging Chamber Loading Stand

A fuel element may be positioned or a support stand will be provided for loading the charging chamber. A flanged ring on the platform simulating the furnace valve face will provide support and guidance features for positioning the charging chamber with the building crane. The mating half of the electrical connector will provide for operation.

8.4.7 Spacer Pallet

A machined graphite spacer pallet will be installed between blocks in the furnace to transfer the centering and orientation positioning of the lower block to the block seated on it and to serve as a means of handling the blocks as they progress through the furnace and are removed from the discharge chamber.

8.4.8 Thermal Gradient

The furnace design will provide a temperature profile from 200°C in the top section up to a maximum temperature of 1800°C in the center section and then back down to 200°C in the bottom section.[3] The temperature up to 1000°C will be for carbonization and between 1000 and 1800°C will be for annealing. The temperature profile will be accomplished by use of five heating zones at the top of the furnace followed by three cooling zones. Two of the cooling zones will be in the main portion of the furnace and the final cooling zone in the discharge chamber.

8.4.9 Heat Removal System

Heat will be removed from the process chamber walls, the retractable support plungers, the elevator platen, the walls of the discharge chamber, and the high-current heater leads.

The cooling water required for the furnace will be supplied from an existing process water system in Building 4508. The water will be circulated through cooling jackets built into the furnace structure. A portion of the water will be recirculated to minimize waste.

8.4.10 Fire Protection

The existing fire protection system in Building 4508 will be extended for added sprinklers inside and beneath the control room. The remainder of the furnace area will be protected by existing sprinklers.

8.4.11 Furnace Purge Gas

Because of the high temperature in the furnace and the oxidizing characteristics of the furnace internals and fuel blocks, no oxygen can be allowed in the furnace. Either nitrogen or argon will be supplied to the furnace as a purge to ensure the removal of oxygen. Purge gas will be supplied from trailers to be located outside Building 4508 to a control panel in the furnace area. Individual argon lines will extend from the panel to the various connection points on the furnace.

8.4.12 Compressed Air

Compressed air, extended from an existing system in the building, will be required to actuate pneumatically operated mechanisms, including the upper and lower valves of the furnace, the discharge chamber door clamps, the material support forks, and the control valves. A supply header [0.7 MPa gage (100 psig)] will be routed to the furnace area and individual lines extended from the header to the service points.

8.4.13 Off-Gas

Furnace off-gases containing hydrocarbons and soot will be carried by ductwork to the scrubber where tars and soot will be removed from the gases in the spray tower by perchloroethylene.

8.4.14 Environmental Control

The existing air-conditioning supply ducts will be extended to diffusers in the ceiling of the new control room. The ductwork will be galvanized steel designed for low velocity and low pressures. Louvers in the door will permit flow of air from the control room to the surrounding high-bay area.

Before the furnace is charged, air and moisture will be purged from the charging chamber by argon. About 19 std liters/sec (40 scfm)

of the inert gas plus 28 liters/sec (60 cfm) of ambient air will be removed by ductwork connected to two existing exhaust ducts in the pit. These ducts discharge into a room exhaust duct to the HEPA filter exhaust systems.

About 14 std liters/sec (30 scfm) of off-gas fumes will be exhausted from the furnace during normal operation. This gas will pass through a perchloroethylene scrubber, demisters, and an after-cooler for cleaning. A pressure controller sensing the pressure in the furnace will control a ball valve on the exhaust duct to maintain a positive pressure in the furnace. An exhaust duct will connect to the duct used for the argon purge of the charging chamber. The ventilation system will be provided with emergency power.

8.4.15 Instrumentation and Control Systems

These will include the following: argon gas supply and off-gas control panels, cooling water measurement and control instrumentation, mechanical sequential operation control instrumentation, and safety interlock and alarm instrumentation.

8.4.16 Electrical

This will consist of the following:

1. A power distribution panel and a motor control center will be installed in the northwest end of Building 4508. Relocation of an existing motor control center will be necessary to allow space for new equipment.

2. Conduit and cabling are required between the distribution panel, the instrumentation and control room, and the furnace heaters. Controllers will regulate power to the heaters. Zones 4 and 5 of the furnace will be heated by high-current graphite heaters, which will require the installation of two high-current, low-voltage transformers. Water-cooled cables will carry the high current (1500–2000 A) from the transformer to the graphite heaters.

3. Conduit and cabling will be installed between the motors, the instrumentation and control room, and the motor control center.

4. Conduit and cabling will be required between the instrumentation and control room and the motor control center to provide a protective interlocking system for equipment.

5. An approved fire alarm system will be installed and connected to the existing building fire alarm system.

6. A system ground will be installed and connected to the existing building ground system.

8.5 REFERENCES

1. D. R. Johnson, P. Angelini, J. E. Rushton, S. R. McNeany, R. W. Knoll, R. A. Bradley, and R. M. Delozier, "Fuel Rod Fabrication (Work Unit 2105)," *Thorium Utilization Program Prog. Rep. Jan. 1, 1974–June 30, 1975*, ORNL-5128, pp. 176–90.
2. D. R. Johnson, A. J. Caputo, and W. G. Cobb, "Fuel Element Assembly," *Thorium Utilization Program Prog. Rep. Jan. 1, 1975–June 30, 1975*, ORNL-5128, pp. 191–94.
3. G. A. Llewellyn, *Thermal Design and Analysis of the HTGR Fuel Element Vertical Carbonizing and Annealing Furnace*, ORNL-Eng-TM-1 (to be published).

ORNL-5266
UC-77 — Gas-Cooled
Reactor Technology

INTERNAL DISTRIBUTION

1–2. Central Research Library
3. Document Reference Section
4–5. Laboratory Records Department
6. Laboratory Records, ORNL RC
7. ORNL Patent Office
8. R. D. Ackley
9. P. Angelini
10. S. P. Baker
11. B. J. Baxter
12. R. J. Beaver
13. R. J. Braatz
14. R. A. Bradley
15. R. E. Brooksbank
16. W. D. Burch
17. A. J. Caputo
18. J. A. Carpenter
19. W. L. Carter
20. H. E. Cochran
21. D. A. Costanzo
22. F. L. Culler
23. F. C. Davis
24. R. G. Donnelly
25. B. C. Duggins
26. W. P. Eatherly
27. G. G. Fee
28. D. E. Ferguson
29. C. L. Fitzgerald
30. T. M. Gilliam
31. R. W. Glass
32. P. A. Haas
33. C. C. Haws
34 F. E. Harrington
35. L. C. Hensley
36. R. F. Hibbs, UCC
37–39. M. R. Hill
40. R. M. Hill
41. F. J. Homan
42. L. N. Howell
43. J. O. Hylton
44. J. D. Jenkins
45. D. R. Johnson
46. M. J. Kania
47. S. V. Kaye
48–55. P. R. Kasten
56. R. K. Kibbe
57. J. J. Kurtz
58. W. J. Lackey
59. K. H. Lin
60. E. L. Long, Jr.
61–70. A. L. Lotts
71. J. E. Mack
72. A. P. Malinauskas
73. M. M. Martin
74. S. R. McNeany
75. F. H. Neill
76–78. K. J. Notz
79. A. R. Olsen
80. W. H. Pechin
81. S. Peterson
82. H. Postma
83. R. H. Rainey
84. D. P. Reid
85. A. D. Ryon
86. J. E. Rushton
87. T. F. Scanlan
88. C. D. Scott
89. J. H. Shaffer
90. W. D. Shults
91. G. M. Slaughter
92. P. E. Stein
93. D. P. Stinton
94. R. R. Suchomel
95. S. M. Tiegs
96. T. N. Tiegs
97. J. E. Till
98. D. B. Trauger
99. V.C.A. Vaughen
100. J. R. Weir, Jr.
101. R. P. Wichner
102. R. G. Wymer

EXTERNAL DISTRIBUTION

103–104. ERDA DIVISION OF REACTOR NUCLEAR RESEARCH AND APPLICATIONS, Washington, DC 20545

Director

105–106. ERDA DIVISION OF REACTOR DEVELOPMENT AND DEMONSTRATION, Washington, DC 20545

Director

107. ERDA IDAHO OPERATIONS OFFICE, P.O. Box 2108, Idaho Falls, ID 83401

Barry Smith

108. ERDA OFFICE PROGRAM MANAGEMENT, RESEARCH AND SPACE PROGRAMS, P.O. Box 81325, San Diego, CA 92138

J. B. Radcliffe

109. ERDA SAN FRANCISCO OPERATIONS OFFICE, 1333 Broadway, Wells Fargo Building, Oakland, CA 94612

Manager

110–113. ERDA DIVISION OF WASTE MANAGEMENT, PRODUCTION AND PROCESSING, Washington, DC 20545

Acting Assistant Director for Reprocessing
Chief, Technology Branch
Chief, Projects Branch
Chief, Industrial Programs Branch

114–116. ERDA OAK RIDGE OPERATIONS DIVISION, P.O. Box E, Oak Ridge, TN 37830

Director, Research and Technical Support Division
Director, Reactor Division
F. E. Dearing, Reactor Division

117–294. ERDA TECHNICAL INFORMATION CENTER, P.O. Box 62, Oak Ridge TN 37830

For distribution as shown in TID-4500 Distribution Category, UC-77 (Gas-Cooled Reactor Technology).